The American Mineralogist

Journal of the Mineralogical Society of America

VOL. 45 SEPTEMBER-OCTOBER, 1960 Nos. 9 and 10

LIBRARY
7 1960
CHICAGO

Contents

X-ray spectrochemical analysis: An application to certain light elements in clay minerals . . . . . M. W. Molloy and P. F. Kerr 911
The crystallography of mcgovernite, a complex arsenosilicate . . . . . Bernhardt J. Wuensch 937
Thermal transformations and properties of cryptomelane . . . . . G. M. Faulring, W. K. Zwicker and W. D. Forgeng 946
Classification of silicates and other minerals with tetrahedral structures . . . . . Tibor Zoltai 960
Proto-amphibole, a new polytype . . . G. V. Gibbs, F. D. Bloss and H. R. Shell 974
Infrared spectra of some tectosilicates . . . . . Robert G. Milkey 990
Serpentinite-limestone contact at Taleri Mohammad Jan, Zhob Valley, West Pakistan . . . . . S. A. Bilgrami 1008
Selective staining of K-feldspar and plagioclase on rock slabs and thin sections . . . . . E. H. Bailey and R. E. Stevens 1020
Crystal chemical studies of some uranyl oxide hydrates . . . . . C. L. Christ and J. R. Clark 1026
A second find of euhedral bornite crystals on barite . . . . . G. Kullerud, G. Donnay and J. D. H. Donnay 1062
An interstratified mixture of mica clay minerals . . . S. Shimoda and T. Sudo 1069
Ranquilite, a calcium uranyl silicate . . . . . M. J. de Abeledo, M. R. de Benyacar and E. E. Galloni 1078
Notes and News: *X*-ray crystallography of larderellite, $NH_4B_5O_6(OH)_4$ . . . . . Joan R. Clark 1087
  Crystal structure of potarite, PdHg, with comments on allopalladium . . . K. Terada and F. M. Cagle, Jr. 1093
  A note on so-called "pressure independent" minerals . . . . . Carl W. F. T. Pistorius 1097

(*Continued on Cover 2*)

EDITOR: LEWIS S. RAMSDELL

BOARD OF ASSOCIATE EDITORS:

D. JEROME FISHER
GEORGE W. BRINDLEY
RICHARD H. JAHNS
GEORGE T. FAUST (1958–60)
ADOLF PABST (1959–61)
EDWIN W. ROEDDER (1960–62)

Published bi-monthly by the Society

(*Contents continued*)

Preparation and use of a gelatin mounting medium for repeated oil immersion of minerals.......................Gordon W. Olcott 1099
Dehydration studies by infrared spectroscopy..........J. M. Serratosa 1101
X-ray diffraction technique for small samples.........Ronald K. Sorem 1104
A natural occurrence of nickel hydroxide................K. L. Williams 1109
Dehydration and rehydration of ferrimolybdite.......................................H. G. Golding, P. Bayliss and N. Trueman 1111
The preparation and use of polished thin sections........G. C. Amstutz 1114
Variations in interference figures in single crystals of zoned smoky quartz ....L. F. Dellwig and W. E. Hill, Jr. 1116
Calciostrontianite from Virginia..........................R. V. Dietrich 1119
Occurrence of orthopyroxene with low optic axial angle......J. F. Lewis 1125
Birefringence of synthetic garnets.......A. B. Chase and R. A. Lefever 1126
New Mineral Names.. 1130

Mineralogical Society of America

ASSOCIATED WITH THE GEOLOGICAL SOCIETY OF AMERICA

President: Joseph Murdoch, University of California at Los Angeles, Los Angeles 24, California.
Past-President: Ralph E. Grim, University of Illinois, Urbana, Illinois.
Vice-President: E. F. Osborn, Pennsylvania State University, University Park, Pennsylvania.
Secretary: George Switzer, U. S. National Museum, Washington 25, D. C.
Treasurer: Marjorie Hooker, U. S. Geological Survey, Washington 25, D. C.
Editor: Lewis S. Ramsdell, University of Michigan, Ann Arbor, Michigan.
Councillors:
(1958–60) Richard H. Jahns, California Institute of Technology, Pasadena, California.
(1958–60) Charles Milton, U. S. Geological Survey, Washington 25, D. C.
(1959–61) Wilfrid R. Foster, Ohio State University, Columbus 10, Ohio.
(1959–61) Edward W. Nuffield, University of Toronto, Toronto 5, Ontario, Canada.
(1960–62) Julian R. Goldsmith, University of Chicago, Chicago 37, Illinois.
(1960–62) Horace Winchell, Yale University, New Haven, Connecticut.
Advertising Manager: Martin L. Ehrmann, 1135 S. Beverly Drive, Los Angeles 35, California.

The enlarged issues of this journal for 1960 are made possible by a grant from the Penrose Fund of the Geological Society of America.

The American Mineralogist—Journal of the Mineralogical Society of America

The journal, containing articles on mineralogy, crystallography, and allied sciences, is issued every two months. Contributions are invited.

The general conduct of the journal is in the hands of the editor, Lewis S. Ramsdell, Department of Mineralogy, University of Michigan, to whom all manuscripts should be submitted.

Second class postage paid at Menasha, Wisconsin. Acceptance for mailing at the special rate of postage provided for in section 1103, Act of Oct. 3, 1917, paragraph 4 section 429 P. L. & R. authorized March 13, 1922.

Notice of change of address, orders, and remittances should be sent to Marjorie Hooker, c/o U. S. Geological Survey, Washington 25, D. C.

Printed by the George Banta Company, Inc., Menasha, Wisconsin
Printed in the United States of America

Leitz® **first in precision optics**

NEW
POLARIZING
MICROSCOPE SM-pol

Leitz sets a new standard with this student polarizing and chemical microscope of modern design, with dual, low-position focusing controls and large field of view. A reasonably priced polarizing microscope, the model SM-pol, has rugged, one-piece construction with Bertrand lens and pinhole diaphragm built into the tube. Inclined monocular tube will accommodate wide-field eyepieces and the microscope can be used faced away from the observer, permitting easy accessibility to the stage.

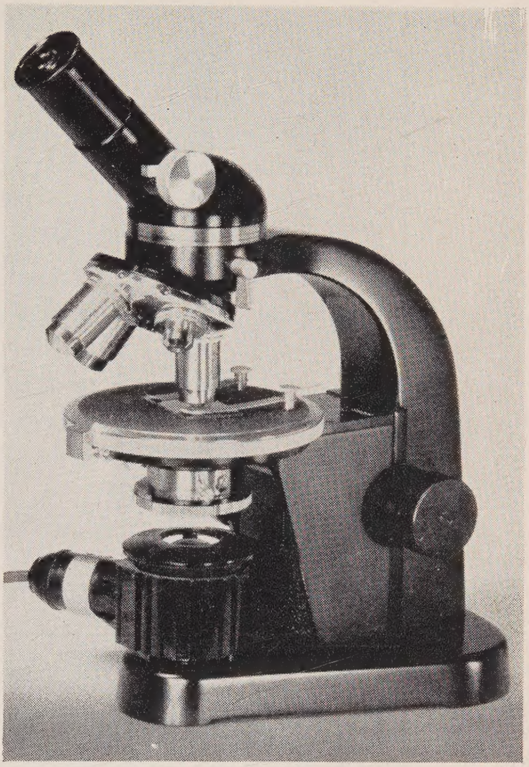

A reputation for integrity and a tradition of service have led thousands of scientific workers to bring their optical problems to Leitz. If you have problems in this field, why not let us help you with them?

See your Leitz dealer and examine these Leitz instruments soon. Write for information.

E. LEITZ, INC., Dept. AM-10
468 Park Avenue South, New York 16, N. Y.

Please send me the Leitz____________brochure.

NAME________________________

STREET________________________

CITY____________ZONE______STATE________

E. LEITZ, INC., 468 PARK AVENUE SOUTH, NEW YORK 16, N. Y.
Distributors of the world-famous products of
Ernst Leitz G. m. b. H., Wetzlar, Germany—Ernst Leitz Canada Ltd.
LEICA CAMERAS · LENSES · PROJECTORS · MICROSCOPES · BINOCULARS

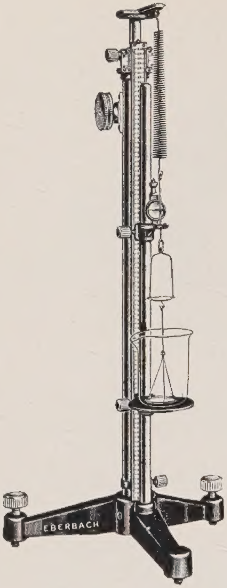

KRAUS JOLLY BALANCE

For Speedier Specific Gravities

This professional model is mentioned in *Mineralogy* by Kraus, Hunt and Ramsdell, in *Dana's Manual of Mineralogy* by Hurlbut and *Elements of Mineralogy* by Winchell.

The Kraus Jolly balance simplifies the determination of specific gravity; only two readings and a division are necessary; older forms of the balance require more extensive computation. The balance is especially well adapted for the rapid and accurate determination of specific gravity of solids, such as minerals, rocks, coal, precious stones, etc.

Send for our bulletin.

Eberbach
CORPORATION
P. O. Box 1024 Ann Arbor, Michigan

MINERAL SPECIMENS

Large variety of crystals, crystal groups, rare minerals, and ore minerals for collectors, universities and museums.

Mineral Catalog 25¢, or sent free when requested on official letterhead.

Filer's are interested in buying or exchanging for good quality minerals, especially from foreign countries. Correspondence is invited.

FILER'S
P. O. Box 372, Redlands, California

Our Specialty is

SELECTED MINERAL SPECIMENS
FROM WORLD-WIDE LOCALITIES FOR COLLECTORS AND MUSEUMS

we also carry a complete line of
MINERALIGHTS, DETECTRON GEIGER COUNTERS, ESTWING PROSPECTOR PICKS, MINERALOGICAL BOOKS, ETC.

Send for free current bulletin

SCHORTMANN'S MINERALS
6 McKinley Avenue Easthampton, Massachusetts

For Mineralogists:

Index of Refraction Liquids

Range: 1.35 to 2.11 index; available in sets of limited range, or in sets with various intervals, or in any selection. Note that liquids 2.01 to 2.11 are now available.

Write for Price List Nd-AM

Allen Reference Sets for Microscopical Studies in Mineralogy and Petrology

Six sets of Authentic materials for use as standards for refractive index, for standard materials mounted in balsam to be compared with unknowns, and for demonstration of typical optical characteristics under microscopical study.

Write for descriptive material A-AM

Text: Practical Refractometry by Means of the Microscope

By ROY M. ALLEN, D.SC.

Describes the technique of the immersion method of microscopy, with particular reference to the identification of minerals. Written primarily for elementary instruction, but this text will be very useful also to advanced workers. Price $1.00. Copy will be sent on approval.

Heavy Liquids

Formulated especially for determination of specific gravity of minerals, but special formulations are being made to order for various procedures. If you have any special problem in this field of separation of minerals or other materials by differences in specific gravity, please write us about your problem. Or, just write for leaflet HL-AM.

Gems, Testing For Identity and For Defects

The CARGILLE-ALLEN GEM TESTING SET is the title of our new book describing the properties of gems and also the equipment for certain identification of gems by a new simple procedure. Price $1.00; this amount applicable to purchase price of any of the items listed in the book.

R. P. Cargille Laboratories, Inc.
117 Liberty St., New York 6, N.Y.

MINERAL SPECIMENS *For Sale or Exchange*
MICROSCOPES BOOKS · GEOLOGICAL SUPPLIES

Catalog on request

SCOTT J. WILLIAMS
Mineralogist

440 N. SCOTTSDALE ROAD · SCOTTSDALE, ARIZONA, U.S.A.

The Lapidary Journal

SUBSCRIBE NOW

THE ORIGINAL GEM MAGAZINE

for gem cutters, gem collectors
and jewelry craftsmen

A non-technical craft publication, not a gemological or mineralogical magazine. Most quoted publication in its field. Bimonthly. Now in its 14th year.

RATES: $3.00 in U.S., North and South America
$3.50 in other foreign countries

Address: P.O. Box 518G, Del Mar, California

ADVANCED COLLECTORS

and Museums buy from us regularly. Choice mineral specimens and crystals. Visit our show room in San Diego or see us at the shows in your area.

Plummer's Minerals, 4720 Point Loma Ave., San Diego 7, Calif.

d. m. organist

petrographic
laboratory

BOX 176, NEWARK, DELAWARE

THIN SECTIONS OF

ROCKS, MINERALS, ORES, CERAMICS
PREPARED ROCK SECTIONS FOR
STUDENT USE
PHOTOMICROGRAPHS
PETROGRAPHIC ANALYSIS

Books from McGraw-Hill

PETROLEUM RESERVOIR ENGINEERING: Physical Properties

By James W. Amyx, Daniel M. Bass, and Robert L. Whiting, all of Agricultural and Mechanical College of Texas. 640 pages, $17.50

This volume develops the fundamental concepts of rock and fluid properties on which reservoir engineering is based. Procedures are presented for reduction and organization of reservoir rock, fluid and production measurements for use in reservoir engineering studies. Materials are presented in the quantitative sense, and adequate work charts are provided. A complete treatment of composite volume factors has been included.

PHOTOGEOLOGY

By Victor C. Miller, Miller & Associates, Inc., Denver, Colorado. Ready in Spring, 1961.

A text for graduate and advanced undergraduate courses in photogeology or photogeologic interpretation covering briefly the concepts of aerial photography and photogrammetric instrumentation, and then, in greater detail, stereoscopy and procedures. Of especial interest is the final third of the text which contains stereo-pair aerial photographic illustrations accompanied by individual texts, exercises, and pertinent topographic or geologic maps, sketches and cross-sections.

PRINCIPLES OF PETROLEUM GEOLOGY

New Second Edition

By William L. Russell, Agricultural and Mechanical College of Texas. 503 pages, $9.50

An up-to-date, carefully revised edition of one of the most important books in this academic area. The book gives students and geologists a description of the principles and processes that are important in petroleum geology. New information on the origin and accumulation of petroleum is discussed at length. The concept of traps for oil and gas is described and illustrated. A brief discussion of well logging methods and of geophysics is given.

Send for copies on approval

McGRAW-HILL BOOK COMPANY, INC.
330 WEST 42ND STREET, NEW YORK 18, N. Y.

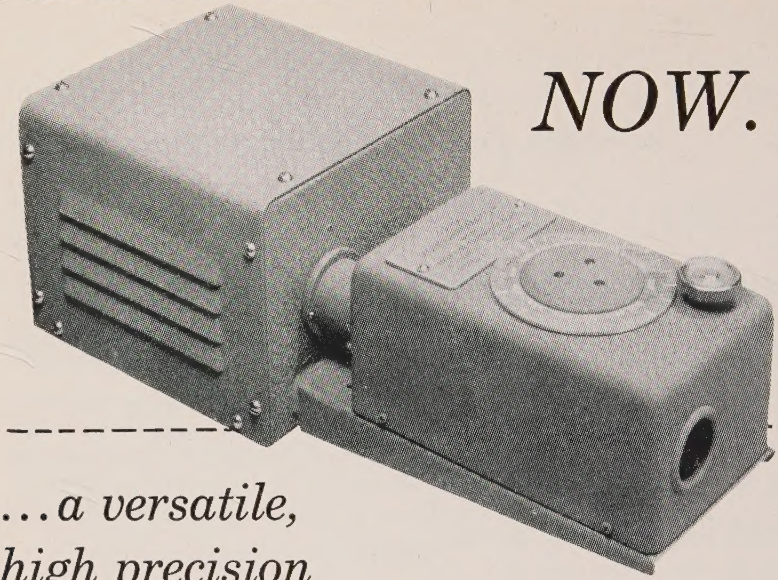

NOW...

...a versatile, high precision

CAMBION® Monochromato

with light source

- **Cold Intense 100 Watt Zirconium Arc Light**
- **Point Source — .08″ Diameter**
- **Convenient Circular Light Aperture**
- **Wide Range of Wavelengths — 4500A to 6400A**
- **Narrow Pass Band Width — 40A to 120A**

Here's the ideal monochromator for optical crystallography determinations. Can be used with both microscope and refractometer. Utilizes the rotary dispersion of quartz to provide a continuous selection of wavelengths. Combines highest intensity light source with large aperture. Power source, light, and lenses in compact, portable unit. Overall length 14″; height 5″; width 6″. Crackle grey finish. Send coupon for complete details.

CAMBRIDGE THERMIONIC CORPORATION
CAMBION
The guaranteed electronic components

Cambridge Thermionic Corporatio
503 Concord Avenue
Cambridge 38, Massachusetts

Please send complete details on CAMBION Monochromator.

Name. . . . .

Title. . . . .

Address. . . . .

City . . . . *Zone*. . . . *State*. . . .

FIRST: LOOK AT UNITRON'S NEW POLARIZING MICROSCOPE

Here is a precision measuring instrument for both orthoscopic and conoscopic observations, designed to meet the exacting requirements of science, education, and industry. Its many features make it ideal for work in chemistry, crystallography, mineralogy and biology as well as in the technology of paper, glass, textiles and petroleum.

CHECK THESE OPTICAL & MECHANICAL FEATURES

Note that UNITRON'S new Model MPS comes complete with optics and accessories and includes features usually associated only with much more costly models.

- **EYEPIECES:** Micro 5X providing measurements to 0.0025mm. and cross-hair 10X. The eye lenses focus to produce sharp reticle images and are keyed to prevent rotation.
- **OBJECTIVES:** 4X(N.A.0.1), 10X(N.A.0.25), 40X(N.A.0.65), achromatic, strain-free, each with centerable mount.
- **NOSEPIECE:** quick-change type for critical centering.
- **CONDENSER and POLARIZER:** three-lens condenser with upper elements on a swing-out mounting, provides either parallel or convergent light. A dovetail-slide focusing mount and iris diaphragm insure optimum illumination and resolution.
- **POLAROID POLARIZER:** rotatable through 360° and graduated every 45°. Plano-concave mirror.
- **ANALYZER:** Polaroid, in sliding metal mount.
- **BERTRAND LENS:** for the study of interference figures, fixed-focus lens is centerable and mounted in a slideway.
- **STAGE:** diameter 115mm., revolves through 360°, graduated in degrees and reads to 6′ with vernier. The top is calibrated in mms. in two directions and is drilled and tapped for an accessory mechanical stage. Stage clips.
- **COMPENSATORS:** two compensators are included; a quarter-wave plate and first order red plate. These fit into a slot above the objective lens.
- **FOCUSING:** coarse and micrometric fine adjustments.
- **STAND:** heavy stand, arm inclines to horizontal position.

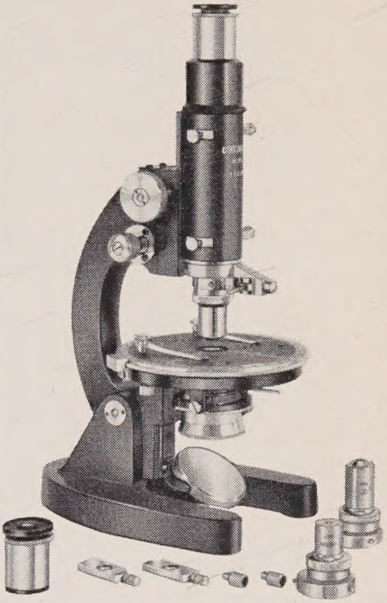

1 Iris diaphragm
2 Polarizer
3 Swing-out lever
4 Focusing lock
5 Focusing slide

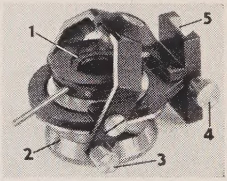

Condenser and Polarizer

THEN: LOOK AT THE PRICE!

Model MPS complete as described, in fitted cabinet . . . . . . $269 FOB BOSTON
Quantity prices on three or more.
Accessory mechanical stage. $14.75

AVAILABLE ON FREE 10 DAY TRIAL

Send for complete catalog on UNITRON Microscopes.

UNITRON
INSTRUMENT DIVISION OF UNITED SCIENTIFIC CO.
204-206 MILK STREET • BOSTON 9, MASSACHUSETTS

Please rush UNITRON Catalog on Microscopes.

Name ____________________
Company ____________________
Address ____________________
City ____________ State ____________

THE TREND IS TO UNITRON

Complete Hydrothermal Apparatus and Supplies :: High Temperature X-ray

". . . one experiment is worth ten thousand expert opinions . . ."

Well! perhaps more than one, but if you want it done at **high temperatures** and/or **high pressures** we can do it for you or help you significantly with the proper research equipment.

TEM-PRES RESEARCH INC.
STATE COLLEGE, PENNSYLVANIA

o 2400°C :: Precise, ultra sensitive (0.001 cal) DTA :: Recording balances with

controlled atmospheres :: Pure synthetic phases :: Co-operative or contract research :: Various services

THE AMERICAN MINERALOGIST

JOURNAL OF THE MINERALOGICAL SOCIETY OF AMERICA

VOL. 45 SEPTEMBER-OCTOBER, 1960 Nos. 9 and 10

X-RAY SPECTROCHEMICAL ANALYSIS: AN APPLICATION TO CERTAIN LIGHT ELEMENTS IN CLAY MINERALS AND VOLCANIC GLASS

MARTIN W. MOLLOY* AND PAUL F. KERR, *Columbia University, New York, New York.*

ABSTRACT

Recent developments in instrumentation have extended the range of *x*-ray spectrochemical analysis (*x*-ray fluorescence) to the lighter elements in the range of atomic number 12 to 22. This includes the significant rock-forming elements aluminum, silicon, potassium and calcium, in addition to phosphorus, sulfur, and titanium. Improved procedure provides a rapid, non-destructive, quantitative, semiquantitative, and qualitative analytical method useful in the examination of aluminosilicate minerals and mineraloids. It is also capable of wider application.

The analytical method has been applied to volcanic and related materials from the Marysvale, Utah, uranium area. The *x*-ray instrument has been calibrated through the use of artificial mixtures of chemical compounds containing the constituent elements. Previously analyzed reference clay minerals of the American Petroleum Institute Research Project 49 have served to establish the calibration. *X*-ray analytical data have been obtained for a selection of specimens from the Mt. Belknap Series which forms part of the Late Tertiary volcanic cover of the Marysvale region. The materials examined include rhyolitic obsidian, volcanic ash, granular igneous rocks and argillitic alteration specimens. *X*-ray spectrochemical analyses of the Mt. Belknap Series show a limited compositional range. This indicates that the tuffs, glasses and rhyolites of this series are derived from a uniform magma.

INTRODUCTION

The objective of this study has been twofold: (1) to explore what appears to be a rapid *x*-ray method for the approximate analysis of the important rock- and ore-forming elements, and (2) to apply a considerable group of approximate analyses obtained by the *x*-ray method to the interpretation of a mineralogic-geologic field problem.

The investigation has concentrated on the extent to which *x*-ray spectrochemical analysis may be utilized for rapid analysis of minerals which contain elements with atomic numbers greater than magnesium ($Z=12$). It involves the application of the *x*-ray spectrochemical method as one phase in the field study of a sequence of Tertiary tuffs and glasses of the Mt. Belknap Volcanic Series near Marysvale, Utah.

---

* Present address: Texaco, Inc., P. O. Box 3247, Ventura, California.

The term x-ray spectrochemical analysis has been used by Parrish (1956*a*) to describe qualitative and quantitative analysis using the emission spectra of elements in the x-ray wavelength region (0.1 to 100 Å). The name emphasizes the similarity of the method to spectrochemical analysis utilizing the emission spectra of elements in the optical wavelength region. "X-ray spectrochemical analysis" is preferable to "x-ray spectroscopy," a somewhat misused term first applied to x-ray powder diffraction using the diffractometer. The terms "x-ray fluorescence spectroscopy," "x-ray emission spectroscopy" or "fluorescent x-ray spectrographic analysis" are also less desirable. All of these seek to express, in the words of von Hevesy (1932), "chemical analysis by x-rays."

The discovery by Barkla (1908–1911) of the "characteristic" nature of x-rays emitted by different elements furnished the basis for x-ray spectrochemical analysis. Although initial successes, such as the discovery of the element hafnium (von Hevesy, 1932) proved the utility of the method, it was not generally accepted as a means of chemical analysis until recently developed electronic devices replaced earlier photographic methods of intensity measurement.

With the introduction of automatic programing in 1956, x-ray spectrochemical instruments have found application on the production line as well as in the laboratory. In the important field of metallurgical alloys (Brissey, Liebhafsky and Pfeiffer, 1953; Whittig, 1959) this development has had special significance. The application of x-ray spectrochemical analysis to mineralogical problems has been somewhat delayed. This has been caused primarily by the relatively recent development of reliable instrumentation, and the limitation of the analysis to elements with atomic numbers greater than 22. The last factor has been the most serious; although 80 of the 102 known elements could be analyzed, those which could not, include the important rock-forming elements C, O, Na, Mg, Al, Si, P, S, Cl, K, Ca and Ti. Within the past two years the range of analysis has been extended to Mg, leaving only C, O and Na as rock-forming elements still beyond reach. It is worthy of mention, however, that Siegbahn, using a vacuum x-ray spectrograph, has analyzed metals as light as Li ($Z=3$).

The basic theory of x-ray spectrochemical analysis has been covered in particular by Compton and Allison (1935), von Hevesy (1932), the Symposium of the American Society for Testing Materials (Friedman, Birks and Brooks, 1954) and in papers by Parrish (1956a). The immediate problem has concerned the modification of the standard x-ray spectrograph to permit the detection of light elements, and the application of the modified instrument to the analysis of materials such as clay minerals and volcanic glass.

INSTRUMENTATION

Complete absorption of Al Kα radiation ($\lambda = 8.3$ Å) occurs in the 34 cm. air path used in the standard Norelco spectrograph. However, enclosure of the system with a flexible rubber bag permits replacement of the air with helium, which in turn allows 85 per cent transmission of the same radiation. Diffraction of such long wavelength radiation may be accomplished by the use of large single crystals of ammonium dihydrogen phosphate (ADP) which are cleaved along the reflecting plane, $2d = 10.6$ Å. ADP crystals diffract Al Kα radiation within goniometer range with greater efficiency than gypsum ($2d = 15.2$ Å) and mica ($2d = 19.9$ Å). The flow proportional counter developed by Hendee, Fine and Brown (1956) provides a one hundred-fold increase in peak to background ratio over the most sensitive Geiger-Müller counter developed for use in the soft x-ray region. The least absorptive window for the flow proportional counter is 0.1 mm. mylar, which transmits 55 per cent Al Kα radiation.

Other items in the standard Norelco spectrograph are the tungsten target x-ray tube and the collimator. The former, normally operated at 35 Kv. and 27 Ma. for the detection of heavier elements, is given the heaviest possible loading without excessive overheating (50 Kv. and 40 Ma.) when working with light elements. A 100 Kv. tube has recently been manufactured, but this requires a more powerful basic unit which has not been available for this study. In the case of the collimation, a four-fold increase in counting rate can be obtained by substituting a bundle of coarse nickel tubes for the closely spaced nickel foil collimator. The corresponding loss in resolution is not critical for the widely spaced reflections in the long wavelength region, but for the closely spaced reflections of elements heavier than titanium, such resolution loss cannot be tolerated. For this reason, the standard collimation was retained, thus avoiding realignment of the instrument upon transfer from light to heavy element determinations.

Operational requirements include helium for the instrument path, methane-argon gas (P10) and a linear amplifier for the flow proportional counter, and electronic pulse discrimination by means of a Pulse Height Analyzer. The linear amplifier preserves the energy to pulse height relationship resolved by the detector while amplifying the pulse by a factor of several thousand. The Pulse Height Analyzer consists of a single channel or window of variable width, which can be set to accept pulses with energy corresponding to that of the radiation being studied while rejecting all others including hard background radiation and detector tube noise.

Modifications of the standard *x*-ray spectrograph for light element detection are summarized in Fig. 1.

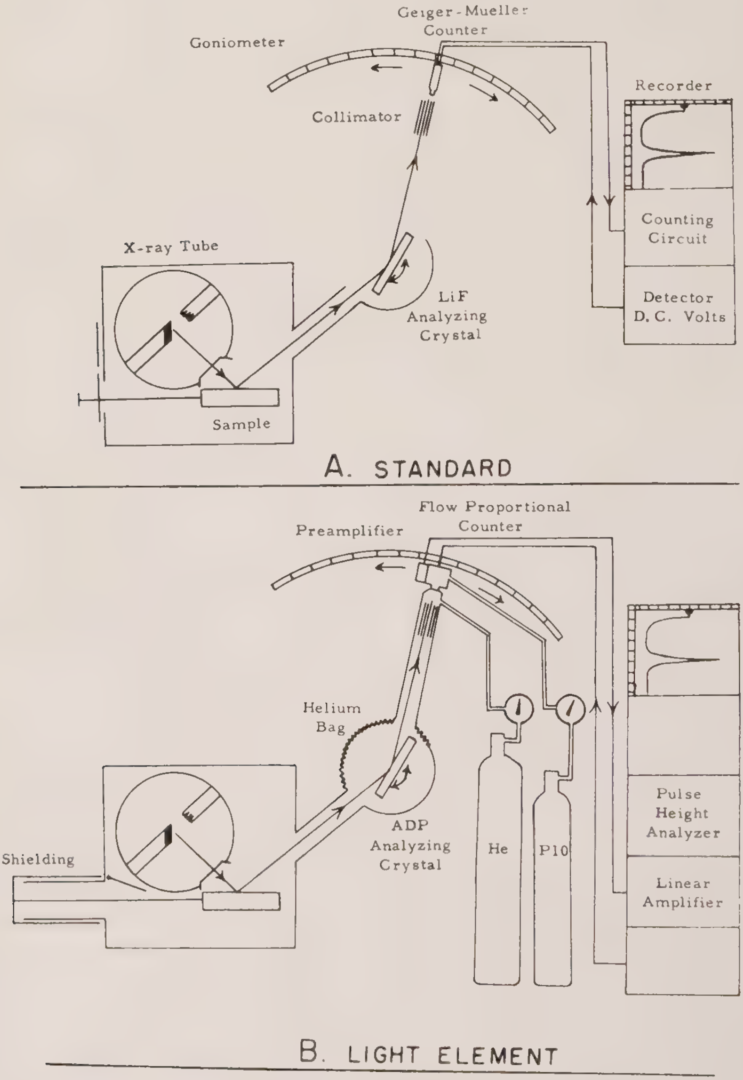

FIG. 1. Schematic diagram of equipment.
A. The standard *x*-ray spectrograph.
B. Modifications of the *x*-ray spectrograph for "light element" ($Z=12$ to 29) detection.

Matrix Effects

If problems caused by the presence of the matrix could be overlooked, x-ray spectrochemical analysis of a sample could be limited to an initial calibration, and a routine scan for detection. However, the associated matrix elements and the physical-chemical form of the specimen affect both qualitative and quantitative measurements. Physical state, particle size, and sample preparation must first be standardized. The major and minor associated elements in the sample are then ascertained to determine the importance of inter-element interferences. These interferences have been summarized (Molloy, 1959) in terms of x-ray emission and absorption interactions of three types: emission absorption, emission enhancement, and competitive absorption.

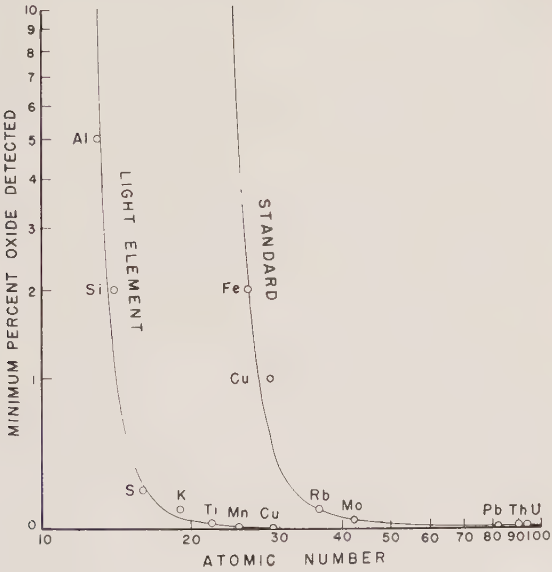

Fig. 2. Estimated limits of minimum detection.

In emission absorption the intensity of a wavelength emitted by one element is decreased by the selective absorption of that wavelength by another element present in the sample. Emission enhancement may be caused either by the overlap of adjacent emission lines, or the absorption of additional energy by one element in the range in which another element is emitting. Competitive absorption may occur with insufficient excitation potential, in which case a decrease in emission intensity may be noted if two or more elements absorb energy in the same range.

The basic limitation in analysis with the *x*-ray spectrograph is the minimum amount of an element that can be detected (Fig. 2). If the element exceeds this minimum, analysis is possible.

The intensity of the secondary radiation emitted by the sample is a direct measurement of the amount of the element present. Quantitative analysis is therefore possible, but, in all except simple systems, this intensity must be corrected for inter-element interferences. Thus the adjustment of intensity measurements to a standard calibration curve becomes the major problem in quantitative *x*-ray spectrochemical analysis.

The accuracy of quantitative analysis is limited, therefore, by the amount of the element present, the atomic number and amount of interfering elements in the sample, the sensitivity of the instrument, and the nature of the detector. At the threshold of light element analysis, only large amounts of Mg and Al can be detected, and with only semi-quantitative accuracy. In the neighborhood of titanium, 0.01 weight per cent oxide may be determined with quantitative accuracy. Titanium is at the threshold of the standard spectrograph, and normally this instrument will not detect less than 1% TiO_2 with the scintillation counter.

MATRIX CORRECTIONS

Hower (1959) and others have pointed out that the matrix corrections for most elements in the trace element analysis of rocks and minerals are satisfied by the correction of the gross *x*-ray absorption coefficient of the sample with reference to a standard. This gross absorption coefficient is essentially dependent on the bulk element composition, and may be expressed in terms of the mass absorption coefficient of the sample calibrated against a standard. Corrections for the major elements are more involved, but may be approximated by the addition of an internal standard which reacts in a manner similar to the element under study. Such theoretical corrections make possible precise, quantitative *x*-ray spectrochemical analysis.

At present, such precise analysis is limited to simple mineral systems, or to restricted applications with well established alloys and chemicals. Bulk analysis of samples with unknown composition is semi-quantitative. However, within a restricted compositional range, certain modifications permit extension of precise, alloy-type analysis to silicate mineral systems.

X-ray spectrochemical analysis of alloys is best accomplished by calibration with previously analyzed standards which are nearly identical in composition to the samples. For each significant change in the proportions of the components, a suitable standard must be prepared. In an instrument such as the Autrometer (Behr, 1956), an automatic *x*-ray comparison spectrometer, the alloy sample and a suitable standard are alternately placed in the detection position as a record is made of element intensities. This immediate comparison of sample and standard forms the basis of quantitative analysis performed with the *x*-ray spectrograph. Absorption and emission interferences are corrected by the analyzed standard which closely approximates the sample in composition and preparation.

The extreme compositional range of rocks and minerals requires strict limitation in the compositional range of a particular study. An approximate quantitative analysis must be confined to a particular mineral or mineral group, or, at most, a small rock suite. In the quantitative analysis of such groups, two factors must be considered: (1) although synthetic mixtures may approach the mineral or rock in composition, the comparative intensities will probably differ because of slightly differing mass absorption coefficients, and (2) an unrecognized interfering element may destroy the accuracy of the analysis.

INSTRUMENT CALIBRATION

Maximum accuracy in quantitative analysis with the *x*-ray spectrograph may be obtained through the application of counting statistics (Parrish, 1956*b*). However, the large number of analyses desired has led to the use of a more rapid method, which may be described as graphic, continuous stripchart recording. Scanned or oscillated peak heights and corrected peak height (minus background) readings may be used for semi-quantitative estimates, but lack sufficient reproducibility for quantitative work.

An integrated peak height method was developed to provide the necessary accuracy. This involves several steps: the goniometer is set for the maximum intensity of the selected peak, the Pulse Height Analyzer is adjusted if required, the proper scale factor and multiplier are selected to retain the peak within the chart range, the maximum time constant (16 sec.) is chosen to permit integration of the signal, and the recorder is allowed to reach the maximum position and continue running for several minutes. The result is a plateau (Fig. 3) which is smooth when a large number of counts are recorded (ThO_2), and irregular when only a few counts are detected (SiO_2). The Scale Factor (S.F.) notations refer to the settings on the electronic circuit panel of the instrument. Because many instrument settings are required, it is advisable to complete the work with each element, determining the calibration curve with standards and analyzing the unknown specimens, before changing the settings to analyze for another element.

Several stages have been employed in the development of calibration curves: (1) the initial calibration utilizing mixtures of simple chemical compounds or elements, (2) calibration with reference clay minerals and previously analyzed clay and volcanic glass specimens, (3) calibration curves corrected to consider absorption or emission interferences. The third calibration is only required where interferences are encountered. Instrument background has not been removed from the data curves.

Figures 4*a* and 4*b* show the chemical calibration curves for silicon and silica in a matrix of aluminum oxide. The linearity of the points in both cases demonstrates that the determination is proportional to the amount of the element present, and that the integrated peak height method compares favorably with the counting statistics technique. For convenience in comparison with mineral and rock analyses the curves are recorded in terms of oxides.

The *x*-ray spectrograph has been calibrated with standard sample

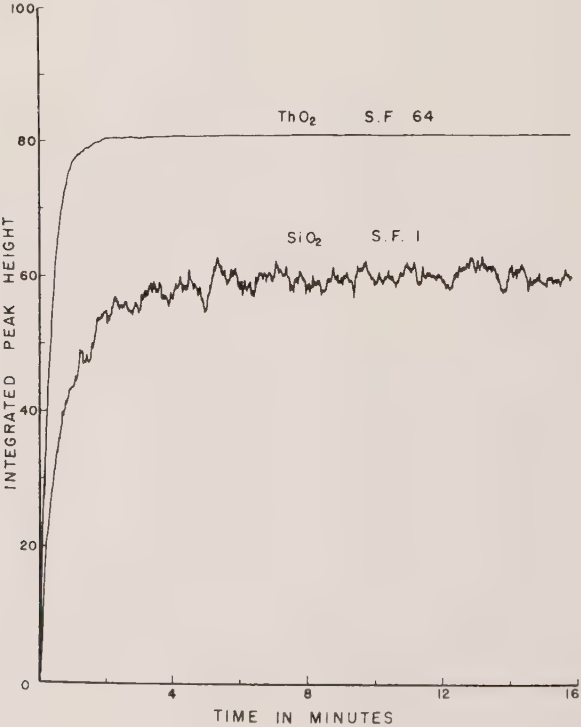

FIG. 3. The integrated peak height method. The upper curve shows the stability obtained with a large number of counts (ThO_2, scale factor 64). The lower curve shows the variation about a mean when only a few counts register (SiO_2, scale factor 1).

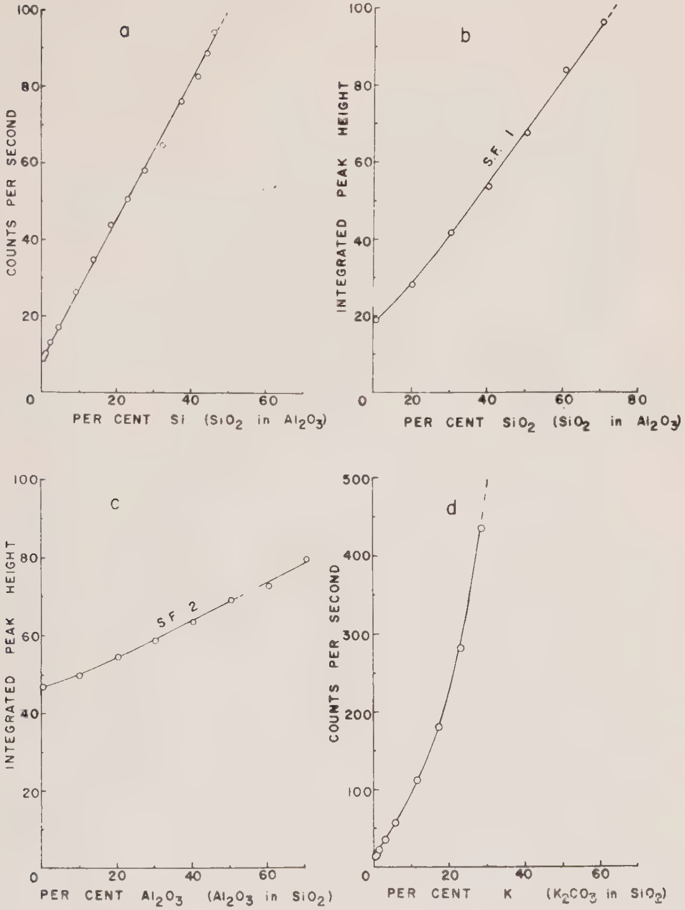

FIG. 4. Chemical calibration curves for mixtures. Weight per cent element or oxide *vs* counts per second or integrated peak height.

a) Silicon, SiO_2 in Al_2O_3.
b) Silica, SiO_2 in Al_2O_3, scale factor 1.
c) Aluminum oxide, Al_2O_3 in SiO_2, scale factor 2.
d) Potassium, K_2CO_3 in SiO_2.

sequences containing Al_2O_3, K_2CO_3, Fe, Cu, ThO_2 and U_3O_8 in weighed amounts disbursed in finely ground silica. For the calibration of silica, the aluminum oxide set was used. The chemical calibration curves obtained from these preparations illustrate the accuracy and sensitivity of the *x*-ray spectrochemical method for the analysis of simple chemical systems.

Figure 4*c* shows the chemical calibration curve for aluminum oxide in silica, derived from a set consisting of eight prepared mixtures. While the agreement between the points and the curve is good, the slope of the curve is too gradual to provide desirable accuracy. Several factors account for this situation. The long wavelength of aluminum radiation is considerably absorbed by helium; the primary *x*-ray beam is inefficient in the aluminum excitation region; and the detector is relatively insensitive to extremely soft radiation. These three factors combine to reduce the number of counts recorded for each per cent of aluminum oxide in the sample. This in turn results in the gradual slope of the calibration curve over the range of interest (0 to 70% Al_2O_3). In such a case the determinations will have a minimum variation of about ±10% of the amount present, which may be attributed to reproducibility and reading factors alone. This is to be expected for determinations at the threshold of detection of the fluorescence technique.

The chemical calibration curve for silica (Fig. 4*b*) shows a more definitive slope which results from the detection of a much larger number of counts for each per cent silica in the sample. Both the sensitivity and accuracy of the determination benefit from the improved detection.

The large number of counts recorded in the determination of potassium in silica (Fig. 4*d*) shows that the analysis of this element, and others which are greater in atomic number, lies well within the range of maximum sensitivity and accuracy of the instrument. In simple systems detection of less than 1% K_2O is routine, with an accuracy approaching ±5% of the amount present.

Determinations of iron oxide (Fig. 5*a*), copper (Fig. 5*b*), thorium oxide (Fig. 5*c*), and uranium oxide (Figs. 5*d* and 6*a*) in silica are similarly uncomplicated. The accuracy and sensitivity of the determinations improve with the increase in atomic number, again in response to the larger number of counts detected. Figures 5*c* and 5*d* demonstrate the limitation on this increase in sensitivity. When too many counts are available, the detector becomes saturated and fails to record all of the impulses. The curve tends toward a plateau at the upper end, precluding the accurate analysis of samples containing large amounts of these oxides. This is overcome by decreasing the primary *x*-ray beam intensity, thus decreasing the secondary emission from the specimen, and the number of counts recorded by the detector. Figure 6*a* is a small portion of the uranium oxide calibration curve (Fig. 5*d*), recorded with a different Scale Factor, showing the straight line characteristic of a calibration curve over a limited concentration range.

The influence of the mass absorption coefficient of an alumino-silicate matrix and the effect of interfering elements upon these chemical calibration curves have been established by additional calibration with the set of original analyzed specimens of seven reference clay minerals from the American Petroleum Institute Research Project 49 collection. These specimens include kaolinite, halloysite, montmorillonite, and illite, and cover the principal range of clay minerals previously established for the Marysvale, Utah uranium area (Kerr *et al.*, 1957, p. 60). Table 1 lists the chemical analyses for these reference clay minerals.

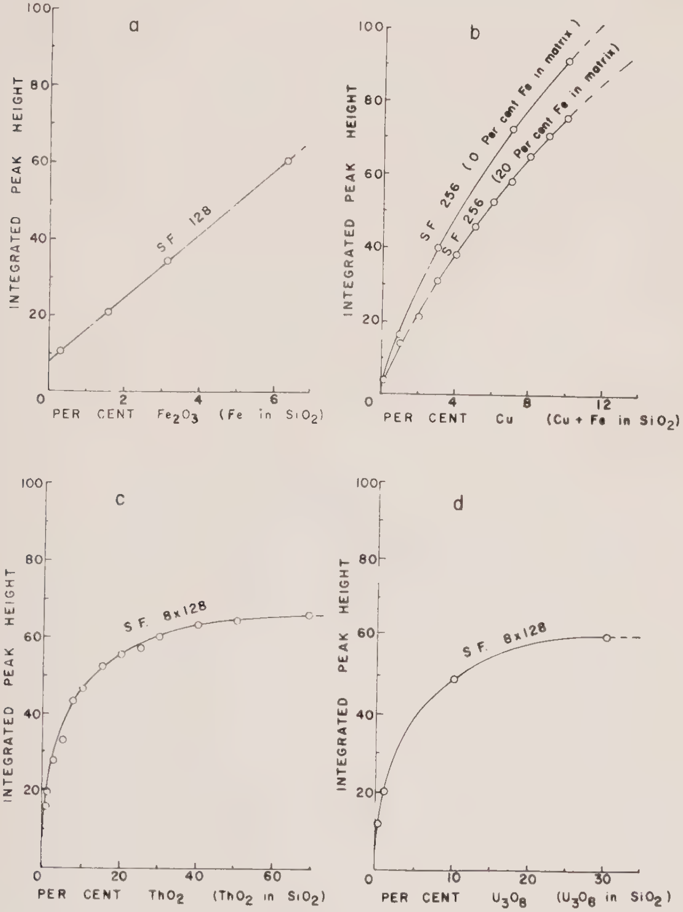

FIG. 5. Chemical calibration curves for mixtures. Weight per cent element or oxide *vs.* integrated peak height.

a) Iron oxide, Fe in SiO_2, scale factor 128.

b) Copper, intensity partly absorbed by iron in matrix, Cu+Fe in SiO_2, scale factor 256.

c) Thorium oxide, saturation of detector is responsible for increasing lack of sensitivity, ThO_2 in SiO_2, scale factor 8×128.

d) Uranium oxide, U_3O_8 in SiO_2, scale factor 8×128.

The curves obtained by plotting the chemical analysis of these standards against the integrated *x*-ray intensity were checked by the *x*-ray spectrochemical analysis of three chemically analyzed specimens of clay and volcanic glass from Marysvale, Utah. These three analyzed specimens were studied in 1953 by Kerr and Hamilton during the previous investigation of vitrophyre ores and alteration in the Central Mining District of the Marysvale Uranium Area. Table 2 shows a comparison of the wet chemical analyses of these Marysvale specimens (by the New Brunswick Laboratory of the U. S. Atomic Energy Commission) and the *x*-ray spectrochemical analyses utilizing the techniques outlined in this study. The agreement between the conventional chemical and *x*-ray spectrochemical analyses was sufficient to encourage proceeding to the analysis of unknown specimens of similar composition, on the basis of the reference clay calibration curves and the analyzed Marysvale specimens.

TABLE 1. CHEMICAL ANALYSES FOR AMERICAN PETROLEUM INSTITUTE REFERENCE CLAY MINERALS*

	Kaolinite		Halloysite	Montmorillonite		Illite	
	API 1a Murfreesboro Ark.	*API 9a* Mesa Alta N. M.	*API 13* Eureka Utah	*API 19* Polkville Miss.	*API 23* Chambers Ariz.	*API 35* Fithian Ill.	*API 36* Morris Ill.
SiO_2	45.47%	46.07%	43.98%	50.95%	49.91%	56.91%	57.41%
Al_2O_3	38.84	38.07	38.46	16.54	17.20	18.50	17.96
Fe_2O_3	.19	.33	—	1.36	2.17	4.99	4.99
FeO	—	—	.03	.26	.26	.26	.26
MgO	.17	.01	Trace	4.65	3.45	2.07	2.25
CaO	.24	.38	.32	2.26	2.31	1.59	.64
Na_2O	.24	.27	.14	.17	.14	.43	.15
K_2O	.42	.43	.48	.47	.28	5.10	5.75
H_2O^+	13.66	13.47	14.59	8.28	7.70	5.98	6.70
H_2O^-	.71	.43	2.58	15.01	15.77	2.86	2.97
TiO_2	.86	.50	.01	.32	.24	.81	.82
MnO_2	—	—		.01	.04		
SO_3		Trace					
C		—		.01	Trace		
LiO_2					—		
Impurities	2.81	3.61	7.1				
Absorbed H_2O	.70	.44	2.56				
Total	100.81	99.96	100.59	100.28	99.47	99.50	99.90

* Kerr *et al.*, 1950, Report No. 7, pp. 43, 45, 49, 52, 53, 57.

TABLE 2. COMPARISON OF WET CHEMICAL AND *X*-RAY SPECTROCHEMICAL ANALYSES OF THREE MARYSVALE, UTAH, STANDARD CLAY AND GLASS SPECIMENS[1]

	Wet Chemical Analysis			*X*-ray Spectrochemical Analysis		
Per cent oxide	Brown glass[2]	Pink clay[3]	Green clay[4]	Brown glass	Pink clay	Green clay
C						
F						
Na	1.88	1.52	.45			
Mg	.32	1.59	3.62			
Al	11.54	14.33	20.24	10.1	15.6	21.9
Si	63.60	56.39	56.02	(65)	(55)	(61)
P						
S	.98	.25	.12	.87	.32	1.20
Cl						
K	3.79	1.09	2.17	3.6	1.5	1.6
Ca	1.76	1.83	.61	1.78	—[5]	.59
Ti	.07	.10	.14	.07	.13	.19
V						
Mn	.05	.02	.02	.04	.03	.02
Fe[6]	5.088	8.061	3.566	(.6)	(3.65)	(1.3)
Cu	.01	.01	.01	.01	.01	.01
Sr						
Mo	.29	.69	.09	.1	.7	.4
Ba						
Pb	.01	.01	.01	.01	.01	.005
U	.42	.02	.02	.02	.02	.02

Semiquantitative data are given in parentheses.

[1] Analyses by New Brunswick Laboratory, U.S. Atomic Energy Commission.

[2] Sample 600-11, brown glass from vitrophyre dike, Bullion Monarch Mine.

[3] Pink clay alteration from same dike.

[4] Greenish clay from same dike.

[5] No determination.

[6] Iron oxides converted to total Fe_2O_3.

On the final calibration curves, the points representing the Marysvale specimens are shown as closed circles.

When the nature of the instrument response to chemical mixtures was considered established by the chemical calibration curves discussed above, preparation of such chemical standards was discontinued. For the final calibration of calcium oxide (Fig. 6*b*), titanium oxide (Fig. 6*c*), and manganese oxide (Fig. 6*d*), the curves obtained from reference clay minerals and checked with the analyzed Marysvale standards were considered sufficient.

For those specimens which had been initially calibrated through the use of standard sets of chemical mixtures, a final calibration was also performed. In these instances, the calibration curves of the chemical mixtures and the reference clay minerals show the same slope for the same element. The displacement that may be noted is caused solely by

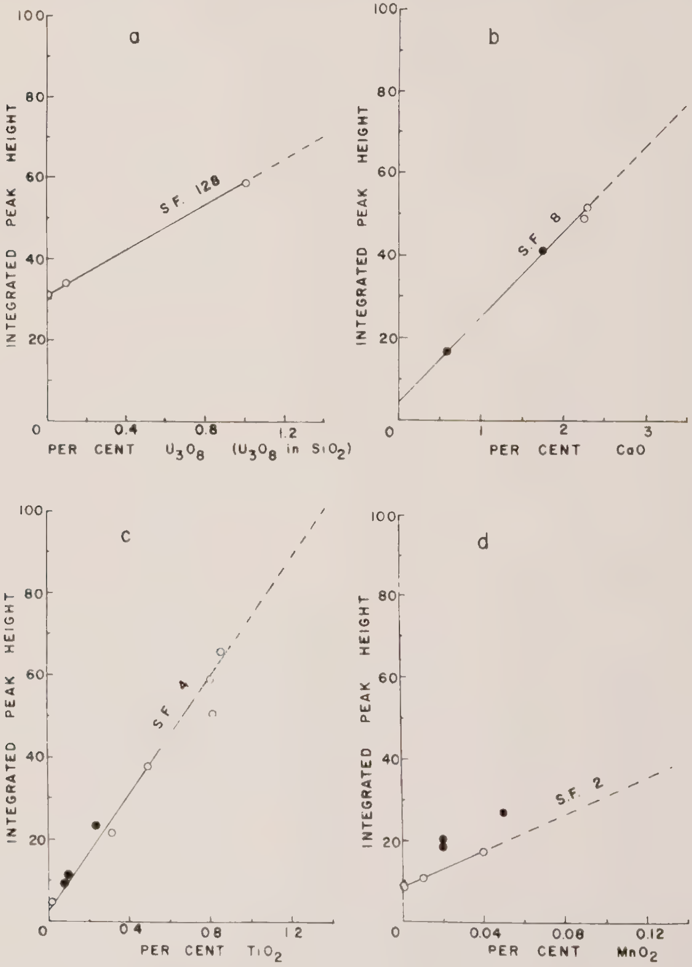

FIG. 6*a*. Chemical calibration curve for a mixture. Weight per cent oxide *vs.* integrated peak height.

a) Uranium oxide, 0 to 1.4 per cent, illustrating the linear character of a short portion of a calibration curve, U_3O_8 in SiO_2, scale factor 128.

6*b*–6*d*. Clay matrix calibration curves. Points represent analyses in Tables 1 and 2.

b) Calcium oxide, scale factor 8.

c) Titalium oxide, scale factor 4.

d) Manganese oxide, scale factor 2.

the difference in mass absorption coefficient between the matrices of the two materials.

Final calibration for aluminum oxide (Fig. 7*a*) met with the same limitations encountered in the initial calibration. At the threshold of detection, the determination of aluminum would be aided by substitution of coarser collimation for the standard nickel foil system. Pulse amplitude discrimination for aluminum radiation would reject most of the increased interference encountered with the coarse collimation, and would result in an appreciably increased signal-to-background ratio. While the selection of chemical standards (Fig. 4*c*) permitted control over the desired range of analyses, the close similarity in aluminum oxide content of the A.P.I. clay specimens (Table 1) and Marysvale standards (Table 2) precluded similar control during the final calibration. Despite the encouraging comparison of the aluminum oxide determinations in Table 2, calibration for aluminum is only slightly better than semiquantitative, in view of the small number of counts recorded and the poor control afforded by the reference clay standards.

Determination of potassium oxide in the range of interest (0 to 7%) was more successful, as the final calibration curve (Fig. 7*b*) shows.

In the case of the calibration of silica and iron oxide, Figs. 7*c* and 7*d* respectively, the presence of interfering elements caused the displacement of points above and below the calibration curves. This is caused by the enhancement and absorption of the initial radiation. The effect of such emission absorption is seen in Fig. 5*b*, in which the addition of iron to a set of copper standards resulted in the downward displacement of the emission intensities, caused by selective absorption of copper radiation by iron.

Such inter-element interferences may be ascertained from Fig. 8, where the absorption edges and emissions arising from elements encountered in this study have been plotted. The overlap of the emission of copper (Cu $K\alpha_1$, 1.540 Å) and the absorption edge of iron (Fe K_{AB}, 1.740 Å) accounts for the downward displacement of emission intensities encountered in Fig. 5*b*.

A similar displacement is seen in the calibration curve for silica (Fig. 7*c*), and is interpreted as the absorption of silicon emission (Si $K\alpha_1$, 7.125 Å) by aluminum (Al K_{AB}, 7.99 Å). The grouping of the points in the silica plot reflects the aluminum content of the specimens. From left to right the points represent: the first group of three –kaolinites and halloysite; the first pair –montmorillonites; second pair –Marysvale dike clays; third pair –illites; and the last point –Marysvale dike glass. Empirical correction of peak intensities for the amount of interfering aluminum in the specimens is afforded by the correction curve seen on

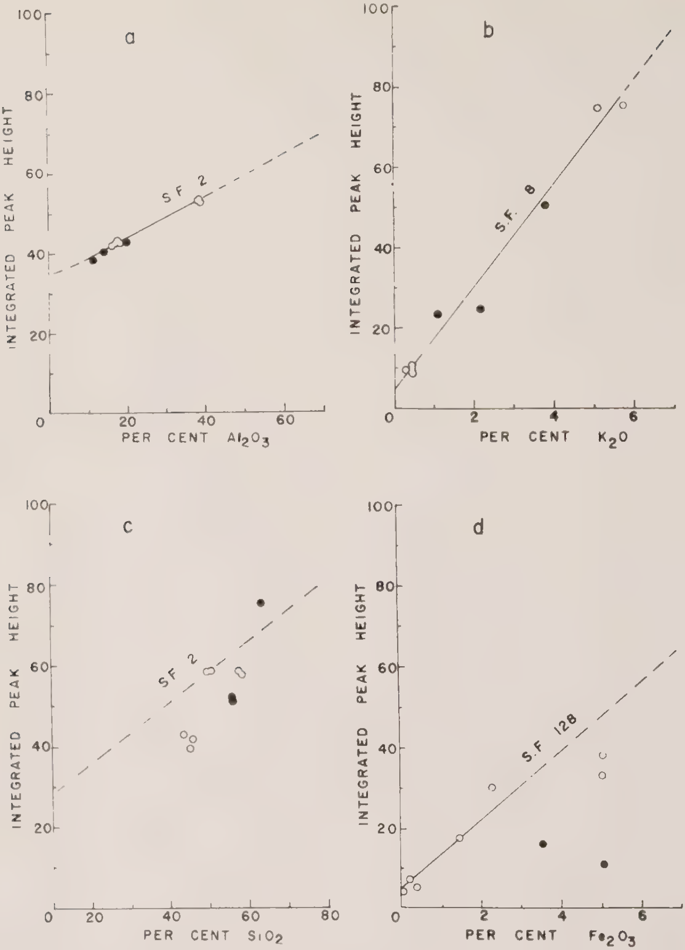

FIG. 7*a*–7*b*. Clay matrix calibration curves. Points represent analyses in Tables 1 and 2.
a) Aluminum oxide, scale factor 2.
b) Potassium oxide, scale factor 8.
7*c*–7*d*. Uncorrected calibration curves. Points represent analyses in Tables 1 and 2.
c) Silica, scale factor 2.
d) Iron oxide, converted to total Fe_2O_3, scale factor 128.

the lower right side of Fig. 9. Application of the correction factor from this plot to the points in Fig. 7*c* results in the corrected per cent SiO_2 final calibration curve of Fig. 9.

A similar grouping of points is not apparent in the calibration curve of iron (Fig. 7*d*). The displacements observed in this plot result from the combined effects of enhancement and absorption. Emission enhancement of Fe radiation by Sr and competitive absorption by Mn are possible, in addition to emission absorption, by traces of V and Cr. In the absence of determinations for Sr, V and Cr from the reference clay minerals, a similar correction could not be established. However, the points from specimens high in Mn are displaced downward, and those high in Ca are displaced upward. The geochemistry of Sr indicates that it is admitted into the structure of Ca minerals in place of the larger radius Ca ion. Strontium would therefore be expected to increase in specimens high in Ca. Indeed, the uncalibrated spectrochemical determinations for Sr in the reference clay minerals show an increase in Sr emission intensity for those specimens high in Ca.

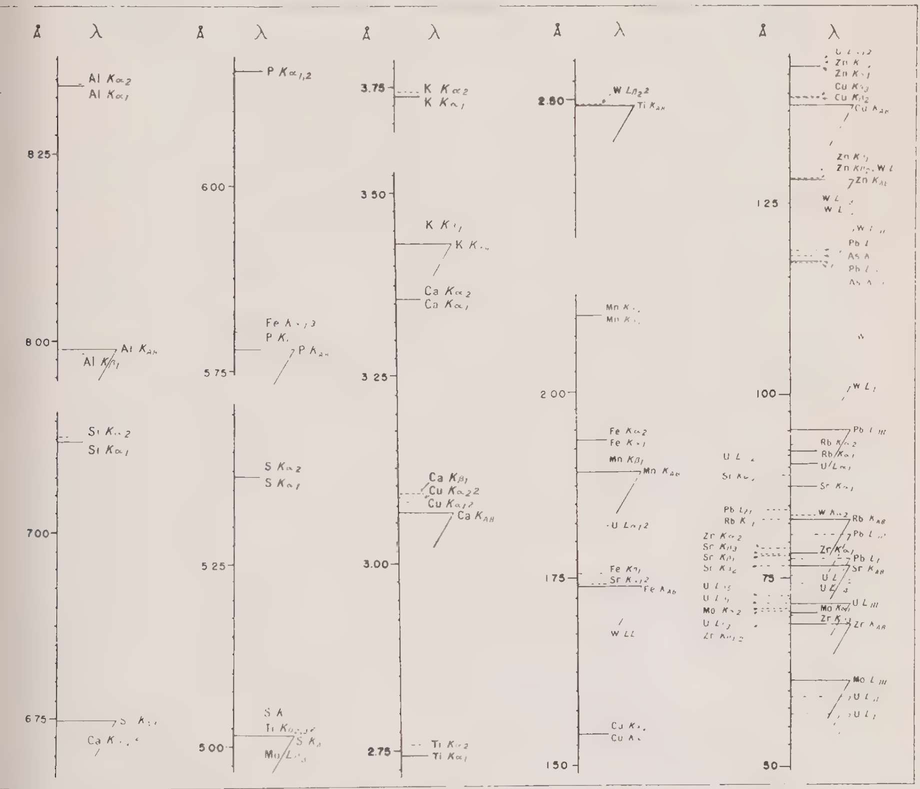

Fig. 8. Plot of inter-element interferences.* The elements chosen are encountered in the x-ray spec-
hemical analysis of clay minerals and volcanic glass. The notation used is the following: Cu $K_{\alpha 1}$
esents the alpha 1 emission of the first order of the K series of copper, while Mo L_{III} represents the
absorption edge of the L series of molybdenum.

* Compiled from Fine and Hendee (1954) and Powers (1957).

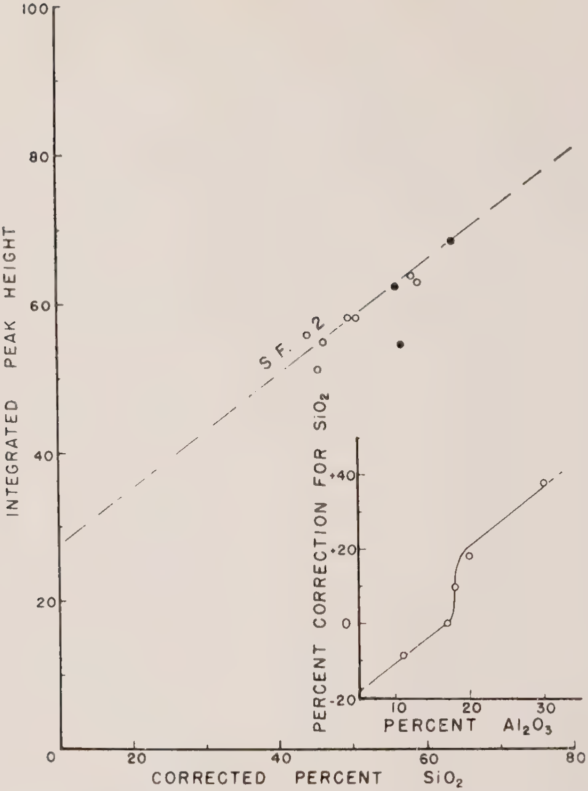

FIG. 9. Clay matrix calibration curve for silica, and correction curve for aluminum interference. Per cent SiO_2 *vs.* integrated peak height, scale factor 2, reference clay minerals. Points represent SiO_2 analyses in Tables 1 and 2, corrected for aluminum absorption.

EVALUATION OF *X*-RAY SPECTROCHEMICAL ANALYSES

Several conventional chemical analyses of clay and glass specimens (Table 2), when compared with *x*-ray spectrochemical analyses, suggest limitations of the *x*-ray method as well as useful applications. Aside from determinations of Na and Mg which lie beyond the present detection range of the *x*-ray spectrograph, some form of analysis was possible for all elements reported.

Determinations for Ca, Ti, Cu and Pb appear reliable, and show a range in minimum sensitivity from 0.01 to 1% in this study. Such determinations would be considered quantitative in accuracy for the purpose of this paper.

S, K, Mo and U analyses showed similar sensitivity to small amounts, but contained a somewhat larger margin of error. These determinations would be considered approximately quantitative in accuracy.

The figures for Al were consistently low by about 10% of the amount present, and those of Mn consistently high by about 50% of the amount present. This indicates a somewhat different mass absorption coefficient for these elements in the Marysvale specimens, in contrast to the reference clay minerals. The calibration curves were therefore corrected by this amount prior to the analysis of the unknown Marysvale samples. These analyses are also considered approximately quantitative. Further study of matrix conditions would probably result in improved analyses for Al and Mn.

Inconsistencies in the analyses of Si and Fe have been discussed. Silicon determinations have been corrected for aluminum absorption, and the figures obtained then lowered by a uniform correction of 10%. The absence of Sr, V, and Cr determinations for the reference clay minerals fails to provide a similar correction for Fe. While the Si analyses are relatively reliable (semi-quantitative in accuracy) those of Fe are unreliable.

X-Ray Spectrochemical Analysis of Specimens from the Mt. Belknap Volcanic Series, Marysvale, Utah

The Marysvale, Utah, uranium area (Kerr, Brophy, Dahl, Green and Woolard, 1957) has been under study at intervals by the mineralogy group in the Department of Geology, Columbia University, since the project was begun in 1951 under the auspices of the Division of Raw Materials of the United States Atomic Energy Commission. Initial interest in the association of uranium mineralization and extensive vulcanism has recently become focused on the relation of the mineralization and alteration to glassy dikes which penetrate the uranium mining area (Kerr *et al.*, 1957, pp. 47–48). These glassy dikes are of Late Tertiary age and form part of the Mt. Belknap Series of tuffs, glasses and rhyolites. A study of the Mt. Belknap volcanics in the Tushar Mountains adjoining the area mapped by Kerr *et al.* was begun in 1958. In connection with this work a considerable suite of specimens has been collected, in order to apply *x*-ray spectrochemical analysis to the interpretation of the volcanic sequence, to study the chemical nature of the rock, and to examine the alteration types.

Several factors have served to facilitate this study. Much data have already been established on the compositional nature of the volcanics as well as the mineralization and the alteration (Kerr *et al.*, 1957). Clay minerals and volcanic glass are known to comprise the bulk of the rock suite collected. Hence the *x*-ray spectrograph has been calibrated for the clay-glass compositional range with a set of clay mineral standards

(Kerr *et al.*, 1950), and analyzed clays and glass from the Marysvale area. Standard preparation procedure of samples and standards minimizes differences of a physical nature. Complete scans were made of each specimen in both the light and normal element range ($Z=12$ to 102) to insure that the effect of inter-element interferences could be considered for each element under analysis. Among the 42 samples studied Al, Si, P, S, K, Ca, Sc, Ti, Mn, Fe, Cu, Zn, Rb, Sr, Zr, Th, and U were found to be significant, and the spectrograph was calibrated for either a quantitative or semi-quantitative determination of each of these elements. The 70 elements which are not reported were either entirely absent, or present in amounts below the minimum sensitivity of the instrument.

Discussion of the analyses of the Marysvale rock suites is limited in the present study to salient points, or to features which are consistent throughout the analyses. A more detailed investigation of minor points which are established by the analyses is planned, and will include a mineralogical study by *x*-ray diffraction, differential thermal, and optical techniques.

Examination of the spectrochemical analyses of the clay specimens (Tables 3A and 3B) shows high Al, Ti, and Fe, occasionally high Ca, low P, and extremely variable Si. These clays were collected from altera-

TABLE 3. CLAY SPECIMENS; MT. BELKNAP VOLCANIC SERIES, MARYSVALE, UTAH

A. Description

M1	Alteration, clay, Beaver Canyon.
M5	Alteration, clay, Phillips 66 tunnel, Beaver Canyon.
M6	Alteration, hematitic clay, Beaver Canyon.
M7	Alteration, clay, Beaver Canyon.
M14	Alteration, hematitic clay, Beaver Canyon.
M15	Alteration, hematitic clay, Beaver Canyon.

*B. X-ray Spectrochemical Analysis**

	Al	Si	K	Ca	Ti	Mn	Fe	Cu	Additional Determinations	Trace
M1	19.8	(66)	5.6	.31	.12	.04	(.7)	.01		P, Rb, Zr
M5	17.9	(62)	5.0	.33	.16	.15	(1.2)	.01		Rb
M6	16.9	(60)	.95	.96	.90	—	(5.7)	.01	1.0 S	Sr
M7	19.3	(37)	4.3	3.2	.76	.08	(6.4)	—		Cr, Rb, Pb
M14	24.2	(58)	5.5	2.8	.82	.02	(5.2)	—		Rb, Sr
M15	22.3	(68)	3.9	.30	.11	.02	(.6)	.01		V, Rb

* In per cent oxide, total iron oxides reported as Fe_2O_3.

TABLE 4. TUFF SPECIMENS; MT. BELKNAP VOLCANIC SERIES, MARYSVALE, UTAH

A. Description

M3	Lithophysae and tuff, Beaver Canyon.
M4	Tuff, slightly radioactive, Nallick claim, Mt. Barrette.
M9	Altered tuff, Beaver Canyon.
M10	Tuff, summit of Gold Mt.
M11	Laminated, weathered tuff, Beaver Canyon.
M13	Columnar welded tuff, Beaver Canyon.
M17	Fragmental tuff, Beaver Canyon.
M19	Joe Lott tuff, upper columnar section, Sam Stowe Canyon.
M20	Joe Lott tuff, dark brown fragmental section, Sam Stowe Canyon.
M31	Fragmental red tuff, south of V.C.A. mine, Marysvale Valley.
M34	Bleached tuff, Beaver Canyon.
M35	Vesicular tuff, Beaver Canyon.
M36	Fragmental tuff, Beaver Canyon.
M41	Red fragmental tuff, Beaver Canyon.

*B. X-ray Spectrochemical Analysis**

	Al	Si	K	Ca	Ti	Mn	Fe	Cu	Additional Determinations	Trace
M3	17.9	(69)	4.9	.30	.17	.08	(1.2)	.01		P, V, Zn, Rb, Zr, Pb
M4	15.1	(68)	5.2	.30	.15	—	(.7)	.01		P, Rb, Zr
M9	20.2	(67)	5.4	.27	.14	—	(.7)	.01		Rb, Zr, Pb
M10	19.2	(72)	4.6	.28	.10	.03	(.2)	.01		Rb
M11	17.8	(70)	6.9	.29	.07	—	(.3)	.01		Rb
M13	13.5	(68)	4.9	.31	.17	—	(.4)	.01		Rb
M17	19.6	(71)	5.1	1.77	.07	.03	(.4)	.01		P, Rb
M19	21.1	(71)	4.3	1.12	.09	.04	(.5)	.01		P, Rb
M20	17.7	(76)	4.5	.71	.08	.03	(.4)	.01		Rb
M31	13.7	(68)	4.4	.68	.09	.07	(.7)	.01		Rb
M34	9.9	(71)	4.7	.27	.14	—	(.6)	.01		P, Rb, Sc
M35	21.0	(69)	4.5	.32	.14	.01	(.8)	.01		Cr, Rb
M36	15.9	(71)	4.7	.28	.01	.02	(.6)	.01		P, Rb
M41	13.1	(68)	4.7	.31	.13	.03	(.9)	.01		Rb, Th

* In per cent oxide, total iron oxides reported as Fe_2O_3.

tion zones, which in the Mt. Belknap Series are localized about fracture systems.

Analyses of the tuff samples (Tables 4A and 4B) are characterized by low Mn, S and Fe, together with consistently high K and a complete absence of Sr. The latter indicates a distinction between the tuffs and local glassy dikes which are high in Sr. Although the glassy dikes and the tuff are closely associated, the spectrochemical data indicate that the dikes were not the source of the major tuff accumulations, which attain a thickness of 3,000 feet in places. Recent field evidence supports this conclusion, indicating that the source of the tuffs was considerably removed from the Marysvale area. In general, the tuff specimens, with their expected homogeneity, are quite similar in spectrochemical analysis, far more so than any other group.

The volcanic glass specimens (Tables 5A and 5B) were among the most interesting examined, both in view of their field occurrence and analyses. The specimens included examples of surficial flow glass and intrusive dike glass, ranging in color from jet black to light brown, and in appearance from obsidian to perlite. Analysis shows frequent traces of strontium and phosphorus, and also distinguishes the dike glasses from the flows. The former (M25 and M29) are lower in K and at the same time higher in Ca, and are thus set apart from the others which are all flow glasses. Field relationships indicate that the glassy flows are

TABLE 5. GLASS SPECIMENS; MT. BELKNAP VOLCANIC SERIES, MARYSVALE, UTAH

A. Description

M22	Gray glass, Deer Creek Canyon.
M23	Gray glass, Teacup Structure (vent), Marysvale Valley.
M24	Black glass, Beaver Hill.
M25	Brown glass from dike, Beaver Canyon.
M26	Gray glass, Beaver Canyon.
M27	Isoclinally folded gray glass, Gray Hills.
M28	Glass from fault zone at mouth of Beaver Creek.
M29	Brown glass from dike, 300 foot level, Prospector mine.
M30	Black glass from Black Knob, Marysvale Valley.

*B. X-ray Spectrochemical Analysis**

	Al	Si	K	Ca	Ti	Mn	Fe	Cu	Additional Determinations	Trace
M22	19.7	(68)	4.3	.62	.09	.05	(.4)	.01		P, Rb, Sr
M23	16.9	(69)	3.5	.97	.20	.03	(1.1)	.01		P, Sr
M24	19.0	(67)	4.7	.37	.13	.06	(.7)	.01		Rb
M25	14.6	(69)	2.1	1.77	.09	.07	(.7)	.01		P, Rb, Sr
M26	19.8	(63)	4.2	1.06	.27	.04	(1.2)	.01		Rb, Sr, Zr
M27	16.0	(68)	4.3	.32	.10	.06	(.8)	.01		P, Rb, Zr
M28	16.5	(75)	4.9	.35	.08	.05	(.6)	.01		P, Rb, Sr, U
M29	17.4	(75)	2.5	1.88	.07	.05	(.5)	.01		V, Rb, Sr, Zr, Pb
M30	14.2	(75)	4.6	.33	.07	.05	(.7)	.01		P, Cr, Rb

* In per cent oxide, total iron oxides reported as Fe_2O_3.

part of the valley sequence of rhyolites and tuffs, associated with local vent structures. The glassy dikes, while also common in the valley area, show a closer relation to both the high mountain tuff sequences and the period of regional mineralization.

As has been pointed out, the rhyolites (Tables 6A and 6B) of the Marysvale area are principally associated with local valley vents. These are the red rhyolites of the lower volcanic sequence, and must be distinguished from the gray rhyolite specimens (M8, M37 and M38) of the upper, high mountain sequence. These gray specimens, as indicated by their characteristic contorted flow-folding, flowed along a regional slope from their original area of deposition in the high mountain region down into the valleys below, building up into a great thickness. A gray flow (M18) from a valley vent structure unrelated to the upper volcanic

TABLE 6. RHYOLITE SPECIMENS; MT. BELKNAP VOLCANIC SERIES, MARYSVALE, UTAH

A. Description

M8	Dense gray flow, Beaver Canyon.
M16	Layered rhyolite from intrusive core, Marysvale Valley.
M18	Gray rhyolite from Teacup Structure (vent), Marysvale Valley.
M21	Red rhyolite, Deer Creek Canyon.
M32	Red rhyolite porphyry, south of V.C.A. mine, Marysvale Valley.
M33	Flow-banded rhyolite, Beaver Canyon.
M37	Flow-banded gray rhyolite, Beaver Canyon.
M38	Gray rhyolite capping, summit of Mt. Belknap.
M40	Red rhyolite, Dome Hill.
M42	Red rhyolite porphyry, Beaver Canyon.

*B. X-ray Spectrochemical Analysis**

	Al	Si	K	Ca	Ti	Mn	Fe	Cu	Additional Determinations	Trace
M8	16.5	(75)	5.4	.26	.10	—	(1.0)	.01		P, Rb, Zr
M16	22.1	(68)	5.6	1.9	.09	.06	(.5)	.01		Rb, Zr
M18	18.0	(63)	3.5	1.02	.90	—	(.2)	.01	6.0 S	Sr
M21	20.1	(72)	3.2	1.18	.09	.06	(.6)	.01		Zn
M32	13.3	(67)	4.7	.36	.11	.04	(.7)	.01		P, Rb
M33	11.3	(63)	6.1	.29	.14	—	(.6)	.01		V, Rb, Cr
M37	16.4	(74)	4.4	.31	.11	.04	(.7)	.01		P, Rb
M38	17.3	(77)	4.6	.32	.12	.01	(.6)	.01		P, Rb
M40	12.6	(63)	4.5	1.37	.09	—	(.6)	.01		Rb
M42	19.6	(73)	5.1	.36	.29	.04	(1.2)	.01		P, Rb

* In per cent oxide, total iron oxides reported as Fe_2O_3.

sequence is distinguished from three other gray rhyolites (M8, M37, and M38) by lower Si and exceptionally high S content. The analyses underline the variability among the rhyolites, which as a group are less homogeneous than any of the others.

Specimens of uranium mineralization, silica and carbonate alteration (Tables 7A and 7B) are sharply distinguished from the normal rock types by spectrochemical analysis. All show a trace of scandium, which, with the exception of a hydrothermally bleached tuff (M34) is found only in specimens associated with mineralization and alteration. Similarly, the uranium ore is unusually high in Fe, Ca, S and U, and low in Al, Si, K, Ti and Rb. M12 represents a zone of silica enrichment surrounding a glassy dike (M25) characterized by 2 to 3 inch lithophysae imbedded in a ground-mass of pink and white perlite and green clay. The lithophysae were almost pure silica, and often showed a central cavity lined with small quartz crystals. Analysis of this material is high in silica, and low in iron, potassium and titanium. Otherwise the composition resembles the tuff specimen (M3) into which this altered material intergrades.

Finally, there is a constant trace of rubidium, copper and titanium in all specimen types.

CONCLUSIONS

The observed sensitivity of *x*-ray spectrochemical analysis in the case of minor amounts of P, S, Sc, Ti, Mn, Cu, Zn, Rb, Sr, Zr, Mo, Pb, Th, and

TABLE 7. OTHER SPECIMENS; MT. BELKNAP VOLCANIC SERIES, MARYSVALE, UTAH

A. Description

M2	Mineralization, uranium ore, Phillips 66 claims, Beaver Canyon.
M12	Alteration, silica nodule from dike, Beaver Canyon.
M39	White alteration, effervescent coating, Beaver Canyon.

*B. X-ray Spectrochemical Analysis**

	Al	Si	K	Ca	Ti	Mn	Fe	Cu	Additional Determinations	Trace
M2	7.8	(5)	.95	9.1+	.02	—	(2.7)	—	.68 S 10.1 U	P, V, Zn, Pb, Sc
M12	15.5	(73)	3.5	.28	.05	.02	(.2)	.01		P, Rb, Sc
M39	6.8	(18)	2.1	21.6+	—	.01	—	—		P, Sr, Sc

* In per cent oxide, total iron oxides reported as Fe_2O_3.

U holds promise for the ultimate quantitative detection of these elements by the *x*-ray spectrographic technique.

Approximate quantitative sensitivity has been developed in complex alumino-silicate systems for K, Ca, Ti, Mn, Cu, Mo, Th, and U in the range from .01 to 10 per cent oxide by weight.

Somewhat larger amounts of Al, Si, and Fe oxides are easily detected, but gross matrix absorption and interelement interferences provide serious problems for precise quantitative analysis. These important elements appear limited at present to semi-quantitative determination, thus restricting conclusions that might otherwise be drawn.

The semi-quantitative analyses for P, S, Sc, V, Cr, Zn, As, Rb, Sr, Zr, and Pb indicate that calibration of the instrument for quantitative determination of these elements should be attempted. For such calibration, a set of previously analyzed standards must be available.

With a capacity for a large number of approximate quantitative determinations, the *x*-ray spectrograph provides a useful supplement for conventional chemical analysis. However, for many determinations where quantitative accuracy is essential, the customary chemical method is preferred. The application of *x*-ray spectrochemical analysis to an increasing number of quantitative determinations shows that further improvement of the method may provide much data now obtained by conventional analyses.

The general uniformity of analyses from the Marysvale specimens emphasizes the homogeneity of the magma which supplied the complex of tuffs, glasses and rhyolites which blanket the region. The analyses also indicate that chemical data may be conveniently assembled with an *x*-ray spectrograph controlled by standards. Several significant relationships are shown by the spectrochemical data: (1) enrichment of Fe, Ti, Al and Ca, and depletion of P in clay alteration zones which follow fracture systems; (2) the chemical distinction between the tuffs and local glassy dikes which might have served as feeder vents; (3) the unusual homogeneity of the tuff specimens; (4) a distinction in K-Ca ratio between flow and dike glasses, indicating that these particular dikes were not feeders for the flow glasses; (5) separation of the red rhyolites of the lower, valley sequence, from the gray rhyolites associated with the tuffs of the upper, high mountain sequence; (6) and finally, the sharp chemical distinction between the carbonate-silica-uranium mineralization and the normal rock types of the Marysvale region.

Acknowledgments

A graduate fellowship from the Union Carbide Ore Company, Division of Union Carbide Corporation, aided in completing this study.

The writers express their appreciation to Prof. T. I. Taylor, Department of Chemistry, and Prof. Brian Mason, Department of Geology, Columbia University, for critically reading the manuscript and offering suggestions. We are grateful to Mr. Frank Nallick, Marysvale, Utah, and Mr. Allen Taylor, Phillips 66 Petroleum Company, for samples of uranium ore from the Mt. Belknap Volcanic Series. Mr. Steve Bender, formerly with the Application Laboratory of North American Philips, Incorporated, Mount Vernon, New York, has been particularly helpful in solving problems which arose with the *x*-ray instrumentation. To our coworkers in the mineralogical section of the Department of Geology, Columbia University, the late Miss Peggy-Kay Hamilton, Dr. William A. Bassett, Messrs. Samuel Kamhi and George Megrue, we express our thanks for many helpful suggestions.

REFERENCES

BEHR, F. A. (1956), The autrometer; an automatic comparison spectrometer: *Norelc Reporter*, **III,** 80–82.

BRISSEY, R. M., LIEBHAFSKY, H. A., & PFEIFFER, H. G. (1953), Examination of metalli materials by *x*-ray emission spectrography: *A.S.T.M. Sp. Tech. Publication*, No. **157**, 43–56.

COMPTON, A. H., & ALLISON, S. K. (1935), *X*-rays in Theory and Experiment: D. van Nostrand Company, Inc., New York, 2nd ed., 828 pp.

FINE, S., & HENDEE, C. F. (1954), A table of *x*-ray K and L emission and critical absorption energies for all the elements: *Philips Tech. Rept.*, **86.**

FRIEDMAN, H., BIRKS, L. S., & BROOKS, E. J. (1954), Basic theory and fundamentals o fluorescent *x*-ray spectrographic analysis: *A.S.T.M. Sp. Tech. Publication*, No. **157**, 3–26.

HENDEE, C. F., FINE, S., & BROWN, W. B., (1956), Gas-Flow proportional counter for soft *x*-ray detection: *Rev. Sci. Instr.*, **27,** No. 7, 531–535.

VON HEVESY, G. (1932), Chemical Analysis by *X*-rays and its Applications: McGraw-Hill Book Company, Inc., New York, 325 pp.

HOWER, J. (1959), Matrix corrections in the *x*-ray spectrographic trace element analysis of rocks and minerals: *Am. Mineral.*, **44,** 19–32.

KERR, P. F., *et al.* (1950), Analytical data on reference clay minerals: Am. Petroleum Inst., Project 49, Prelim. Rept. 7, Columbia Univ., New York.

KERR, P. F., BROPHY, G. P., DAHL, H. M., GREEN, J., & WOOLARD, L. E. (1957), Maryvale, Utah, Uranium Area: *Geol. Soc. Am. Sp. Paper* **64.**

MILLER, D. C. (1957), Some considerations in the use of Pulse Height Analysis with *x*-rays: *Norelco Reporter*, **IV,** 2, 37–40.

MOLLOY, M. (1959), A comparative study of ten monazites: *Am. Mineral.*, **44,** 510–532.

PARRISH, W. (1956*a*), *X*-ray spectrochemical analysis: *Philips Tech. Rev.*, **17,** 269–287.

——— (1956b), *X*-ray intensity measurements with counter tubes: *Philips Tech. Rev.*, **17,** 7–8, 206–221.

POWERS, M. C. (1957), *X*-ray fluorescent spectrometer conversion tables: Philips Electronics, Inc., New York.

WITTIG, W. J. (1959), Production control analyses using the automatic *x*-ray spectrograph: *Norelco Reporter*, **VI,** 1, 17–21.

Manuscript received January 6, 1960.

THE AMERICAN MINERALOGIST, VOL. 45, SEPTEMBER-OCTOBER, 1960

THE CRYSTALLOGRAPHY OF MCGOVERNITE, A COMPLEX ARSENOSILICATE

BERNHARDT J. WUENSCH, *Crystallographic Laboratory,*
Massachusetts Institute of Technology, Cambridge,
Massachusetts.

ABSTRACT

Mcgovernite has been found to have the largest unit cell yet discovered for an inorganic material which is not a stacking polytype. The mineral has probable space group $R\bar{3}2/c$ and unit cell dimensions $a=8.22$ Å, $c=205.5$ Å, as determined from oscillation photographs and confirmed by precession photographs. The primitive rhombohedral cell contains 6 $Mn_9Mg_4Zn_2As_2Si_2O_{17}(OH)_{14}$. The cell dimensions indicate a close relationship to dixenite, another complex arsenosilicate.

INTRODUCTION

Mcgovernite is a complex arsenosilicate occurring in the zinc deposits at Sterling Hill, New Jersey. Well crystallized material occurs in slightly deformed, mica-like "books" and in coarse granular masses. The mineral is brittle with a very perfect micaceous cleavage. Nearly perfect crystals have a deep red-brown, somewhat bronzy color, while masses have a pearly appearance and a light brown color. The specimens examined were uniaxial positive with a barely detectable birefringence, and had $n_o=1.761\pm.002$.

The mineral was first reported by Palache and Bauer (1927) who were not able to determine a simple and satisfactory formula. The simplest empirical expression representing the results of their analysis was

$$21(Mn, Mg, Zn)O\cdot 3SiO_2\cdot \tfrac{1}{2}As_2O_3\cdot As_2O_5\cdot 10H_2O.$$

This formula and the physical properties of the material indicated that it might be related to dixenite, $21(Mn, Ca, Fe)O\cdot 4SiO_2\cdot 4As_2O_3\cdot 5H_2O$ (Flink, 1920), and also more remotely related to the friedelite-schallerite group (Bauer and Berman, 1928).

PREPARATION OF CRYSTALS

Cleavage plates taken from well crystallized specimens appeared to be single crystals and, because of the brittle nature of the flakes, were easily broken into fragments of size suitable for *x*-ray analysis. Diffraction patterns subsequently showed, however, that these plates were not single crystals. Upon examination with an optical goniometer, it was observed that each cleavage surface gave rise to a series of reflections originating from different layers within the volume of the crystal, indicating that the cause of this trouble was partial cleavages in the plate induced by the breaking, rather than twinning or plastic deformation. In some cases, interference fringes were visible along the partially cleaved surfaces.

After considerable difficulty, single-crystal fragments were obtained from extremely thin cleavage plates which could be broken to appropriate size with application of only very slight pressure.

X-RAY EXAMINATION

Since the basal cleavage plane was the only morphological feature of aid in orienting the crystals, a c-axis rotation photograph was first obtained. This pattern indicated a (001) spacing which was so enormous that it would prove impossible to resolve the various l levels with the layer-line screens required in any moving-film method. The unit cell and space group were consequently determined with the oscillation method. Although this technique is not as powerful as the moving-film methods (Buerger, 1942*a*), it was nevertheless possible to unambiguously index all reflections and to determine the unit cell and space group of the crystal.

Five 20° oscillation photographs were obtained at 20° intervals to determine the symmetry along the c axis. MoKα radiation was used in order to obtain a large number of values of h and k. These photographs indicated diffraction symmetry $\bar{3}m$ and exhibited rhombohedral and c-glide space-group extinctions. Different photographs are obtained when the oscillation range is centered about each of two neighboring symmetry planes in a rhombohedral lattice. By comparing the observed l values with those predicted for each of these cases, it was possible to identify the oscillation range. This permitted indexing of all reflections on the films exhibiting the plane of symmetry of the Laue group. Within certain narrow limits, this indexing fixed the orientation of the crystal about c with respect to the x-ray beam, so that the remaining films in the set of oscillation photographs could be indexed.

An approximate value of a was graphically determined in the normal fashion (Buerger, 1942*b*) from ξ values measured with the aid of a Bernal chart; c was computed from measurements made on a c-axis rotation photograph which was taken with FeKα radiation to increase the separation of the closely spaced l levels. The unit-cell dimensions, as improved from measurements on precession photographs, were:

Referred to hexagonal axes	*Referred to rhombohedral axes*
$a = 8.22 \pm 0.02$ Å	$a = 68.7 \pm 0.3$ Å
$c = 205.5 \pm 1$	$\alpha = 6°52'$

Space group $R3c$ or $R\bar{3}2/c$

The two possibilities for the space group differ only by a center of symmetry and therefore cannot be distinguished by x-ray measurements. A test for piezoelectricity was made with an apparatus similar to that described by Stokes (1947) and yielded negative results. This test does not entirely eliminate the acentric possibility, but does lend support to $R\bar{3}2/c$ as the most probable space group.

Within the limits imposed by the extreme size of the cell, it was desired to obtain a direct record of the reciprocal lattice. Reflections recorded in this fashion are more readily examined for possibilities of twinning and evidences of substructures. Figure 1 gives a *c*-axis MoKα precession photograph adjusted for zero-level geometry. The hexagonal nature of the lattice is clear in this photograph, but, since the separation of neighboring levels is very small, the upper levels could not be eliminated by the layer-line screen. These levels were also recorded along with the zero level. This record is therefore a projection of a small slice of the reciprocal lattice onto the zero level and thus has a falsely high symmetry. The various levels were also not resolved on *c* cone-axis photographs, but appeared as nearly continuous smears of coherent radiation.

Figure 2 shows a zero-level MoKα precession photograph taken about [11·0]. The reflections on this photograph have indices of the form $h\bar{h}\cdot l$; the space group allows such reflections to be present only if l is even. It is interesting to note that reflections up to $l=246$ are observable on this film. Figure 3 shows an upper-level precession photograph taken about [11·0] giving general reflections having extinctions due only to the rhombohedral lattice.

TWINNING AND POLYTYPISM

Large cells are suspect since they may have been determined from twinned crystals of material having a smaller cell (Buerger, 1954). No "strange" extinctions were observed in the present study, however. No twinning model based on a smaller cell could be devised to give the observed patterns.

For materials exhibiting a basal cleavage, cells with large spacings are also good candidates for stacking polytypes. Although there is no evidence for a substructure in the photographs of Figs. 2 and 3, several samples from all specimens of mcgovernite available from the Harvard collection* were examined for polytypism. Cleavage flakes, usually imperfect, were optically aligned with their *c* axes parallel to the spindle of a precession apparatus, and a precession photograph of each was taken about a random direction in the (00·1) plane. By this procedure only $00\cdot l$ reflections were recorded, but these were a sufficient check on the length of *c*. This method eliminated the time-consuming necessity of orienting the flakes and a search for highly perfect cleavage flakes.

Although the specimens differed widely in physical appearance and

---

* Harvard Catalog Numbers 90380, 104668, 104674, 105531 (used for the unit cell and space group determination), 105532, 105533 and 105534.

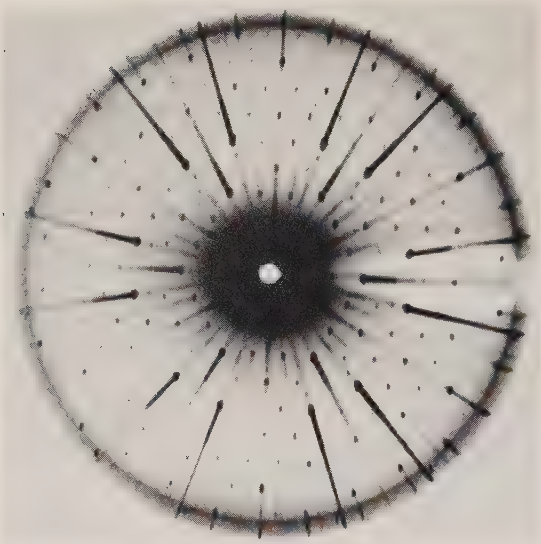

FIG. 1. Precession photograph of mcgovernite, c-axis, with settings for zero-level geometry. MoKα, 35 kv, 15 ma, 68 hours, $\bar{\mu}=25°$. It was not possible to eliminate all neighboring levels with the layer-line screen. The record is therefore essentially a thin slice of the reciprocal lattice projected parallel to c^*.

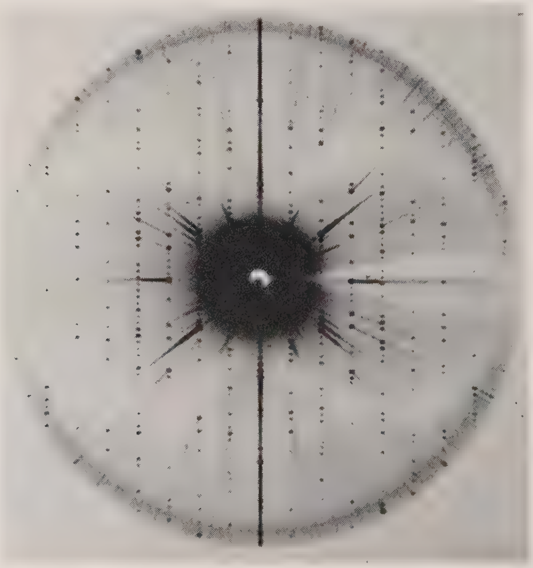

FIG. 2. Precession photograph of mcgovernite, [11.0] axis, zero level. MoKα, 35 kv, 15 ma, 59 hours, $\bar{\mu}=25°$. Reflections are all of special type $h\bar{h}\cdot l$ and exhibit both rhombohedral and c-glide extinctions.

grain size, no polytypes or further evidences for twinning were discovered.

CHEMICAL FORMULA

Because of the large variety of atomic species present, including the unusual occurrence of arsenic in two oxidation states, Palache and Bauer could assign no satisfactory formula to the mineral. Knowledge of the unit-cell dimensions now permits computation of the numbers of each type of atom in the unit cell, but because of the large cell volume the numbers tend to be large and subject to considerable uncertainty. The determination of a formula is therefore still somewhat arbitrary.

The triple hexagonal unit cell has a volume of 12,000 Å^3, which, when combined with an experimental density of 3.719 gr./cm.^{3}, results in a molecular weight per cell of 26,900. In Table 1 this is divided among the various atoms on the basis of Palache and Bauer's analysis. This leads to an empirical content for the primitive rhombohedral cell of

$$\mathrm{Mn_{54.1}Mg_{25.1}Zn_{11.3}Fe_{1.9}\overset{+3}{As}_{4.0}\overset{+5}{As}_{9.7}Si_{13.3}O_{191.5}H_{84.6}}$$

Space group $R\bar{3}2/c$, when referred to rhombohedral axes, has 12-, 6-, and 4-fold equipoints with at least one variable parameter, one symmetry-fixed 6-fold, and two symmetry-fixed 2-fold equipoints. Space group $R3c$ has only 6-fold and 2-fold equipoints with variable parameters. After possibilities for substitution have been taken into account, the number of atoms contained in the cell must correspond to multiples of the multi-

TABLE 1. CHEMICAL COMPOSITION OF MCGOVERNITE

Component	Mol. wt.	Weight fraction (after Palache and Bauer, 1927)	$\frac{\text{Wt. fract.}}{\text{mol. wt.}}$	Molecules per hexagonal cell. $\left(\text{Equals } \frac{\text{wt. fract.}}{\text{mol. wt.}} \times \text{mol. wt./cell}\right)$	Metal	Oxygen
SiO_2	60.09	.00892	$14.8(10)^{-4}$	39.9	39.9	79.8
MnO	70.94	.4272	60.2	162.2	162.2	162.2
FeO	71.85	.0153	2.1	5.7	5.7	5.7
MgO	40.32	.1127	28.0	75.4	75.4	75.4
ZnO	81.38	.1022	12.6	34.0	34.0	34.0
As_2O_3	197.82	.0445	2.2	5.9	11.9	17.8
As_2O_5	229.82	.1248	5.4	14.6	29.1	72.8
H_2O	18.016	.0849	47.1	126.9	253.8	126.9
		$\sum = 1.0008$				$\sum = 574.6$

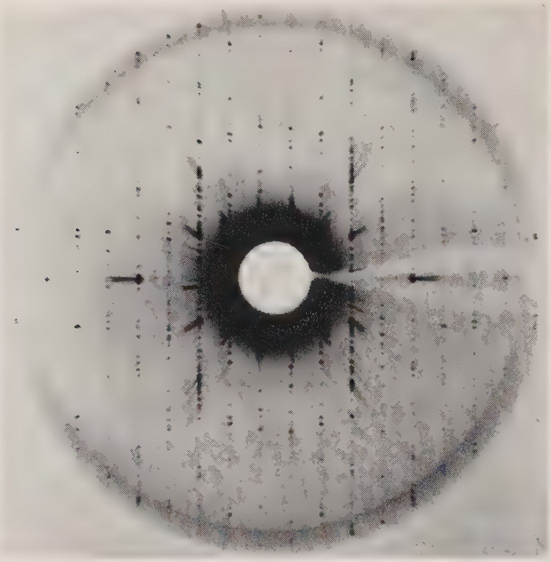

FIG. 3. Precession photograph of mcgovernite, [11·0] axis, first level. MoKα, 35 kv, 15 ma, 64 hours, $\bar{\mu}=20°$. Reflections are general and exhibit only extinctions due to the rhombohedral lattice.

plicities of the available equipoints. Although the correct space group is not definitely established, the number of atoms must still be multiples only of 6 and 2.

No further analyses of mcgovernite are available, so it is not known to what extent there is substitution present among the metal atoms. It may be noted, however, that, with the exception of the small amount of iron, all metals are present in near-multiples of 6. Hydrogen is arbitrarily assigned to hydroxyl radicals. Hey (1956) has shown that, in the chemically similar friedelite family, As does not substitute for Si and that As radicals do not substitute for OH. Accordingly, it is assumed that the As present is not in substitution with another species. With these assumptions, the rhombohedral cell contents may be written as

$$6\,Mn_{9.0}Mg_{4.2}(Zn, Fe)_{2.2}\overset{+3}{As_{x}}\overset{+5}{As}_{2.3-x}Si_{2.2}O_{17.8}(OH)_{14.1}$$

with $x=.66$. This suggests as an ideal formula for the As^{+5} end member of the series:

$$Mn_9Mg_4Zn_2\overset{+5}{As_2}Si_2O_{17}(OH)_{14}$$

More analyses are necessary before the exact nature of the substitutions and formula are established.

Relation to Dixenite

The unit cell dimensions determined for mcgovernite show a remarkable relation to those reported by Wickman (1950) for dixenite.†

Dixenite (*Långban, Sweden*)	8.22 Å	37.44 = 2×18.72 Å
Mcgovernite (*Sterling Hill, New Jersey*)	8.22	205.5 = 11×18.68

The empirical rhombohedral unit-cell contents for dixenite, scaled by a factor of 11/2 to permit direct comparison with those of mcgovernite, are as follows:

Dixenite (×11/2):

$$\overset{+2}{Mn}_{69.6}Mg_{1.3}\overset{+2}{Cu}_{4.3}\overset{+2}{Fe}_{6.4}Ca_{.5} \qquad \overset{+3}{As}_{31.1}P_{.1}Si_{14.5}O_{176.8}H_{37.7}$$

$$\overset{+3}{Mn}_{10.7}\overset{+2}{Mn}_{63.9}Mg_{.8}\,\overset{+2}{Cu}_{4.6}\overset{+3}{Fe}_{5.0}Ca_{.7}Na_{.4}K_{.6} \qquad \overset{+3}{As}_{34.1} \quad Si_{9.3}\,O_{179.9}H_{32.6}$$

Mcgovernite:

$$\overset{+2}{Mn}_{54.1}Mg_{25.1}Zn_{11.3}\overset{+2}{Fe}_{1.9} \qquad \overset{+3}{As}_{1.0}\overset{+5}{As}_{9.7}Si_{13.3}O_{191.5}H_{84.6}$$

The cell contents for dixenite are based on analyses given by Mauzelius (Wickman, 1950) and Johansson (Wickman, 1951), respectively. The latter analysis is the more reliable and, furthermore, was determined from the material used for the measurement of the lattice constants given above.

In order to deduce an ideal formula for dixenite, it was necessary for Wickman to assume different valence states for some of the metal atoms. The two results for dixenite may then be expressed:

$$(Mn^{+2}, Fe^{+2}, Cu^{+1})_{15}As_5^{+3}(Si, As^{+5})_3O_{25}(OH)_7$$

$$(Mn^{+2}, Fe^{+2}, Cu^{+2}, As^{+3})_{20}(Si, As^{+5})_3O_{26}(OH)_6,$$

respectively. Mcgovernite may be written:

$$(Mn^{+2}, Mg, Zn)_{15}As_2^{+5}Si_2O_{17}(OH)_{14}.$$

It may be seen that there is a strong similarity between the unit cell contents of the two minerals, although the numbers of atoms contained in the cells are not quite in the same ratio as the lengths of their *c* axes. Assumptions slightly different from those made in this paper had to be made by Wickman in deducing the ideal formulae for dixenite. Since the space group of dixenite has not been reported, and in view of the fact that only three chemical analyses exist for two minerals of such variable composition, there is as yet no real basis for establishing the true relation between the formulae.

---

† The cell dimensions for dixenite, reported in kX units, have been converted to A.

DISCUSSION

Referred to hexagonal axes, mcgovernite has the largest cell edge yet discovered as a basic translation in an inorganic material. It is true that a few larger cells have been reported, but only as members of a set of polytypes of certain crystals. In such instances the large period is due to a curious compounding of a simpler period and is not a fundamental characteristic of the structure. For example, Honjo *et al.* (1950) have discovered a SiC modification, type 594*R*, with *c* approximately equal to 1500 Å.

The formula determined above suggests that, in spite of its perfect basal cleavage, mcgovernite is not a phyllosilicate. The lack of evidence in the diffraction patterns for a substructure equal to a submultiple of *c*, the brittle nature of the cleavage flakes, the negligible birefringence (indicating the absence of more loosely bound electrons perpendicular to the sheets), and the absence of polytypes despite the large cell size, all confirm the unlikelihood of a mica-like sheet structure.

Despite the difficulties encountered when a unit cell contains a larg number of atoms, some progress has been made in a crystal-structur analysis of the two minerals.

ACKNOWLEDGMENTS

The writer gratefully acknowledges the kindness of Professor Cliffor Frondel in supplying the specimen of mcgovernite used in this study and in permitting access to the remaining specimens in the Harvard collection. The writer is also indebted to Professor Martin J. Buerger for many discussions and much encouragement in view of the incredulity with which one usually regards a large unit cell. Thanks are also due Professo Adolf Pabst for calling the writer's attention to the interesting relations between the unit cells of mcgovernite and dixenite.

This work, in part, was made possible under a grant by the National Science Foundation.

REFERENCES

BAUER, L. H. AND BERMAN, HARRY (1928), Friedelite, schallerite and related minerals *Am. Mineral.* **13,** 341–348.

BUERGER, M. J. (1942*a*), *X*-ray Crystallography. John Wiley and Sons, New York p. 162–165, 214.

BUERGER, M. J. (1942*b*), op. cit., p. 160.

BUERGER, M. J. (1954), The diffraction symmetries of twins. *Anais. Acad. Brazil. Cienc.* **26,** 111–121.

FLINK, G. (1920), Trigonit och dixenit. *Geol. Fören. Förhandl.*, **42,** 436–452.

HEY, MAX H. (1956), The empirical unit cell contents of the friedelite family. *Am. Mineral.* **41,** 134–138.

Honjo, Goro; Miyake, Shizuo; and Tomita, Takanori (1950), Silicon carbide of 594 layers. *Acta Cryst.*, **3,** 396–397.

Palache, C. and Bauer, L. H. (1927), Mcgovernite, a new mineral from Sterling Hill, New Jersey. *Am. Mineral.*, **12,** 373–374.

Stokes, Ralph G. (1947), An improved apparatus for detecting piezoelectricity. *Am. Mineral.*, **32,** 670–677.

Wickman, Frans E. (1950), From the notes of the late K. Johansson. IV. Dixenite. *Geol. Fören. Förhandl.*, **72,** 64–65.

Wickman, Frans E. (1951), From the notes of the late K. Johansson. VII. A revised chemical analysis of dixenite from Långban. *Geol. Fören. Förhandl.*, **73,** 637–638.

Manuscript received January 18, 1960.

THE AMERICAN MINERALOGIST, VOL. 45, SEPTEMBER-OCTOBER, 1960

THERMAL TRANSFORMATIONS AND PROPERTIES OF CRYPTOMELANE

G. M. Faulring, W. K. Zwicker, and W. D. Forgeng,
*Metals Research Laboratories, Union Carbide Metals
Company, Division of Union Carbide Corporation,
Niagara Falls, New York.*

Abstract

An unusual occurrence of needles of cryptomelane in cavities in a manganese ore from western Australia is described. X-ray diffraction data for the acicular crystals are indexed in terms of a body-centered tetragonal unit cell although optical examination of the crystals indicates a pseudotetragonal cell. The powder data are more detailed than those previously reported for cryptomelane. Fiber patterns obtained from the crystals, heat-treated in air at various temperatures and times, establish the following thermal transformations and relative orientations parallel to the [001] axis of cryptomelane.

$$\underset{\text{cryptomelane}}{[001]} \xrightarrow{\Delta} \underset{\text{bixbyite}}{\overset{[110]}{[100]}} \xrightarrow{\Delta} \underset{\text{hausmannite}}{[100]} \xrightarrow{\Delta} \underset{\text{spinel}}{[110]}$$

A transformation product of cryptomelane indexed in terms of a spinel structure, $a_0 = 8.42$ Å, is reported.

A correlation of thermogravimetric data with phase determinations shows that on continuous heating at 6° C. per minute, fibered cryptomelane does not transform completely to bixbyite before the formation of hausmannite begins. At this heating rate, the critical temperature for formation of bixbyite from the acicular crystals of cryptomelane is approximately 600° C., for the hausmannite approximately 825° C., and for the spinel approximately 1050° C.

In 1932, Ramsdell (1) showed that the hard, compact manganese oxide, usually known as psilomelane, was actually any one of several distinct minerals, the most common of which he termed "true psilomelane." This mineral was characterized by a distinctive *x*-ray diffraction pattern, the presence of potassium and the virtual absence of barium. In 1942, Richmond and Fleischer (2) determined the chemical composition and physical properties of several specimens of the mineral and gave *x*-ray data which were in close agreement with those given in a second report by Ramsdell (3). They proposed that the term "true psilomelane" be discontinued in favor of a new name "cryptomelane." Although they considered cryptomelane to be isostructural with the manganese minerals hollandite and coronadite, they were unable to determine its space group.

The present authors' interest in cryptomelane arises from studies designed to establish the properties and geochemistry of the different structural types of manganese oxides. During the course of this investigation a manganese ore sample was received from western Australia, which consisted of a dense, dark-gray matrix containing a few small cavities partly filled with aggregates of acicular crystals, hereafter designated "needles." The needles were shiny and black in reflected light, and frequently oriented toward the centers of the cavities (Fig. 1).

A few of the needles were gently crushed for petrographic examination. Upon crushing, the needles split into fine fibers as shown in Fig. 2. The fragments were dark brown, and nearly opaque except when very thin. They were weakly anisotropic with parallel or nearly parallel extinction. Since the sign of elongation changed as the thin fibers were rotated, it appears that they are biaxial rather than uniaxial in nature.

CHEMICAL ANALYSIS

The limited supply of cryptomelane needles (ca 150 mg.) necessitated the use of micro-analytical techniques and restricted the number of determinations that could be made. The chemical analyses of the needles and the matrix material are compared to those reported by Richmond and Fleischer (2) for various specimens of cryptomelane in Table 1. The relatively large amount of Fe_2O_3 and SiO_2 in the matrix material is due to the presence of hematite and quartz. The calculated chemical formulae in Table 1 are based on similarities of atomic radii and possible substitutions. "*A*" represents large ions (chiefly K^+ with substitution by Ba^{++} and Na^+), and "*R*" represents small ions (chiefly Mn^{+4}, with substitu-

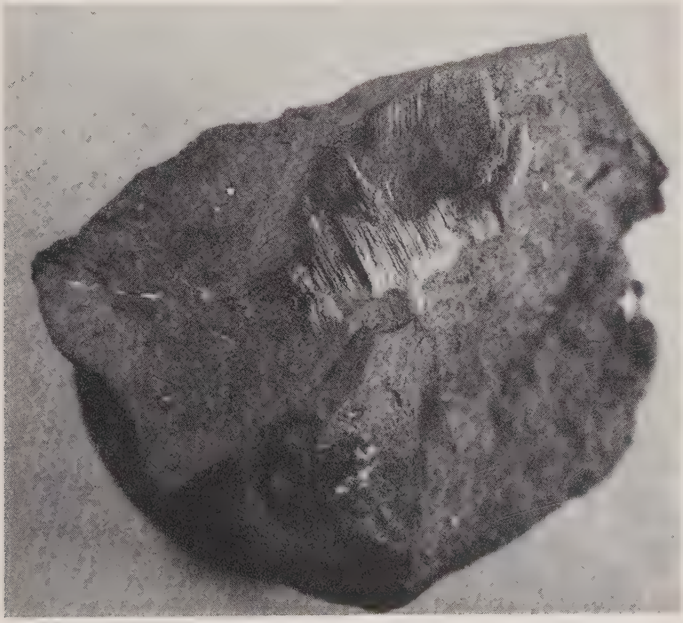

FIG. 1. Needles of cryptomelane in cavity. 5×.

tion of Mn^{+2}, Zn^{+2}, Al^{+3}, Cu^{+2}, Co^{+2}, and Fe^{+3} to maintain electrostatic balance). A chemical formula was not calculated for the matrix material, because of the relatively large amount of Fe_2O_3. Gruner (4) reports the chemical formula, $Mn^4{}_{7.4}(Mn^2,R^2)_{0.81}(K,Na)_{0.7}(Ba_{0.0216}\cdot(H_2O))_{1.31}$, and considered that H_2O molecules could also occupy the position of the "*A*" ions. Bystrom and Bystrom (5) gave the general chemical formula, $A_{(2-y)}B_{(8-z)}X_{16}$,* and suggested that a portion of these "*A*" positions may be vacancies. Mathieson and Wadsley (6) contend that sodium cannot replace potassium in the cryptomelane structure, but the present investigators consider sodium and potassium are somewhat interchangeable in this structure.

The compositions of the various specimens in Table 1 are similar in many respects. The presence of potassium, the absence of a significant amount of barium, and the fact that lead was not detected, establish that

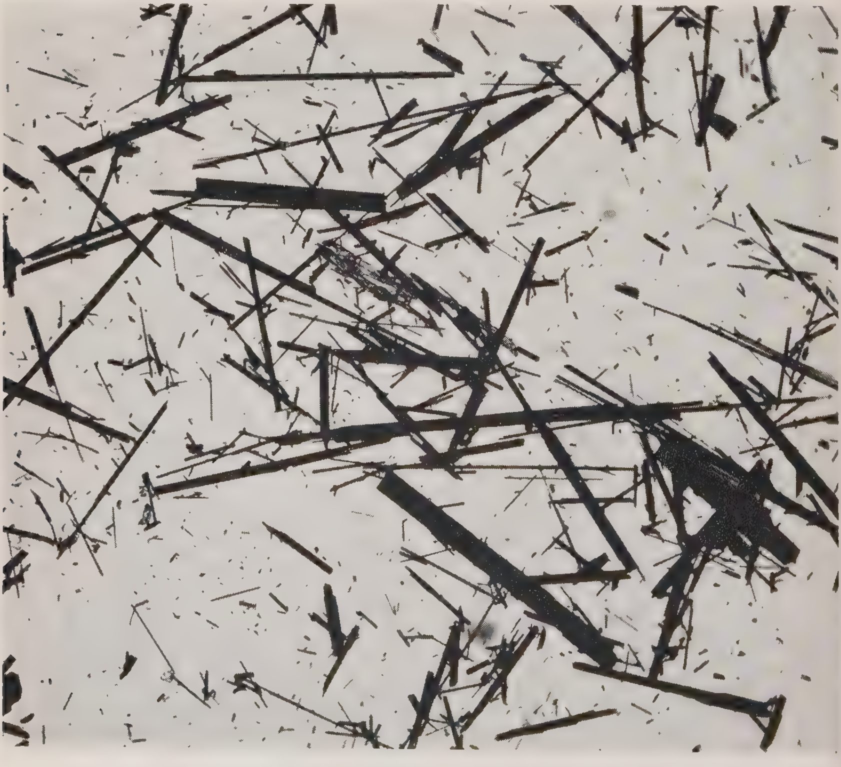

FIG. 2. Isolated fibers of cryptomelane needles. Transmitted light. 100×.

---

* In this formula y is approximately unity, z falls within the limits 0.1–0.5, A represents large ions, B represents small ions, and X represents O or OH anions.

TABLE 1. CHEMICAL ANALYSES OF CRYPTOMELANE SPECIMENS

	1	2	3	4	5	6
MnO_2	83.13	86.54	81.75	87.09	84.2	73.11
MnO	2.08	3.92	3.50	2.49	3.3	5.16
CuO	0.12	0.44	0.06	None	0.08	0.05
NiO	None	None	0.02	None	++	0.02
CoO	None	0.21	0.21	0.08	0.10	0.06
ZnO	5.23	None	None	1.69	++	None
MgO	0.05	None	0.02	0.07	0.08	0.06
BaO	0.13	1.04	None	None	0.08	0.29
SrO	None	0.21	None	None	++	0.16
CaO	0.27	0.30	0.28	None	0.05	
Na_2O	0.44	0.47	0.56	0.48	0.38	0.84
K_2O	3.5	3.88	3.84	3.10	4.4	2.35
H_2O	0.81	0.21	0.38	0.60	++	3.25
H_2O^+	2.58	1.62	3.45	3.58	++	
Al_2O_3	0.37	None	1.37	0.39	0.77	1.9
Fe_2O_3	0.46	0.36	4.00	0.19	1.86	10.3
SiO_2	0.58	0.03	0.35	0.18	0.30	3.0
TiO_2	0.01	None	None	None	++	0.88
P_2O_5	0.07	0.19	None	None	++	++
Total	99.83	99.42	99.79	99.94	95.6	100.4
Chemical Formula	$A_{0.7}R_8O_{16}$	$A_{0.79}R_8O_{16}$	$A_{0.74}R_8O_{16}$	$A_{0.64}R_8O_{16}$	$A_{0.8}R_8O_{16}$	

1. Tombstone, Arizona—Richmond and Fleischer.
2. Deeming, New Mexico—Richmond and Fleischer
3. Sugar Stick Prospect near Mena, Arkansas—Richmond and Fleischer.
4. Philipsburg, Montana—Richmond and Fleischer.
5. Cryptomelane needles—Western Australia—present investigators.
6. Matrix material—Western Australia—present investigators.

++ = not determined.

both the needles and matrix material are predominantly cryptomelane and not the isostructural minerals, hollandite (barium predominant in "*A*" type ions) or coronadite (lead predominant in "*A*" type ions).

The naturally-occurring mineral cryptomelane has not been reported without potassium, although Dubois (7) and Mathieson and Wadsley (6) report manganese oxides, having *x*-ray diffraction patterns like those of cryptomelane, can be produced in the absence of potassium.

X-RAY DIFFRACTION STUDIES

Fiber photographs revealed that the needles were not single crystals but bundles of acicular crystals all oriented randomly around a common *c* axis. This was confirmed by Weissenberg photographs.

Rotation photographs of needles oriented along the c axis could be indexed with the values reported by Ramsdell as body-centered tetragonal ($a_0 = 9.82$ Å, $c_0 = 2.86$ Å, $c/a = 0.29$). Richmond and Fleischer (2) reported a body-centered tetragonal unit cell $a_0 = 9.82$ Å, $c_0 = 2.83$ Å, $c/a = 0.288$. Mathieson and Wadsley (6) reported cryptomelane to be monoclinic ($a_0 = 9.79$ Å, $b_0 = 2.88$ Å, $c_0 = 9.94$ Å, $\beta = 90°37$). The present Weissenberg photographs did not show any deviation from tetragonal symmetry, but this is not conclusive, since the needles always consisted of more than one crystal. Powder photographs also failed to reveal any monoclinic deformation of the unit cell. The optical properties of the needles suggest a pseudotetragonal (monoclinic?) symmetry, which would verify Mathieson and Wadsley's results. As Bystrom and Bystrom suggest, however, since the reported deviation of the monoclinic angle from 90° is very small, the monoclinic and tetragonal forms may be considered as essentially the same from an x-ray structural standpoint.

The x-ray diffraction powder patterns, using iron radiation, were obtained from the needles and the matrix material. In Table 2, the observed and calculated interplanar spacings and observed intensities of the x-ray diffraction powder pattern obtained from thoroughly crushed needles are compared to the powder and fiber data for cryptomelane reported by Ramsdell. It may be noted that (1) the powder data reported by Ramsdell account for approximately 50 per cent of the powder data reported by the present investigators, (2) the powder data of the crushed needles may be correlated with those of Ramsdell's, if his powder and fiber data are combined, and (3) the additional very weak reflections, not observed by Ramsdell, may be indexed with the unit cell he reported (body-centered tetragonal $a_0 = 9.82$ Å, $c_0 = 2.86$ Å, $c/a = 0.29$).

X-ray patterns of the matrix surrounding the cryptomelane needles indicated the presence of cryptomelane, hematite, and quartz. The interplanar spacings and relative intensities of the cryptomelane in this sample and the powder data reported by Ramsdell are shown in Table 3. The lack of correlation of the relative intensities, particularly in the low angle range, is attributed, partially, to a difference in technique. Ramsdell's data were obtained from film measurements (CuKα and MoKα radiation), whereas, the present data were obtained with a diffractometer (iron radiation).

THERMAL TRANSFORMATIONS

There have been studies made on thermal transformations of various oxides of manganese, some of which include data concerning the thermal transformations of cryptomelane. However, no thermal studies have been made with naturally occurring, fibered cryptomelane. Cole, Wadsley, and

TABLE 2. *X*-RAY DIFFRACTION POWDER DATA FOR CRYPTOMELANE NEEDLES

$d_{(\text{obs.})}$	Relative Intensity	*hkl*	$d_{(\text{calc.})}$	Ramsdell $d_{(\text{obs.})}$
6.94	S	110	6.944	6.92 (F & P)
4.92	S	200	4.910	4.91 (F & P)
3.48	W	220	3.472	3.47 (F & P)
3.10	S	130	3.105	3.11 (F & P)
2.45	W	400	2.455	2.46 (F & P)
2.39	M	121	2.389	2.40 (P)
2.32	VW	330	2.315	2.325 (F)
2.20	W	240	2.196	(2.205) (F)
				(2.210) (P)
2.15	M	301	2.148	2.16 (P)
1.97	VW	321	1.968	—
1.92	W	150	1.926	1.935 (F)
1.83	M	141	1.827	1.835 (P)
1.73	VW	440	1.736	1.74 (F)
1.69	VW	350	1.684	1.69 (F)
1.64	M	600	1.637	1.64 (F & P)
1.61	VW	501	1.617	—
1.54	M	260	1.553	1.55 (F)
		251	1.536	1.54 (P)
1.39	VVW	(170)		
		(550)	1.389	1.39 (F)
1.43	W	002	1.424	1.43 (P)
1.402	VW	611	1.405	—
1.350	VW	451	1.350	1.35 (P)
1.297	VW	370	1.290	1.295 (F & P)
1.232	VW	402	1.2317	1.24 (P)
1.215	VW	332	1.2128	1.22 (P)
1.193	VW	422	1.1947	—
1.158	VW	660	1.1573	(1.16) (F)
		561	1.1502	(1.15) (P)
1.116	VW	811	1.1199	—
1.075	W	190	1.0844	1.09 (F)

P = powder *x*-ray diffraction data.
F = fiber *x*-ray diffraction data.

Walkley (8) report that a cryptomelane, made by ammonia digestion of anodic deposits from the electrolysis of zinc sulfate solutions containing manganese as an impurity, was partially transformed to bixbyite* after heating at 500° C. for 13 hours. McMurdie and Golovato (9) studied the changes of cryptomelane by using differential heating curves and powder diffraction data. They reported that cryptomelane may convert directly to hausmannite* or may go through an intermediate stage of bixbyite, and considered this to be due to the effect of impurities. They also reported that a specimen of massive cryptomelane from Tombstone, Arizona transformed to an unidentified phase upon heating above 1200° C. and that a sample of high-purity pyrolusite (MnO_2) transforms to a Mn_3O_4 phase stable above 1170° C. This Mn_3O_4 phase has a spinel-type structure and an $a_0 = 8.70$ Å. Delano (10) also studied the transformations of natural cryptomelane and found that it converted first to bixbyite and then to hausmannite.

---

* Bixbyite—chemical formula $(FeMn)_2O_3$—varies in composition from nearly pure Mn_2O_3 to 59% Fe_2O_3, cubic—$a_0 = 9.365$.

Although changes occurring upon heating cryptomelane powders have been reported, it was of interest to investigate the transformations by rotating crystal and fiber methods. These techniques would not only be expected to reveal changes in structure and crystal orientation, but should also show variations in crystal size. Some of the cryptomelane needles were heated at different temperatures for various times and air-cooled. The single-crystal photographs were made with copper radiation ($\lambda = 1.542$ Å). The long direction or the c axis of the original cryptomelane needle was mounted perpendicular to the x-ray beam.

Rotation photographs of the cryptomelane needles heated at either 500 or 600° C. for 2 hours were identical to those of the cryptomelane needles in their original state (Fig. 3*a*).† Upon heat-treatment at 600° C. for 5 hours the patterns showed the first evidence of the formation of Mn_2O_3.‡ A weak reflection corresponding to the interplanar spacing, $d = 2.72$ ($hkl = 222$), of this phase was evident on the zero layer of the rotation pattern of the cryptomelane. The elongation of this particular reflection in a direction parallel to the c axis of the cryptomelane in a fiber photograph indicated that the Mn_2O_3 phase consisted of small crystallites slightly misoriented perpendicular to the needle axis. It was also concluded from the fiber photograph that the randomness of orientations and crystallite sizes of the cryptomelane phase after this treatment were not different from those of the original cryptomelane needle.

A needle heated at 600° C. for 17 hours showed an increase in the amount of Mn_2O_3. The Mn_2O_3 was polycrystalline and highly orientated

---

* Hausmannite—chemical formula—

$$Mn_3O_4\text{—Fe:Mn} = 1:23 \text{ tetragonal } a_0 = 5.75$$
$$c_0 = 9.42$$

† Cryptomelane is represented by the chemical formula KMn_8O_{16} in Figures 3 and 7 to emphasize the predominance of the K^+ and Mn^{+4} ions in this mineral.

‡ This transformation phase is regarded as Mn_2O_3, not bixbyite, since the original sample contains only 1.86% Fe_2O_3, and the x-ray data agree closely with those of the synthetic Mn_2O_3 reported by Gruner ($a_0 = 9.24$ Å) (11).

TABLE 3. X-RAY DIFFRACTION POWDER DATA FOR CRYPTOMELANE IN MATRIX MATERIAL

Matrix Material		Ramsdell's Powder	
$d_{(obs.)}$	$I_{(obs.)}$	$d_{(obs.)}$	$I_{(obs.)}$
6.94	7.6	6.92	W
4.92	7.6	4.91	W
3.48	1.5	3.47	VW
3.10	9.3	3.11	M
2.46	0.2	2.46	VW
2.39	10.0	2.40	S
2.20	3.0	2.21	W
2.15	6.8	2.16	W
1.83	7.0	1.835	M
1.64	3.3	1.64	W
1.54	2.9	1.54	M
1.43	1.2	1.43	W

in both the [100] and the [110] directions which coincided with the original [001] axis of the cryptomelane. No change in the randomness of orientation or crystallite size of the cryptomelane phase in the needles was evident from a fiber photograph. The fiber spots of the Mn_2O_3 phase were more elongated after the 17-hour treatment than after the 5-hour treatment, thus indicating an increase in the amount of randomness of orientations perpendicular to the needle axis with increasing time at this temperature.

After a heat-treatment at 700° C. for 2 hours, there was a definite increase in the amount of Mn_2O_3, and the Mn_2O_3 crystals were oriented slightly more in the [100] direction than in the [110] direction (Fig. 3*b*). Although this figure does not clearly show a difference in intensity corresponding to these orientations, it was quite evident on the original photograph. After 17 hours at 700° C., the amount of Mn_2O_3 increased markedly, and the amount oriented in the [100] and [110] directions appeared to be equal (Fig. 3*c*). When the time at 700° C. was increased to 68 hours, there was again a definite trend toward a preferred orientation in the [100] direction for the Mn_2O_3 phase, and since a fiber photograph showed that the elongated spots of the Mn_2O_3 were discontinuous, it appears that some recrystallization had taken place.

Mn_2O_3 was the only constituent detected in a cryptomelane needle heated at 800° C. for 17 hours. The rotation photograph showed the Mn_2O_3 to consist of small crystals more randomly arranged than in previous heat-treatments but with some preference for the [100] over the

[110] direction. Needles heated for 68 or 110 hours at 850° C. were similar to those heated at 800° C. for 17 hours. A heat-treatment at 875° C. for 24 hours, however, lessened the orientation of the Mn_2O_3 along the [110] axis appreciably (Fig. 4*a*).

Mn_3O_4 appeared as a minor constituent in a cryptomelane needle heated at 900° C. for $1\frac{1}{2}$ hours. The predominant constituent was Mn_2O_3 with the same preferred orientations as in the needles treated at 800° C. for 17 hours. There was a slight increase in the crystal size of the Mn_2O_3 after this heat-treatment as compared to that in the needles heated at lower temperatures. The Mn_3O_4 occurred as a group of crystals randomly oriented with a common [100] axis. The [100] axis of the Mn_3O_4 crystals was parallel to the [001] axis of the original cryptomelane needle.

A rotation photograph of a needle heat-treated to 1000° C. at a rate of 6° C./min., however, showed only Mn_3O_4 with a predominant orientation along the *a* axis, [100] (Fig. 4*b*). This heat-treatment was the only one

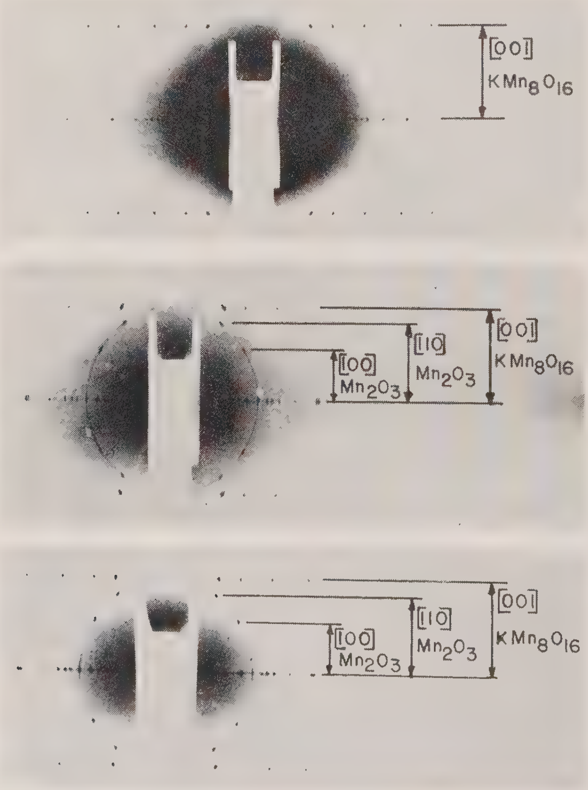

FIG. 3. Rotation patterns of cryptomelane needles. (*a*) As received, Cryptomelane; (*b*) 700° C. for 2 hours, Cryptomelane and Mn_2O_3; (*c*) 700° C. for 17 hours, Cryptomelane and Mn_2O_3.

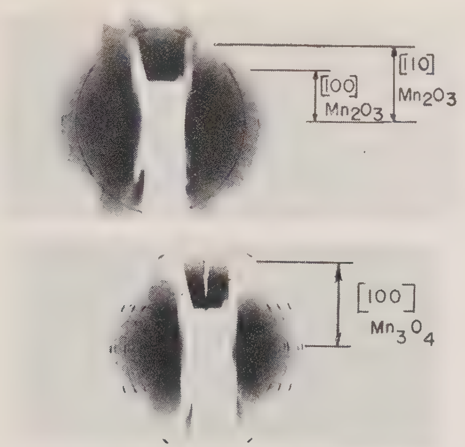

FIG. 4. Rotation patterns of heat-treated cryptomelane needles. (*a*) 875° C. for 24 hours, Mn_2O_3; (*b*) 1000° C. for 6 minutes, Mn_3O_4.

of those used that produced a rotation pattern of only Mn_3O_4. The temperature-time relationship appeared to be more critical for the formation of the Mn_3O_4 than the other thermal products.

Upon heating a cryptomelane needle at 900° C. for 17 hours, a phase with a cubic diffraction pattern similar to that of a spinel was obtained. The [110] axis of the spinel is parallel to the [001] axis of the original cryptomelane needle. The diffraction spots of the spinel are very diffused, indicating a high degree of structural imperfection. The major constituent is again Mn_2O_3 in a polycrystalline state, orientated primarily along its [100] direction.

The only constituent detected after heating the needles at 950° C. for 48 hours is the spinel in a polycrystalline state with a preferred orientation along its [110] axis. With an increase in time at 950° C. to 68 hours, the degree of orientation of the spinel along its [110] axis increases. A heat-treatment at 1000° C. for 92 hours produces a more random orientation of the crystallites of the spinel. The change in degree of orientation of the spinel with increasing time and temperature is shown in Fig. 5. In Table 4 are presented the powder diffraction data (iron radiation) and calculated interplanar spacings of the spinel.

The cell dimensions of the cryptomelane, Mn_2O_3, Mn_3O_4, and spinel remained constant throughout the described thermal treatments. The observed cell diminsions and orientations are represented schematically in Fig. 6.

THERMOGRAVIMETRIC STUDY

Thermogravimetric determinations were made in air with a rate of temperature increase of 6° C. per minute. The graphs obtained by plot-

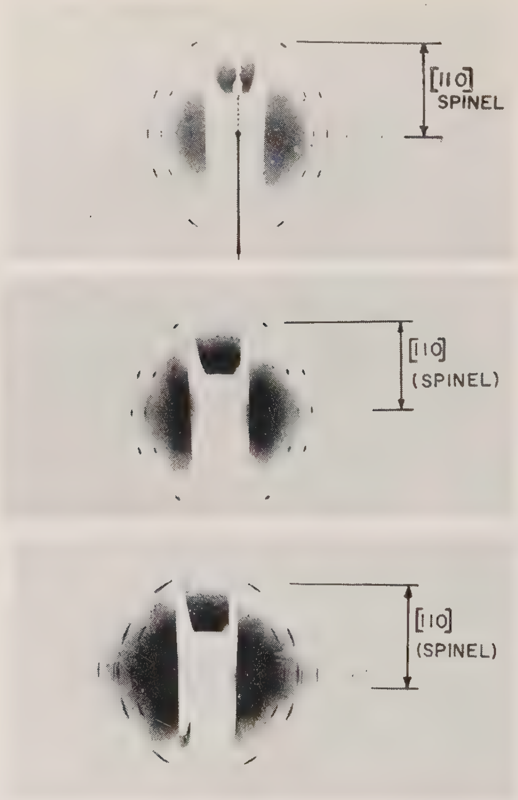

FIG. 5. Rotation patterns of cryptomelane needles heat-treated to produce "Spinel" phase.

ting weight loss versus temperature for the matrix material and the needles were similar. However, the weight loss values for the needles were less accurate because of the limited amount of sample.

A graph of the thermogravimetric results obtained from the matrix material is shown in Fig. 7. The weight loss due to adsorbed water (below 110° C.) is negligible and between 110 and 500° C. the loss of 2.5% is attributed to zeolitic water. (Chemical analysis shows a total water content of 3.25%.) The total weight loss recorded was 11.3%, and 8.8% of this occurred between temperatures of 500 and 1050° C. The theoretical weight loss due to oxygen in this sample for the transformation of MnO_2 and MnO in cryptomelane to Mn_3O_4 is 8.6%.

Cryptomelane needles were heated to 650, 850, 1000 and 1200° C. at the same rate of temperature increase (6° C./min.) used for the thermogravimetric determination. Powder photographs were made of these heat-treated samples. The results of this investigation are included in

TABLE 4. INTERPLANAR SPACINGS AND RELATIVE INTENSITIES FOR SPINEL FORMED BY HEAT-TREATMENT OF CRYPTOMELANE NEEDLES

h k l	$d_{(\text{calc.})}$	$d_{(\text{obs.})}$	$I_{(\text{obs.})}$
111	4.86	4.86	5
220	2.98	2.98	5
311	2.54	2.54	10
222	2.42	2.43	1
400	2.10	2.10	5
422	1.719	1.718	2
511 333	1.623	1.620	5
440	1.488	1.488	6
533	1.284	1.284	2
444	1.217	1.215	1
642	1.126	1.126	1
731 553	1.099	1.096	4

Fig. 7. The powder photograph of the cryptomelane needles heated to 1000° C. (6° C./min.) revealed a trace of cryptomelane remaining. As previously noted, the rotation photograph of a needle heated under the same conditions showed only Mn_3O_4 (Fig. 4*b*). This indicates that a small amount of untransformed cryptomelane may be present in the core of the needles. The Mn_2O_3 phase was not detected after this heat-treatment.

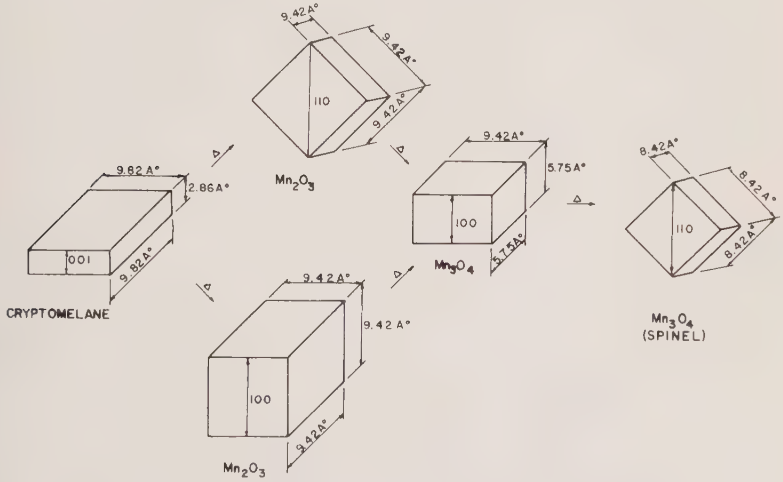

FIG. 6. Relationships of cell dimensions and orientations of thermal transformation products of cryptomelane.

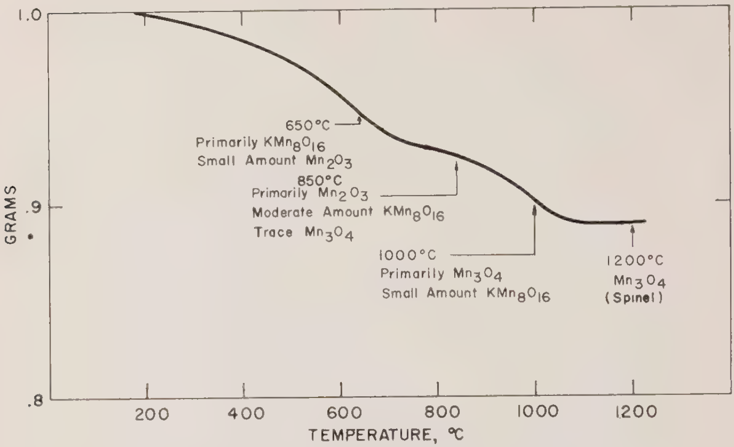

FIG. 7. Thermogravimetric results from matrix material.

probably because of the rapidity with which it transforms to Mn_3O_4 at this temperature.

A minimum rate of weight loss with temperature occurs between approximately 750 and 850° C. and a maximum rate between about 850 and 950° C. The minimum rate may be due to a slow rate of diffusion of oxygen through a relatively thick layer of Mn_2O_3.

The thermogravimetric data in correlation with the phases present indicate that cryptomelane, at a heating rate of 6° C. per min., does not transform completely to Mn_2O_3 before formation of Mn_3O_4 begins, and that Mn_3O_4 forms from the intermediate Mn_2O_3 phase. At this heating rate, the critical temperature for formation of Mn_2O_3 from the needles is approximately 600° C., for the Mn_3O_4 approximately 825° C., and for the spinel approximately 1050° C.

SUMMARY

Cryptomelane needles and their surrounding matrix material were examined. Chemical analyses established that the needles and the principal constituent in the matrix material were cryptomelane. Fiber photographs revealed the needles were bundles of crystals randomly oriented around a common *c* axis. X-ray diffraction data from powder patterns of the needles are tabulated and indexed in terms of a body-centered tetragonal cell, although optical data indicate a pseudotetragonal cell.

The cryptomelane needles were heat-treated at various temperatures for different times and examined by rotation and fiber methods. A manganese oxide phase with a spinel-type structure, $a_0 = 8.42$ Å, occurs after

heating the needles at temperatures greater than 900° C. for prolonged times. The following representation shows the thermal transformations and relative orientations parallel to the [001] axis of cryptomelane.

$$\begin{array}{cccc} & [110] & & \\ [100] \xrightarrow{\Delta} & [100] \xrightarrow{\Delta} & [100] \xrightarrow{\Delta} & [110] \\ \text{cryptomelane} & Mn_2O_3 & Mn_3O_4 & \text{Spinel} \\ & & & (R_3O_4 \text{ type}) \end{array}$$

Thermogravimetric data, correlated with identified phases, indicate that the Mn_3O_4 phase forms from the Mn_2O_3 phase. At a heating rate of 6° C. per minute, the critical temperature for formation of Mn_2O_3 from the cryptomelane needles is approximately 600° C., for Mn_3O_4, approximately 825° C., and for the spinel, approximately 1050° C.

ACKNOWLEDGMENT

The authors wish to thank P. F. Forsyth for the thermogravimetric data, R. A. Lannoye for the chemical analyses, and H. R. Spedden who furnished the cryptomelane sample.

REFERENCES

1. Ramsdell, L. S., *Am. Mineral.* **17,** 143 (1932).
2. Richmond, W. E. and Fleischer, M., *Am. Mineral.* **27,** 607 (1942).
3. Ramsdell, L. S., *Am. Mineral.* **27,** 611 (1942).
4. Gruner, J. W., *Am. Mineral.* **28,** 497 (1943).
5. Bystrom, A. and Bystrom, A. M., *Acta Cryst.* **3,** 146 (1950), and *Acta Cryst.* **4,** 469 (1951).
6. Mathieson, A. McL. and Wadsley, A. D., *Am. Mineral.* **35,** 99 (1950).
7. Dubois, P., *Ann. Chimie* **5,** 411 (1936).
8. Cole, W. F., Wadsley, A. D., and Walkley, A., *Trans. Electrochem. Soc.* **92,** 133, (1947).
9. McMurdie, H. F. and Golovato, E., *J. Research National Bureau of Standards,* **41,** 589 (1948).
10. Delano, P. H., *Eng. Chem.,* **42,** 523 (1950).
11. Gruner, J. W., *Am. Mineral.* **28,** 174 (1943)

Manuscript received December 26, 1959.

THE AMERICAN MINERALOGIST, VOL. 45, SEPTEMBER-OCTOBER, 1960

CLASSIFICATION OF SILICATES AND OTHER MINERALS WITH TETRAHEDRAL STRUCTURES

Tibor Zoltai, *Crystallographic Laboratories, Massachusetts Institute of Technology, Cambridge, Massachusetts.**

Abstract

The conventional geometric classification of the silicates is no longer sufficient to classify the ever-increasing number of determined ionic tetrahedral structures. More detail is desirable in the classification, and consequently, new classification criteria are necessary to provide a larger number of subdivisions. The study of the relative energies of isolated rings of tetrahedra suggests that the size of the tetrahedral loops may be used as one additional criterion. It is suggested that another criterion may be based on the different nature of the corner sharing of tetrahedra. A numerical expression, called the sharing coefficient, is derived to cover this criterion. In the proposed classification these two criteria are added to the customary silicate classification, and, consequently, the classification proposed is basically in accordance with the conventional scheme.

A large number of silicates can be classified differently depending on whether we consider all tetrahedra of the structure, or only the silicon and aluminum tetrahedra. This problem is not treated consistently in the literature. In some cases aluminum tetrahedra are disregarded or other tetrahedra, like boron, are accepted. It is suggested that all tetrahedrally coordinated cations should be considered as part of the tetrahedral frame of a silicate. This suggestion is supported by the similarity of the observed ionic radii and electronegativity of other four-coordinated cations with that of silicon and aluminum, and by the analytical data indicating the random distribution of silicon and other cations in different tetrahedra of certain silicates.

Introduction

The classification of things of scientific interest is not merely a filing system, but is also a basis for evaluation and comparison. As such, it constitutes a step in the progress of science and may lead to the better understanding of nature, and to the establishment of new directions of research. The classification conceived by Machatschki (1928) and developed by Bragg (1930) was an excellent system for classifying a large number of silicates. It also explained many of the important physical properties of silicates. Consequently, the classification was of considerable importance in the understanding of the silicates and other crystals with similar tetrahedral structures. Since 1928 the number of tetrahedral structures determined has grown so tremendously that the Machatschki-Bragg classification is no longer adequate, especially for structures with a three-dimensional network of tetrahedra. There is a definite need for an improved classification, first, to provide more subdivisions in the system of classification and, second, to point out minor, but important, similarities between different tetrahedral structures.

---

* Present address: Department of Geology and Mineralogy, University of Minnesota, Minneapolis 14, Minnesota.

After the structure of coesite was determined (Zoltai and Buerger 1959) and compared with structures of other forms of silica, the significance of tetrahedral loops in the tetrahedral structures became apparent. In the conventional classification the geometric forms of the tetrahedral structures are related to the cleavage, hardness and the optical properties of the crystals; similarly the size of the tetrahedral loops are related to the energies of the tetrahedral structures (Zoltai and Buerger 1960). The importance of the size of the tetrahedral loops in a structure and its prospective application as a natural classification criterion stimulated an investigation of tetrahedral structures and the construction of an improved classification.

Other geometric features of tetrahedral structures were observed during the course of this study. Most of them are applied in the proposed classification system. The classification criteria are discussed in detail in their order of application.

The Geometrical Forms

The conventional classification is based on geometrical forms created by the linkage of tetrahedra. These forms are referred to as "types" in the literature. They are: isolated tetrahedra, groups, chains, rings, sheets and three-dimensional networks of tetrahedra. These features are important, and are widely accepted. Consequently they are adopted in this classification. Minor revisions, however, are made in order to group these types systematically, and to cover all the possible ionic tetrahedral structures. Some of the types have distinct directions in which the tetrahedral structures extend to infinity. In others the tetrahedral structures are terminated in all directions. Consequently, if the tetrahedral structures are extended to infinity in zero-, one-, two- and three-dimensions, four major types of tetrahedral structures are possible. These four types are:

(1) Isolated groups of tetrahedra.
(2) One-dimensionally non-terminated structures of tetrahedra.
(3) Two-dimensionally non-terminated structures of tetrahedra.
(4) Three-dimensionally non-terminated structures of tetrahedra.

It is theoretically possible for a crystal to be composed of two or more different types of tetrahedral structures. To cover such possibilities a fifth type is established:

(5) Mixed-types of tetrahedral structures.

All these types can be divided into subtypes. In the first three types the subtypes can be defined according to the complexity of the tetrahedral structure of the type. That is, in the first type the number of tetrahedra can serve as a basis for the subdivisions and in the others the number of single chains, single rings and single sheets welded together. In the fourth type the subtypes can be defined according to an important characteristic of these structures, that is, according to the sharing of tetrahedral corners only, or the sharing of one or more tetrahedral edges or faces also.

The types and subtypes are listed in the first two columns of Table 1.

CORNER SHARING IN TETRAHEDRAL STRUCTURES

A brief study of the tetrahedral structures revealed that different number of tetrahedral corners can be shared and still make up the same type, and even the same subtype structure. For example, two single

TABLE 1. SHARING COEFFICIENTS AND CATION-ANION RATIOS OF THE TYPES AND SUBTYPES OF TETRAHEDRAL STRUCTURES

Types	Subtypes	Sharing coefficients	Cation-anion ratios
1. Isolated groups of tetrahedra	a. single tetrahedron	1.00	1:4
	b. pair of tetrahedra	1.25	1:3½
	c. large groups	1:25–1.50–(1.75)*	1:3½–1:3–(1.2½)
	d. mixed groups	1.25–1.50–(1.75)	1:3½–1:3–(1:2½)
2. One-dimensionally non-terminated structures of tetrahedra	a. single chains	1.50	1:3
	b. single rings	1.50	1:3
	c. double chains	1.50–1.75	1:3–1:2½
	d. double rings	1.50–1.75	1:3–1:2½
	e. multiple chains	(1.50)–1.75–2.00	(1:3)–1:2½–1:2
	f. multiple rings	(1.50)–1.75–2.00	(1:3)–1:2½–1:2
	g. mixed chains and rings	(1.50)–1.75–2.00	(1:3)–1:2½–1:2
3. Two-dimensionally non-terminated structures of tetrahedra	a. single sheets	1.50–1.75	1:3–1:2½
	b. double sheets	(1.50)–1.75–2.00	(1:3)–1:2½–1:2
	c. multiple sheets	(1.50)–1.75–2.00	(1:3)–1:2½–1:2
	d. mixed sheets	(1.50)–1.75–2.00	(1:3)–1:2½–1:2
4. Three-dimensionally non-terminated structures of tetrahedra	a. networks with corners shared	1.75–4.00	1:2½–1:1
	b. networks with one or more edges shared	4.00–8.00	1:1–1:½
	c. networks with one or more faces shared	8.00–	1:½–
5. Mixed types			

---

* Sharing coefficients in parentheses indicate theoretically possible but practically improbable ranges.

chains can be welded into a double chain if each tetrahedron of the first chain is connected to a tetrahedron of the second chain. Two single chains can also be welded into a double chain if only every second tetrahedron of the first chain is connected to every second tetrahedron of the second chain. In the former case six tetrahedral corners are shared per two tetrahedra and in the latter only five. The general geometric form, however, still remains a double chain. A similar situation exists in the sheet structures. A sheet can be constructed if each tetrahedron shares three corners with other tetrahedra. A sheet also can be constructed if certain tetrahedra share only two corners. Once again, the number of tetrahedral corners shared is the only difference between the two sheets. In the three-dimensional network usually all four corners are shared. In some structures a few corners are left unshared, and consequently the average number of tetrahedral corners shared becomes less than four.

In these examples it was tacitly assumed that only two tetrahedra can share a tetrahedral corner. This is not a necessary restriction. Several three-dimensional networks of tetrahedra are actually known in which three or even more tetrahedra share a tetrahedral corner. In order to distinguish between such structures, the number of tetrahedral corners shared is no longer sufficient. It has to be supplemented with the number of tetrahedra participating in the sharing of a corner.

It is possible to derive a single numerical value which can express both the number of tetrahedral corners shared and the number of tetrahedra participating in the sharing, if we make two assumptions:

A. The difference between the smallest and the largest number of tetrahedra participating in the sharing of a tetrahedral corner in a structure can not be more than one.

B. No edges of tetrahedra can be shared unless the corners are shared between more than four tetrahedra, and no faces can be shared unless the corners are shared between more than eight tetrahedra.

Assumption *A* means, for example, that as long as there are free corners present in a structure, no corners can be shared between more than two tetrahedra; or if some corners are shared between two tetrahedra only, no corners can be shared between more than three tetrahedra. Assumption *B* means that edges and faces can be shared only in very dense tetrahedral structures. In certain structures the density of the tetrahedra may require geometrically the sharing of edges, and in even denser structures the sharing of faces.

Under these conditions the average number of tetrahedra participating in the sharing of a tetrahedral corner in a structure also defines the number of corners shared. The average number of tetrahedra participating in the sharing of a corner in a structure is called the sharing coefficient of the structure. It can be either an integer or a fraction. An integral number defines a state in which each corner of each tetrahedron is shared between n tetrahedra, where n is the integer in question A fractional number, on the other hand, defines a state in which some corners are shared between n tetrahedra and others between $n+1$ tetrahedra, where n is the integral part of the sharing coefficient. The fractional part, further, defines the ratio of the number of corners shared between n and $n+1$ tetrahedra. A sharing coefficient of $n+\frac{1}{4}$ means, for example, that all the corners are shared between at least n tetrahedra and in addition every fourth corner is shared between $n+1$ tetrahedra; or a sharing coefficient of $n+(1/20)$ means that all the corners are shared between at least n tetrahedra and in addition every twentieth corner is shared between $n+1$ tetrahedra.

There is a simple relationship between the sharing coefficient and the cation-anion ratio in the tetrahedral radical of the chemical formula. The relationship is obvious when a tetrahedral corner is shared between two or more tetrahedra. Then the same anion simultaneously belongs to two or more cations. The cation-anion ratio in a single tetrahedron is 1:4 and in a pair of tetrahedra it is $1:3\frac{1}{2}$, and the corresponding sharing coefficients are 1:00 and 1.25 respectively. Consequently the sharing coefficient not only describes a geometric feature, but also defines part of the chemical formula. A list of possible sharing coefficient ranges for the types and subtypes of the tetrahedral structures, and the corresponding cation-anion ratios, are tabulated in the third and fourth columns of Table 1.

Assumptions *A* and *B* were found, empirically, to hold for dominantly ionic crystals. These assumptions are generalizations of Pauling's third rule which states, briefly, that the sharing of edges and particularly of faces of ionic polyhedra decreases the stability of the structure. This is because such sharing necessitates the close approach of two cations and thus increases the potential energy of the system. Assumptions *A* and *B* can be supported by similar arguments. When more tetrahedra share a tetrahedral corner, more tetrahedra come in contact, and the high valence cations approach each other, thereby increasing the potential energy of the system. Since a system tends toward the lowest energy state possible, the corners should be shared by the least possible number of tetrahedra. Thus no corner is shared by three tetrahedra unless there is no lower energy state available. Similarly no tetrahedral corners will be shared between three tetrahedra in a double chain when a multiple chain or other geometric form represents lower energy with the corners shared between two tetrahedra only. The same argument restricts the sharing of edges and of faces to structures where it is necessitated by geometry, in extremely dense three-dimensional networks.

REPEAT UNITS AND LOOPS OF TETRAHEDRA

With the exception of the isolated groups of tetrahedra, the single chains, and the three-dimensional networks with one or more faces shared, all the tetrahedral structures contain loops of tetrahedra. These loops are outstanding features. They are also important in the consideration of the energies of structures. Consequently the tetrahedral loops are simple and non-artificial criteria. Modern investigators of the tetrahedral and other polyhedral structures noticed the significance of these loops, and, in one form or other, they applied the loop concept to the subclassification of certain types of tetrahedral and polyhedral structures. Wells subdivided the polyhedral networks according to the size of the loops formed by polyhedra. Tetrahedral networks are also included in his classification (Wells 1954, Part 2). However, he considered only the highly regular tetrahedral networks with a sharing coefficient of 1.75 and 2.00.

Liebau (1956) classified the tetrahedral silicate structures on the basis of the number of tetrahedra in the periodic unit of the tetrahedral structure. Liebau's classification subclassifies the simpler tetrahedral structures very conveniently, but fails to give a sufficient number of subdivisions for the three-dimensional networks.

The combination and extension of Wells' and Liebau's principles could conveniently be applied to the subclassification of all types of tetrahedral structures. The structures containing no loops of tetrahedra can be subdivided according to the number of tetrahedra in the periodic unit of the tetrahedral structure, and structures containing loops of tetrahedra can be subclassified according to the number of tetrahedra in the loops. The former term is called the repeat unit of tetrahedra, and the latter the loop of tetrahedra.

The repeat unit of tetrahedra in the isolated groups of tetrahedra would be simply the number of tetrahedra in the groups. If there are different kinds of groups in the structure, several units will be listed and one number will represent each kind of group.

In an endless single chain the repeat unit of tetrahedra is the number of tetrahedra in the motif of the chain which is repeated by translation to form the chain. If, for example, all the tetrahedra of the chain are similarly oriented and are translation equivalents, the repeat unit is one tetrahedron. But if every second tetrahedron is oriented differently from the first one, then only every third tetrahedra are translation equivalents, and the repeat unit of the chain is two tetrahedra (Liebau 1956, p. 75).

In most of the other types of tetrahedral structures there are loops of tetrahedra, and every tetrahedron of the structure is part of one or more loops. These structures can be subclassified either (1) by the size of the

Table 2 Classification of Tetrahedral Structures

Types	Subtypes	Sharing coefficients	Repeat-units and loops of tetrahedra	Structure families	Members
1. Isoiated groups of tetrahedra	a. Single tetrahedron	1.00	1		Olivine, garnet, sphene, apatite, gypsum etc.
	b. Pair of tetrahedra	1.25	2		Ilvaite, tilleyite, $ZrPO_4$ lawsonite
	c. Large groups	1.40	5		Zunyite
	d. Mixed groups	1.111	1-2		Idocrase
		1.167	1–2	Epidote	Clinozoisite, allanite
2. One-dimensionally non-terminated structures of tetrahedra	a. Single chains	1.50	2	Pyroxenes	Enstatite, diopside, augite etc.
		1.50	3	Wollastonite	
		1.50	5	Rhodonite	
	b. Single rings	1.50	3	Benitoite	Catapleite, wadeite
		1.50	4	Axinite	
		1.50	6	Tourmaline	Dioptase, caledonite
	c. Double chains	1.583	8	Xonotlite	
		1.625	6	Amphiboles	Tremolite, hornblende etc.
		1.75	4	Sillimanite	
	d. Double rings				
	e. Multiple chains				
	f. Multiple rings				
	g. Mixed chains and rings				
3. Two-dimensionally non-terminated structures of tetrahedra	a. Single sheets	1.75	4–8	Apophyllite	Datolite
		1.75	4–8	Gillepsite	
		1.75	6	Mica	Clay, chlorite etc.
		1.75	6	Sepiolite	Beryllonite, V_2O_5
		1.833	5	Melilite	Hardystonite, gehlenite, åkermanite
	b. Double sheets	2.00	4–6	Hex. Celsian	α Celsian
	c. Multiple sheets				
	d. Mixed sheets				
4. Three-dimensionally non-terminated structures of tetrahedra	a. Networks with corners shared	1.75	10	P_2O_5	
		1.821	8–10	$12CaO \cdot 7Al_2O_3$	
		2.00	3–6	GeS_2	
		2.00	4–5–8	Scapolites	Marialite etc.
		2.00	4–6	Sodalite	Ultramarine, helvite, danalite, hauynite
		2.00	4–6–8	Paracelsian	Danburite, hurlbutite
		2.00	4–6–8	Analcite	Leucite, pollucite
		2.00	4–6–8–9	Coesite	
		2.00	4–6–8–10	Feldspars	Sanidine, orthoclase, plagioclase etc.
		2.00	4–6–8–12	Chabazite	
		2.00	4–6–8–12	Gmelinite	
		2.00	4–6–9	Beryl	Cordierite
		2.00	4–6–9	Milarite	Osumilite
		2.00	4–6–12	Faujasite	
		2.00	4–6–12	Cancrinite	
		2.00	4–8	Natrolite	Edingtonite, thomsonite
		2.00	5–6	Petalite	
		2.00	5–6–8	Heulandite	Philippsite (?)
		2.00	5–7–8	Keatite	

TABLE 2 (*continued*)

Types	Subtypes	Sharing coefficients	Repeat-units and loops of tetrahedra	Structure families	Members
		2.00	6	Cristobalite	Carnegieite, cuprite, Na_2CaSiO_4, $K_2Al_2O_4$ $Na_2Al_{24}O$,BPO_4, $BAsO_4$ etc.
		2.00	6	Tridymite	Nepheline, $BaAl_2O_4$, $BaFe_2O_4$, $KAlSiO_4$, $K_2MgSi_3O_8$ etc.
		2.00	6–8	Quartz	Berlinite, hi-eucryptite, $AlPO_4$, $AlAsO_4$ etc.
		2.75	3-4-6	Bertrandite	
		2.75	3-4-6-8	Hemimorphite	
		2.75	3-4	B_2O_3	
		3.00	3-4	Ag_2HgI_4	
		3.00	3-4-5	Phenacite	Willemite
		4.00	3	Sphalerite	BeO, MgTe etc.
		4.00	3	Wurtzite	BeS, BeTe etc.
	b. Networks with one or more edges shared	4.00	3	Cubanite	
		4.00	4	Cooperite	
		6.00	3	Zn_3P_2	Bi_2O_3
		8.00	Octahedron	Fluorite	ZrO_2, ThO_2 etc., also antifluorite structures: Na_2O, K_2O, Li_2O etc.
	c. Networks with one or more faces shared				
5. Mixed types					

smallest loop of the structure, or (2) by the list of the different sizes of loops occurring in the structure, or (3) by the list of all the symmetrically non-equivalent loops, in order of the increasing size of the loops. The first alternative has only five or six subdivisions, which is not sufficient to distinguish between a large number of possible structures, especially in the three-dimensional networks. The second alternative increases the number of subdivisions considerably. The third alternative, however, increases it to such an extent that almost every known structure has a different list of loop sizes.

Although the third alternative offers a greater number of subdivisions than the second, the second has been chosen for this classification for the following reasons: because the determination of the symmetrically non-equivalent loops is difficult and, in complicated structures, might become confusing; secondly because the number of subdivisions offered by the much simpler second alternative seems to be sufficient since only very similar structures have the same loop sizes.

The loop sizes can be determined either by simple observation or by a more systematic approach offered by the symmetry of the structure: all the possible loops of the structure must include the tetrahedra of the tetrahedral motif of the structure. The number of tetrahedra in the motif is usually less than five. Unfortunately in complicated structures there might be a very long list of loop sizes, especially for the larger loops. In order to avoid an unnecessarily long list, the loop sizes can be limited arbitrarily. At the present time it seems to be satisfactory to limit the number of loop sizes of a structure to four, and the size of the largest loop to twelve.

As the sharing coefficient increases above 4.00, tetrahedral edges are shared, and, in addition to the loops, incomplete polyhedral openings are present. When the sharing coefficient approaches 8.00 certain openings become complete polyhedra, but when the sharing coefficient reaches 8.00, all the edges are shared and all the openings are polyhedral. For example, the openings in the fluorite structure are octahedral. In structures with a sharing coefficient higher than 8.00, the polyhedral openings start to disappear, making room for solid bodies of tetrahedra. With a sharing coefficient at and above 8.00 there are no more loops of tetrahedra. Instead of units and loops these structures can be subdivided according to the shape of their polyhedral openings.

STRUCTURE FAMILIES

After the tetrahedral structures are classified according to types, subtypes, sharing coefficients, and repeat units or loops of tetrahedra, there remain only very similar structures in each category of the classification. They are in most cases isomorphic, isotypic, or derivative structures. It is theoretically possible, however, that two structures can be so similar that they have the same tetrahedral loops, yet their tetrahedral linkages are different; these should not be left in the same final group. Two such structures are apophyllite and gillepsite. They are similar in every respect, except in the linkage of tetrahedra. In both structures the tetrahedra are oriented so that they form triangular pyramids with their bases in the plane of the sheet of the layered structure. In apophyllite the three basal corners of the pyramids are shared, but in gillepsite the two basal corners and the apices of the pyramids are shared. Such structures should be separated as two different structure families, so that in the final column of the classification there are only closely related structures.

CLASSIFICATION OF SILICATES

There is a complication in the structures of the silicates which makes their classification difficult. This is the presence of tetrahedrally coordinated Al, B, Be and other cations. This complication is usually neglected by most authors and gives rise to an inconsistency in the treatment of various silicates. The problem can be illustrated briefly by three points:

(1) It is generally accepted that Al can replace Si, and when it does, the Al tetrahedra still remain part of the tetrahedral framework of the silicates. In some cases, however, the Al tetrahedra are not so regarded. For example, cordierite is usually classified as a six-membered single-ring structure, where the tetrahedra of the ring are Si tetrahedra. But Al tetrahedra connect these rings into a continuous three-dimensional network.

(2) In other cases other cations occur in tetrahedra and they are sometimes accepted as part of the frame and sometimes not. For example, B in danburite is accepted as part of the frame, and danburite is classified as a silicate with the three-dimensional network of tetrahedra. Ca occurs in tetrahedral coordination in Na_2CaSiO_4 and is accepted as part of the framework, so that the crystal is a derivative of the cristobalite structure. But tetrahedrally coordinated Be is not accepted in beryl, phenacite or bertrandite, nor Zn in willemite, hemimorphite or hardystonite.

(3) Almost every author treats this problem differently (Bragg 1930, 1937, Berman 1937, Gruner 1931, Strunz 1937, Swartz 1937). Most authors exclude cations other than Si and Al from the tetrahedral frame of the silicates. In some instances even Si atoms are excluded from the frame as in Na-melilite (Swartz 1937). On the other hand some authors (Strunz 1937, 1957, Eitel 1941) accept two alternate classifications for the silicates containing several cations in tetrahedral coordination.

Without a consistent treatment of the various four-coordinated cations, a classification of silicates based on their tetrahedral structures is somewhat artificial. In order to save the otherwise satisfactory Machatschki-Bragg classification, the problem of the cations must be treated consistently. The acceptance of all the tetrahedrally coordinated cations in the tetrahedral frames of the silicates would not only be the simplest solution, but probably the only satisfactory solution. This is the only way, for example, for the consistent classification of the melilites. The linkage of the tetrahedra in the various melilites is identical although the tetrahedra are occupied by different cations. In Na-melilite there are only Si cations in the tetrahedra, in gehlenite only Si and Al cations, but in hardystonite, there are also Zn and in melilite Mg and Fe cations.

Geometrically there are several cations which can substitute for silicon in a tetrahedron without changing significantly the size of the tetrahedron. Table 3 is a list of some cations which can be found tetrahedrally coordinated in silicate structures, and some which might conceivably be present in tetrahedral coordination. They are listed in order of increasing cation-oxygen radius ratio. The minimum radius ratio geometrically required for a tetrahedron is .225, so that any of the cations from B to Ca, listed in Table 3, can fit into an oxygen tetrahedron. Due to its large size, however, Ca distorts the tetrahedron considerably. Most of these cations also have similar electronegativity, so that their substitution for Si would not be expected to change significantly the nature of the chemical bond (Pauline 1939, p. 58). The list of the observed cation-oxygen distances indicates that the variation in the size of the tetrahedron is even less than indicated by the theoretical radius ratios. Except in the case of B and Ca

TABLE 3. SOME IMPORTANT TETRAHEDRALLY COORDINATED CATIONS IN SILICATES

Cation	Radius ratio (calculated)	Observed M—O distance ±.05 Å	Electro-negativity	Examples
B^{3+}	.25	1.50	2.0	Danburite, datolite, homolite
Be^{2+}	.28	1.60	1.5	Beryl, phenacite
As^{5+}	.30	—	2.0	—
P^{5+}	.34	—	2.1	Stillwellite
Si^{4+}	.38	1.60	1.8	Silicas, silicates
Li^{+}	.39	—	1.0	—
Al^{3+}	.41	1.78	1.5	Aluminosilicates
Ge^{4+}	.43	1.80	1.8	Many silicates
Ga^{3+}	.46	—	1.5	Many silicates
Mg^{2+}	.47	1.80	1.2	Melilite, åkermanite
Fe^{2-3+}	.48–.50	1.80	1.5–2.0	Staurolite, cordierite
Zn^{2+}	.50	1.82	1.8	Hemimorphite, hardystonite
Ti^{4+}	.55	1.82	1.6	Schlorlomite, astrophyllite
Ca^{2+}	.67	1.90	1.0	Na_2CaSiO_4

Data from Pauling (1940), Hori (1954), Smith (1954).

tetrahedra, the different cation-oxygen distances are almost equal to the cation-oxygen distances observed in the Si and Al tetrahedra.

In many silicate structures containing several tetrahedrally coordinated cations the different cations appear to occupy symmetrically different tetrahedra. In beryl the Si cations appear to occupy the tetrahedra of the hexagonal rings, and the Be cations the tetrahedra which connect these rings into continuous networks of tetrahedra. This separation of the two cations is probably not complete except in a state of high order. The milarite structure is similar to the beryl structure, except that milarite has double hexagonal rings. At room temperature there are $(Si_{.90}Be_{.10})$ cations in the tetrahedra of the hexagonal rings and $(Si_{.40},Be_{.27}Al_{.33})$ cations in the connecting tetrahedra (Ito and Sadanaga 1952). Consequently Be can be present in both tetrahedra, and the rejection of the connecting tetrahedra in the consideration of the tetrahedral frame of milarite or beryl is artificial. The only consistent treatment is the acceptance of all tetrahedra, and the classification of milarite and beryl as structures containing three-dimensional networks of tetrahedra.

There is only one important criterion which can lead to discarding a tetrahedron from consideration as part of the tetrahedral frame, namely the nature of its bonding. The tetrahedral structure of a silicate can be regarded as the frame of the crystal. This frame is a strong unit within the structure, since in each tetrahedron half or more of the cation's bond strength is expended in holding the tetrahedral frame together and less than half is expended in connecting the cation to the rest of the structure. Any tetrahedron can be part of the frame, provided that half or more of the cation's bond strength is distributed within the tetrahedral frame. If less than half of the bond strength of the cation is distributed within the frame, the tetrahedron belongs to the rest of the structure, rather than to the frame. A good example is offered by axinite. Here the four-membered rings of Si tetrahedra are connected by Al tetrahedra, but the Al's contribute less than half their bond strength to connect the Si tetrahedra and more than half to connect the Fe octahedra and B triangles.

Of course, it is expected that in a silicate a large number of tetrahedra are Si tetrahedra in order to classify the crystal chemically as a silicate. If the replacement of Si by another cation goes as far as the complete replacement of all the Si, the compound should not be called a silicate chemically, although structurally it still might be included in the silicates. An example is yttro-garnet, in which practically all the Si is replaced by Al (Yoder and Keith 1950).

By accepting the tetrahedrally coordinated cations in the tetrahedral frame of the silicates, some changes have to be made in the conventional classification of beryl, cordierite, hemimorphite, phenacite, willemite, bertrandite and melilites. Beryl and cordierite are three-dimensional networks instead of single rings, and hemimorphite, phenacite and willemite are three-dimensional networks instead of pairs of tetrahedra. Bertrandite is also a three-dimensional network instead of a complex of chains and groups of tetrahedra. In the melilites the pairs of tetrahedra become sheets of tetrahedra.

In hemimorphite, phenacite, willemite and bertrandite, all of the cations are tetrahedrally coordinated. These tetrahedra build up a neutral network, somewhat similar to that of the pure silicas. The cation-anion ratio in these minerals is higher than in SiO_2, and consequently the sharing of one oxygen by two cations would no longer give a neutral structure. In order to obtain neutrality, the oxygens are shared by up to three cations, and some of the O^{--} is replaced by $(OH)^-$.

ACKNOWLEDGMENT

The author is deeply indebted to Professor M. J. Buerger for his suggestions and constructive criticism during the preparation of this paper.

APPENDIX

The sharing coefficient of a tetrahedral structure can be obtained from the subscripts of the tetrahedrally coordinated cation (T) and anion (A) in the chemical formula. An equation has been derived for this calculation.

There is a total number of $4T$ tetrahedral corners in a chemical-formula unit, x of these are joined to anions shared by $n+1$ tetrahedra and $4T-x$ to anions shared by n tetrahedra. Then the average number of tetrahedra participating in the sharing of a corner is:

$$\begin{aligned}\text{sharing coefficient} &= \frac{x(n+1) + (4T - x)n}{4T} \\ &= \frac{x}{4T} + n \qquad (1)\end{aligned}$$

A is the number of anions per chemical formula and is the sum of the number of corners shared between $n+1$ and n tetrahedra:

$$\begin{aligned}A &= \frac{x}{n+1} + \frac{4T - x}{n} \\ &= \frac{xn + 4T(n+1) - xn - x}{n^2 + n} \\ x &= 4T(n+1) - A(n^2 + n) \qquad (2)\end{aligned}$$

Equations (1) and (2) can be combined to obtain the sharing coefficient in terms of T, A and n:

$$\begin{aligned}\text{sharing coefficient} &= \frac{4T(n+1) - A(n^2+n)}{4T} + n \\ &= n + 1 - \frac{A}{4T}(n^2 + n) + n \\ &= 2n + 1 - \frac{A}{4T}(n^2 + n) \qquad (3)\end{aligned}$$

The only unknown in equation (3) is n. Fortunately, n can be obtained from the ratio of the number of available tetrahedral corners to the number of shared corners: $4T/A$. This ratio does not express the proportion of corners shared by $n+1$ and by n tetrahedra, but it is equal to the sharing coefficient when its value is an integer. Between integers the integral part of $4T/A$ is equal to the integral part of the sharing coefficient, that is, to n in equation (3). Consequently:

$$n = \text{the integer of } \frac{4T}{A} \qquad (4)$$

In conclusion, the sharing coefficient of a tetrahedral structure can be obtained from the structural chemical formula by using equations (4) and (3).

REFERENCES

BERMAN, H. (1937), Constitution and classification of the natural silicates. *Am. Mineral.* **2,** 342–408.

BRAGG, W. L. (1930), The structure of silicates. *Zeit. Krist.* **74,** 237–305.

BRAGG, W. L. (1937), Atomic structure of minerals. Cornell Univ. Press.

EITEL, W. (1941), Physikalische Chemie der Silikate. J. A. Barth Verl. Leipzig.

Gruner, J. W. (1931), Structure of some silicates. *Am. Mineral.* **16,** 437–454.

Hori, F. (1954), On the diadochic substitution in silicates. *Mineral. Journ. Japan.* **1,** 109–125.

Ito, T., and Sadanaga, R. (1952), The crystal structure of milarite. *Acta Cryst.* **5,** 209–213.

Machatschki, F. (1928), Zur Frage der Struktur und Konstitution der Feldspate. *Zbl. Min. Geol. Palaeo. A*, 97–104.

Liebau, F. (1956), Bemerkungen zur Systematik der Kristallstrukturen von Silikaten mit hochkondensierten Anionen. *Zeit. Phys. Chem.* **206,** 73–92.

Pauling, L. (1939), The nature of chemical bond. Cornell Univ. Press.

Swartz, C. K. (1937), Classification of the natural silicates. *Am. Mineral.* **22,** 1073–1087, 1161–1174.

Smith, J. V. (1954), A review of the Al—O, Si—O distances. *Acta Cryst.* **7,** 585–595.

Strunz, H. (1937), Systematik und Struktur der Silikate. *Zeit. Krist.* **98,** 60–83.

Strunz, H. (1957), Mineralogische Tabellen. Akad. Verl. Geest and Portig.

Wells, A. F. (1954–56), The geometrical basis of crystal chemistry. Part 1–6. *Acta Cryst.* **7,** 535–554, 842–853, **8,** 32–36, **9,** 23–27.

Yoder, H. S., and Keith, M. L. (1950), Complete substitution of aluminum for silicon: the system $3MnO.Al_2O_3.3SiO_2$—$3Y_2O_5.5Al_2O_3$. *Bull. Geol. Soc. Amer.* **61,** 1516–1517.

Zoltai, T., and Buerger, M. J. (1959), The structure of coesite, the dense, high pressure form of silica. *Zeit. Krist.* **111,** 129–141.

Zoltai, T., and Buerger, M. J. (1960), The relative energies of rings of tetrahedra. *Zeit. Krist.* **114,** 1–8.

References for Structure Data

Strukturbericht. Band I-VII. *Zeit. Krist.* (1913–1939).

Structure Reports. Vol. 8–15. Intern. Union Cryst. (1940–1951).

Berger, S. V. (1952), Crystal structure of B_2O_3. *Acta Cryst.* **5,** 388–389.

Berghoff, G., Bauer, W. H., and Nowacki, W. (1958), Über die Kristallstruktur des Faujasits. *Neues Jb. Min. Mh.* **9,** 193–200.

Brauner, K., and Preisinger, A. (1956), Struktur und Entstehung des Sepioliths. *Tscherm. Min. Petr. Mitt.* **6,** 120–140.

Dent, L. S., and Smith, J. V. (1958), Crystal structure of Chabasite, a molecular sieve. *Nature* **181,** 1794–1796.

Heide, H. G. (1954), Die Struktur des Dioptas. *Naturwiss.* **41,** 402–403.

Henshaw, D. E. (1955), The structure of wadeite. *Min Mag.*, **227,** 585–595.

Ito, T., and Takeuchi, Y. (1952), The crystal structure of axinite. *Acta Cryst.* **5,** 202–208.

Ito, T., and Mori, H. (1953), The crystal structure of datolite. *Acta Cryst.* **6,** 24–32.

Miyashiro, A. (1956), Osumilite, a new silicate mineral and its crystal structure. *Am. Mineral.* **41,** 104–116.

Smith, J. V. (1953), The crystal structure of paracelsian $BaAl_2Si_2O_8$. *Acta Cryst.* **6,** 613–620.

Strunz, H. (1956), Die Zeolithe Gmelinit, Chabasit, Levyn. *Neues Jb. Min. Mh.* **7,** 250–259.

Takeuchi, Y., and Donnay, G. (1959), The crystal structure of hexagonal $CaAl_2Si_2O_8$. *Acta Cryst.* **12,** 465–470.

Ventriglia, U. (1955), La struttura della heulandite. Period. Min. **24,** 49–83.

Zemann-Hedlik, A., and Zemann, J. (1955), Die Kristallstruktur von Petalit $LiAlSi_4O_{10}$. *Acta Cryst.* **8,** 781–787.

Zviagin, B. B. (1957), Determination of the structure of celadonite by electron diffraction. *Russ. Phys. Cryst.* **2,** No. 3, 388–394.

Manuscript received December 20, 1959.

THE AMERICAN MINERALOGIST, VOL. 45, SEPTEMBER-OCTOBER, 1960

PROTO-AMPHIBOLE, A NEW POLYTYPE

G. V. Gibbs, F. D. Bloss, and H. R. Shell,* *Electrotechnical Experiment Station, Bureau of Mines, U. S. Department of the Interior, Norris, Tenn.*

Abstract

An orthorhombic amphibole ($a_0=9.330$, $b_0=17.867$, $c_0=5.286$ Å, ± 0.05 per cent with space group *Pnmn* or *Pn2n*) has been identified as a phase within the system Li_2O—MgO—MgF_2—SiO_2. Its unit cell is one half that of anthophilite ($a_0=18.5$, $b_0=17.9$, $c_0=5.28$ Å; space group *Pnma*). A new structure type for amphibole, based on the space group *Pnmn*, is proposed. The term proto-amphibole is used to describe this new polytype, since it appears structurally related to the amphiboles in the same way that proto-enstatite is to the pyroxenes.

Chemical analysis reveals the proto-amphibole studied in greater detail to have the following formula: $Li_{.64}Na_{.05},Li_{.48}Mg_{1.52}.Mg_{5.00}Si_{7.93}:O_{21.91}F_{2.09}$.

Its optical constants for sodium light are: $\alpha=1.5759$, $\beta=1.5870$, $\gamma=1.5928$, $2V_{(calc.)}=71.4°$, $2V_{(meas.)}=74°$. The presence of lithium and the absence of calcium in the melts studied seems essential to the formation of proto-amphibole, a monoclinic fluor-amphibole being otherwise developed.

Introduction

The synthetic asbestos investigations of the Electrotechnical Experiment Station of the Federal Bureau of Mines at Norris, Tenn., recently led to the synthesis of some orthorhombic amphiboles which, on preliminary study, appeared to the fluoride analogs of anthophyllite. Powder diffraction data at first seemed to confirm this identification. However, precession, cone-axis, and rotation diagrams of single crystals revealed: (1) A repeat unit along the *a*-axis which was one-half that of anthophyllite and (2) a space group which was *Pnmn* or *Pn2n* rather than *Pnma* as is known for anthophyllite.

These amphiboles thus belong to a distinct new structural type which, for reasons to be developed, may be referred to as proto-amphibole. Details of the study are here presented to establish this new structure and to indicate criteria for the recognition of natural representatives. One of us (G.V.G.) is currently testing the postulated structure by Fourier synthesis at The Pennsylvania State University.

Chemical Synthesis

An orthorhombic fluor-amphibole was first observed as a phase in the system Li_2O—MgO—MgF_2—SiO_2. Following this observation a number of melts (19-43, et seq.) were studied to determine the bulk composition most favorable for the formation of this phase.

---

* Academic addresses for F.D.B. and G.V.G. are, respectively, Department of Geology, Southern Illinois University, Carbondale, Ill., and Department of Mineralogy, Pennsylvania State University, University Park, Pa.

The procedure used was to melt the well-mixed raw materials in a graphite crucible, which was itself protected from oxidation by being sealed in a fire-clay crucible. After melting was effected (within the range 1350°–1450° C.), the temperature was rapidly lowered by 100°, then at a rate of 10°–15° C. per hour to 1000° C. For melt compositions subject to reduction by graphite, the procedure was varied in that only a sealed fire clay crucible was used. Consequently, it was necessary to cool these melts more rapidly in order to prevent excessive contamination. Raw materials were LiF, Li_2CO_3, MgF_2, MgO, SiO_2 (−200 mesh quartz sand), $CaCO_3$, and various oxides or carbonates.

The experiments of Table 1, as well as others, appear to indicate that Li^+ is essential for the formation of proto-amphibole. The efficacy of Li^+, however, appears affected by the nature of the other ions in the melt. For example, when Al^{+++} is present, the Li^+ combines with Al^{+++} to form β-spodumene but no fluor-amphibole; if Cl^- is present, the Li^+ containing phase is LiCl, and again no fluor-amphibole is formed.

Neither Na^+ nor K^+ yielded proto-amphibole when substituted completely for Li^+ in otherwise favorable batch compositions. With Na^+, the monoclinic fluor-amphibole, $Na \cdot NaMg \cdot Mg_5 \cdot Si_8{:}O_{22}F_2$, was obtained instead. *X*-ray and optical data on this substance will be reported separately (Miller and Gibbs, in press). K^+ always yielded a sheet structure (Shell, et al., 1958). If the lithium content was maintained (Na^+ and K^+ absent), orthorhombic fluor-amphibole was formed even when Mn^{++}, Co^{++}, Cu^{++}, Fe^{++}, or Zn^{++} were partially substituted for Mg^{++} in the batch composition. However, if Ca^{++} was substituted to the extent of $\frac{1}{2}$ or $\frac{2}{7}$ of the amount of Mg^{++} in the batch composition, monoclinic rather than orthorhombic fluor-amphiboles were formed (Table 1, 19-12). MgO—MgF_2—SiO_2 systems (Fujii, T. and Eitel, W., 1957) did not yield orthorhombic amphiboles even when Fe^{++} was partially substituted for Mg^{++}. 1 or 2 Ni^{++}, substituted for equivalent Mg^{++}, favored silicates with a sheet structure.

The fluoride content of the batch compositions strongly affected the yield of orthorhombic amphibole. Batch compositions may be compared to the theoretical fluoride content in fluor-amphiboles which is $2F^-$ per unit formula (e.g. fluor-richterite, $Na \cdot Na\,Ca \cdot Mg_5 \cdot Si_8{:}O_{22}F_2$; or to that in fluor-micas which is $4F^-$ (e.g. fluor-phlogopite, $K_2 \cdot Mg_6 \cdot Al_2Si_6{:}O_{20}F_4$). These may be written alternately as $Na \cdot Na\,Ca \cdot Mg_5 \cdot (F_2)\,(Si_4O_{11})_2$ and $K_2 \cdot Mg_6 \cdot (F_4)(Al\,Si_3O_{10})_2$, respectively.

In the Li_2O—MgO—MgF_2—SiO_2 system, an 7:O ratio of 1:5 yielded fluor-micas or fluor-montmorillonites as the major phase; whereas F:O ratios approaching 1:11 gave fluor-amphibole as the major phase. This tendency was not necessarily true for all cationic substitutions, some of which (e.g. $\mathrm{Zn^{++}}$) never yielded a fluor-mica.

TABLE 1.—BATCH COMPOSITIONS AND RESULTING PHASES

Exp. No.	Batch Composition	Phases formed; remarks
19-41	$\mathrm{Li \cdot LiMg \cdot Mg_5 \cdot Si_8 : O_{21}F_4}$	97% water-swelling fluor-montmorillonoid; 3% acicular proto-amphibole
19-43	$\mathrm{Li \cdot Ca_2 \cdot Mg_5 \cdot BSi_7 : O_{21}F_4}$	Monoclinic fluor-amphibole major phase
19-45	$\mathrm{Li \cdot Mg_2 \cdot Mg_5 \cdot AlSi_7 : O_{21}F_4}$	Humites are major phases; some beta spodumene; mica and amphibole absent
19-47	$\mathrm{Li \cdot MnMg \cdot Mg_5 \cdot BSi_7 : O_{21}F_4}$	10% water-swelling platy mineral; 90% orthorhombic fluor-amphibole
19-48	$\mathrm{Li \cdot LiMg \cdot Mg_5 \cdot B_2Si_6 : O_{20}F_4}$	95% fluor-montmorillonoid; 5% norbergite, fluor-amphibole
19-49	$\mathrm{Li \cdot LiCo^{++} \cdot Mg_5 \cdot Si_8 : O_{21}F_4}$	20% fluor-montmorillonoid; remainder orthorhombic fluor-amphibole
19-50	$\mathrm{Li \cdot LiCu^{++} \cdot Mg_5 \cdot Si_8 : O_{21}F_4}$	Similar to 19–49, but 50% or more of $\mathrm{Cu^{++}}$ was as oxide
19-52	$\mathrm{Li \cdot LiNi^{++} \cdot Mg_5 \cdot Si_8 : O_{21}F_4}$	Very fine, fluor-montmorillonoid; no fluor-amphibole
19-53	$\mathrm{Li \cdot LiZn^{++} \cdot Mg_5 \cdot Si_8 : O_{21}F_4}$	Fluor-montmorillonoid absent; orthorhombic fluor-amphibole present
19-64	$\mathrm{Li \cdot LiMg \cdot Mg_5 \cdot B_2Si_6 : O_{20.5}F_3}$	75% fluor-montmorillonoid; 25% proto-amphibole (see 19-47)
19-65	$\mathrm{Li \cdot LiMg \cdot Mg_5 \cdot B_2Si_6 : O_{22}F_2}$	Fluor-montmorillonoid minor; largely orthorhombic fluor-amphibole (see 19-47, 19-64)
19-69	$\mathrm{Li_{.5} \cdot Mg_2 \cdot Mg_5 \cdot Si_8 : O_{21.25}F_4}$	95% fluor-montmorillonoid; 5% tridymite; no fluoramphibole
19-71	$\mathrm{Mg_{.5} \cdot Mg_2 \cdot Mg_5 \cdot Si_8 : O_{21.5}F_4}$	No fluor-amphibole or fluor-montmorillonoid
19-73	$\mathrm{Li \cdot LiMg \cdot Mg_5 \cdot Si_8 : O_{21.95}F_{2.1}}$	20% fluor-montmorillonoid; 80% proto-amphibole
25-160	$\mathrm{Li \cdot LiCa \cdot Mg_5 \cdot Si_8 : O_{21.5}F_3}$	Major phase formed was monoclinic fluor-amphibole
19-12	$\mathrm{Li \cdot LiCa \cdot Mg_5 \cdot Si_8 : O_{21.5}F_3}$	Monoclinic fluor-amphibole was a major phase (75%); fluor-montmorillonoid phase minor (25%); fluor-amphibole phase contained 8. wt. % CaO
19-86	$\mathrm{Li \cdot LiMg \cdot Mg_5 \cdot Si_8 : O_{22.5}F_1}$	Fluor-montmorillonoid, 10%; orthorhombic fluoramphibole, 55%, enstatite$_1$ 35%
19-87	$\mathrm{Li \cdot LiMg \cdot Mg_5 \cdot Si_8 : O_{23}F_0}$	Note that fluoride was *absent* from batch; products were: clinoenstatite, 50–60%; cristobalite, 20%; "Mg equivalent of petalite," 30%; differential thermal curves showed a phase ($\mathrm{Li_2MgSiO_4}$?) with reversible inversion at 880° C.

CHEMICAL FORMULA

The proto-amphibole synthesized from batch composition 19-41 (Table 1) was chemically analyzed and its ionic composition was calculated by two different methods. In the first method the total mass units (ZM) of the unit cell were determined from the standard formula:

$$ZM = \frac{\rho V \times 10^{24}}{1.66 \times 10^{-24}}$$

where ρ and V represent the crystal's measured density and unit cell volume. For this particular proto-amphibole, as is discussed later, these were determined to be 2.928 g. cm.$^{-3}$ (at 21° C.) and 881.22 Å^3, respectively. Inserting these values in the foregoing equation, ZM can be calculated to be 1554.258 mass units. The chemical analysis (col. 1, Table 2) permits calculation of the amount of the mass units of each chemical component in the unit cell (col. 2, Table 2). Consequently, the relative numbers of different cations and fluoride ions in the unit cell (col. 4) were calculated by dividing the value in col. (2) by the equivalent weight in col. (3). Assuming $Z=2$, the chemical formula for proto-amphibole is determined, except for oxygen, by halving the values in col. (4). Thus $Na_{.04}\ Li_{1.12}\ Mg_{6.50}\ Si_{7.89}\ O_xF_{2.09}$. Assuming sufficient oxygen to neutralize

TABLE 2. CHEMICAL ANALYSIS OF PROTO-AMPHIBOLE AND IONIC FREQUENCIES

	(1) Analysis (wt. %)	(2) Mass units in unit cell*	(3) Equivalent weight of oxides, etc.	(4) Number of ions per unit cell
SiO_2	60.68	948.43	60.06	Si 15.79
MgO	33.51	523.76	40.32	Mg 12.99
Li_2O	2.14	33.45	14.94	Li 2.24
CaO	0.0	—	—	
Na_2O	0.17	2.66	30.99	Na 0.08
F	5.07	79.25	19.00	F 4.17
Ignition loss 350°	0.40	—		
	101.97	1587.55		
Less O=F	2.13	33.30		
Total	99.84	1554.25		

* Results in col. (1) multiplied by 1554.258/99.44. It will be noted that in this method the total of 1554.25 is obtained first, then the portions comprising the total are calculated from the chemical analysis in weight %.

all unsatisfied cations, as well as grouping the ions according to their presumed structural positions, the formula becomes

$$\mathrm{Na_{.04}Li_{.62}\cdot Li_{.50}Mg_{1.50}\cdot Mg_{5.00}\cdot Si_{7.89}\colon O_{21.82}\cdot F_{2.09}}.$$

Calculating the formula on the basis of 24 anions using the method of Shell and Craig (1956), the result is

$$\mathrm{Na_{.05}Li_{.64}\cdot Li_{.48}Mg_{1.52}\cdot Mg_{5.00}\cdot Si_{7.93}\colon O_{21.91}\cdot F_{2.09}}.$$

The two formulae, each calculated on a different basis, thus show excellent agreement.

OPTICAL DATA

The optical properties of the proto-amphiboles studied were obtained using a 5-axis universal stage, a monochromator, and the standard single variation technique. All crystals were biaxial negative and exhibited parallel extinction. The optical data for typical proto-amphiboles are summarized in Table 3 (A, B, and C); the α and β indices cited are believed accurate to ± 0.0005. Each measured value for $2V_D$ (presented as footnotes to the table) represents an average of eighteen measurements on nine different crystals; 95 per cent of these individual measurements varied by less than one degree from the average value.

The close physical and chemical resemblance of the synthetic proto-amphibole to anthophyllite invites comparison between their optical properties. Accordingly, the data for two natural anthophyllites (Rabbitt, 1948, p. 291) were tabulated (D and E, Table 3), these two particular anthophyllites being chosen for their chemical similarity to the proto-amphibole synthesized. Compared to these anthophyllites, the synthetic proto-amphibole possessed significantly lower dispersion ($N_f - N_c$) and a smaller 2V. In addition proto-amphibole 19-41A, as well as two others examined microscopically, was optically negative for all wavelengths of light used whereas Rabbitt indicates the optic sign of anthophyllite to be often positive. The generally lower indices of the proto-amphibole compared with the natural anthophyllites may be the result of the complete substitution of fluorine for hydroxyl. Such substitution has been shown to lower the indices of refraction in the case of both fluor-phlogopite (Kohn and Hatch, 1955, p. 15) and fluor-tremolite (Comeforo and Kohn, 1954, p. 543).

MORPHOLOGY

Synthetic proto-amphibole crystallized in an acicular habit, the needles consisting of several parallel-to-sub-parallel individuals, each elongated parallel to the *c*-axis. Individual crystals with well developed faces were rare. The best developed faces were of the {110} form. The {100} form occasionally occurred as narrow, poorly developed faces. An

TABLE 3. COMPARISON OF OPTICAL CONSTANTS OF SYNTHETIC PROTO-AMPHIBOLE WITH NATURAL ANTHOPHYLLITES

λ(Å)	γ	β	α	$\gamma-\alpha$	$\gamma-\beta$	Optic sign; 2V
A. Synthetic proto-amphibole No. 19-41A						
F (4861)	1.5989	1.5930	1.5816	0.0173	0.0061	(−); 71° (calc)
D(5893)	1.5928	1.5870	1.5759	0.0169	0.0058	(−); 71.4° (calc)[a]
C (6563)	1.5903	1.5845	1.5736	0.0167	0.0057	(−); 71.8° (calc)
N_f-N_c	.0086	.0085	.0080			
B. Synthetic proto-amphibole No. 18-64B						
F (4861)	1.5987	1.5923	1.5808	0.0181	0.0064	(−); 71.3° (calc)
D(5893)	1.5938	1.5869	1.5742	0.0196	0.0069	(−); 72.3° (calc)[b]
C (6563)	1.5918	1.5847	1.5714	0.0204	0.0071	(−); 71.8° (calc)
N_f-N_c	.0069	.0076	.0094			
C. Synthetic proto-amphibole No. 19-73C						
F (4861)	1.6049	1.5996	1.5920	0.0129	0.0053	(−); 79.4° (calc)
D(5893)	1.5979	1.5926	1.5812	0.0167	0.0053	(−); 68.2° (calc)[c]
C ((6563)	1.5950	1.5897	1.5766	0.0184	0.0053	(−); 64.5° (calc)
N_f-N_c	.0099	.0099	.0154			
D. Natural Anthophyllite (Rabbitt, 1948, p. 291, No. 29)						
F (4861)	1.6451	1.6365	1.6365	0.0146	0.0086	(+); 80°
D(5893)	1.6354	1.6270[d]	1.6180	0.0174	0.0084	(−); 88°
C (6563)	1.6315	1.6230	1.6127	0.0188	0.0085	(−); 84°
N_f-N_c	0.0136	0.0135	0.0178			
E. Natural Anthophyllite (Rabbitt, 1948, p. 291, No. 30)						
F (4861)	1.6505	1.6430	1.6340	0.0165	0.0075	(−); 85°
D(5893)	1.6410	1.6280	1.6162	0.0248	0.0130	(+); 88°
C (6563)	1.6372	1.6205	1.6092	0.0280	0.0167	(+); 79°
N_f-N_c	0.0133	0.0225	0.0248			

[a] By direct measurement $2V_D=74°$

[b] By direct measurement $2V_D=75.2°$

[c] By direct measurement $2V_D=73°$

[d] Rabbitt's original paper has 1.6370, but this is presumed to be 1.6270.

excellent cleavage occurred parallel to {110}. The angle between the (110) and $(1\bar{1}0)$ faces was determined with an Eichner two circle goniometer to be 55°02′; individual measurements varied as much as 10′ from these averages (although usually they were within 5′).

DIFFRACTION DATA

The x-ray diffraction data for synthetic proto-amphibole were obtained by means of a Norelco diffractometer from a glass slide smear of a mixture of powdered proto-amphibole and a synthetic spinel ($MgAl_2O_4$) internal standard. The smear was prepared by the standard technique of mixing a small portion of powder with a lacquer of 10 parts cellulose acetate dissolved in acetone and carefully spreading the resultant slurry over the slide as a uniformly thin, translucent layer.

The instrumental settings of the diffractometer were: Time constant, 4 seconds; multiplier, 1.0; scale factor, 8 and 16; divergence and scatter slits, 1°; receiving slits, 0.006″; scanning speed, $\frac{1}{4}$ degree 2θ per minute; chart scale, $\frac{1}{2}$ degree per inch; filtered Cu Kα radiation.

Three diffraction records were made within the range 5 to 70 degrees 2θ. Following each scan of this range, the smear mount was moved slightly in the clip-holder to alter the portion of the smear being x-rayed. The 2θ Bragg reflections recorded on the diffraction charts were located by measuring the centers of the peaks at two-thirds height as proposed by Donnay and Donnay (1952). This method of peak location was, however, only considered suitable when the α_1 and α_2 spectral components were completely resolved. For unresolved or partially resolved maxima, the peak locations were obtained by measuring their centers at half height (Smith and Sahama, 1954). The Bragg reflections were corrected by means of an internal standard and comparable 2θ values from the three separate charts were averaged and converted into Q-values from the Donnay and Donnay (1951) tables. The resultant diffraction data (Table 4) were indexed on the basis of the following orthorhombic cell dimensions:

$$a_0 = 9.330, \qquad b_0 = 17.867, \qquad c_0 = 5.286 \text{ Å}(\pm 0.05\%).$$

On the basis of powder diffraction data only, proto-amphibole may be mistaken for anthophyllite. For example, the values in Table 4 could also have been indexed on an orthorhombic cell comparable in size to that of anthophyllite (i.e. in our case $a_0 = 18.661$, $b_0 = 17.867$, and $c_0 = 5.286$ Å). The resultant indexing is very similar to that for anthophyllite (Table 5). However, even when thus indexed, proto-amphibole can be differentiated from anthophyllite since for it there is an absence of all reflections for which h is odd indication that the value of a used in indexing is double the true value.

To confirm the dimensions of the unit cell, as well as to determine the space group, single crystal data from proto-amphibole were obtained. Cone-axis and rotation diagrams about [100], [010], and [001], confirmed the cell edges a 9.330, b 17.867, c 5.286 Å. Particular attention was given

TABLE 4. *X*-RAY POWDER DIFFRACTION DATA FOR SYNTHETIC PROTO-AMPHIBOLE
Cu Kα = 1.54178 Å, Cu Kα_1 = 1.54050 Å

hkl	I/I$_1$	Observed values			Calculated values*			Q×10^5
		d	2θ**	Q	*d*	2θ	Q	
020	5	8.962	9.85(α)	.01245	8.934	9.90(α)	.01253	−8
110	67	8.276	10.69(α)	.01460	8.270	10.70(α)	.01462	−2
130	4	5.019	17.67(α)	.03970	5.020	17.67(α)	.03968	2
200	14	4.666	19.02(α)	.04593	4.665	19.02(α)	.04595	−2
040	28	4.469	19.868(α)	.05008	4.467	19.876(α)	.05012	−4
220	1	4.137	21.48(α)	.05844	4.136	21.49(α)	.05847	−3
131	16	3.645	24.428(α)	.07532	3.640	24.45(α)	.07546	−14
150	6	3.339	26.697(α)	.08969	3.337	26.71(α)	.08978	−9
221	13	3.260	27.358(α)	.09411	3.258	27.38(α)	.09425	−14
240	33	3.226	27.631	.09612	3.228	27.62	.09603	9
310	100	3.063	29.134	.10663	3.064	29.12	.10651	12
231	7	3.017	29.581(α)	.10967	3.017	29.61(α)	.10990	−23
151	22	2.822	31.709(α)	.12559	2.822	31.71(α)	.12557	2
330	25	2.759	32.424	.13138	2.757	32.45	.13156	−18
102	13	2.543	35.253	.15455	2.543	35.26	.15460	−5
161 251	21	2.499	35.90	.16009	2.500	35.89	.16002	7
350	4	2.346	38.33(α)	.18166	2.346	38.33	.18167	−1
400	4	2.334	38.577(α)	.18361	2.333	38.59(α)	.18377	−16
261	7	2.268	39.708	.19442	2.268	39.71	.19448	−6
171 080	8	2.233	40.360	.20059	2.233	40.35	.20047	12
421	4	2.077	43.54	.23185	2.076	43.56	.23209	−24
361	7	1.993	45.48	.25185	1.992	45.49	.25191	−6
510	8	1.856	49.038	.29028	1.856	49.038	.29028	0
530	4	1.781	51.26	.31537	1.781	51.26	.31535	2
461	8	1.735	52.726	.33236	1.735	52.723	.33232	4
480	3	1.613	57.05	.38438	1.613	57.04	.38424	14
1.11.0	5	1.600	57.56	.39069	1.600	57.54	.39049	20
372	2	1.581	58.31	.40004	1.581	58.30	.39993	11
561	14	1.515	61.098	.43544	1.515	61.117	.43569	−25
0.12.0	10	1.489	62.303	.45105	1.489	62.303	.45105	0
661	11	1.334	70.55	.56214	1.334	70.53	.56204	10

* Based on the following direct and reciprocal lattice constants:
$a_0 = 9.330$; $b_0 = 17.867$; $c_0 = 5.286$ Å ± 0.005
$a^{*2} = .0114860$; $b^{*2} = .0031323$; $c^{*2} = .035767$

** Values for Cu Kα_1 radiation unless otherwise indicated.

TABLE 5. COMPARISON BETWEEN OBSERVED DIFFRACTION DATA FOR SYNTHETIC PROTO-AMPHIBOLE AND NATURAL ANTHOPHYLLITE

Synthetic proto-amphibole No. 19-41A			Natural Anthophyllites					
			Specimen from Falun, Sweden[a]			Gedrite from Inverness-Shire[b]		
hkl	d_{hkl}	I/I_1	*hkl*	d_{hkl}	I[c]	*hkl*	d_{hkl}	I/I_1
(020)	8.962	5				—	8.99	50
(210)	8.276	67	(210)	8.22	4	(210)	8.28	70
						—	7.19	50
(230)	5.019	4	(230)	5.05	2			
(400)	4.666	14						
(040)	4.469	28	(040)	4.52	3	(040)	4.45	30
(420)	4.137	1	(420)	4.13	3	(420)	4.11	30
			(131)	3.88	1	(131)	3.87	15
(231)	3.645	16						
			(321)	3.67	3	(321)	3.63	50
(250)	3.339	6	(331)	3.34	1			
(421)	3.260	13						
(440)	3.226	33	(440)	3.24	5	(440)	3.21	85
(610)	3.063	100	(610)	3.05	8	(610)	3.04	100
(431)	3.017	7						
			(521)	2.87	2	—	2.87	50
(251)	2.822	22	(251)	2.84	3	—	2.81	50
(630)	2.759	25	(630)	2.75	2	(630)	2.74	50
			(351)	2.69	3			
			(161)	2.59	3	—	2.66	50
(202)	2.543	13	(202)	2.54	4	(202)	2.56	50
						—	2.53	50
(451)	2.499	16	(451)	2.51	3	(451)	2.49	50
(261)			(261)					
(650)	2.346	4	(302)	2.43	2			
(800)	2.334	4	(551)	2.32	1	(551)	2.31	30
			(402)	2.29	1			
(461)	2.268	7						
(271)	2.233	8						
(080)								
			(502)	2.15	3	(502)	2.14	30
			(561)	2.14	4	(561)	2.12	30
(821)	2.077	4	(840)	2.065	2	(840)	2.06	15
(661)	1.993	7	(661)	1.998	2			
			(751)	1.982	1	(751)	1.98	15
			(571)	1.965	1			

[a] Calculated from data of Johannson (4, pp. 35–36) using 1.9373 as wavelength Fe K_α.

[b] As given by American Society for Testing Materials card 7-289 for gedrite.

[c] As given by Johannson (4).

TABLE 5 (*continued*)

Synthetic proto-amphibole No. 19-41A			Natural Anthophyllites					
			Specimen from Falun, Sweden[a]			Gedrite from Iverness-Shire[b]		
hkl	d_{hkl}	I/I_1	*hkl*	d_{hkl}	I[c]	*hkl*	d_{hkl}	I/I_1
			(702)	1.872	1			
			(191)	1.867				
(10.1.0)	1.856	8						
			(860)	1.837	3	(860)	1.84	15
(10.3.0)	1.781	4						
(861)	1.735	8	(861)	1.735	2	—	1.73	15
			(812)					
(880)	1.613	3	(961)	1.618	4	—	1.61	15
			(880)					
			(2.11.0)					
(2.11.0)	1.600	5						
			(053)	1.584	2			
(672)	1.581	2						
(12.0.0)	1.56	3	(12.0.0)	1.546	2	(12.0.0)	1.54	15
(10.6.1)	1.52	14	(10.6.1)	1.513	2			
			(0.12.0)	1.505	4	(0.12.0)	1.51	50
			(6.11.0)	1.451	1			
			(11.0.2)	1.421	2			
			(11.6.1)	1.418	3	(11.6.1)	1.42	15
						—	1.41	30
			(663)	1.364	2			
(12.6.1)	1.33	11	(12.6.1)	1.331	3	—	1.33	15

to determining the repeat unit along the *a*-axis (since for proto-amphibole this value was one-half that for anthophyllite, the only other orthorhombic amphibole known until now). An intentionally over-exposed (113 hour) rotation diagram about [100] (Fig. 1) confirmed the a_0 spacing of proto-amphibole as 9.330 Å.

Additional data support the accuracy of the cell parameters. The calculated specific gravity, 2.940 g. cm.$^{-3}$, is in close agreement with that measured by the sink-float method, 2.928 g. cm.$^{-3}$ at 21° C. (± 0.002). The angle $(110)\wedge(1\bar{1}0)$ calculated from the values of a_0 and b_0 is 55°06′; the goniometrically measured value was 55°02′.

Precession diagrams (Figs. 2, 3) indexed on the basis of the following orthorhombic cell dimensions

$$a_0 = 9.330, \qquad b = 17.867, \qquad c = 5.286 \text{ A}(\pm .005.)$$

indicated the following conditions for Bragg reflection: *hkl*, no conditions; $0kl$, $k+l=2n$; $h0l$, no conditions; $hk0$, $h+k=2n$; $h00$ $h=2n$; $0k0$, $k=2n$; and $00l$, $l=2n$. The space groups obeying these rules are *Pnmn* and *Pn2n*. The distribution of intensities of the diffraction spots recorded on the precession diagrams indicated orthorhombic symmetry. Transmission Laue diagrams further confirmed this.

Postulated Structure

There is little doubt that the material under investigation is an amphibole since: (1) The observed intensities for proto-amphibole are very similar to the intensities of corresponding reflections recorded for amphibole minerals; (2) The values of the repeat units, b_0 and c_0 (i.e. 17.867 an 5.286) are typical for an amphibole chain; (3) The goniometrically measured angle for the prismatic cleavage, 55°02′, is also typical and (4). Th ratio Si:O:F found in the unit cell is very close to 8:22:2, values characteristic of fluor-amphiboles. Of the two space groups possible for proto amphibole, i.e. *Pnmn* or *Pn2n*, only *Pnmn* can be reconciled to an amphi bole chain. Thus *Pnmn* is the more likely of the two space groups.

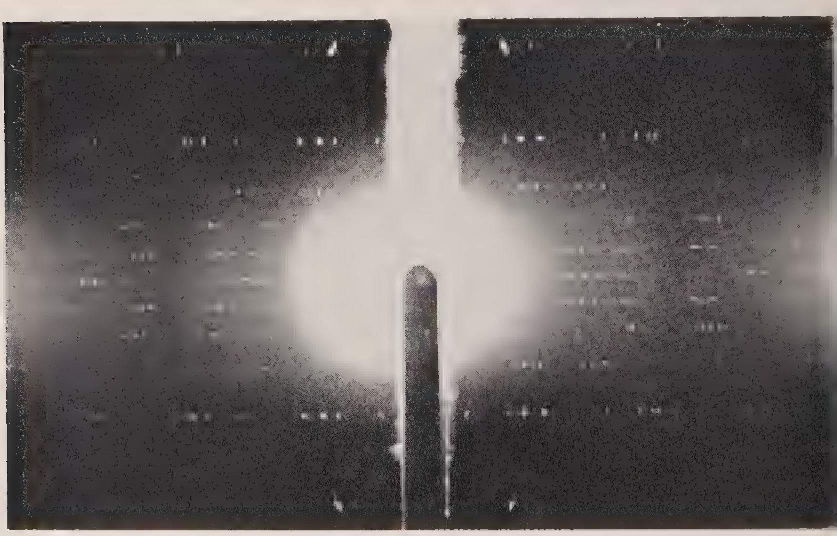

Fig. 1. *X*-ray rotation diagram about the *a* axis of proto-amphibole; Cu Kα radiation, 113 hour exposure.

Employing atomic coordinates largely based on those found for proto enstatite (Smith, 1959), a structure whose atoms are consistent with th space group *Pnmn* has been proposed for proto-amphibole (Figs. 4, 5) The structure is derived from that of proto-enstatite by placing a mirro plane parallel to (010) so as to produce a doubling of the pyroxene-typ

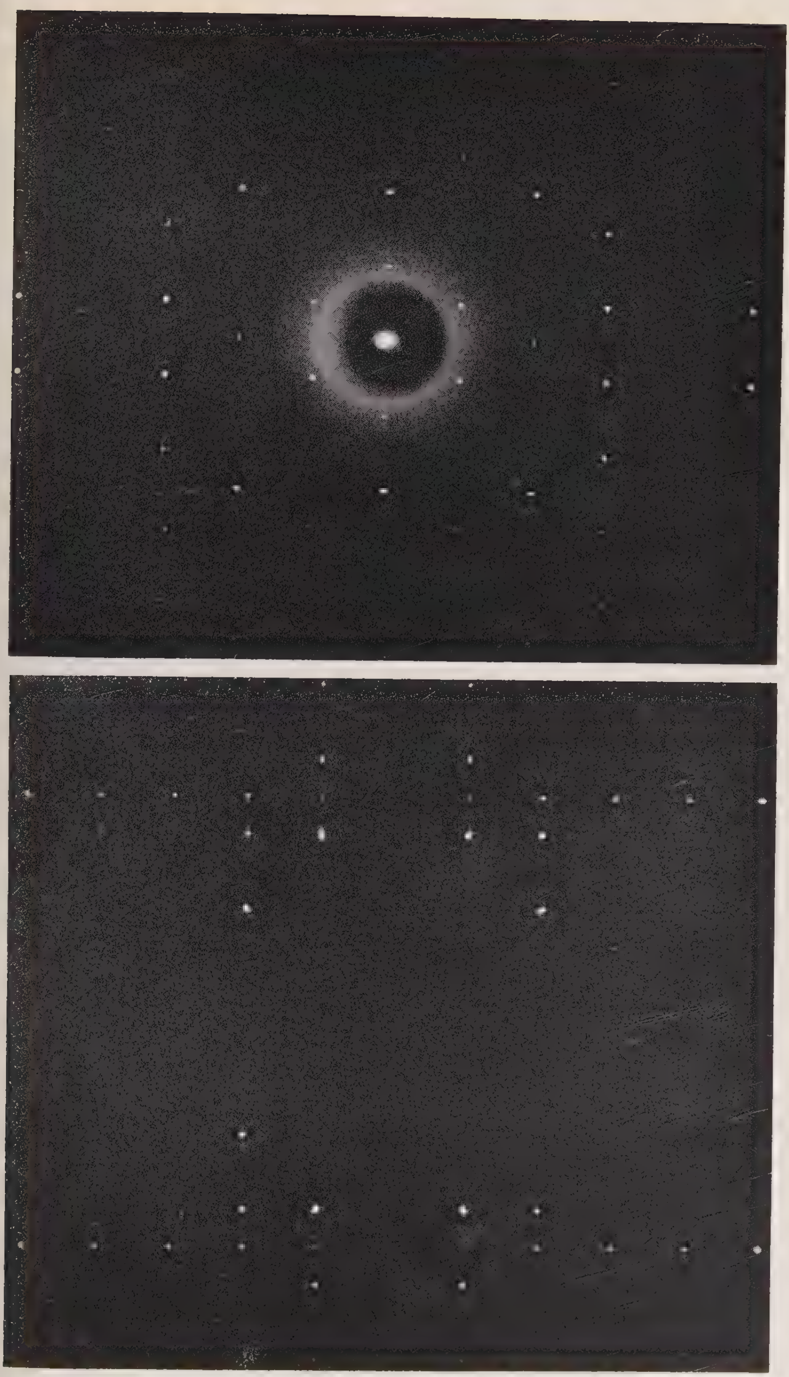

FIG. 2. (*a*) An *hk*0 precession diagram of proto-amphibole; Cu Kα radiation, 18 hour exposure; a^* horizontal, (*b*) An *hk*1 precession diagram; a^* horizontal.

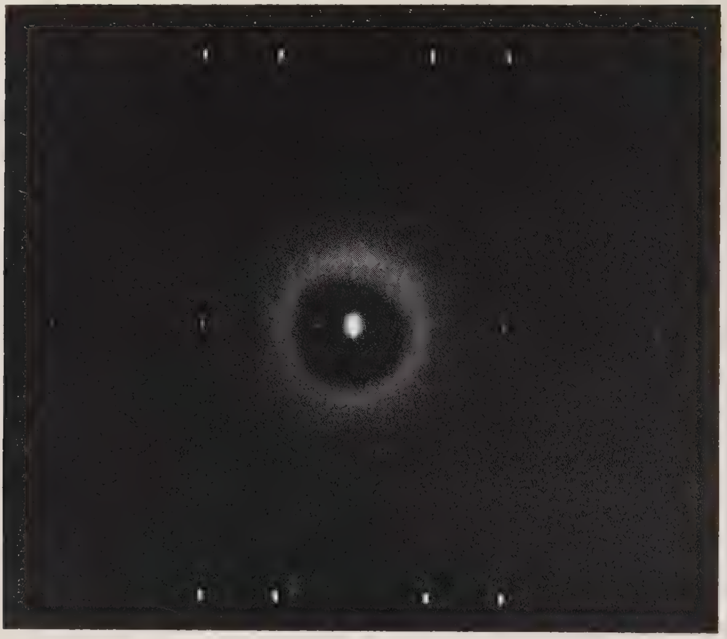

FIG. 3. An $h0l$ precession diagram of proto-amphibole; Cu Kα radiation, 18 hour exposure; a^* horizontal.

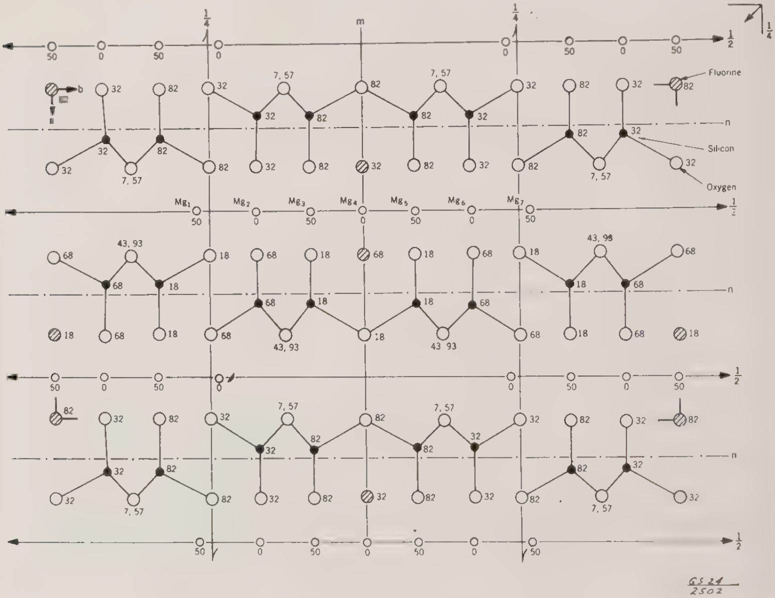

FIG. 4. Proposed structure for proto-amphibole projected on (001).

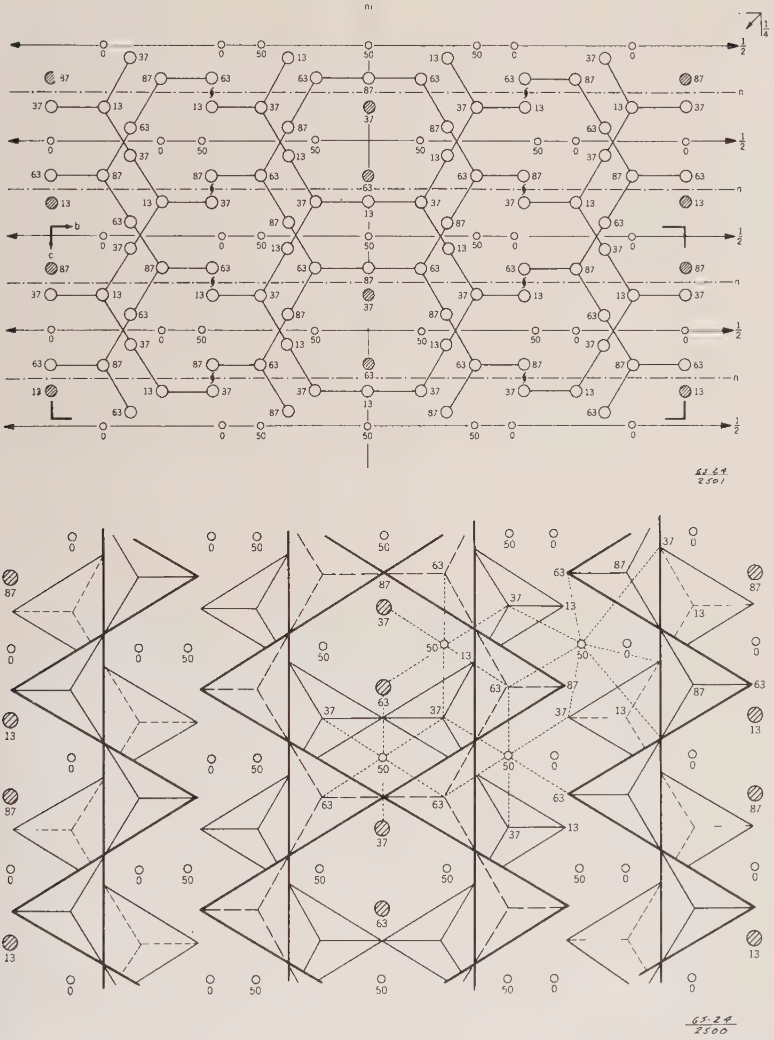

FIG. 5. (*a*) Proposed structure for proto-amphibole projected on (100). (*b*) (100) projection showing silicon-oxygen tetrahedra.

chains of proto-enstatite. This operation is similar to that used by Warren (1929) to derive the structure of tremolite from that of diopside. The resultant structure for proto-amphibole differs from that of the typical amphibole in that neighboring chains are slightly shifted relative to each other along the *c*-axis, a feature necessary to produce the orthorhombic symmetry without doubling the cell as in anthophyllite.

In Figs. 4, 5 the eight-fold-coordinated cation sites are labelled Mg_1 and Mg_7; the six-fold sites, Mg_2–Mg_6. The cation sites of twelve-fold coordination are not labelled. The details of the occupancy of these different cation sites by Mg^{++} and Li^+ are not known, the questions posed by Zussman (1955, p. 301) remaining unanswered with respect to proto-amphibole pending its structural analysis. Some conjectures may be made, however. For example, the inter-chain shift in proto-amphiboles as compared to tremolite restricts the space available for cation positions Mg_1 and Mg_7. Subject to revision following a structural analysis, the extent and significance of this restriction can be assessed by comparing the various Mg_7—O inter-atomic distances of the postulated structure with the corresponding Ca—O inter-atomic distances given by Zussman (1955, Fig. 3, p. 305) for actinolite (Table 6). Comparison of these distances with the average of the Goldschmidt, Pauling, and Zachariasen inter-atomic distances for Li^+—$O^=$, Mg^{++}—$O^=$, and Ca^{++}—O, i.e. 2.08, 2.09, and 2.39 Å, respectively, indicates that, in contrast to its role in monoclinic amphiboles, calcium ions are too large to occupy the Mg_1 and Mg_7 sites in proto-amphibole. The chemical data supports this explanation: batch compositions to which calcium was added always yielded monoclinic amphiboles rather than proto-amphiboles (Table 1).

Table 6. Comparison of Cation-Oxygen Distances of the Eight-fold Coordinated Sites in Proto-Amphibole and Actinolite

	Inter-atomic distances (Å)			
Mg_7-O (proto-amphibole)	2.1	1.9	2.0	3.0
Ca-O (actinolite)	2.32	2.34	2.6	2.7

Acknowledgments

The writers are indebted to Mr. Irving L. Turner for the optical measurements, Mr. David Cummings for aid in drafting, Mr. M. V. Denny for the density determination, to Mr. R. L. Craig for chemical analyses, and to Drs. J. V. Smith and William L. Brown for their critical readings of the manuscript. Dr. John Koster's encouragement was appreciated.

References

Comeforo, J. E. and Kohn, J. A. (1954), Synthetic asbestos investigations, I: Study of synthetic fluor-tremolite, *Am. Mineral.*, **39**, 537–548.

Donnay, G. and Donnay, J. D. H. (1951), *Tables for the interpretation of X-ray diffraction data:* Baltimore, Crystallographic Laboratory, The Johns Hopkins University.

——— (1952), The symmetry change in the high-temperature alkali-feldspar series: *Am. J. Sci.*, Bowen vol., 115–132.

Fujii, Takashi, and Eitel, Wilhelm (1957), Solid state reaction in the system MgO-MgF_2-SiO_2: *University of Toledo, Inst. Silicate Res., Inf. Circ.* No. 11.

Johansson, K. (1930), Vergleichende Untersuchungen an Anthophyllit, Grammatit und Cummingtonit, *Zeits. f. Krist.*, 31–51.

Kohn, J. A. and Hatch, R. A., (1955), Synthetic mica investigations, VI: *X*-ray and optical data on synthetic fluor-phlogopite, *Am. Mineral*, **40,** 10–21.

Rabbitt, J. C. (1948), A new study of the anthophyllite series, *Am. Mineral.*, **33,** 263–323.

Shell, H. R. and Craig, R. L., (1956), Synthetic mica investigations, VIII: Chemical analysis and calculation to unit formula of fluor-silicates, *Bureau of Mines, Report of Investigations*, No. **5158,** pp. 1–29.

———, Comefero, J. E., and Eitel, W. (1958), Synthesis of fluoramphiboles from melts, *Bureau of Mines, Report of Investigations*, No. **5417.**

Smith, J. V. and Sahama, T. G., (1954), Determination of the composition of natural nephelines by an *X*-ray method, *Min. Mag.*, **30,** 439–449.

Smith, J. V., (1959), The crystal structure of proto-enstatite, $MgSiO_3$, *Acta Cryst.*, **12,** 515–519.

Warren, B. E., (1929), The structure of tremolite $H_2Ca_2Mg_5(SiO_3)_8$, *Zeits. f. Krist.*, **72,** 42–57.

——— and Modell, D. I. (1930), The structure of anthophyllite $H_2Mg_7(Si_2O_3)_8$, *Zeits. f. Krist.*, **75,** 161–178.

Zussman, J., (1955), The crystal structure of an actinolite, *Acta Cryst.*, **8,** 301–308.

Manuscript received December 29, 1959.

THE AMERICAN MINERALOGIST, VOL. 45, SEPTEMBER-OCTOBER, 1960

INFRARED SPECTRA OF SOME TECTOSILICATES*

Robert G. Milkey, *U. S. Geological Survey, Washington 25, D. C.*

Abstract

In the spectra of the tectosilicates analyzed, the major absorption peaks, which are due to the primarily bond-stretching vibrations of the

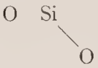

linkages, occur within a narrow range of the spectrum from 9.1 to 10.2μ. The spectra may be used in some cases, such as for orthoclase and microcline, to distinguish between similar materials. For others, such as noselite, hauynite, and lapis lazuli, the spectra are too similar for purposes of identification. The specificity of such spectra might be increased by extending the study to include wavelengths longer than 15 microns.

The wavelengths of the major absorption peaks show an irregular, but definite, shift toward longer wavelengths as the aluminum-silicon ratio increases: the introduction of aluminum into the framework increases some of the bond-lengths and decreases bond force constants, resulting in lower frequencies of vibration for the major absorption bands. The infrared spectra could generally be correlated in groups according to similarities in tetrahedral frameworks. However, dissimilar spectra obtained from some tectosilicates with identical frameworks but differing cations, indicated that in some cases the comparatively weak bonds between cation and framework may produce alterations in absorption.

The major absorption peak of most of the tectosilicates showed a high intensity, reflecting the substantial ionic character of the silicon-oxygen bond. As little as a few micrograms of some of the tectosilicates may be detected from their absorptions.

Introduction

In the literature there have appeared some infrared spectra of various silicates. Hunt, Wisherd, and Bonham (1950), in a survey of some minerals and inorganic compounds, have presented the infrared spectra of some layer silicates and tectosilicates. Launer (1952) has offered the infrared spectra of some silicates of each class, including 4 silica minerals and 9 tectosilicates. Keller, Spotts, and Biggs (1952) also presented several minerals of each silicate class in a similar type of survey. However, no comprehensive survey has been attempted of any of the major classes of silicates.

In this paper, the infrared spectra of 57 tectosilicates are presented, and also some correlations and interpretations of the various absorption bands.

Experimental Procedure

The mineral samples analyzed were obtained from the National Museum, Washington, D. C., from Dr. Frank Schairer, Geophysical Laboratory, and from Jewell Glass, David Stewart, John Hathaway, and the collection of Esper S. Larsen, Jr., all of the U. S. Geological Survey. Confirmation of identification of the samples from the National Museum was, in each case, made by optical means, and, when necessary, also by *x*-ray and spectrographic analyses. Compositions of the plagioclase feldspars were determined by method of extinction angles, and their compositional error is estimated to be within 5 per cent. *X*-ray analyses were performed by Daphne Ross, optical analyses by Sam Rubinstein and W. W. Virgin, and spectrographic analyses by Katherine Hazel, all of the U. S. Geological Survey.

---

* Publication authorized by the Director, U. S. Geological Survey.

Each sample was prepared for infrared analysis using the potassium-bromide imbedding-window method:

Two-tenths milligram of the finely divided silicate was mixed with reagent grade KBr which had been ground to pass 300-mesh screen, dried at 110° C. for several days, and thereafter stored over drierite. The silicate was dispersed throughout the KBr by mixing manually in a mullite mortar for about 20 minutes, or alternately by agitation in the bakelite capsule of a mechanical agitator. The mixture of sample and KBr was pressed in a tool-steel die at a pressure of nearly 100,000 psi too form a more-or-less transparent pellet, or window, having a 0.5-inch diameter and a thickness of approximately 0.4 mm. The window was placed in the sample beam of the infrared spectrophotometer.

The infrared spectra were obtained using a Perkin-Elmer Model 21 double beam infrared spectrophotometer, with sodium chloride optics. Instrument settings were: Resolution 927, gain 5, response 1, source amperage 0.3, suppression 2, and speed of recording 1 minute per micron. For wavelengths longer than 7 microns, calibration of the spectrophotometer was made by reference to the polyethylene absorption peaks at 8.662 microns (1154 cm.^{-1}), 9.724 microns (1028 cm.^{-1}), and 11.035 microns (906 cm.^{-1}). The $\Delta(\text{cm}^{-1})$ for these three peaks was -1 cm.^{-1}, $+2$ cm.^{-1}, and -1 cm.^{-1}, and for each peak, the $\Delta\mu$ shown by two successive spectra obtained under the same operating conditions was 0.01μ or less.

OBSERVATIONS OF THE SPECTRA

The spectra were obtained covering the infrared region of the spectrum from 2 to 15 microns. However, the significant absorption peaks of the tectosilicates occurred at wavelengths longer than 8 microns. Therefore only that portion of the spectra between 8 and 15 microns is presented. The spectra are shown in Figs. 1 to 12.

As can be seen from the figures, the absorption spectra of the tectosilicates analyzed showed a general similarity in the region 8 to 15 microns. Most have one major broad absorption peak, the base of which extends over more than a micron. The apex of the peak, for most of them, is situated in the region of the spectrum between 9 and 10.1 microns. Only a few exceptions to this rule (plagioclase feldspars, danalite, helvite) have the peak of their major absorption outside this range, and in no case at a wavelength longer than 10.8 microns. Thus, the peak of absorption of these tectosilicates can generally be correlated within a relatively narrow segment of the spectrum.

This is advantageous for characterizing them as a group. However, it also reduces the usefulness of the spectra for analysis, because the main absorption bands of individual silicates thus commonly overlap; and, therefore, if a spectrum is obtained of a mixture of silicates, there may be difficulty in distinguishing the absorption peaks arising from the individual components. Similarly, for the identification of pure silicate samples, the usefulness of the spectra may also be somewhat limited because of the close similarity of shape that was shown by some of the spectra.

However, others of the spectra are sufficiently distinctive to indicate that the spectra may often be used for purposes of identification or analysis of the pure materials. Thus, for some of the tectosilicates, such as scolecite, mesolite, helvite, eucryptite and marialite, the major absorption bands have a distinctive sequence of two or more discrete absorption peaks whose wavelengths may be used to identify pure samples of these materials. Also, the spectra of others of the tectosilicates, such as quartz, danalite, and sodalite have various sharp secondary peaks at distinctive wavelengths; the occurrence of such peaks outside the range of the major absorption band are helpful for indicating the presence of these latter silicates in a mixture, as well as useful for identifying the pure materials.

From the standpoint of general application to analysis, the specificity of the curves is affected by some materials and unaffected by others. Thus, borates, phosphates, and perchlorates, as well as clay minerals, are examples of types of materials whose spectra exhibit conflicting absorptions, as they all produce strong absorption bands in the 9 to 10 micron range. On the other hand, the tectosilicates can be detected in the presence of such materials as polyvanadates, selenates, bromates, iodates, chromates, and permanganates, all of these inorganic materials having their major absorptions at wavelengths longer than 10 microns, and carbonates, nitrates, and thiocyanates, which have their major absorptions at wavelengths shorter than 8 microns. Of course, a sample producing no strong absorption at 9 to 10.1 microns indicates the absence of most tectosilicates.

Comparisons of the major absorption bands of the curves also indicate the relative ease of detection of these tectosilicates, because in each case two-tenths milligram of the mineral was used in obtaining the spectra. Each curve, however, represented the absorption resulting from only 0.06 mg. of silicate, as approximately only 30% of the face of the potassium bromide window subtended the light beam. At the wavelength where maximum light absorption occurred, the per cent of the incident light beam that was absorbed by the sample ranged from 39% for oligoclase to 86% for quartz. More than half of the silicates absorbed 60% or more of the incident light beam at the wavelength of maximum absorption, and almost all absorbed more than 50%. At the lower limit of detection, experiments indicated that as little as 3.7 micrograms of quartz absorbed about 10% of the incident light beam at the wavelength of maximum absorption. It is evident, therefore, that their infrared spectra may serve to detect almost trace amounts of these silicates, either as pure materials or in mixtures with other substances.

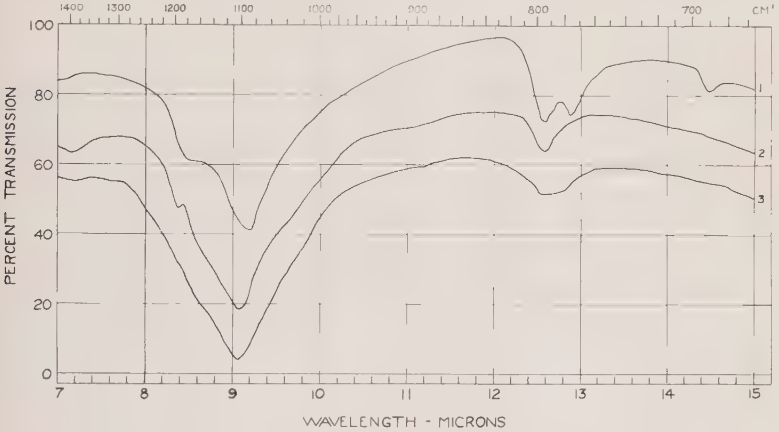

FIG. 1. Spectra of modifications of silica: (1) quartz, (2) α-cristobalite, (3) opal.

Other comments on specific spectra are of interest.

Because much infrared work has been done with the varieties of silica, only quartz, α-cristobalite, and opal of this subgroup were analyzed; the spectra obtained were similar to spectra of these minerals that have appeared in the literature (Plyler, 1929; Keller and Pickett, 1949; Hunt, Wisherd, and Bonham, 1950; Lippincott, Van Valkenburg, Weir, and Bunting, 1958), and generally similar to each other. It may be noted that their major absorption band occurs at shorter wavelengths (9.1 to 9.2 microns) than for any other of the tectosilicates.

The spectra of quartz may be readily distinguished from that of cristobalite by the secondary absorption near 12.6μ; cristobalite had only the one broad peak at near 12.6μ, whereas, in quartz, this absorption occurs as a doublet, at 12.56 and 12.84μ. The absorptions in this region are thought to occur when the silicate structure contains tetrahedra connected together in regular closed rings, as occurs in quartz (Schaefer, Matossi, and Wirtz, 1934; Matossi and Krueger, 1936). The occurrence of the 12.6μ band in the spectra of opal, similar to those of cristobalite and quartz, indicates concurrence with x-ray studies that opal contains in its structure, zones with periodic ordered arrangements of the tetrahedra.

The feldspar minerals, like the modifications of silica, have been the subject of various infrared investigations (Thompson and Wadsworth, 1957; Laves and Hafner, 1956). Moreover, the complex relationships of the minerals of this group merit a detailed treatment. The feldspar

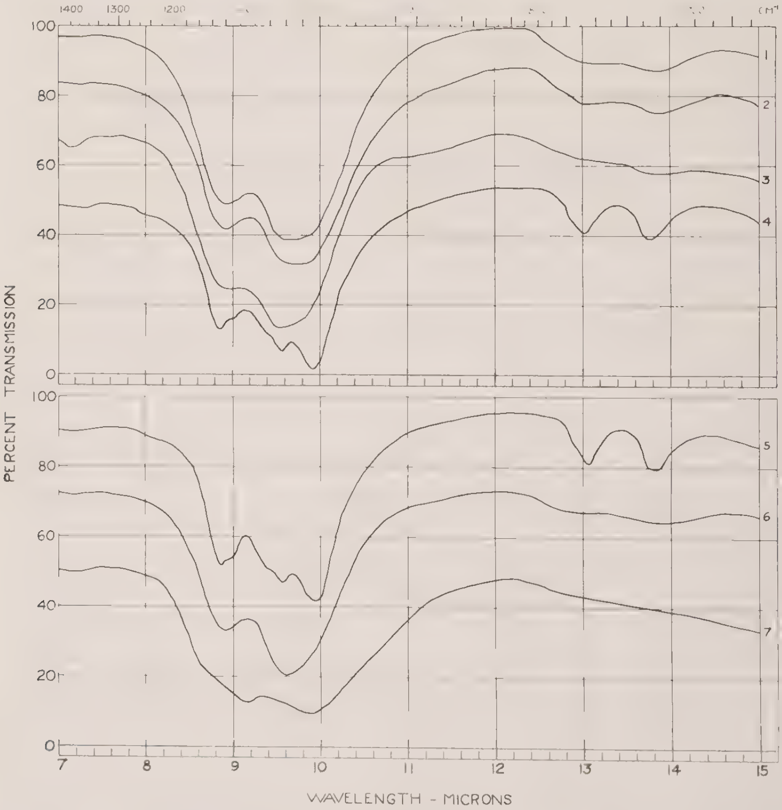

FIG. 2. Spectra of feldspars: (1) orthoclase (Rubidoux Mountains, California), (2) orthoclase (Bearpaw Mountains, Montana), (3) adularia (Miask, Urals, Russia), (4) green microcline and (5) white microcline (Amelia, Virginia), (6) anorthoclase (Essex Co., New Jersey), (7) anemousite, (Skagit River, Washington).

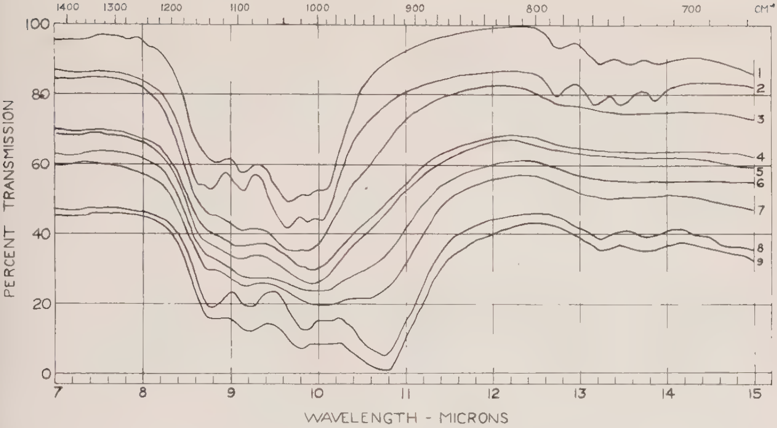

FIG. 3. Spectra of plagioclase feldspars: (1) albite, (2) oligoclase ($Ab_{90}An_{10}$) (Amelia, Va.), (3) oligoclase ($Ab_{75}An_{25}$), (4) andesine ($Ab_{66}An_{35}$) (Izu, Japan),(5), andesine ($Ab_{57}An_{43}$) (Minsen, Korea), (6) labradorite ($Ab_{40}An_{50}$) (Millard Co., Utah), (7) bytownite ($Ab_{30}An_{70}$), (8) bytownite ($Ab_{18}An_{82}$) Europe, (9) anorthite (synthetic).

spectra presented here, including orthoclase, adularia, microcline, anorthoclase, and a series of 10 plagioclases, represent only a brief reconnaissance of this group.

The spectra obtained of orthoclase and microcline conform to the observations of Keller, Spotts, and Biggs (1952), and Hunt, Wisherd, and Bonham (1950). Orthoclase and microcline can be differentiated by their spectra at wavelengths longer than 13 microns, orthoclase having only a diffuse absorption in this region, whereas microcline has two secondary peaks at 13.0 and 13.75μ. The spectra also indicate a differentiation in the main absorption peak—orthoclase having its major peak at 9.6μ, and microcline having twin major peaks at 9.52 and 9.82μ. The samples of adularia and anorthoclase analyzed produced spectra similar to that of orthoclase.

The spectra of the series of plagioclase feldspars produced a progression similar to that shown in Thompson and Wadsworth (1957). At each end of the series, the spectra show numerous well-defined absorption peaks -(the sample of $Ab_{90}An_{10}$ produced a spectra similar to that of $Ab_{97}An_3$, and at the other end of the series, $Ab_{18}An_{82}$ and synthetic anorthite produced similar absorption peaks); in the intermediate spectra, however, the well-defined peaks are replaced by broad, diffuse absorption bands, which do not provide a picture of progressive changes in structure throughout the series. (The spectra of anemousite is closely similar to that of the andesine ($Ab_{57}An_{43}$) region of the series.)

Thompson and Wadsworth extended the wavelength range beyond 1 microns to obtain further information on the intermediate members o the plagioclases; they utilized an absorption peak which undergoes bathochromic shift from 15.4 to 16.2 microns as the weight per cen anorthite is increased from 0 to 100 per cent, to suggest a definite structural change in the series at a composition of approximately An$_{31}$–An$_{33}$ These authors also pointed out that high and low temperature forms o the plagioclase feldspars were not distinguishable by their infrare spectra.

Among the spectra of the feldspars, it is interesting to note that th sharp, well-defined absorption peaks of microcline, albite, and anorthit are indicative of their regular crystalline structures, in which aluminun

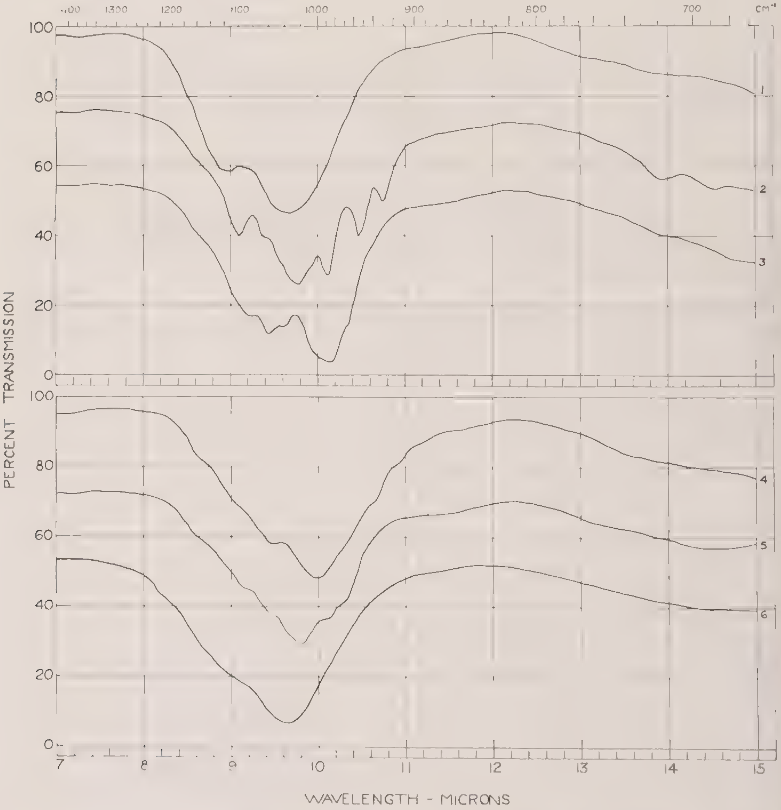

FIG. 4. Spectra of fibrous zeolites: (1) natrolite (Giant's Causeway, Ireland), (2) scolecit (Hyderabad, India), (3) mesolite (Southeast Table Mt., Colorado.), (4) thomsonit (Jefferson Co., Colorado), (5) edingtonite (Bohlet, Sweden), (6) gonnardite (Puy-de-Dom France).

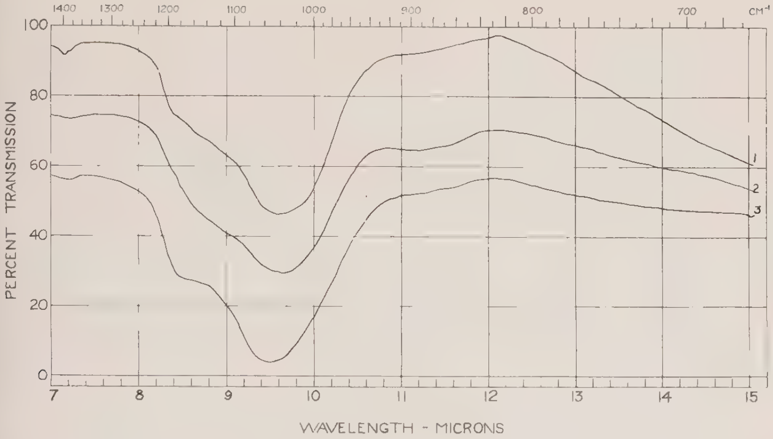

FIG. 5. Spectra of heulandite group: (1) heulandite (Paterson, New Jersey), (2) brewsterite (Argylleshire, Scotland), (3) epistilbite (Bernfiord, Iceland).

and silicon are fully ordered. On the other hand, the broad, diffuse absorption bands and absence of sharp peaks, which characterizes the spectra of orthoclase and the intermediate plagioclases, is a reflection of the irregular structures of these minerals, in which varying degrees of disorder of aluminum and silicon are present.

Among the lamellar zeolites, the minerals of the heulandite subgroup, heulandite, brewsterite, and epistilbite, which are considered to form an isomorphous series, produced spectra which are very similar to each other. Their spectra are also practically identical to the lamellar zeolites

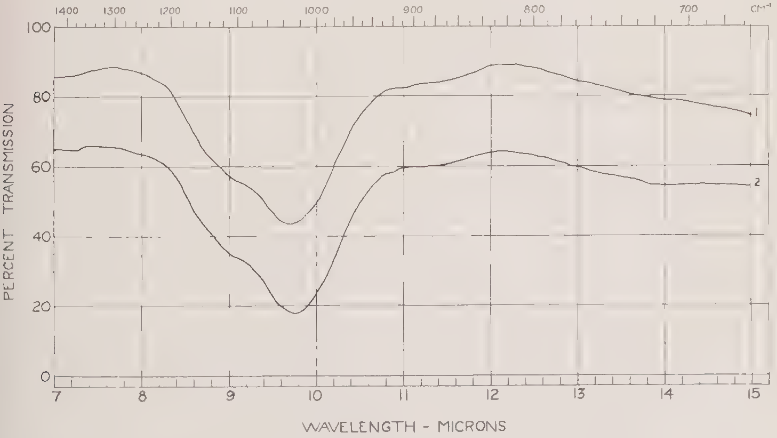

FIG. 6. Spectra of chabazite group: (1) chabazite, (2) levynite (Skye, Scotland).

of the phillipsite group, phillipsite, wellsite, stilbite, harmotome, stellerite, erionite, and gismondite, suggesting that the absorptions are due to similar vibrational modes in all of these zeolites. By contrast, the fibrous zeolites natrolite, scolecite, and mesolite, which are constructed of frameworks similar to each other, have spectra that are distinctively different.

The spectra of helvite and danalite contrast strongly with the spectra of the other minerals in the sodalite group, as well as with the other tectosilicates analyzed, having their major absorption peaks at wavelengths longer than 10.5 microns. Helvite and danalite are also noteworthy among the tectosilicates analyzed, in that all of the substitutions within the tetrahedra take place with beryllium rather than with aluminum; in either mineral the Be:Si ratio is 1:1.

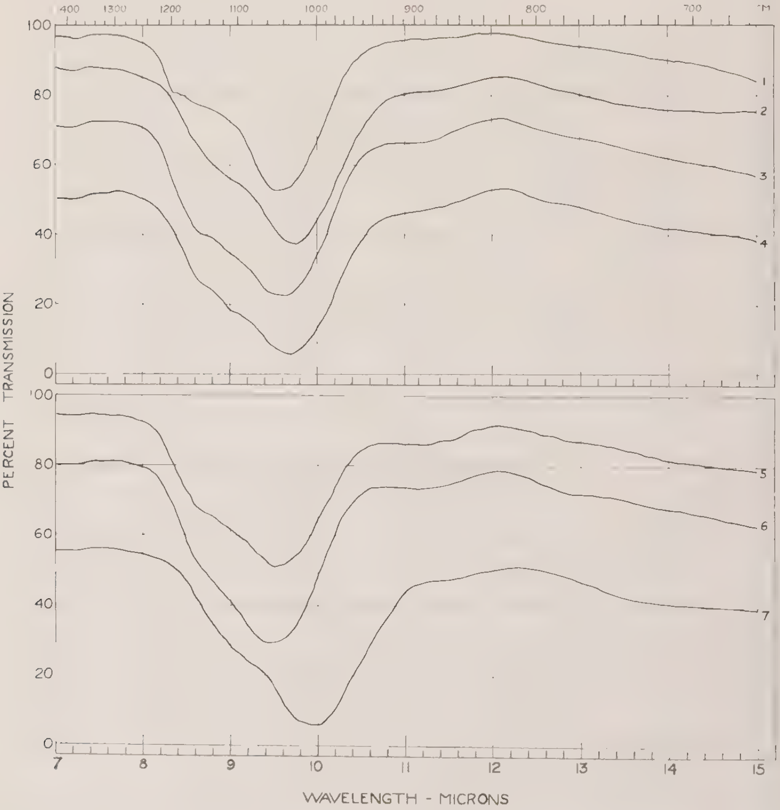

FIG. 7. Spectra of phillipsite group: (1) phillipsite (Antrim, Ireland), (2) wellsite (Cla Co., N. Carolina), (3) stilbite (Faroe Islands), (4) harmotome (Westchester Co., New York), (5) stellerite (Gishu mine, Korea), (6) erionite (Montana), (7) gismondite (Cap di Bove, Italy).

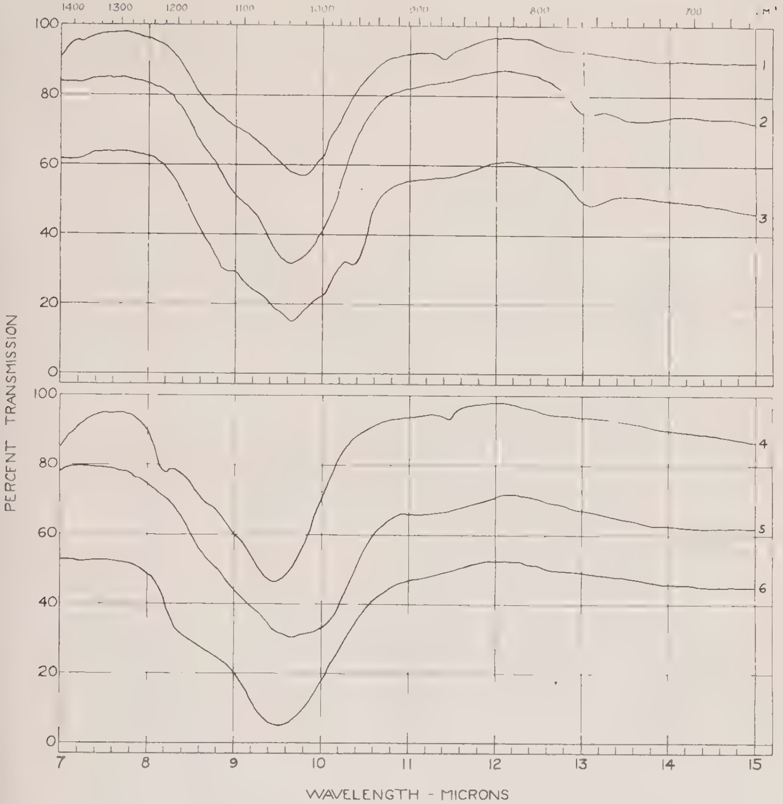

FIG. 8. Spectra of miscellaneous zeolites: (1) faujasite (Hesse, Darmstadt, Germany), (2) analcite (Giant Causeway, Ireland), (3) laumontite (Transylvanian, Hungary), (4) ferrierite (British Columbia, Canada), (5) laubanite (Steinbruch, Silesia), (6) dachiardite (Speranza, Elba).

CRYSTAL VIBRATIONS

The absorption bands of complicated molecules like the tectosilicates, unlike that of some simpler molecules, cannot be assigned by appropriate calculations to specific vibrational modes of the molecule. However, by means of empirical comparisons of spectra, general statements may be made linking absorption bands with the types of vibrations that produced them. Thus, Colthup (1950) has designated the region of absorption of the valence stretching vibration for the Si-O bond as between 9.1 and 10.8 microns, and Wright and Hunter (1947) have used the absorption of polydimethylsiloxanes to assign Si-O absorptions to the 9.1 to 10.0 micron region. As the silicon- (or aluminum-, or beryllium-)

oxygen tetrahedral bond is common to all the silicates, it is inferred that the strong absorption bands shown by most tectosilicates in the wavelength region 9 to 10 microns are due to predominantly bond-stretching vibrations of the

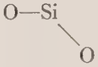

tetrahedral linkage. (As intensity of absorption depends on an effective vibrating charge, the very high level of absorption of these bands is consistent with the highly ionic character of the Si—O bond, reported by Pauling (1930), to be approximately 50% ionic. By contrast a lower intensity of absorption is shown by a more covalent bond, such as the C— bond, which has only 22% ionic character.)

Compared to the bands in the 9 to 10 micron region, the absorptio

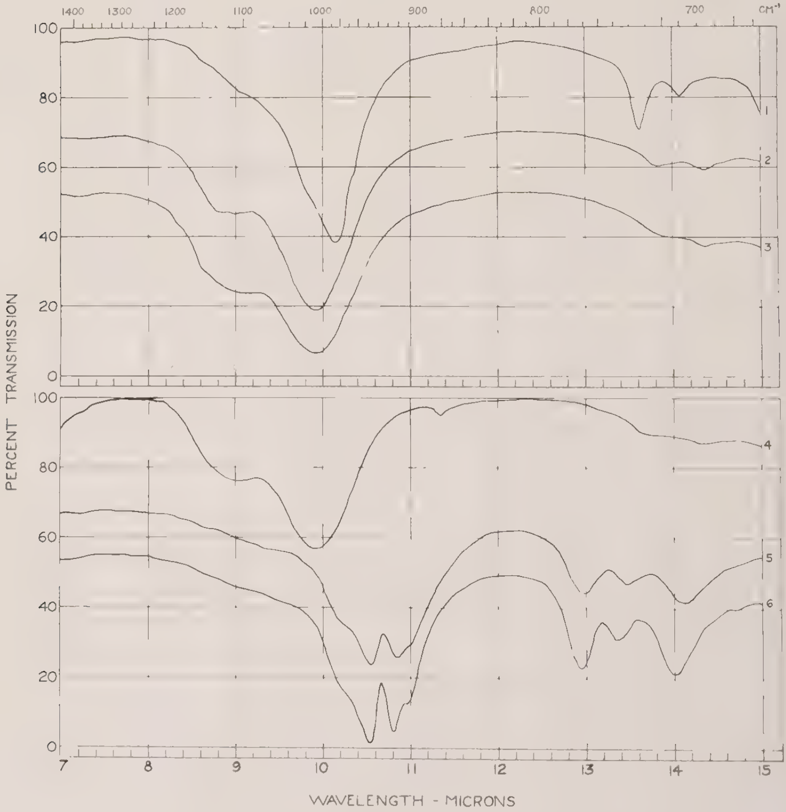

FIG. 9. Spectra of sodalite group: (1) sodalite (Ontario, Canada), (2) noselite (Saach See, Prussia), (3) hauyanite (Deer Lodge, Montana), (4) lapis lazuli (Persia), (5) helvit (Iron Mt., New Mexico), (6) danalite (Rockport, Massachusetts).

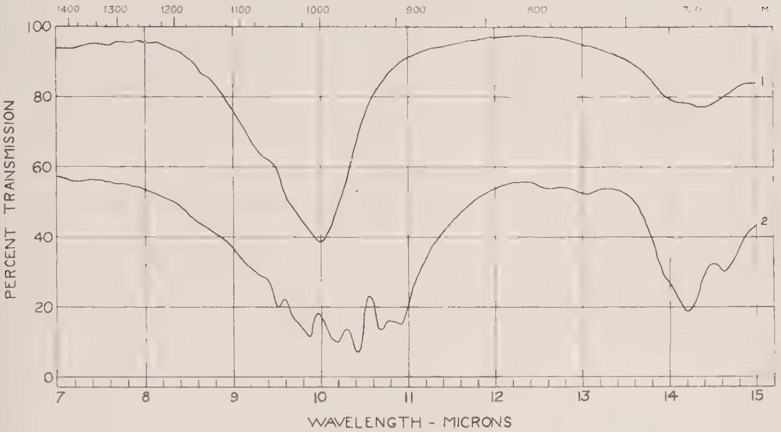

FIG. 10. Spectra of nepheline group: (1) nephelite (Ontario, Canada), (2) eucryptite.

bands that occur at longer wavelengths (including those beyond 15 microns) arise from vibrations in which bond-bending is relatively more important; such absorption bands should be more characteristic of skeletal structure than the primarily bond-stretching vibrations that occur in the 9 to 10 micron region. In the spectra of quartz and cristobalite, for example, the minor absorption bands at 12.5 to 12.8 microns have been termed characteristic of the "ring" structure to be found in quartz in which the silicate tetrahedra are joined together to form rings (Schaeffer, Matossi, and Wirtz, 1934). Probably an extension of the spectra to the wavelength region 15 to 30 microns would reveal greater contrasts and more specific differentiation between spectra that appear generally similar in the 8 to 15 micron region.

EFFECT OF ANION AND CATION

The tectosilicates which are constructed of similar frameworks are most likely to have spectra similar in shape to each other. This is shown by the matching spectra of such groups as orthoclase and adularia, stellerite and stilbite, analcite and pollucite, heulandite, brewsterite and epistilbite, chabazite and levynite, helvite and danalite, or noselite and lapis lazuli. In each case, the members of these groups have similar frameworks of linked tetrahedra, while they have different cations, or differing proportions of the same cation (or, as in the case of noselite and lapis lazuli, different substituted anionic groups). This is similar to what is found in the spectra of simple inorganic compounds, such as metal carbonates, sulfates, and nitrates, in which the shape of the spectra are determined principally by the vibrations of the anion, with only slight effect resulting from the substitution of cation for another.

In the tectosilicate frameworks, the silicon-oxygen and aluminum-oxygen bond distances are in the region of 1.6–1.7 Å. On the other hand, the distance between an oxygen atom and a sodium or calcium cation is comparatively greater; at least 2.5 Å, and sometimes as much as 3.0 Å or more. The distances from H_2O molecules to oxygen atoms are comparable to the distances between oxygen and cations. Moreover, as the coordination number of silicon or aluminum is 4, while that of a cation such as sodium may be 6 or 8, from Pauling's electrostatic valence rule, the electrostatic bond strengths of the Si—O or the Al—O bonds may be as much as 6 to 8 times the strength of the bonds between oxygen and a sodium cation. Thus, the restoring forces between oxygen and silicon (or aluminum) in the framework are much stronger than those between oxygen and a sodium or calcium cation. From this general picture, it is to

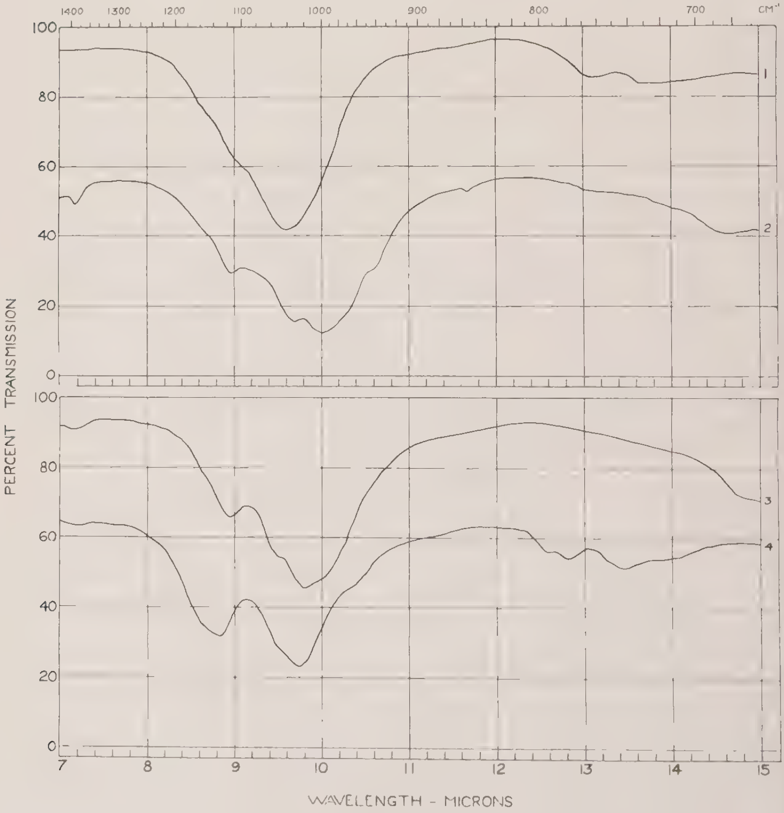

FIG. 11. Spectra of (1) pollucite (Buckfield, Maine), (2) cancrinite (Litchfield, Maine), (3) davyne (Iowa), (4) Milarite (Grisons, Switzerland).

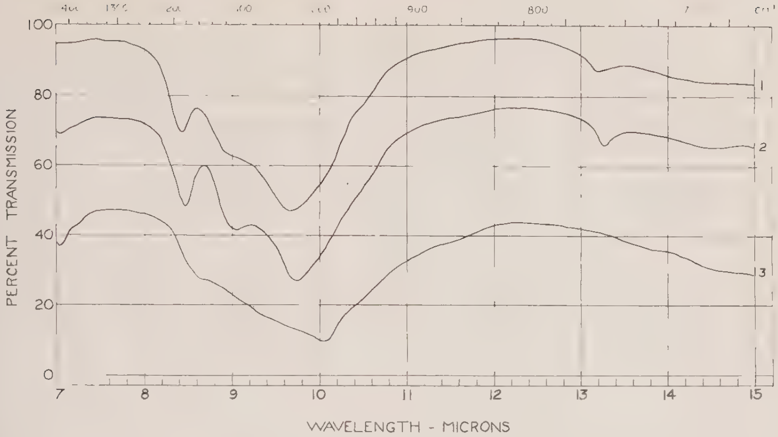

FIG. 12. Spectra of scapolite: (1) marialite ($Ma_{100}Me_0$ to $Ma_{80}Me_{20}$) (French Creek, Pennsylvania), (2) wernerite ($Ma_{80}Me_{20}$ to $Ma_{20}Me_{80}$) (St. Lawrence Co., New York), (3) meionite ($Ma_{20}Me_{80}$ to Ma_0Me_{100}) (Monte Somma, Vesuvius, Italy).

be expected, therefore, that valence stretching vibrations of the strong Al—O and Si—O bonds in the framework should be affected only slightly by changes in the much weaker oxygen-cation bonds, such as by the substitution of one cation for another.

Some of the tectosilicates, notably the fibrous zeolites natrolite, mesolite, and scolecite, showed widely-contrasting spectra, in spite of their being isostructural. However, the frameworks of these fibrous silicates also show other characteristics that differ from those of the more robust, 3-dimensional frameworks of such zeolites as chabazite, analcite, harmotome, or levynite. Thus, the alumino-silicate framework is essentially the same for all alkali-exchanged forms of chabazite from lithium to cesium (Beattie, 1953), and the framework of analcite remains the same when Na^+ is replaced by K^+, NH_4^+, Tl^{+++}, or Rb^+, whereas the fibrous zeolites show a tendency toward lattice changes after outgassing or ion-exchange. Moreover, natrolite, scolecite, and mesolite give off their water at different temperatures, their differential thermal curves are all distinctive and they undergo thermal decomposition at different temperatures (mesolite and scolecite at comparatively low temperatures, 490° and 560° C., while natrolite retains its structure until 940° C. [Peng, 1955]). The decomposition temperatures may be regarded as a measure of bond strengths. In the light of these differences in the characteristics of natrolite, mesolite, and scolecite, their markedly contrasting infrared spectra may serve as additional evidence in support of the hypothesis that these minerals do not constitute an isomorphous series, but rather are independent species.

Effect of Aluminum Substitution

The spectra show a correlation between the wavelength of the main absorption peak, and the degree of aluminum substitution into the crystal. Thus, the spectra of quartz, with no aluminum substitution, has its major peak at 9.18 microns, while the spectra of noselite, sodalite, hauynite, and others, in which the (aluminum):(aluminum+silicon) ratio approaches the limiting value of 0.5, the major peaks occur near 10.0 microns. Those with intermediate ratios have their major peaks located at intermediate wavelengths. In Fig. 13 is shown the relationship between the wavelengths of the peaks of the major absorption bands and the corresponding (Al):(Al+Si) ratio in the tectosilicate frameworks. The abscissae in Fig. 13 are represented by the published range of (Al):(Al+Si) ratios for each mineral, calculated from chemical analyses appearing in the literature (principally in Dana's System of Mineralogy). Some of the spectra, such as those of the plagioclase feldspars, helvite, or milarite, could not be correlated in this way, as they have series of peaks over a broad absorption band, rather than a sharp, major peak. Others,

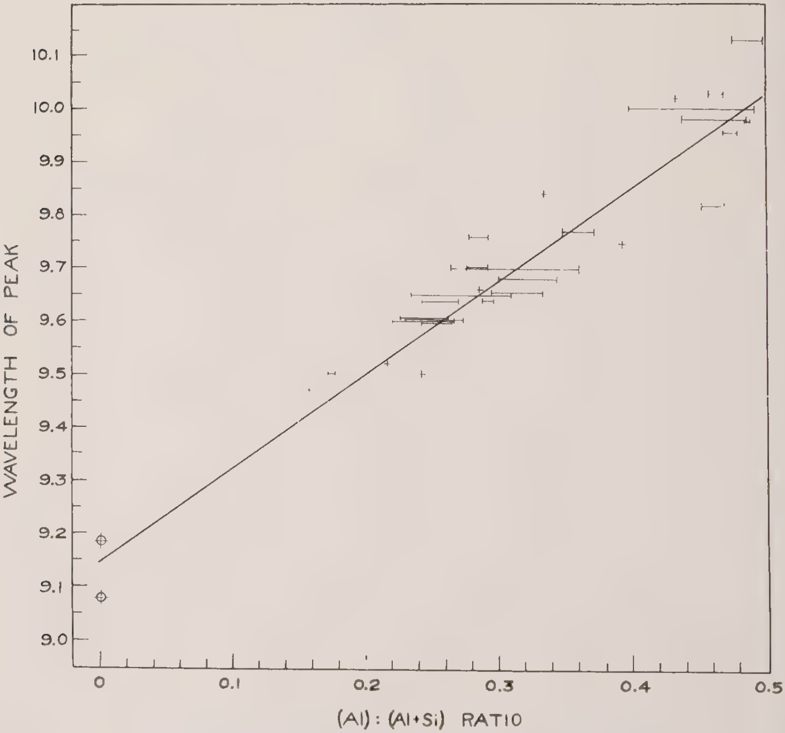

Fig. 13. Relationship of wavelength of absorption peak and published range of (Al):(Al+Si) values of tectosilicates.

such as lapis lazuli and wernerite, were also excluded, as their (Al):(Al+Si) ratios, which may vary appreciably, demand a more specific determination to be useful. The data from 32 of the tectosilicates, are included in the curve.

As the frequency of the valence-stretching vibrations varies inversely with the atomic masses, it might be presumed that the substitution of aluminum, which has a smaller mass than silicon, would result in a higher frequency. However, the vibrational frequency is affected also by the bond force-constant, which varies directly with the electronegativity product of the vibrating nuclei, and inversely with the internuclear distance. As the electronegativity of aluminum is less than that of silicon, and as the internuclear distance of the aluminum-oxygen bond is greater than that of the silicon-oxygen bond, the substitution of aluminum for silicon results in a decreased force constant. Accordingly, the stretching vibrational frequency, which varies directly with the force constant, is also decreased, and therefore the absorption peak is shifted, as is seen in Fig. 13, toward the longer wavelengths.

An idea of the wavelength shift to be expected from the effects of these various factors can be arrived at by calculation of the valence stretching frequency of the metal-oxygen bond, using the expression for an harmonic oscillator, $v = 1307\sqrt{k/u}$, where v is vibrations per centimeter, k is force-constant, dynes per centimeter ($\times\ 10^{-5}$), and u is the reduced mass of the vibrating nuclei of the bond. Force constant values for Al—O and Si—O bonds were obtained from Gordy's (1946) empirical formula for the force constants of tetrahedral AB_4 molecules,

$$k = 3.29\left(\frac{x_A x_B}{d^2}\right)^{3/4} - 0.40,$$

where x_A and x_B are electronegativities of the atoms, and d is internuclear distance, Angstroms. (Although such calculations are not a precise treatment of the stretching vibrations in the framework, as they neglect the effects on a particular vibrating pair caused by bonds from neighboring nuclei, they can be used as an indication of the direction and approximate extent of shift caused by the atom substitution.) Thus, for the case of maximum wavelength shift, when one-half the silicon atoms in the framework have been replaced by aluminum, the calculations indicate a bathochromic shift of 0.5 micron. This is comparable to the actual shift of 0.6 to 0.8 micron shown by those tectosilicates with the one-to-one aluminum-silicon ratio—from the 9.20 microns for quartz, to 10.0 for thomsonite, 10.3 for nephelite, 9.82 for davyne, 10.12 for sodalite, 9.96 for noselite, and 9.97 for hauynite.

The bathochromic shifts shown by beryllium-substituted danalite and helvite are substantially greater than those shown by any of the aluminum-substituted frameworks. The framework structures of both danalite and helvite are similar to the framework of sodalite; and, similar to the Al:Si ratio in sodalite, the Be:Si ratio in danalite and helvite is 1:1. The unique shape of their spectra, however, compared to those of the other members of the sodalite group, suggests that, unlike the substitution of aluminum, the substitution of the small beryllium atom may produce substantial changes in the vibrational modes of the tetrahedrons in the framework.

It is interesting to note the wavelength shift resulting from aluminum substitution in an isomorphous series, as is seen in the spectra of the scapolite group. The changes in Al:Si ratio are reflected in the wavelengths of the absorption peaks. In the sample of marialite analyzed, the peak is at 9.64 microns, and in the sample of meionite, representing a higher Al:Si ratio, the absorption band has shifted toward longer wavelengths, with the peak at 10.02 microns. The sample of wernerite analyzed had a spectra closely similar to that of the marialite, although the peak wavelength has shifted somewhat—from 9.64 to 9.74 microns. The spectra of scapolites should provide a convenient method of characterizing their compositions, since their positions in the isomorphous series ought to bear a direct correlation with the positions of their absorption peaks. Analysis of a series of scapolites for which the Al:Si ratio had been closely determined would provide the curve of the relationship of peak wavelength and aluminum content, from which the Al composition of an unknown could be determined.

Conclusions

Interesting group correlations were made of the infrared spectra of the tectosilicates analyzed, and in many of the spectra features of individual interest occurred. Generally, as little as a few milligrams of the tectosilicates could be detected from their major absorption peaks. The occurrence of the major absorption bands within a relatively narrow wavelength interval of the spectrum was advantageous in characterizing the spectra as a group; however, the accompanying lack of specificity of the spectra has the result of limiting the quantitative or qualitative detection of the tectosilicates in mixtures. Thus, only a few of the spectra, such as those of quartz, danalite, helvite, sodalite, and marialite have discrete substantial absorption peaks outside the wavelength range of the major absorption bands. Perhaps the extension of the spectra from the 15 micron region to the 28 or 30 micron region would prove of particular value, as it is possible that the region of longer wavelengths, where the lower-energy, bond-bending absorption bands occur, might reveal greater contrast among the spectra.

REFERENCES

BEATTIE, I. R. (1953), The structure of ion-exchanged forms of chabazite: *Nature*, **172,** 999–1000.

COLTHUP, N. B. (1950), Spectra-structure correlations in the infrared region: *Jour. Optical Soc. Amer.*, **40,** 397–400.

GLASS, JEWELL J. (1935), The pegmatite minerals from near Amelia, Virginia: *Am. Mineral.*, **20,** 751, 765.

GORDY, WALTER J. (1946), A relation between bond force constants, bond orders, bond lengths, and the electronegativities of the bonded atoms: *Jour. Chem. Phys.*, **14,** 305–320.

HUNT, J. M., WISHERD, M. P., AND BONHAM, L. C. (1950), Infrared absorption spectra of minerals and other inorganic compounds: *Anal. Chemistry*, **22,** 1478–1501.

KELLER, W. D., AND PICKETT, E. E. (1949), The absorption of infrared radiation by powdered silica minerals: *Am. Mineral.*, **34,** 855–868.

KELLER, W. D., SPOTTS, J. H., AND BIGGS, D. L. (1952), Infrared spectra of some rock-forming minerals: *Am. Jour. Sci.*, **250,** 453–471.

LARSEN, E. S., JR. (1948), Batholith and associated rocks of Corona, Elsinore, and San Luis Rey quadrangles, Southern California: *Geol. Soc. America Memoir* **29.**

LAUNER, P. J. (1952), Regularities in the infrared absorption spectra of silicate minerals: *Am. Mineral.*, **37,** 764–784.

LAVES, F., AND HAFNER, ST. (1956), Order/disorder and infrared absorption: *Zeit. Krist.*, **108,** 52–63.

LIPPINCOTT, E. R., VAN VALKENBERG, ALVIN, WEIR, C. E., AND BUNTING, E. N. (1958), Infrared studies on polymorphs of silicon dioxide and germanium dioxide: *Jour. Research, U. S. Natl. Bur. Standards*, **61,** 61–70.

MATOSSI, F., AND KRUEGER, H. (1936), An *x*-ray investigation of the feldspars: *Zeitschr. Physik*, **99,** 1–23.

PAULING, L. (1930), The structure of some sodium and calcium aluminosilicates: *Proc. [U. S.] Natl. Acad. Sci.*, **16,** 453–459.

PENG, C. J. (1955), Thermal analysis study of the natrolite group: *Am. Mineral.*, **40,** 834–856.

PLYLER, E. K. (1929) Combination frequencies of the infra-red bands of quartz. *Phys. Rev.*, **33,** 48–51.

SCHAEFER, C., MATOSSI, F., AND WIRTZ, K. (1934), The infrared reflection of silicates: *Zeitschr. Physik*, **89,** 210.

THOMPSON, C. S., AND WADSWORTH, M. E. (1957), Determination of the composition of plagioclase feldspars by means of infrared spectroscopy: *Am. Mineral.*, **42,** 334–341.

WRIGHT, NORMAN, AND HUNTER, M. J. (1947), Organosilicon polymers. III. Infrared spectra of the methylpolysiloxanes: *Am. Chem. Soc. Jour.*, **69,** 803–809.

Manuscript received January 18, 1960.

THE AMERICAN MINERALOGIST, VOL. 45, SEPTEMBER-OCTOBER, 1960

SERPENTINITE-LIMESTONE CONTACT AT TALERI MOHAMMAD JAN, ZHOB VALLEY, WEST PAKISTAN*

S. A. Bilgrami,† *Department of Mineralogy and Petrology,
Harvard University, Cambridge, Mass.*

Abstract

Mineralogical and petrographic description is given of a serpentinite-limestone contact at Taleri Mohammad Jan, West Pakistan. Chemical analyses and optical properties of a diopside, an idocrase and a clinochlore are given and their possible mode of origin discussed.

Introduction

Taleri Mohammad Jan is a small village about seven miles northwest of Hindubagh, West Pakistan (Fig. 1). Here serpentinite is in contact with limestone and an interesting suite of contact minerals (wollastonite, grossularite, idocrase, clinochlore, diopside, etc.) is developed. Unfortunately the area was visited early by amateur mineral collectors, who indiscriminately used explosives to obtain idocrase crystals; consequently at most places the contacts between the igneous and the sedimentary rocks can only be inferred. No work has been done on these rocks before. The present paper is the first attempt at describing the mineralogy and petrology of the rocks of this area and forms a part of the study of the Zhob Valley igneous complex.

Petrography

The rocks described here were collected from the contacts between a stoped limestone block and the enclosing serpentinite. The limestone block is about 2,000 square meters in area and projects above the serpentinite surface from 0 to 30 meters; the downward extent is not known. At the contact the serpentinite is very fine grained and chocolate brown in color. Away from the contact the limestone is buff colored and very fine grained. At the contact, however, recrystallization has taken place and the limestone is also traversed by veins of green idocrase and colorless clinochlore. The veins are from a fraction of a centimeter to 7 or 8 centimeters thick, are several meters long, and do not follow any definite direction or pattern. Intersection of veins is common. In addition, idocrase, clinochlore and grossularite are also developed on joint and fracture planes and it is only here that euhedral crystals of idocrase and grossularite are developed.

---

* Contribution No. 391, Department of Mineralogy and Petrology, Harvard University, Cambridge 38, Mass.

† Present address, Department of Geology, University of Karachi, Karachi, Pakistan.

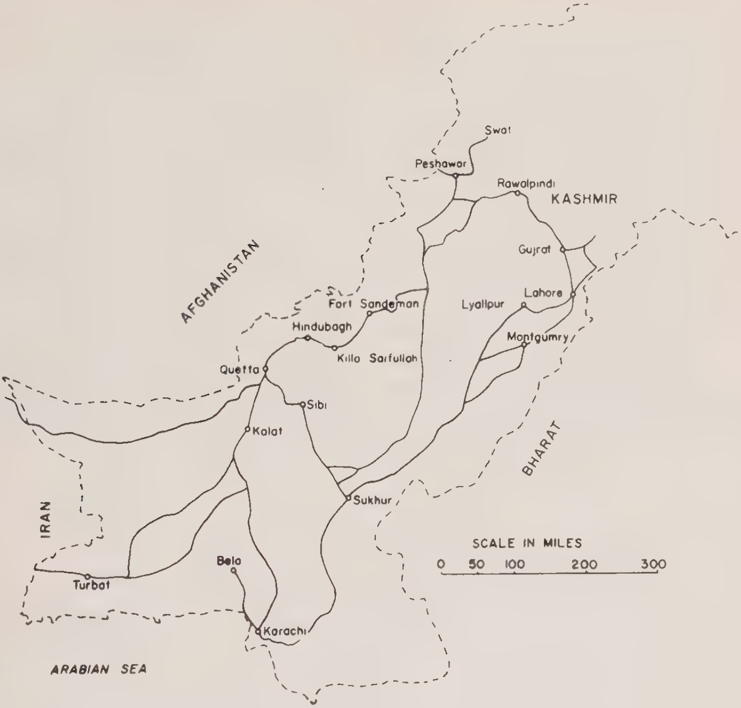

FIG. 1. Map of West Pakistan showing the location of Hindubagh.

Under the microscope the contact serpentinite (Specimen B-7*) is composed of colorless antigorite, euhedral sphene, veins of grossularite, idocrase, clinochlore and a few anhedral crystals of picotite. Rarely diopside crystals also occur. Antigorite is colorless and cryptocrystalline. Sphene is euhedral in form and is markedly pleochroic from pale pink to brown. It occurs as individual grains and in small veinlets. Most of the veins and grains have altered to leucoxene. Grossularite is in clear, colorless, euhedral crystals which when magnified ×300 are of the size of a pinhead. They occur in irregular veins as well as in crystal aggregates. Idocrase in clear colorless crystals is in veins and patches and shows typical abnormal interference colors. The chlorite occurs in very minor amounts, is extremely fine grained and shows abnormal interference colors. Picotite in dark green crystals is also very minor in amount. Colorless diopside and needles of apatite occur in some specimens.

The contact limestone shows greater variation than the serpentinite and it is necessary to describe some of the specimens in detail. Specimen B-1. Very fine grained, buff colored rock in which no minerals can be recognised in the handspecimen. In this section the rock is composed of almost equal proportions of wollastonite, idocrase and grossularite. Wollastonite occurs as prismatic crystals, some of which are poorly developed, are dirty brown in color (probably due to minute inclusions), show one set of perfect cleavages and an extinction angle ($X:c$) of 44°. The mineral is optically negative with a $2V=38°$. Idocrase is in clear, colorless, irregular plates with no cleavages and abnormal interference colors. Grossularite occurs in irregular, pale brown patches and is intergrown with idocrase. All the three minerals appear to have developed simultaneously, although there appear to be second generations of wollastonite and idocrase which form veins and exhibit euhedral form.

---

* Numbers refer to collections in Department of Geology, University of Minnesota, Minneapolis and Department of Mineralogy, Harvard University, Cambridge, Mass.

Variation from the above specimen is exhibited by another contact specimen (B-3) which is extremely fine grained and earthy yellow in color. At the contact with serpentinite the limestone has acquired a greenish tint and a gradation from limestone to serpentinite can be seen. Idocrase and clinochlore are developed on the surface of the specimen. The age relationships of the two minerals are rather confusing but it appears that the two minerals developed simultaneously. In thin section the rock is composed of pale brown, poorly developed garnet, ill-formed crystals and needles of wollastonite, sporadic crystals of idocrase and clinochlore. The last two minerals also form veins. The garnet forms the bulk of the slide and encloses wollastonite and idocrase. The clinochlore veins do not follow any definite direction but show a banded structure under crossed nicols. Branching and closing of idocrase and clinochlore veins is common, although veins composed of one mineral do not intersect those composed of the other. Rarely the two minerals occur in the same vein.

In one contact specimen (B-8) yellow chondrodite is developed in addition to garnet, colorless clinochlore and antigorite, wollastonite and spinel, all cut by later composite veins. Chondrodite is yellow in color, does not show any form, is faintly pleochroic from pale yellow to yellowish brown and in places is altered to a serpentinous mineral. The composite veins consist of idocrase, clinochlore and antigorite. The limestone is traversed by serpentinite veins and at the contact these veins are very fine grained. Under crossed nicols the serpentine (antigorite) shows banded structure (Fig. 2). About one centimeter from the contact antigorite of the vein is replaced by a colorless clinochlore and the line of contact between the two minerals is quite sharp. One centimeter from this contact idocrase makes its appearance in composite veins. It is colorless, anhedral in form and is intergrown with clinochlore (Fig. 3). The mineral

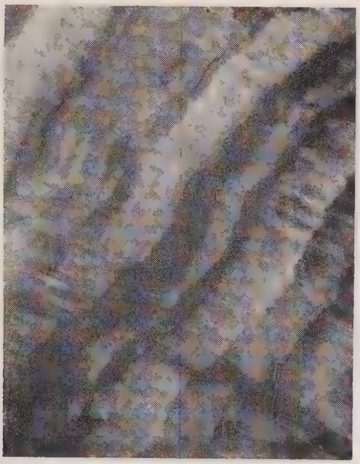

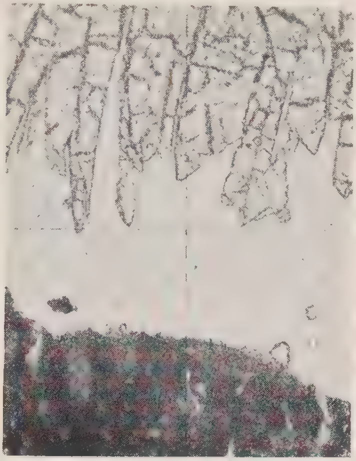

FIG. 2. Photomicrograph showing banded structure in antigorite. Crossed nicols. ×40.
FIG. 3. Photomicrograph of composite vein showing intergrowth between idocrase and clinochlore. ×40.

does not appear to be different from the variety described before. In some composite veins idocrase occurs as inclusions in clinochlore (Fig. 4). Other specimens taken a few centimeters from the contact show development of clear grossularite crystals. Under the microscope these specimens (B-14 and B-14A) are composed of wollastonite, prehnite, grossularite ($a_0 = 11.851$ Å), a little chlorite and biotite. Skeletal crystals of ilmenite are evenly distributed throughout the slide. Prehnite is colorless and anhedral in form with one set of well developed cleavages. The mineral is optically positive with a moderate 2V. Chlorite is pale green in color and markedly pleochroic from pale green to green. Biotite is in very small amounts and is pale brown to colorless. Skeletal crystals of ilmenite are mostly altered to leucoxene. In specimen B-14A, a little clear albite is also present, and prehnite shows bow tie structure. Another contact specimen (B-12), is very fine grained and unusually rich in sphene. The mineral is dark brown in color, is strongly pleochroic and is replaced by idocrase, which occurs in colorless crystals in veins cutting across all other minerals.

In another contact specimen (B-13) pale brown garnet, colorless diopside, apatite and a little sphene are present and are cut by antigorite veins. Garnet shows rounded crystals (Fig. 5) and alteration to a dense brown isotropic material. Other minerals do not show any variation from those described above.

A marked variation from the above described specimens is shown by B-4, which is a medium grained, dark colored rock with euhedral crystals of chromite set in a very fine grained dark matrix. The rock is composed of pale green chlorite, pink garnet, euhedral chromite, spinel and a little kaolinite. Chlorite is pale green, shows one set of well developed cleavages and has a bleached appearance in parts. It shows abnormal interference colors, uniformly in the bleached and unbleached parts; the refractive index γ is 1.585, the 2V is 25° and it is optically negative. Most of the chlorite appears to have formed by the alteration of garnet. Inclusions of minute chromite crystals in chlorite are common. Garnet is pale pinkish brown in color, shows anhedral form and is partly altered to chlorite. Spinel is almost colorless, shows anhedral form and occurs as individual crystals as well as crystal aggregates. Euhedral crystals of chromite are evenly distributed throughout the slide. Kaolinite occurs in small colorless patches, is extremely fine grained and shows wavy extinction, possibly due to its very fine grained nature.

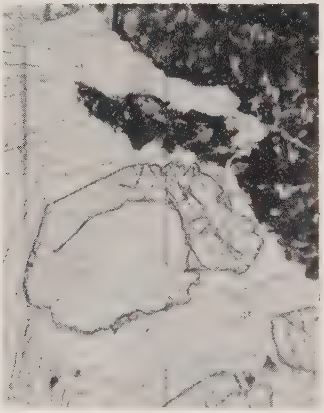
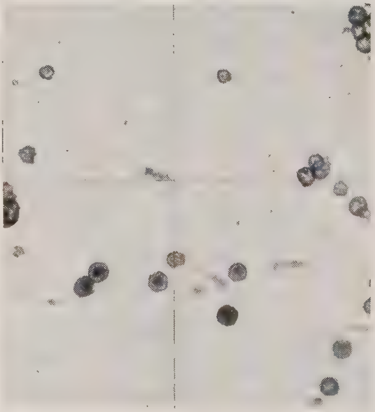

Fig. 4. Photomicrograph of composite vein showing inclusions of idocrase crystals in clinochlore. ×40.

Fig. 5. Photomicrograph showing rounded grossularite crystals in a matrix of colorless antigorite. ×40.

In addition to the above, the limestone is traversed by veins of idocrase. These veins range from a fraction of a centimeter to 7 or 8 centimeters in thickness and do not follow any definite direction. In the hand-specimen the veins seem to be composed almost entirely of massive or crystalline idocrase. In the crystalline veins idocrase crystals are from a millimeter to 2 centimeters long and up to about one centimeter thick. They vary from pale to dark brownish green in color and show a pearly luster. All crystals show perfect prism faces and rarely bipyramidal crystals are also found. In this sections some specimens (B-17, B-17A), exhibit a core of colorless diopside, and brown garnet is often present.

Idocrase is anhedral in form and colorless although some crystals show a pale brown color. The mineral occurs in veins as well as in the groundmass of the thin sections and the former shows a better crystal form. Faint zoning, twinning and undulose extinction are exhibited by some crystals. Garnet does not show any crystal form and appears to be intergrown with diopside and the groundmass idocrase. Diopside is colorless and in very minute crystals which are intergrown with or included in the idocrase. A little wollastonite is present in some slides. The best development of the diopside is exhibited in B-17A, where the mineral forms the core of an idocrase vein about $2\frac{1}{2}$ centimeters thick. The vein consists of pale green idocrase crystals which are 2 to 3 millimeters long and show pearly luster. In thin section the rock is composed of colorless, granular diopside, veins of colorless chlorite and a colorless mineral, possibly chondrodite. Idocrase does not show any variation from the above described varieties. Diopside is granular in form, has two sets of well developed cleavages and often shows simple and multiple twins. Optical properties of the mineral and a chemical analysis with comparisons are given in Tables 1 and 2. Chlorite is colorless, extremely fine grained and shows abnormal interference colors. A few crystals of dolomite enclosing diopside are present in some specimens. A pale yellowish brown idocrase traversed by veins of colorless diopside is present in another veins specimen (B-18). Primary (?) calcite is also present in this slide.

Chemical Mineralogy

Diopside. A chemical analysis of a diopside from an idocrase vein is given in Table 1 (analysis 1) with a comparison. It is higher in MgO and CaO and lower in total iron and alkalies than the diopside from the skarn rock (Table 1, anal. 3). The presence of 0.75% of CO_2 in the analysis may be due to minute calcite or dolomite inclusions in the diopside. The carbonate may be an alteration product of the diopside. The determined refractive indices of this diopside agree well with the values obtained by plotting the analysis on Hess's graphs for refractive indices and chemical composition of clinopyroxenes (Hess, 1949, 641). The structural formula of the diopside calculated on the basis of 6 oxygen atoms is given in Table 3 and is in general agreement with the theoretical formula for the mineral. The summation of the Z positions is slightly lower than the theoretical value of the group and this would seem to confirm the earlier suggestion of the carbonate alteration of the mineral which would decrease its silica content.

Clinochlore. The clinochlore analysis is compared with an analysis of a leuchtenbergite, a variety of clinochlore (Hey, 1954, 280), in Table 1 (anal. 4 and 6). The two analyses show general similarity but the mineral

TABLE 1. CHEMICAL ANALYSES OF DIOPSIDE, CLINOCHLORE AND IDOCRASE WITH COMPARISONS

	1	2	3	4	5	6	7	8	9	10	11
SiO_2	53.46	54.22	53.79	32.39	32.66	31.44	36.91	36.79	36.52	37.75	41.42
Al_2O_3	0.34	0.34	1.41	16.52	16.66	17.62	20.37	16.16	15.12	2.17	0.74
TiO_2	0.00	0.00	0.04	0.05	0.05	—	0.11	0.31	0.31	0.04	tr
Fe_2O_3	0.08	0.09	0.33	0.38	0.38	—	0.07	2.21	4.71	2.94	3.62
FeO	1.39	1.40	2.60	2.78	2.80	tr	0.46	1.51	0.67	2.37	1.12
MnO	0.24	0.24	0.22	0.29	0.29	tr	0.09	0.30	0.30	0.16	0.08
MgO	17.50	17.76	16.64	33.27	33.56	37.64	3.01	3.22	3.18	43.42	40.12
CaO	25.94	25.56	24.66	0.99	0.77	tr	36.36	35.60	36.01	tr	tr
Na_2O	0.00	0.00	0.14	0.03	0.03	—	0.02	0.09	0.25	0.31	nil
K_2O	0.01	0.01	0.04	0.02	0.02	—	0.01	0.02	0.20	0.12	nil
H_2O^+	0.32	0.32	0.10	12.44	12.55	13.19	2.38	2.04	2.70	9.76	12.74
H_2O^-	0.06	0.06	0.04	0.23	0.23	—	0.00	—	—	0.46	0.32
F	—	—	—	—	—	—	0.03	0.76	—	—	—
CO_2	0.75			0.23							
	100.09	100.00	100.01	99.62	100.00	99.89	99.82	99.92	99.97	100.15†	100.16
O−F							0.01	0.31			
							99.81	99.61*			

1. Diopside, Taleri. Analyst C. O. Ingamells.
2. Same as above recalculated to 100% after deducting 1.5% calcite.
3. Diopside, Skarn rock from Clifton Mine, St. Lawrence Co., N. Y. (Hess, 1949, 662, anal. 36). Analyst Lee C. Peck.
4. Clinochlore, Taleri. Analyst C. O. Ingamells.
5. Same as above recalculated to 100% after deducting 0.46% calcite.
6. Leuchtenbergite, colorless to pale green, in metamorphosed limestone, Philipsburg, Mont. (Shannon, 1923). Analyst E. V. Shannon.
7. Idocrase, Taleri. Analyst C. O. Ingamells.
8. Green idocrase, limestone quarry near Sala, Sweden (Wickman, 1950). Analyst K. Johnson.
9. Green idocrase at contact of marble with serpentine and amphibolite. (Sedlacek, 1949). Analyst Sedlacek.
10. Typical dunite of the Hindubagh area. Analyst S. A. Bilgrami.
11. Green lizardite from a serpentine xenolith in rodingite. Analyst R. A. Howie (Bilgrami and Howie, 1960).

* Total includes 0.91% B_2O_3.

† Total includes $Cr_2O_3=0.53\%$ and $P_2O_5=0.12\%$.

TABLE 2. OPTICAL PROPERTIES* OF DIOPSIDE, CLINOCHLORE AND IDOCRASE WITH COMPARISONS

	1	3	4	6	7	8	9
α or e	1.6681	1.6740	1.5911	1.572	1.7122	1.7133	1.722
β	1.6753	1.6805	—	1.572	—	—	—
γ or o	1.6972	1.7029	1.5961	1.575	1.7272	1.7146	1.725
$\gamma-\alpha$	0.0291	0.0289	0.005	0.003	0.0139	0.0023	0.003
2V	$55\frac{1}{2}°$	$56\frac{3}{4}°$	15°–21°	6–14°	—	—	—
Z:c	39°	$39\frac{1}{2}°$		—	—	—	—
s g.	3.255	—	2.722	—	3.368	3.37	3.376

Numbers same as in Table 1.

* All determinations in sodium light. Values ±0.002.

TABLE 3. STRUCTURAL FORMULAE OF DIOPSIDE, CLINICHLORE AND VESUVIANITE

	2		5			7		
Si	1.967		3.075			8.630		9.00
				.925	4.00		0.370	
Al	0.015	1.98	1.845			5.627	4.000	4 00
				.923			1.257	
Ti	0.000		0.003			0.011		
Fe'''	0.002		0.026			0.018		2.00
Fe''	0.053		0.220			0.090		
Mn	0.007		0.022		5.97	0.017		
Mg	0.968		4.707			1.124	0.624	
		2.04					0.500	
Ca	1.012		0.067			9.137		9.65
Na	0.000		0.004			0.008		
K	0.004		0.002			0.002		
OH	—		7.850		7.85	3.72		3.74
F	—		—			0.021		

2. Diopside from Taleri. Cations on the basis of 6(O).
Formula = $(\text{Ca, Mg, Fe})_{2.04}(\text{Si, Al})_{1.98}(\text{O})_6$.
5. Clinochlore, Taleri. Cations on the basis of 18(O, OH, F).
Formula = $(\text{Si, Al})_4(\text{Al, Mg, Fe})_{5.97}(\text{O})_{10}(\text{OH})_{7.85}$.
7. Idocrase, Taleri. Cations on the basis of 38(O, OH, F).
Formula = $(\text{Ca, Mg})_{9.65}(\text{Mg, Fe})_{2.00}\text{Al}_{4.00}\text{Si}_{9.00}(\text{O})_{34}(\text{OH, F})_{3.74}$.
Numbers 2, 5, and 7, same as in Table 1.

described by Shannon (anal. 6) appears to be quite unique in the simplicity of its chemical composition. The Taleri clinochlore when plotted on Hey's diagrams for chlorites (Hey, 1954, Figs. 1*a* and 4) falls within the clinochlore field and the determined refractive indices are in close agreement with those obtained from his diagrams. The structural formula of the mineral calculated on the basis of 18(O, OH) is given in Table 3 and agrees well with the theoretical formula $(\text{Si, Al})_4(\text{Al, Mg, Fe})_6(\text{OH})_8(\text{O})_{10}$. It will be seen that slightly over half the total Al present in the mineral is placed in the Z positions replacing Si. This would cause a charge imbalance and is compensated by the replacement of Mg by Fe''' and Ti.

Idocrase. A chemical analysis of Taleri idocrase is compared with analyses of two specimens from different localities (Table 1, anal. 7–9). The three analyses show close similarity although the Taleri specimen is higher in alumina and lower in total iron and alkalies. The high alumina content of the Taleri specimen is a unique feature and search of the literature has shown that idocrase with comparable alumina content is rare. The structural formula of the mineral calculated on the basis of 38(O, OH, F) is given in Table 3 and is in close agreement with the general formula of the mineral given by Warren and Modell (1931). In calculating the structural formula Si—Al, Al, and Fe—Mg positions were filled to their theoretical values and the excess of Mg was allotted to Ca position to make up part of the deficiency in this group. This deficiency appears to be due to the replacement of calcium by magnesium. Water is slightly lower than the theoretical value and may be due to the fact that silicate minerals do not release all their structural water on being heated in a glass tube. No attempt has been made to correlate the optical properties of idocrase with its chemical composition but it appears from the available data that no simple relationships exist.

Distribution of Trace Elements

The distribution of trace elements in some of the minerals and rocks of the Taleri area is given in Table 4. The trace elements have been determined on an optical spectrograph using D.C. arc and standard samples for comparison. The accuracy of the determinations is considered to be ±30%.

With the notable exception of Ba and Sr most elements in the minerals show values closer to the contact serpentinite than the limestone and this suggests that the serpentinite was the source of these elements. Limestone, however, appears to be the source of Ba and Sr, which are characterstically high in this rock. In idocrase and diopside Ni, Co and Cr follow Mg but clinochlore shows a low content of all the trace elements determined. Copper appears to vary sympathetically with Si and V seems to follow total iron. These trends are in general agreement with the behavior of these elements in the rocks and minerals from other areas (Wager and Mitchell, 1951, Nockolds and Allen, 1953, 1954 and 1956).

Table 4. Distribution of Trace Elements in the Rocks and Minerals of Taleri Mohammad Jan Area

Specimen	All values in parts per million. ±30%						
	Cu	Ni	Co	V	Cr	Ba	Sr
Limestone	<5	<4	<3	<2	8	75	900
Contact serpentinite	220	250	60	12	350	10	25
Idocrase	100	5	3	15	2	10	500
Clinochlore	20	4	5	10	5	<5	10
Diopside	115	70	35	100	150	<5	80

Analyst S. A. Bilgrami.

PETROGENESIS

The rocks and minerals described here appear to be the result of two different but probably related processes.

Contact Metamorphism. The contact metamorphism of the limestone by the dunite will result in the formation of wollastonite and grossularite. At moderately high temperatures no excessive pressure is needed for the formation of these minerals (Fyfe, Turner and Verhoogen, 1958, 156). Fyfe and Turner (1958, 156) are of the opinion that if excess silica is present anorthite and wollastonite would form and since anorthite has not been identified in the rocks of Taleri area there appears to have been a slight deficiency of silica which is also reflected in the chemical composition of the minerals from this area.

Hydrothermal Activity. The extensive serpentinization and the development of hydrous minerals like chlorites and idocrase all point to a large scale hydrothermal activity. The development of clinochlore and idocrase, however, also requires large amounts of alumina, part of which would be available during the serpentinization of the dunite (by breakdown of orthopyroxene and spinels) and the remainder was probably supplied by the limestone. That alumina is released during the serpentinization of dunites is suggested by the fact that natural serpentines do not accommodate much Al in their structure. Analyses of a dunite and a serpentine mineral (lizardite) from the adjoining Hindubagh area (Table 1, anal. 10 and 11) also illustrate this fact. The above postulated hydrothermal activity, however, raises the problem of the stability of grossularite in hydrothermal environment (Flint, McMurdie and Wells, 1941, and Yoder, 1950). Fyfe and Kennedy found that "the synthesis of hydrogarnets is due to loss of silica from the system during the hydrothermal experiment" (Fyfe, Turner, and Verhoogen, 1958, 156). They further noted that hydrogarnets were not formed in the presence of excess silica. The absence of quartz and hydrogarnets from the rocks of Taleri area suggests that in natural environment there might be factors other than the mere deficiency of silica contributing to the formation of hydrogarnets.

Goldschmidt (1911) has suggested that idocrase might form through the reaction of grossularite and wollastonite with the addition of water and MgO. While it is possible that some of the idocrase of the Taleri area might have formed thus, the petrographic evidence is wholly lacking.

Roy and Roy (1955, 156–157) have demonstrated that clinochlore shows a very wide range of temperture and pressure conditions of formation and a fairly wide range of association. From their experimental work on the system $MgO—Al_2O_3—SiO_2—H_2O$ they concluded that high pressures greatly stabilize clinochlore (p. 156). According to them clinochlore is a stable mineral at least as low as 450° C., when it forms at the expense of an aluminous serpentine. This, however, does not mean that clinochlore is not stable below this temperature. These observations, coupled with our knowledge of the paragenesis of idocrase and grossularite, would suggest that the temperature of the hydrothermal solutions responsible for the development of clinochlore in the Taleri area was at least 450° C., and the extensive occurrence of this mineral would also suggest the prevalence of high pressures.

The variation in the mineralogy exhibited by rocks under consideration may be due, in part at least, to the compositional variations in the limestone.

Acknowledgments

The preliminary work for this paper was done at the University of Minnesota, Minneapolis and my sincere thanks are due to Dr. S. S. Goldich for his interest and advice and to Mr. C. O. Ingemalls for three new analyses. To Prof. J. B. Thompson Jr. my sincere thanks are due for a critical reading of the paper and to Mr. J. Ito for help with the spectrographic work. A Fulbright Travel Grant, a Smith-Mundt Fellowship and research library facilities granted by the University of Minnesota, Minneapolis, and Harvard University, Cambridge, are gratefully acknowledged.

References

Bilgrami, S. A. and Howie, R. A. (1960), The mineralogy and petrology of a rodingite dyke, Hindubagh, Pakistan: *Am. Mineral.* **45,** 791–801.

Flint, E. P., McMurdie, H. F. and Wells, L. S. (1941), Hydrothermal and *X*-ray studies of the garnet-hydrogarnet series and the relationship of the series of hydrolysis products of portland cement: *U. S. Bur. Stand. Jour.*, **26,** 13–33.

Fyfe, W. S., Turner, F. J. and Verhoogen, J. (1958), Metamorphic reactions and metamorphic facies: *Geol. Soc. Amer. Mem.* **73.**

Fyfe, W. S. and Turner, F. J., (1958), Chapter V in the above reference.

Goldschmidt, V. M. (1911), Die kontaktmetamorphose im kristianiage beit.

Hess, H. H. (1949), Chemical composition and optical properties of common clinopyroxenes: *Am. Mineral.*, **34,** 621–666.

Hey, M. H. (1954), A review of the chlorites: *Mineral. Mag.*, **30,** 279–292.

Nelson, Bruce, W. and Roy, R. (1958), Synthesis of chlorites and their structure and chemical constitution: *Am. Mineral.*, **43,** 707–725.

Nockolds, S. R. and Allen, R. (1953, 1954, 1956), The geochemistry of some igneous rocks series: *Geochim. et Cosmochim. Acta.* **4, 5, 9,** 109–142, 245–285, 32–77.

Roy, D., and Roy, R. (1955), Synthesis and stability of minerals in the system $MgO—Al_2$-$SiO_2—H_2O$: *Am. Mineral.*, **40,** 147–178.

Sedlacek, M. (1949), Neue mineralvorkommen in neiderosterreichen Waldviertel: *Verh. Geol. Bund. Wein.* Nos. **4/6,** 133–136.

Shannon, Earl V., (1922), Notes on leuchtenbergite from Phillipsburg, Montana: *Am. Mineral.*, **8,** 10.

Wager, L. R. and Mitchell, R. L. (1951), The distribution of trace elements during strong fractionating of basic magma—a further study of the Skaergaard intrusion, East Greenland: *Geochim. et Cosmochim. Acta.*, **1,** 129–208.

Warren, B. E. and Modell, D. J. (1931), The structure of vesuvianite, $Ca_{10}Al_4(Mg, Fe)_2Si_9(OH)_4$: *Zeit. Krist.*, **78,** 422–432.

Wickman, F. E. (1950), From the notes of the late K. Johnson; *Geol. For. Forh.*, **72,** 64–68.

Yoder, H. S. (1950), Stability relation of grossularite: *Jour. Geol.*, **58,** 221–253.

Manuscript received January 26, 1960.

THE AMERICAN MINERALOGIST, VOL. 45, SEPTEMBER-OCTOBER, 1960

SELECTIVE STAINING OF K-FELDSPAR AND PLAGIOCLASE ON ROCK SLABS AND THIN SECTIONS*

Edgar H. Bailey and Rollin E. Stevens,
U. S. Geological Survey, Menlo Park, California.

Abstract

This note describes a new method of selectively staining plagioclase in which a surface etched with hydrofluoric acid is dipped into a solution of barium chloride, rinsed, and treated with a solution of potassium rhodizonate. Plagioclase feldspars other than pure sodium feldspar are thus stained a brick red by barium rhodizonate. This procedure is combined with the cobaltinitrite staining of K-feldspar to stain K-feldspar yellow and plagioclase red on polished rock surfaces and uncovered thin sections.

This paper describes a method for differentially staining K-feldspar yellow and plagioclase red on slab surfaces or uncovered thin sections. Figure 1 shows a specimen of granitic rock that has been stained using the method.

The new method of staining plagioclase feldspar consists of etching the specimen with hydrofluoric acid vapor, dipping it in barium chloride solution, rinsing, and treating the surface with a solution of potassium rhodizonate. Plagioclase is thus stained brick red. This method of staining plagioclase is combined with the cobaltinitrite staining of K-feldspar to stain K-feldspar yellow and plagioclase red. Staining of K-feldspar with cobaltinitrite was proposed by Gabriel and Cox (1929) and further developed in studies by Keith (1939A and B), Chayes (1952) and Rosenblum (1956).

It seems apparent that the etch-residues left after the hydrofluoric acid treatment are stained, and not the feldspars themselves. Unetched feldspars are not visibly stained. In etching the specimen with hydrofluoric acid vapor, silicon is removed as the volatile fluoride, leaving the other elements on the feldspar surface.

Residual potassium from the K-feldspar reacts with cobaltinitrite to form yellow potassium cobaltinitrite. The staining of the plagioclase is accomplished by replacing the calcium ion in the etched feldspar with barium, which reacts with the rhodizonate reagent to form red insoluble barium rhodizonate. Rhodizonic acid or its soluble salts produce insoluble dark red precipitates with barium (see Yoe and Sarver, 1941).

Pure albite did not become stained by the treatment with barium ion and rhodizonate, but albite with calcium corresponding to only 3 per cent of anorthite was stained red. Apparently sodium in the etch-residue from albite is not readily replaced by barium; however, it may be replaced by potassium. After immersing etched albite in a solution of potassium chloride, it may be stained yellow with cobaltinitrite, showing that potassium ion has substituted for sodium in the etch-residue. By this method plagioclase, except perhaps for nearly pure anorthite, as well as the K-feldspar, can be stained yellow with cobaltinitrite.

---

* Publication authorized by the Director, United States Geological Survey.

On surfaces stained by the two-color method, the yellow K-feldspar and red plagioclase are sharply defined. Textures not readily seen when only K-feldspar is stained become clearly visible, and small particles of one feldspar within the other can be seen. In some specimens zoning is brought out by minor differences in color.

Many practical applications of the two-color staining are apparent. For example, rapid and accurate modal analyses can be made on thin sections as the grain boundaries are clearly defined. On stained hand specimens modal analyses can be made, by the methods of Jackson and Ross (1956), by assistants with little or no mineralogical training. Paul C. Bateman, of the U. S. Geological Survey, is successfully using 35 mm. color transparencies of hand specimens stained two colors in making modal analyses of granitic rocks under the microscope (personal communication). Stained slabs should prove particularly effective in demonstrating to students the interrelations of the K-feldspar, plagioclase, quartz, and dark ferromagnesian minerals because of their brilliant color contrasts.

Elimination of Porosity in the Hand Specimens

Porosity causes difficulty in staining plagioclase in some hand specimens. Fluoride absorbed by the porous surface may prevent staining of the plagioclase or cause the red color to bleach on drying. Also barium chloride solution may be absorbed and later come to the surface, causing the yellow-stained K-feldspar to be discolored with red barium rhodizonate.

Porosity can be eliminated by soaking the rock specimen, on which a flat surface has been sawed and roughly polished, in molten paraffin for about 15 minutes. Excess paraffin is then wiped off, and the flat surface is polished with #400 abrasive and dried. Care should be taken not to touch the polished surface and thus transfer paraffin to the surface and prevent its being evenly etched. Other materials, such as plastics which may be sprayed on the specimen, may also be effective in eliminating porosity.

Reagents and Apparatus

Hydrofluoric acid, concentrated, 52% HF. *Caution:* HF can cause painful burns.
Barium chloride solution, 5%.
Sodium cobaltinitrite solution, saturated.

Rhodizonate reagent. Dissolve 0.05 g of rhodizonic acid potassium salt in 20 ml of distilled water. Make fresh in a small dropping bottle, as the reagent solution is unstable.

Etching vessels. Plastic vessels of about 3/4″ depth and various diameters slightly less than those of the specimens to be etched.

Plastic cover vessels, large enough to cover the etching vessels and specimens placed on them for etching.

Plastic or paraffin etching vessel to fit thin sections.

Ribbed vessel to hold the cobaltinitrite solution.

Procedure for Polished Surfaces of Hand Specimens

1. In a well-ventilated hood, pour the concentrated hydrofluoric acid into an etching vessel to about $\frac{1}{4}''$ of the top.

2. Place the rock specimen across the top of the etching vessel, polished surface down.

3. Cover the etching vessel and specimen with an inverted plastic cover vessel to prevent drafts, and let stand 3 minutes.

4. Remove the specimen from the etching vessel, dip in water, and dip twice quickly in and out of the barium chloride solution.

5. Rinse the specimen briefly in water and immerse it face down for 1 minute in the sodium cobaltinitrite solution.

6. Rinse the specimen by gently tilting it back and forth in tap water until the excess of cobaltinitrite reagent is removed from the surface. The K-feldspar is stained bright yellow if the specimen has been adequately etched. If the K-feldspar is not bright yellow, remove the etch residue by rubbing the surface under water, dry, etch again for a longer period, and continue from step 4.

7. Rinse briefly with distilled water, and cover the surface with rhodizonate reagent. Within a few seconds the plagioclase feldspar becomes brick red. When the red is of satisfactory intensity, rinse the specimen in tap water to remove excess rhodizonate.

The procedure for polished surfaces of hand specimens needs to be modified to suit different needs. The procedure above gives brilliant colors which appear grainy under magnification. The brilliant colors are best for demonstrating coarse features in the rock structure and for counting grains with the naked eye. When fine details of structure are to be studied under the microscope a short period of etching is desirable as it gives a thin, tightly adhering etch-residue and smooth, less highly colored stains. The time of etching will also have to be shortened or lengthened somewhat for different rocks, but it should be kept to a minimum as thick etch-residues tend to flake off of the surface and leave areas of unstained feldspar.

The red color on hand specimens may fade on some of the grains of plagioclase when dry, presumably due to the bleaching action of fluorides left in the pores of the specimens.

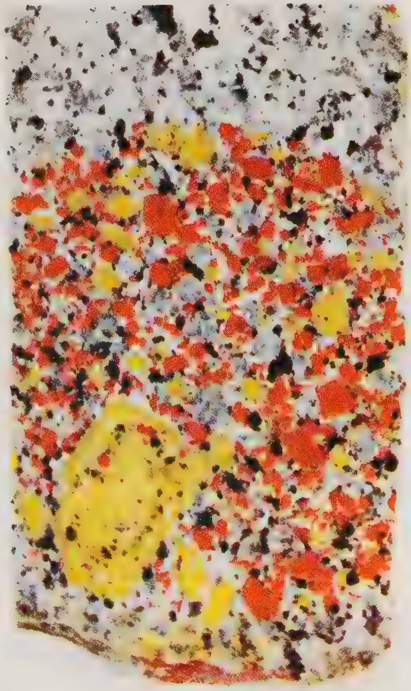

FIG. 1. Granitic rock with K-feldspar stained yellow by cobaltinitrite, and plagioclase stained red by barium rhodizonate. Actual size.

PROCEDURE FOR UNCOVERED THIN SECTIONS

1. Etch the rock surface by leaving it face down for only 10 seconds over hydrofluoric acid at room temperature. *Note:* Rinsing the slide after etching causes the stains to be uneven.
2. Immerse the slide in the saturated sodium cobaltinitrite solution for 15 seconds. The K-feldspar is evenly stained light yellow.
3. Rinse the slide briefly in tap water to remove all of the cobaltinitrite.
4. Dip the slide quickly in and out of the barium chloride solution.
5. Rinse the slide briefly with tap water and then with distilled water.
6. Cover the rock surface with the rhodizonate reagent from the dropping bottle. When the plagioclase feldspar has become pink, rinse the slide in tap water.
7. Allow the slide to dry and cover it in the usual way.

In the stained thin sections under the microscope, the K-feldspar can be seen to be evenly stained a pale yellow and the plagioclase pink. The mineral borders may be outlined by tiny spots of amber red, which seem to be a reaction product of rhodizonate with residual barium chloride left in the cracks between the mineral grains. This defect is not sufficient to interfere with study of the thin section. It was thought that longer washing after the barium chloride treatment would eliminate these amber spots, but after 3 minutes in tap water the K-feldspar also was stained red by the rhodizonate.

REFERENCES

CHAYES FELIX (1952), Notes on the staining of potash feldspar with sodium cobaltinitrite in thin section: *Am. Mineral.*, **37,** 337–340.

GABRIEL, ALTON, AND COX, E. P. (1929), A staining method for the quantitative determination of certain rock minerals: *Am. Mineral.*, **14,** 290–292.

JACKSON, E. D., AND ROSS, D. C. (1956), A technique for modal analysis of medium- and coarse-grained (3–10 mm) rocks: *Am. Mineral.*, **41,** 648–651.

KEITH, M. L. (1939A), Selective staining to facilitate Rosiwal analyses: *Am. Mineral.*, **24,** 561–565.

——— (1939B), Petrology of the alkaline intrusive at Blue Mountain, Ontario: *Bull. Geol. Soc. Am.*, **50,** 1795–1826.

ROSENBLUM, SAMUEL (1956), Improved technique for staining potash feldspars: *Am. Mineral.*, **41,** 662–664.

YOE, J. H., AND SARVER, L. A. (1941), Organic Analytical Reagents: John Wiley and Sons, New York.

Manuscript received January 18, 1960.

THE AMERICAN MINERALOGIST, VOL. 45, SEPTEMBER-OCTOBER, 1960

CRYSTAL CHEMICAL STUDIES OF SOME URANYL OXIDE HYDRATES*

C. L. Christ and Joan R. Clark,
U. S. Geological Survey, Washington 25, D. C.

Abstract

Mineralogical and crystal-chemical studies have been made of the closely related uranyl oxide hydrates becquerelite, billietite, fourmarierite, masuyite, schoepite, and vandendriesscheite. An essential feature of the work is the use of x-ray precession techniques with carefully selected single crystals to determine accurately the crystallographic constants, the symmetry, and the structural relations of these minerals. Indices of refraction and optical orientation were determined on crystals both identified and oriented by the x-ray precession method. Similarly identified crystals were used to obtain the indexed powder pattern data listed. The results obtained on the physical properties, the x-ray crystallography, the x-ray powder data, and the optical properties are listed and compared with the work of other investigators in the 23 tables of the paper.

Crystals of schoepite and of vandendriesscheite that are apparently single, actually consist of several crystallographically distinct phases in parallel intergrowth. The spontaneous alteration from one phase to another that occurs in these crystals results from loss o water of hydration. All six of the minerals studied yield strikingly similar pseudo-hexagona diffraction patterns. A reasonable crystal structure based on these patterns consists o $UO_2(OH)_2$ layers (similar to those proved by Zachariasen to exist in UO_2F_2) parallel to the perfect cleavage (001), with the water of hydration and any cations present in interlayer positions.

Introduction

As part of an extensive program of investigation by this laboratory on the mineralogy and geochemistry of the Colorado Plateau, study was initiated of the crystal structures of some uranyl oxide hydrates and related alkaline earth and lead salts. In the following, these minerals will be referred to simply as uranyl oxide hydrates, the term being taken to include any related salts. Prior to structure analysis, accurate determinations were begun of the unit-cell constants and space groups of the following minerals: becquerelite, billietite, fourmarierite, masuyite, schoepite, and vandendriesscheite. As this work progressed it became apparent that the existing literature on these minerals was confused and often contradictory. Therefore our investigation was extended to include redetermination of the indices of refraction and optical orientation for crystals identified from the x-ray work. In addition, x-ray powder photographs were made from selected crystals of each material. The powder patterns were measured and the lines indexed with the aid of single-crystal x-ray precession patterns. All x-ray and optical data for each mineral have thus been correlated and have been combined with spectrographic analysis whenever enough authentic material was available for such analysis. The results of these studies are presented here. Comparison with earlier findings is given when such comparison appeared warranted, but no exhaustive survey of the literature has been attempted. A comprehensive description of the systematic mineralogy of uranium (including that of the uranyl oxide hydrates) and thorium has recently been published by Frondel (1958).

---

* Publication authorized by the Director, U. S. Geological Survey.

DESCRIPTION OF MINERAL SPECIMENS

All of the mineral specimens used in this study originated in the Shinkolobwe deposit, Katanga district, Belgian Congo. We are greatly indebted to Professor Clifford Frondel, Harvard University, for making available to us the following specimens, each of which is a type specimen from Dr. J. F. Vaes, Union Minière du Haut Katanga: (1) *billietite*, (HM No. 104455), excellent yellow crystals ranging up to 2 mm. in size, associated with green metatorbernite crystals and powdery pale-yellow rutherfordine; (2) *masuyite*, (HM No. 106524), tiny (<0.1 mm.) reddish-orange to brown-orange crystals, associated with large (to 3 mm. length) pale-yellow lath-like crystals of rutherfordine, yellow crystals of becquerelite, and reddish-orange fourmarierite crystals; (3) *vandendriesscheite*, (HM No. 106523), excellent orange crystals (about 0.2 mm. in size), associated with well-developed becquerelite crystals and green metatorbernite crystals, and with powdery pale-yellow rutherfordine.

We are also greatly indebted to Dr. George Switzer, U. S. National Museum, for loaning us the following specimens: (1) *becquerelite* (USNM No. R8387) in fibrous matted crystals; (2) *fourmarierite* (USNM No. R8396), containing orange fourmarierite crystals together with tiny rutherfordine "whiskers" and reddish-brown clumps of goethite crystals; (3) *schoepite* (USNM No. 94712), crystals in various stages of alteration.

DESCRIPTION OF CRYSTALS

Physical properties such as color, habit, and cleavage vary only slightly among the six uranyl oxide hydrates; only billietite and masuyite occur as twins. A summary of these properties for each of the minerals is given in Table 1. It is evident that identification of any one mineral on the basis of these physical properties can be only tentative and *x*-ray and optical studies are also needed for definitive characterization.

The six minerals can be divided into two color classes: a predominantly yellow group, which includes becquerelite (golden to lemon yellow), billietite (deep golden yellow), and altered schoepite (schoepite II and III, yellow), and a predominantly orange group, which includes

Table 1. Physical Properties of Uranyl Oxide Hydrates

Name	Color	Habit	Twinning	Cleavage
Becquerelite	Golden to lemon yellow, less commonly orange yellow	Usually prismatic, elongated [010]; occasionally tabular on {001}	Not observed	Perfect, (001)
Billietite	Deep golden yellow	Tabular on {001}, pseudohexagonal aspect	Usually twins on (110)	Perfect, (001)
Fourmarierite	Reddish orange	Tabular on {001}, elongated [010], pseudo-hexagonal aspect	Not observed	Perfect, (001); secondary, (100)
Masuyite	Reddish to brownish orange	Tabular on {001}, pseudo-hexagonal aspect	Invariably extensively twinned, both on (110) and (1$\bar{3}$0)	Perfect, (001); secondary, (010)
Schoepite I	Amber brown to gold brown	Tabular on {001}, elongated [010], pseudo-hexagonal aspect; (according to Walker (1923) also prismatic elongated [001])	Not observed	Perfect, (001); secondary, (010
Schoepite II, III	Yellow	As for schoepite I	Not observed	
Vandendriesscheite	Yellowish orange to orange	Prismatic, elongated [100], (010) striated parallel to [100]; also tabular on {001}, elongated [100], pseudohexagonal aspect	Not observed	Perfect, (001)

fourmarierite (reddish orange), masuyite (reddish to brownish orange) and vandendriesscheite (yellow orange to orange). Unaltered schoepite (schoepite I) is amber brown to gold brown.

All six minerals are orthorhombic, probably holohedral, and occur in one or both of two common habits: either tabular on {001} with a pseudo-hexagonal outline caused by the presence of forms such as {110}, {111}, {100}, and {010}, or prismatic, elongated along either [100] or [010] and exhibiting a variety of prism forms. Perfect cleavage is always parallel to (001); some secondary cleavages are noted in Table 1. In the present study, billietite, fourmarierite, masuyite, and schoepite were found only as tabular crystals, whereas becquerelite and vandendriesscheite were found both as tabular and as prismatic crystals. Excellent photographs, some in color, of crystals of becquerelite, billietite, fourmarierite, and masuyite-(?) are given by Chervet and Branche (1955). More recently, a remarkably beautiful series of color photographs of a number of uranium minerals, together with brief summaries of the scientific data for these minerals, have been collected in a book by Destas, Vaes, and Guillemin (1958).

Twinning has been reported, and was observed in this study, only for billietite and for masuyite. Billietite twinning was described by Vaes (1947) and Thoreau (1948); single crystals of billietite are rare although some small ones (about 0.2 mm. cross section) were found on the HM No. 104455 specimen. The common twin we observed has twin and composition plane (110). Masuyite twinning was described by Vaes (1947) and we found it to be exactly as he described it: the twins occurring with (110) and with ($1\bar{3}0$) as twin and composition planes. The twinning is persistent and distinctive, providing the only means we found for differentiating masuyite from fourmarierite under the microscope. The mode of twinning in billietite and masuyite was checked by x-ray precession patterns, as well as by optical study. Fourmarierite was always found as tiny, perfect single crystals, whereas single crystals of masuyite for x-ray study were obtained only by careful cutting of twinned crystals.

No attempt has been made during the present investigation to examine crystal morphology in detail, partly because an extensive literature on this subject already exists. Some of the more comprehensive references are: Schoep (1930) on becquerelite, fourmarierite and schoepite, Thoreau (1948) on billietite and vandendriesscheite, and Vaes (1947) on billietite, masuyite, and vandendriesscheite. Previous studies can be readily correlated with the present x-ray findings provided that the perfect cleavage is always taken as parallel to (001), the elongation direction is identified as noted in Table 1, and the optical orientation is followed as given in Table 16. Because the morphology is so similar for all six minerals, x-ray examination, which provides rapid and accurate differentiation, is preferable to any morphologic study for purposes of identification.

X-RAY CRYSTALLOGRAPHY

Single-crystal x-ray studies were made using quartz-calibrated precession cameras with both Mo/Zr and Cu/Ni radiations (λ Mo$K\alpha=0.7107$ Å; λ Cu$K\alpha=1.5418$ Å). Film measurements were corrected for both horizontal and vertical film shrinkage. For all the minerals a characteristic pseudo-hexagonal pattern was obtained for the $hk0$ net, which is the zero level normal to [001] and hence parallel to the cleavage plane (001). A typical pattern is illustrated in Fig. 1. A pseudo-orthohexagonal cell can be defined from these patterns as well as the true orthorhombic cell, and cell constants for each type of cell are given in Table 2. In addition, Table 2 lists the cell volume of the true orthorhombic cell and the possible space groups for each mineral, including alteration forms. Noncentrosymmetric space groups have been included in Table 2 where their possibility exists according to the x-ray data alone. Piezoelectric tests made on an apparatus of the Giebe-Scheibe type gave negative results, and since the morphology of each of the minerals is clearly holohedral the assignment of centrosymmetric space groups is valid.

Table 2 lists probable chemical formulas and cell contents for all the minerals except masuyite and vandendriesscheite; the corresponding calculated and observed specific gravities are compared in this table. New specific gravity determinations were made of becquerelite (12 mg. sample) and vandendriesscheite (2 mg. sample) with the Berman balance, using toluene as the immersion liquid. Values of the specific gravity for the other minerals are taken from the literature. Discussion of the chemical formulas is included in the section on chemical considerations and crystal structure.

Comparison of the data of the present study with previously reported data is made in Tables 3 through 8, and in the text below. Table 3 deals with becquerelite, Table 4 with billietite, Table 5 with fourmarierite, Table 6 with masuyite, Table 7 with unaltered schoepite (schoepite I), and Table 8 with vandendriesscheite.

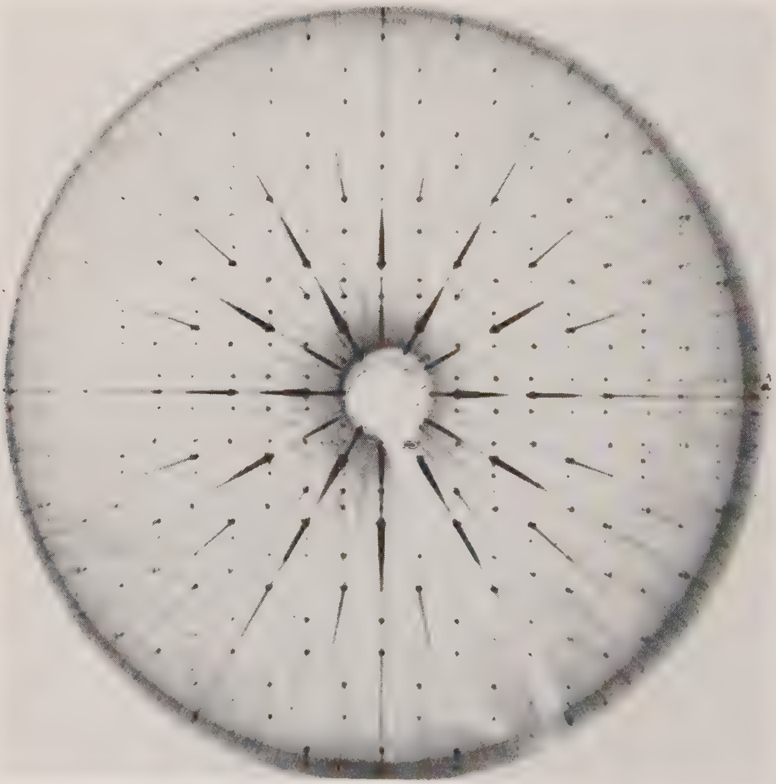

FIG. 1. Characteristic pseudo-hexagonal $hk0$ net, illustrated by schoepite.

TABLE 2. CRYSTAL DATA FOR THE URANYL OXIDE HYDRATES

(Data of present study unless otherwise noted)

	Becquerelite	Billietite	Fourmarierite	Masuyite	Schoepite			Vandendriesscheite	
					I	II	III	I	II
Cell constants[a]									
a	13.86 Å	7.14 Å	14.00 Å	41.93 Å	14.33 Å	13.99 Å	14.12 Å	14.07 Å	14.07 Å
b	12.38	12.08	16.47	24.22	16.79	16.72	16.83	40.85	41.31
c	14.96	15.10	14.39	42.61	14.73	14.73	15.22	43.33	43.33
Pseudo-orthohexagonal cell constants									
a'	$a/2=6.93$	$a/1=7.14$	$a/2=7.00$	$a/6=6.99$	$a/2=7.16$	$a/2=7.00$	$a/2=7.06$	$a/2=7.04$	$a/2=7.03$
b'	$b/3=4.13$	$b/3=4.03$	$b/4=4.12$	$b/6=4.04$	$b/3=4.20$	$b/4=4.18$	$b/4=4.21$	$b/10=4.08$	$b/10=4.13$
c'	$c/2=7.48$	$c/2=7.55$	$c/2=7.20$	$c/6=7.10$	$c/2=7.36$	$c/2=7.36$	$c/2=7.61$	$c/6=7.22$	$c/6=7.22$
Pseudo-hexagonal α'	120.8°	119.4°	120.5°	120.0°	120.4°	120.9°	120.8°	120.2°	120.4°
Volume (true cell) Å^3	2567	1303	3318	43272	3544	3446	3617	24904	25185
Units of $UO_2(OH)_2$ (true cell)	24	12	32	432	32	32	32	240	240
Formula proposed	$CaO \cdot 6UO_3 \cdot 11H_2O$[b]	$BaO \cdot 6UO_3 \cdot 11H_2O$[e]	$PbO \cdot 4UO_3 \cdot 4H_2O$	—	$UO_3 \cdot (2+?)H_2O$	$UO_3 \cdot (2-?)H_2O$	$UO_3 \cdot (2-?)H_2O$	—	
Spec. grav. (calc.)	5.10	5.27	5.76	—	4.83	—	—	—	
Spec. grav. (obs.)	5.14±0.06 5.12±0.02[c] 5.10±0.02[d]	5.28±0.01[f]	5.74±0.05[g]		4.8[h] 4.49[i]	—	—	5.45	
Space Group	*Pnma*- (No. 62), or *Pn2a*- (No. 33)	*Pnmn*- (No. 58), or *Pn2n*- (No. 34)	*Bbmm*- (No. 63), *Bb2₁m*- (No. 36) or *Bbm2*- (No. 40)	—	*Pbca*- (No. 61)	*Pbna*- (No. 60)	*Pbca*- (No. 61)	*Pmma*- (No. 51), *P2₁ma*- (No. 26), or *Pm2a*- (No. 28)	

---

[a] Error ±0.3%.
[b] After Protas (1957).
[c] Mineral, Protas (1957).
[d] Synthetic, Protas (1957).
[e] After Brasseur (1949).
[f] Brasseur (1949).
[g] Brasseur (1948).
[h] Billiet and de Jong (1935).
[i] Bignand (1955).

Becquerelite, billietite, and fourmarierite

Cell constants previously reported for becquerelite and billietite are in good agreement with those found during the present study except that a doubled value for a in billietite was given by Frondel and Cuttitta (1953) (Table 4). The doubled value is found if a twin crystal, instead of a single crystal, is examined by [100] rotation x-ray photographs. This result arises from the fact that in billietite, the twinning on (110), following the classical law for pseudo-hexagonal lattices, brings about the almost parallel alignment of the [110] direction of one member of the twin edifice with the [100] direction of its pseudosymmetrically related member. Since, for billietite, $a=7.14$ Å and $[110]=14.03$ Å, i.e. very nearly $2a$, a rotation pattern made around this common direction will have layer-line geometry leading to the doubled value. The smaller value of a originally given by Brasseur (1949) is correct. The calculated

Table 3. Crystal Data for Becquerelite

Comparison of the results of various investigators

	Present study (Cell constants ±0.3%)	Protas (1957)	Frondel and Cuttitta (1953)	Brasseur (1948)	Billiet and de Jong (1935)
a	13.86 Å	13.86 ± 0.03 Å[b]	13.92 ± 0.005 Å	—[d]	13.9 kX
b	12.38	12.42 ± 0.03	12.45 ± 0.005	—	12.55
c	14.96	14.96 ± 0.03	15.09 ± 0.005	—	14.9
$a:b:c$	1.120:1:1.208	(1.116:1:1.205)[c]	(1.118:1:1.212)	—	1.107:1:1.187
Vol. unit cell	2567 Å	(2575 Å^3)	(2615 Å^3)	—	2600 kX^3
Formula proposed	$CaO\cdot6UO_3\cdot11H_2O$[a]	$CaO\cdot6UO_3\cdot11H_2O$	$7UO_3\cdot11H_2O$	$UO_3\cdot2H_2O$	$2UO_3\cdot3H_2O$
Z	4	4	4	24	13
Space group	*Pnma*- (No. 62), prob., or $Pn2_1a$- (No. 33)	—	*Pmma*	*Pnma*[e]	—
Spec. grav. (calc.)	5.10 ± 0.01	(5.08)	5.60	(4.98)[f]	(5.25)[g]
Spec. grav. (obs.)	5.14 ± 0.06	5.12 ± 0.02 mineral 5.10 ± 0.02 synthetic	5.3 (approx.)	5.090 ± 0.035	5.2

[a] After Protas (1957).

[b] Errors listed are those assigned by original authors.

[c] Quantities enclosed in parentheses calculated by present authors from data of original authors, except as indicated in footnotes f and g below.

[d] Brasseur states that he found values of a, b, and c in agreement with those of Billiet and de Jong (1935).

[e] Brasseur is apparently quoting Wolfe, private communication (1941), in Palache, Berman, and Frondel (1944).

[f] Calculated for a, b, c of present study and cell contents $24[UO_3\cdot2H_2O]$.

[g] Calculated for a, b, c of present study and cell contents $13[2UO_3\cdot3H_2O]$.

TABLE 4. CRYSTAL DATA FOR BILLIETITE

Comparison of the results of various investigators.

	Present Study (Cell constants ±0.3%)	Brasseur (1949)	Frondel and Cuttitta (1953)	
a	7.14_3 Å	7.10 kX	14.25 Å[c]	13.98 Å[d]
b	12.08	12.06	12.04	12.08
c	15.10	15.06	15.06	15.06
a:*b*:*c*	0.591:1:1.250	0.5887:1:1.2486	(1.184:1:1.251)	(1.157:1:1.247)
Vol. unit cell	1303 Å^3	(1290 kX^3)[b]	(2584 Å^3)	(2543 Å^3)
Formula proposed	$BaO \cdot 6UO_3 \cdot 11H_2O$[a]	$BaO \cdot 6UO_3 \cdot 11H_2O$	$BaO \cdot 6UO_3 \cdot 11H_2O$	
Z	2	2	4	
Space group	*Pnmn*-(No. 58), prob., or *Pn2n*-(No. 34)	*Pnnm*	*Pmma*	
Spec. grav. (calc.)	5.27	(5.27)	5.33	5.40
Spec. grav. (obs.)	—	5.28	5.32	5.36

[a] After Brasseur (1949).

[b] Quantities in parentheses calculated by present authors from data of original authors.

[c] Crystal from HM No. 104456; error in lattice constants listed by authors as ±0.005 Å.

[d] Crystal from HM No. 104455; error in lattice constants listed by authors as ±0.005 Å.

angle of obliquity for billietite twinning is 1°11′. Fourmarierite cell constants found in the present study are in reasonable agreement with those reported by Brasseur (1941) (Table 5).

TABLE 5. CRYSTAL DATA FOR FOURMARIERITE

Comparison of the results of various investigators.

	Present study (Cell constants ±0.3%)	Brasseur (1941, 1948)
a	14.00 Å	14.07 kX
b	16.47	16.72
c	14.39	14.52[b]
a:*b*:*c*	0.850:1:0.874	(0.842:1:0.868)[c]
Vol. unit cell	3318 Å^3	(3416 kX^3)
Formula proposed	$PbO \cdot 4UO_3 \cdot 4H_2O$[a]	$PbO \cdot 4UO_3 \cdot 7H_2O$
Z	8	8
Space group	*Bbmm*-(No. 63), prob., *Bb*2_1*m*-(No. 36), or *Bbm*2-(No. 40)	—
Spec. gravity (calc.)	5.76	5.77
Spec. gravity (obs.)	—	5.740±0.051

[a] Best fit to observed specific gravity of Brasseur (1948).

[b] The *a*- and *c*-axes of Brasseur (1941) interchanged to conform to convention of present authors.

[c] Quantities in parentheses calculated by present authors from data of original author.

Masuyite

The large cell edges given for masuyite in Table 2 and in Table 6 are required by the presence of some faint, diffuse, and relatively sparse spots on the precession patterns. Previous investigators have reported smaller cells: Brasseur (1950) gives $a=14.06$, $b=12.06$, $c=14.25$ kX, and J. W. Frondel in Frondel (1958) gives $a=13.90$, $b=12.31$, $c=14.92$ Å. If the faint spots are neglected, the results obtained in the present study lead to cell edges of $a=13.98$, $b=12.11$, and $c=14.20$ Å, in agreement with Brasseur's values. The value for the length of the c-axis found by J. W. Frondel differs significantly from that found by Brasseur and by us. It does, in fact, agree well with the c for becquerelite, and it is possible that the cell constants given by Frondel (1958) for masuyite are actually those of becquerelite. Brasseur gives the space group *Pcna* for masuyite, in agreement with our findings, the faint spots again being neglected. It was not possible to determine the space group of the large cell. Although great care was exercised in trying to use only single crystals in the x-ray work for masuyite, it is possible that the mineral is twinned on a fine scale, and that this twinning could lead to the large cell edges found. The results of Brasseur and Frondel for masuyite are compared with the results of the present study in Table 6.

Schoepite

Crystals of schoepite that are apparently single yield multiple diffraction patterns. These multiple patterns correspond to the presence of two out of three possible distinct orthorhombic phases in parallel inter-

TABLE 6. CRYSTAL DATA FOR MASUYITE

Comparison of the results of various investigators.

	Present study (Cell constants ±0.3%)	Present study—neglecting very weak *hkl*	Brasseur (1950)	Frondel (1958)[a]
a	41.93 Å	13.98 Å	14.06 kX	13.90 Å
b	24.22	12.11	12.06	12.31
c	42.61	14.20	14.24	14.92
a:b:c	1.731:1:1.759	1.154:1:1.172	1.166:1:1.181	1.129:1:1.212
Vol. unit cell	43272 Å^3	2404 Å^3	2415 kX^3	2553 Å^3
Formula proposed	—	—	—	$UO_3 \cdot 2H_2O$[b]
Space group	—	*Pcna*-(No. 50)	*Pcna*-(No. 50)	—

[a] Crystallography by J. W. Frondel. The crystal data may be for becquerelite (see Table 3).

[b] Chemical analysis by F. Cuttitta. Note, however, that Vaes (1947) described masuyite as a Pb-bearing mineral.

TABLE 7. CRYSTAL DATA FOR SCHOEPITE I (UNALTERED SCHOEPITE)
Comparison of the results of various investigators.

	Present Study (Cell constants ±0.3%)	Billiet and de Jong (1935)	Palache (1934); Schoep (1932)
a	14.33 Å	14.40 kX	—
b	16.79	16.89	—
c	14.73	14.75	—
a:*b*:*c*	0.854:1:0.877	0.852:1:0.873	0.8516:1:0.8745[b]
Vol. unit cell	3544 Å^3	3590 kX^3	—
Formula proposed	$UO_3 \cdot 2H_2O$[a]	$4UO_3 \cdot 9H_2O$	$3UO_3 \cdot 7H_2O$[c]
Z	32	8	—
Space group	*Pbca*-(No. 61)	—	—
Spec. grav. (calc.)	4.83	4.83	—
Spec. grav. (obs.)	—	4.8	4.96[c]

[a] See Frondel (1958) and discussion in text of present paper.

[b] Mean of measurements by Walker (1923), Ungemach (1929), and Palache (1934), as reported by Palache (1934).

[c] Schoep (1932).

growth in the crystal. The three phases are designated schoepite I, II and III; data are given for these in the appropriate tables of this report.

Examination of the specimen USNM No. 94712 showed that the schoepite crystals are present in various stages of alteration. Commonly, crystals occur that have an amber-brown core completely or partially surrounded by a golden-yellow alteration product. *X*-ray examination shows that the amber-brown part consists chiefly of schoepite I with small amounts of schoepite II present, and that the yellow alteration product consists either of schoepite II, or of schoepite III, usually with small amounts of schoepite I also present. The fact that schoepite II and schoepite III were not found together in any of the crystals studied does not preclude the possibility that they can occur together, since no exhaustive search was made to test this point. Completely yellow crystals answering the description given for paraschoepite by Schoep and Stradiot (1947) are also present on the specimen. These give the schoepite III pattern. Because of the distinctive *x*-ray pattern given by the yellow crystals and the excellent agreement of the optical measurements obtained in the present study with those originally given by Schoep and Stradiot in 1947, there can be little doubt as to the validity of paraschoepite. Entirely amber-brown crystals are also present on the specimen. Although these appear to be completely unaltered, they show a weak *x*-ray pattern corresponding to schoepite II along with the expected strong pattern of schoepite I. The cell constants for schoepite I agree well with those given by Billiet and de Jong (1935) for "schoepite" (Table 7). Data for schoepite II have not been reported previously. Figure 2 illustrates a portion of an *hk*0 *x*-ray precession pattern of a schoepite crystal showing the results obtained when two phases are present.

Vandendriesscheite

X-ray patterns of vandendriesscheite are also multiple, corresponding to the presence of two distinct orthorhombic phases present in parallel intergrowth in apparently single crystals. These phases are designated vandendriesscheite I and II and the data for these are given in the appropriate accompanying tables. Crystals of vandendriesscheite occur containing mostly phase I with small amounts of phase II present; crystals with the reverse proportions were also found. Unlike schoepite, the crystals of vandendriesscheite do not change appearance on phase change. However, this phase change does manifest itself in the variability of the β and γ indices of refraction, as well as in the *x*-ray patterns.

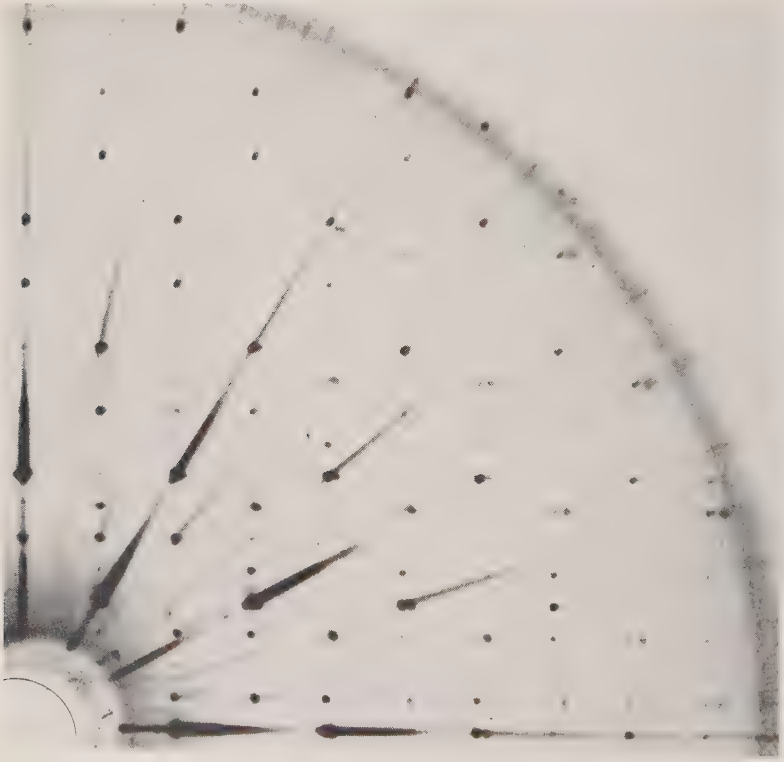

FIG. 2. Enlarged portion of the same pattern shown in Fig. 1 showing the presence of diffraction spots due to two phases in parallel intergrowth.

The weaker reflections leading to the large *b*-length for both phases of vandendriesscheite (Table 2) are sharp, plentiful, and easily visible on the precession patterns. However, the weaker reflections requiring the large *c*-axis are, as in masuyite, very faint, diffuse, and relatively sparse. J. W. Frondel in Frondel (1958) has reported values of *a*, *b*, and *c* for four different crystals of vandendriesscheite. The results she obtained are compared with the results of the present study in Table 8. It can be seen from this table that the two sets of results are not in very good agreement. The variability in the cell constants reported in Frondel (1958) was not encountered in the present study, where, however, only crystals from a single specimen were examined. It is stated in Frondel (1958) that a weak set of *x*-ray reflections was found superimposed on and irrationally related to the main diffraction pattern in Weissenberg photographs of vandendriesscheite. In the present investigation the weak set was found to be unequivocally rational to the main set of reflections. In contrast to masuyite, there was absolutely no indication of any twinning in vandendriesscheite, and consequently no doubt about the validity of the large cell for this reason.

Schoepite and vandendriesscheite appear to alter by spontaneous dehydration at room temperatures. The evidence for this conclusion and a discussion of the complexity of the alteration are given below in the section on chemical considerations and crystal structure. Precession patterns of altered crystals show the usual sharp spots for the parent phase and diffuse spots for the phase resulting from the alteration, due to the fine-grained nature of the alteration product.

X-Ray Powder Data

A 114.59 mm. diameter powder camera was used with Cu/Ni and Cr/V radiations (λ CuK$\alpha = 1.5418$ Å; λ CrK$\alpha = 2.2909$ Å) to obtain the powder films. Tables 9 through 15 give powder pattern data for the minerals, as follows: becquerelite, Table 9; billietite, Table 10; fourmarierite, Table 11; masuyite, Table 12; schoepite, Table 13; dehydrated schoepite, $UO_2(OH)_2$, Table 14; vandendriesscheite, Table 15. Measurements from the patterns for becquerelite, fourmarierite, and vandendriesscheite were corrected for film shrinkage; measurements from the other patterns were not, but film shrinkage corrections were negligible for these, as shown by the good agreement between the observed and calculated interplanar spacings. The lower limit measurable for 2θ was about 6°. Calculated interplanar spacings were based on the values of the cell constants as given in Table 2. Indexing of the powder lines was checked by examination of the intensities of the corresponding reflections on the single-crystal precession photographs; estimated in-

TABLE 8. CRYSTAL DATA FOR VANDENDRIESSCHEITE

Comparison of the results of various investigators.

	Present study (Cell constants ±0.3%)		Present study—neglecting very weak *hkl*		Frondel (1958)[a]			
	I	II	I	II	Crystal 1	Crystal 2	Crystal 3	Crystal 4
a	14.07 Å	14.07 Å	14.07 Å	14.07 Å	13.96 Å	14.12 Å	14.01 Å	13.99 Å
b	40.85	41.31	13.62	13.77	14.36	16.75	16.80	16.44
c	43.33	43.33	14.44	14.44	14.41	14.72	14.68	14.30
$a:b:c$	0.344:1:1.061	0.341:1:1.049	1.033:1:1.061	1.022:1:1.049	0.972:1:1.003	0.843:1:0.879	0.834:1:0.874	0.851:1:0.870
Vol. unit cell	24904 Å^3	25185 Å^3	2767 Å^3	2798 Å^3	(2889 Å^3)[b]	(3481 Å^3)	(3455 Å^3)	(3289 Å^3)
Formula proposed					$PbO\cdot 7UO_3\cdot 12H_2O$[c]	$PbO\cdot 7UO_3\cdot 12H_2O$[d]	$PbO\cdot 7UO_3\cdot 12H_2O$[c]	
Z	—				(4)	(4)	(4)	(4)
Spec. grav. (calc.)	—				5.61	4.66	4.69	—
Spec. grav. (obs.)	5.45				5.46	—	4.72	—

---

[a] Crystallography by J. W. Frondel.

[b] Quantities in parentheses calculated by present authors from data of original authors.

[c] Chemical analysis by F. Cuttitta.

[d] Chemical analysis by F. A. Gonyer.

tensities for the single-crystal reflections are included in the tables, where feasible. All calculated interplanar spacings are given for $d \geq 2.5$ Å except in Table 15 for vandendriesscheite, where, because of the large cell, the listing is for $d \geq 3.0$ Å. However, all observed spacings smaller in value than these could be satisfactorily accounted for. Tables 9 through 15 also give observed powder data found by other investigators and believed by us to be reliable.

Each of these six uranyl oxide hydrates can be identified from its powder pattern provided certain precautions are observed. Material chosen for the powder spindle should, of course, be carefully selected for homogeneity. A sharp clear pattern with maximum line resolution is required. With the commonly used 114.59 mm. diameter camera, a small diameter (*ca.* 0.2 mm.) powder spindle is desirable, and line-focus, rather than spot-focus, radiation is recommended. With good patterns, becquerelite, billietite, and schoepite can be promptly identified. Powder patterns of schoepite always show lines corresponding to each of the two or three possible phases, but their presence does not prevent correct overall identification of the material as schoepite. Fourmarierite, masuyite, and vandendriesscheite can easily be distinguished as a group from the other three minerals, but identification of any one of the three is more difficult. Comparison of the powder data given in Tables 11, 12, and 15 shows that fourmarierite, masuyite and vandendriesscheite can be differentiated if the powder patterns are good. However, single-crystal *x*-ray studies, preferably by precession methods, provide the best and certainly the most rapid and convenient means of unambiguously distinguishing among these various uranyl oxide hydrates and their alteration products.

OPTICAL DATA

Indices of refraction were measured with Na light ($\lambda = 589$ mμ). Cargille's High Series liquids were used and the indices of the liquids were checked on a Leitz-Jelley refractometer. No special effort was made to keep the temperature constant; room temperatures were $25° \pm 5°$ C. Optical orientation was in each case checked on crystals for which crystallographic directions had been identified by precession *x*-ray work.

Values found in the present study for the indices of refraction and observed V_α, as well as data on pleochroism and optical orientation, are summarized in Table 16. Comparison between data of the present study and data reported by other investigators is made in Tables 17 through 23. Table 17 is for becquerelite, Table 18 for billietite, Table 19 for fourmarierite, Table 20 for masuyite, Table 21 for schoepite I, Table 22 for schoepite III, and Table 23 for vandendriesscheite.

All the uranyl oxide hydrates are biaxial negative with $X = c$ in each

TABLE 9. *X*-RAY POWDER DATA: BECQUERELITE

Calculated		Present Study			Frondel and Cuttitta (1953)[1]		Protas (1957)			
		Measured			Measured		Measured d(Å)			
		Single Crystal	d(Å)	Powder Cu/Ni $\lambda=1.5418$ Å	d(Å)	Cu/Ni	Natural Mineral		Synthetic Mineral	
hkl	d_{hkl}	I	I	d_{hkl}	d_{hkl}	I	d_{hkl}	I	d_{hkl}	I
101	10.17	*								
011	9.54	*			(8.51)[2]	1				
111	7.86	*								
002	7.48	VS	100	7.44± .05	7.50	10	7.54	FF	7.48	FF
200	6.93	a								
102	6.58	S	3	6.56± .04	6.63	2	6.59	mf	6.59	mf
201	6.29	a								
020	6.20	*	1	6.21± .04	6.24	1	6.22	mf	6.22	mf
210	6.05	w					6.05	mf	6.05	mf
112	5.81	a					5.81[3]	mf	5.81[3]	mf
211	5.61	m	1	5.59± .03	5.63	1				
121	5.29	*								
202	5.08	a							4.78	ff
022	4.77	w								
212	4.70	w								
103	4.69	m	6	4.68± .02	4.71	6	4.71	mf	4.71	mf
013	4.63	a								
220	4.62	w								
122	4.51	*								
301	4.41	w			4.31	1			4.40	f
221	4.41	a								
113	4.39	a								
311	4.16	a								
203	4.05	w							4.05	f
031	3.981	a								
302	3.931	w-							3.92	f
222	3.930	*								
213	3.848	a							3.84	f
131	3.826	a								
312	3.747	a								
123	3.740	a								
004	3.740	VS	30	3.73± .015	3.75	8	3.74	m	3.73	m
104	3.611	m	3	3.61± .02					3.61	f
321	3.595	a								
230	3.548	VS	21	3.54± .015	3.56	8	3.55	F.FF	3.55	F.FF
132	3.498	w-								
114	3.467	w-								
400	3.465	VS	4	3.45± .015	3.48	2	3.47	m	3.46	m
231	3.452	m								
303	3.389	S								
223	3.388	a	4	3.37± .015	3.39	2	3.40	m	3.39	m
401	3.376	VS								
410	3.337	w-								
322	3.319	a								
204	3.291	a								
313	3.269	*								
411	3.257	a								
232	3.206	VS	35	3.20± .01	3.22	9	3.21	F.FF	3.20	F.FF
024	3.202	w-								
214	3.181	w								
033	3.181	w								
402	3.144	VS	4	3.14± .01	3.13	1	3.15	mF	3.14	mF
124	3.120	w								
133	3.100	w								
040	3.098	w							3.10	f
412	3.048	a								
420	3.024	a								
331	3.016	a								
323	2.973	*								
421	2.964	m	3	2.959± .007	2.97	2	2.97	mf	2.97	mf
141	2.963	a								
105	2.925	w								
015	2.908	a								
304	2.907	w								
224	2.907	a								
233	2.891	m	3	2.894± .006	2.88	3				
042	2.862	w								

---

[1] See also Frondel, Riska, and Frondel (1956).

[2] Must be β reflection for 002.

[3] Possibly a typographical error and should be 5.61.

TABLE 9 (*continued*)

Calculated		Present Study			Frondel and Cuttitta (1953)[1]		Protas (1957)			
		Measured			Measured		Measured d(Å)			
		Single Crystal	d(Å)	Powder Cu/Ni λ=1.5418 Å	d(Å)	Cu/Ni	Natural Mineral		Synthetic Mineral	
332	2.847	a								
115	2.846	a								
403	2.846	m	3	2.848 ± .006			2.86	mf	2.85	mf
314	2.830	*								
240	2.828	a								
422	2.804	a								
142	2.803	a								
241	2.779	a								
413	2.773	*								
205	2.747	w	3	b{2.74 to 2.71	2.73	1				
501	2.726	a								
134	2.718	w								
215	2.682	a								
511	2.662	w-							2.67	f
430	2.654	a								
242	2.645	a								
125	2.645	a								
324	2.632	*								
333	2.620	*								
431	2.614	a								
502	2.599	a								
423	2.586	*								
143	2.585	a								
234	2.574	m	9	2.566 ± .006	2.58	7	2.58	m	2.58	m
512	2.544	w-								
404	2.542	m	1	2.53 ± .01			2.55	mf	2.54	mf
341	2.536	a								
305	2.511	w								
225	2.511	a								
432	2.502	a								
			2	2.483	2.47	2			2.49	ff
			4	2.441	2.44	2			2.45	f
			3	2.378	2.38	2	2.40	mf	2.38	mf
			3	2.305	2.31	3	2.31	m	2.31	m
									2.25	f
			2	2.197	2.21	1	2.22	f	2.21	f
			4	2.102	2.11	2			2.12	f
			3	2.065	2.07	3	2.07	mf	2.07	mf
			6	2.036	2.04	4	2.04	mf	2.04	mf
							2.02	f	2.02	f
			4	1.989	1.994	4	2.00	m	2.00	m
			6	1.935	1.943	5				
			2	1.891	1.893	2				
			3	1.869	1.875	2				
			3	1.846	1.848	2				
			1	1.826						
			2	1.807	1.814	1				
			4	1.771	1.773	3				
			4	1.721	1.725	3				
			2	1.686	1.681	2				
			3	1.670						
			3	1.615	1.614	2				
			3	1.597	1.600	2				
			3	1.560	1.564	2				
			2	1.541	1.541	1				
		Plus many additional weak lines. a = observed to be absent. b = broad. * = not measured. Film No. 7861, corrected for shrinkage.			Plus many additional weak lines.					

TABLE 10. X-RAY POWDER DATA: BILLIETITE

		Present Study			Frondel and Cuttitta (1953)[1]		Protas (1956)			
Calculated		Measured			Measured		Measured d(Å)			
		Single Crystal	d(Å)	Powder Cu/Ni λ=1.5418 Å	d(Å)	Cu/Ni	Natural Mineral		Synthetic Mineral	
hkl	d_{hkl}	I	I	d_{hkl}	d_{hkl}	I	d_{hkl}	I	d_{hkl}	I
011	9.43	a					(7.74)[2]	m-F	(7.69)[2]	mF
002	7.55	VS	100	7.56± .05	7.53	10	7.40	FF	7.40	FF
101	6.46	*	2	6.51± .04						
110	6.15	w	2	6.13± .03						
020	6.04	w								
111	5.69	*	2	5.73± .03						
102	5.19	*								
112	4.77	a								
022	4.72	m	6	b 4.70 to 4.62	4.59	2	4.68	f	4.61	f
013	4.65	m								
121	4.41	w								
103	4.12	a								
122	3.936	a								
113	3.895	a								
031	3.890	a								
004	3.775	VS	25	3.78± .015	3.77	9	3.74	F.FF	3.74	F.FF
200	3.571	S	9	3.58± .015	b3.54	5	3.51	mF	3.47	mF
130	3.507	VS	18	3.51± .01						
201	3.476	w								
131	3.416	w	1	3.42± .01						
123	3.400	w								
211	3.340	*								
104	3.338	a								
202	3.228	S	18	3.23± .01						
114	3.217	w-								
024	3.201	w								
132	3.181	VS	35	3.183± .008	3.17	8	3.19	F.FF	3.16	F.FF
033	3.144	a								
212	3.119	a								
220	3.074	w								
040	3.020	m	2	3.030± .008	3.02	1	3.01	ff	3.01	ff
221	3.012	*								
015	2.930	w	2	2.928± .007	2.89	1	2.91	ff		
124	2.921	a								
203	2.913	a								
133	2.878	a								
222	2.847	*	1	2.85± .01					2.85	ff
213	2.832	a								
042	2.804	S	3	2.798± .007	2.79	2	2.79	ff	2.78	ff
105	2.782	a								
141	2.735	w								
115	2.711	w-								
231	2.631	*								
223	2.624	*								
142	2.610	w	6	b 2.60 to 2.56	2.56	3	2.57	mf	2.55	mf
204	2.594	m								
134	2.570	S								
214	2.537	a								

[1] See also Frondel, Riska, and Frondel (1956).

[2] Possibly β reflection for 002, otherwise not indexable.

TABLE 10 *(continued)*

Calculated		Present Study			Frondel and Cuttitta (1953)[1]		Protas (1956)			
		Measured			Measured		Measured d(Å)			
		Single Crystal	d(Å) Powder Cu/Ni $\lambda=1.5418$ Å		d(Å)	Cu/Ni	Natural Mineral		Synthetic Mineral	
hkl	d_{hkl}	I	I	d_{hkl}	d_{hkl}	I	d_{hkl}	I	d_{hkl}	I
125	2.527	w								
232	2.519	*								
006	2.517	S	4	2.520± .006	2.49	4	2.50	mf	2.50	mf
			3	2.313	2.30	2	2.31	mf	2.29	mf
			2	2.271						
			1	b{2.21 to 2.19	d 2.19	1	2.20	f	2.19	f
			4	2.124	2.10	3	2.12	f	2.11	f
			9	2.053	2.03	6	2.05	m	2.03	m
			2	2.015						
			4	1.983	1.970	4				
			6	1.950	1.940	2				
					1.898	1				
			4	1.888	1.872	3				
					1.812	1				
			3	1.803	1.790	2				
			2	1.705	1.676	3				
			2	1.664	1.654	4				
		Plus many additional weak to moderate lines.			Plus many additional weak to moderate lines.					
		Film No. 7829, not corrected for shrinkage.								
		b = broad d = diffuse a = observed to be absent * = not measured								

case. Since the cleavage and tabular habit favor appearance of {001}, β and γ indices are readily determined. The birefringence, γ-β, is usually small, the largest difference being 0.02. Accurate measurement of the α index is more difficult, and for the poor quality, thin crystals of masuyite this difficulty was not overcome. For billietite, fourmarierite, and unaltered schoepite (schoepite I), the optic angle $2V_\alpha$ was measured by universal-stage methods on crystals having the tabular habit, and the corresponding α index calculated from the standard equation:

$$\alpha = (\gamma\beta \sin V_\alpha)(\gamma^2 - \beta^2 \sin^2 V_\alpha)^{-1/2}.$$

No calculated V_α angles are listed because examination of the equations given by Mertie (1942) shows that for large indices of refraction, a large error (10 to 15°) is associated with a calculated V_α. The indices of refrac-

TABLE 11. *X*-RAY POWDER DATA: FOURMARIERITE

Calculated		Present Study			Bignand (1955)	
		Measured			Measured	
		Single Crystal	d(Å)	Powder Cu/Ni $\lambda = 1.5418$ Å	d(Å)	Cu/Ni
hkl	d_{hkl}	I	I	d_{hkl}	d_{hkl}	I
101	10.04	*				
111	8.57	*	1	8.55± .06		
020	8.23	w				
002	7.20	VS	100	7.20± .04	7.12	FF
200	7.00	m				
210	6.44	m	3	6.42± .03	6.36	f
121	6.37	*				
022	5.42	a				
220	5.33	w				
202	5.02	m	1	5.04± .02		
131	4.82	m	3	4.82± .02		
212	4.80	w				
103	4.54	w				
301	4.44	w				
113	4.38	S	9	4.36± .02	4.31	f
230	4.32	m				
311	4.29	a				
222	4.29	*				
040	4.12	m	2	4.13± .015		
123	3.975	*	3	b 4.00 to 3.90		
321	3.908	S				
141	3.809	a				
232	3.704	m				
004	3.599	VS	50	3.58± .015	3.53	FF
042	3.574	w				
240	3.549	VS	18	3.55± .015		
400	3.500	VS	6	3.50± .01		
133	3.499	*				
331	3.451	w				
410	3.424	m				
303	3.345	w				
024	3.297	w				
313	3.279	w	1	3.28± .01		
420	3.221	a				
204	3.200	a				
242	3.183	VS	50	3.178± .008	3.16	FF
402	3.147	VS	12	3.143± .007		
214	3.142	a				
151	3.129	S				
323	3.099	*				
412	3.091	S	2	3.095± .007		
143	3.050	*		3.046± .007		
341	3.018	w				
224	2.983	*				
250	2.980	m	<1	2.97± .01		
430	2.952	w				
422	2.940	w-				
333	2.857	*				
105	2.820	a				
115	2.779	w-				
234	2.765	*				

TABLE 11 (*continued*)

		Present Study			Bignand (1955)	
Calculated		Measured			Measured	
		Single Crystal	d(Å)	Powder Cu/Ni $\lambda = 1.5418$ Å	d(Å)	Cu/Ni
hkl	d_{hkl}	I	I	d_{hkl}	d_{hkl}	I
252	2.753	a				
501	2.749	a				
060	2.744	m				
432	2.730	S	4	$2.724 \pm .006$	2.71	m
511	2.711	w				
044	2.709	w	<1	$2.70 \pm .01$		
125	2.667	*				
153	2.666	*	1	$2.65 \pm .01$		
440	2.666	w				
161	2.648	w				
351	2.645	a				
521	2.607	w				
343	2.596	*				
062	2.564	w				
260	2.555	w				
244	2.527	*	9	$2.520 \pm .006$	2.51	m
404	2.509	S	4	$2.503 \pm .006$		
135	2.508	*				
442	2.500	m				
			4	2.389		
			<1	2.340		
			<1	2.311		
			2	2.229		
			2	2.181		
			2	2.136		
			3	2.056		
			4	2.030	2.02	mf
			4	2.010		
			12	b 1.987 to 1.972	1.96	F
			4	1.951	1.93	f
			3	1.900	1.88	f
			4	1.793	1.83	f
			4	1.767	1.75	mf
			4	1.719	1.70	f
			2	1.698		
			4	1.600	1.58	mf

a = observed to be absent
b = broad
* = not measured

There are additional weak lines with I $\lesssim 2$ for $d_{hkl} < 1.97$ Å; these are not listed.

Film No. 11911, corrected for shrinkage.

Plus 3 additional weak lines.

Original data of Bignand (1955) given in kX units.

TABLE 12. *X*-RAY POWDER DATA: MASUYITE

Calculated		Measured	
		d(Å) Cu/Ni	
hkl	d_{hkl}	I	d_{hkl}
006	7.10	100	7.08 ± .05
		6	4.36 ± .02
		6	4.30 ± .02
0.0.12	3.551	35	3.56 ± .01
660	3.496	70	3.52 ± .01
12.0.0	3.494	21	3.48 ± .01
666	3.137	12	3.16 ± .01
12.0.6	3.135	50	3.12 ± .01
12.0.12	2.491	6	2.51 ± .01
6.6.12	2.491	12	2.484 ± .007
		4	2.38 ± .01
0.0.18	2.367	9	2.36 ± .01
		4	2.27 ± .01
		4	2.12 ± .01
0.12.0	2.019	18	2.008 ± .004
18.6.0	2.017		
		9	1.973 ± .008
		b 17	1.95 ± .01
		4	1.79 ± .01
		12	1.766 ± .004
		9	1.745 ± .006
		4	1.72 ± .006
		9	1.690 ± .004
		4	1.613 ± .006
		4	1.598 ± .006
		6	1.578 ± .006
		4	1.559 ± .006

Plus additional weak lines.

Film No. 11912, not corrected for shrinkage.

b = broad

tion measured in the present study are considered good to ±0.005 unless otherwise noted, and an estimated error has been assigned to the calculated α values from study of the limits of error attached to the associated observed data.

Whenever the presence of two or more phases was indicated by x-ray study, as in the cases of schoepite and vandendriesscheite, the indices of refraction were found variable within a given range, the variability affecting chiefly the β and γ indices. Schoepite I was identified as original, unaltered schoepite, not only by comparison of its cell constants with

TABLE 13. *X*-RAY POWDER DATA: SCHOEPITE

Schoepite								Dehydrated Schoepite	
Calculated			Measured—Sample 1			Measured—Sample 2		Measured	
Phase	*hkl*	d_{hkl}	d(Å) I	Cu/Ni d_{hkl}	d(Å) Cr/V d_{hkl}	d(Å) I	Cu/Ni d_{hkl}	d(Å) I	Cu/Ni d_{hkl}
III	002	7.61	6	7.59 ±.05	7.56 ±.05				
I, II	002	7.37	100	7.28 ±.05	7.35 ±.05	100	7.35 ±.05		
			70	5.08 ±.02	5.07 ±.02			100	5.09 ±.02
			1	4.43 ±.03		1	4.46 ±.03		
III	004	3.805	3	3.78 ±.015	3.79 ±.01				
I, II	004	3.682	15	3.66 ±.015	3.69 ±.01	50	3.66 ±.01		
I	240	3.622				1	3.62 ±.02		
III	240	3.614							
II	240	3.588	6	3.59 ±.015	3.585±.007	1	3.58 ±.02		
I	400	3.582							
III	400	3.530							
II	400	3.498	12	3.51 ±.01	3.495±.007	2	3.49 ±.01		
			25	3.44 ±.01	3.430±.006			25	3.45 ±.01
			9	3.39 ±.01	3.380±.006			17	3.39 ±.01
III	242	3.265							
I	242	3.250				9	3.24 ±.01		
II	242	3.227	12	3.22 ±.01		3	3.21 ±.01		
I	402	3.222							
III	402	3.202							
II	402	3.159	6	3.162±.008	3.165±.006	3	3.162±.008		
			12	2.885±.007	2.872±.005			7	2.890±.007
						1	2.81 ±.01		
III	404	2.588							
I	404	2.568				4	2.571±.006		
III	006	2.537							
			12	2.539±.006	2.539±.003	1	2.53 ±.01	6	2.542±.003
II	404	2.536							
			9	2.481±.006	2.480±.003			b 7	2.48 ±.01
I, II	6	2.455	1	2.45 ±.01		9	2.446±.006		
			1	2.11 ±.01	Film No.	<1	2.31 ±.01		
					12262, cor-			4	2.117
					rected for	<1	2.09 ±.01		
			4	2.053±.002	shrinkage.			4	2.060±.002
			9	2.018±.002				5	2.023±.002
			Plus many additional weak lines.			Plus many additional weak lines.		Plus many additional weak lines.	
			Film No. 12119, not corrected for shrinkage.			Film No. 11904, not corrected for shrinkage.		Film No. 12293, not corrected for shrinkage.	
								b = broad	

those reported by Billiet and de Jong (1935) but also by the close agreement of its indices of refraction with those originally given by Walker (1923), as shown in Table 21. Schoepite III has indices of refraction in accord with those reported by Schoep and Stradiot (1947) for paraschoepite (Table 22). One reason that schoepite II has been considered an intermediate product is that crystals identified by *x*-ray study as principally schoepite II invariably gave values of β and γ indices of refraction ranging somewhere between the values given by schoepite I and those given by schoepite III. Vandendriesscheite crystals also undergo an alteration process similar to the one that occurs in schoepite, and have more

Table 14. *X*-Ray Powder Data: Dehydrated Schoepite

Present Study		Bignand (1955)		Zachariasen (1944)	
Measured		Measured		Calculated[2]	
d(Å)	Cu/Ni	d(kX)	Cu/Ni		
I	d_{hkl}	I	d_{hkl}	d_{hkl}	hkl
100	5.09	F	5.05	5.10	002
		f	(3.76)[1]		
25	3.45	FF	3.44	3.43	200
17	3.39			3.41	111
		f	3.16		
7	2.890	m	2.85	2.85	202
		f	2.72		
6	2.542	m	2.53	2.55	004
b 7	2.48	m	2.45	2.48	113
4	2.117	f	2.12	2.13	020
4	2.060	f	2.05	2.05	204
5	2.023				
4	1.993	mF	1.97	1.98	311
4	1.954			1.97	022
4	1.826				
<4	1.80			1.81	220
6	1.774	mF	1.77	1.78	115
<4	1.72			1.733	313
				1.725	400
4	1.698	m	1.69	1.708	222
				1.698	006
<4	1.67				
<4	1.63	m	1.63	1.636	024
				1.626	402
<4	1.541	m	1.52	1.52	206
<4	1.484	m	1.48		
<4	1.444	m	1.43		
<4	1.350	mf	1.35		

Film No. 12293, not corrected for shrinkage.
b = broad

[1] Possibly β reflection for $d = 3.44$.

[2] Calculations based on face centered orthorhombic cell with $a = 6.86 \pm .03$, $b = 4.27 \pm .03$, $c = 10.19 \pm .06$ Å.

TABLE 15. *X*-RAY POWDER DATA: VANDENDRIESSCHEITE

Calculated		Measured				
Phase I		Single Crystal	Powder			
			d(Å) Cu/Ni		d(Å) Cr/V	
hkl	d_{hkl}	I	I	d_{hkl}	I	d_{hkl}
006	7.22	VS	100	7.25±.05	S	7.23±.05
210	6.93	m	2	6.94±.04		
060	6.81	m	2	6.81±.04		
230	6.25	w	3	6.33±.04		
240	5.79	m	2	5.77±.04		
236	4.72	(w)[1]	2	4.71±.04		
119	4.53	w-	10	4.53±.03	w-	4.55±.03
246	4.52	(m)				
270	4.49	w				
129	4.45	m	10	4.45±.02	w-	4.45±.03
0.0.12	3.611	VS	100	3.61±.015	S	3.62±.007
0.10.6	3.566	m	b 25	3.53±.03	w-	3.56±.01
0.2.12	3.556	m				
2.10.0	3.532	VS			w	3.53±.01
400	3.517	VS				
410	3.504	m			w-	3.49±.01
2.1.12	3.203	(w)	b 75	3.17±.03	b m	3.18±.03
0.6.12	3.190	w				
349	3.190	(w-)				
2.2.12	3.173	(w-)				
2.10.6	3.173	(VS)				
406	3.162	VS				
416	3.153	(m)				
2.4.12	3.064	(m)	2	3.06±.01		
470	3.013	m	2	3.01±.01		
			2	2.94		
			b 8	2.80		
			5	2.722		
			2	2.66		
			25	2.522	b w	2.531
			10	2.401	w	2.418
			b 3	2.29		
			b 3	2.18		
			5	2.058		
			15	2.034		
			40	1.985		
			3	1.961		
			2	1.914		
			2	1.877		
			2	1.861		
			10	1.800		
			3	1.791		
			8	1.773		
			2	1.726		
			2	1.716		
			Plus additional lines with I≤10. Film No. 11903, not corrected for shrinkage. b=broad		Plus additional weak lines. Film No. 12337 corrected for shrinkage. b=broad	

---

[1] Parentheses used for intensities extrapolated from lower-level patterns,

Table 16. Optical Data for Uranyl Oxide Hydrates[a]

(Data of present study unless otherwise noted)

	Becquerelite	Billietite	Fourmarierite	Masuyite	Schoepite I (unaltered)	Schoepite III (paraschoepite)	Vandendries-scheite
α	1.730	1.730[c]	1.85 ± 0.01[d]	1.785[e]	1.690 ± 0.003[f]	1.700	1.780
β	1.825	1.800	1.885 ± 0.01	1.895 ± 0.01	1.714 ± 0.003[f]	1.750	1.850 ± 0.01
γ	1.830	1.805	1.890 ± 0.01	1.915 ± 0.01	1.735 ± 0.003[f]	1.770	1.860 ± 0.01
$2V_\alpha$ (obs.)	$32°\pm3°$[b]	$37°\pm2°$	$50°\pm2°$	$\sim50°$[e]	$75°\pm2°$	$40°\pm$[g]	$60°\pm2°$
X	*c*, pale yellow	*c*, pale greenish yellow	*c*, colorless[d]	*c*, pale yellow[e]	*c*, pale yellow	*c*, pale yellow	*c*, colorless
Y	*a*, deep yellow	*a*, greenish yellow	*a*, pale amber yellow	*b*, amber yellow	*b*, golden yellow	*b*, golden yellow	*b*, golden yellow
Z	*b*, deep yellow	*b*, deep yellow	*b*, amber yellow	*a*, amber yellow	*a*, golden yellow	*a*, golden yellow	*a*, golden yellow

[a] Dispersion, $r>v$ for all. Values for α, β, γ are ±0.005 unless otherwise indicated.

[b] Protas (1957).

[c] Brasseur (1949).

[d] Larsen and Berman (1934). Error in α estimated by present authors.

[e] Frondel (1958).

[f] Walker (1923).

[g] Schoep and Stradiot (1947).

TABLE 17. OPTICAL DATA FOR BECQUERELITE

	Present Study	Protas (1957)	Frondel and Cuttitta (1953)	Brasseur (1948)	Schoep and Stradiot (1948)	Palache and Berman (1933)
				($\lambda = 578\ m\mu$)		
α	1.730 ± 0.005	1.725	1.730		1.725	1.735
β	1.825 ± 0.005	1.815	1.805	$1.79_8 \pm 0.007$	1.825	1.820
γ	1.830 ± 0.005	1.825	1.720	$1.82_2 \pm .006$	1.83	1.830
2Vα (obs.)		32° ± 3°	~30°		30° ±	30°
X	*c*, pale yellow	colorless	*c*, pale yellow		*c*, colorless	*c*, colorless
Y	*a*, deep yellow	yellow	*a*, deep golden yellow		*a*, yellow	*b*, yellow
Z	*b*, deep yellow	yellow	*b*, deep golden yellow		*b*, yellow	*a*, yellow

TABLE 18. OPTICAL DATA FOR BILLIETITE

	Present Study	Frondel and Cuttitta (1953)		Brasseur (1949) ($\lambda = 578\ m\mu$)	Schoep and Stradiot (1948)	Vaes (1947)
		H.U.M. No. 104456	H.U.M. No. 104455			
α	1.76 ± 0.05*	1.730	1.725	1.730	1.73	
β	1.800 ± 0.005	1.810	1.780	1.822	1.82	
γ	1.805 ± 0.005	1.815	1.790	1.8285	1.83	
2Vα (obs.)	37° ± 2°	~35°	~35°	47°	36° ±	36°
X	*c*, pale greenish yellow	*c*, pale yellow		*c* Dichroism	*c*, colorless	*b*, colorless
Y	*a*, greenish yellow	*a*, deep golden yellow		*a*, of Vaes (1947)	*a*, yellow	*c*, greenish yellow
Z	*b*, deep yellow	*b*, deep golden yellow		*b*, confirmed	*b*, deep yellow	*a*, amber

* Value for α calculated from observed values of β, γ and V_α.

TABLE 19. OPTICAL DATA FOR FOURMARIERITE

	Present Study	Frondel (1958)	Larsen and Berman (1934)
α	$1.863 \pm .025$*	1.865	1.85
β	1.885 ± 0.01	1.900	1.92
γ	1.890 ± 0.01	1.904	1.94
$2V_\alpha$ (obs.)	50° ± 2°	55°	large
X	*c*	*c*, colorless	*a*, colorless
Y	*a*, pale amber yellow	*b*, pale yellow	*c*, pale yellow
Z	*b*, amber yellow	*a*, yellow	*b*, deeper yellow

* Value for α calculated from observed values for β, γ and V_α.

TABLE 20. OPTICAL DATA FOR MASUYITE

	Present Study	Frondel (1958)	Vaes (1947)
α		1.785	
β	1.895±0.01	1.906	between 2.11 and 2.15
γ	1.915±0.01	1.917	
$2V_\alpha$ (obs.)		~50°	large
X	*c*	*c*, pale yellow	*b*
Y	*b*, amber golden yellow	*b*, deep golden	*a*†, orange yellow
Z	*a*, amber golden yellow	*a*, deep golden	*c*, orange yellow

† Vaes (1947) gives $n_m = a$ but states that the P.O.A. is perpendicular to *c*.

TABLE 21. OPTICAL DATA FOR SCHOEPITE I

	Present Study	Larsen and Berman (1934)	Walker (1923)
α	1.70±0.01*	1.690	1.690±0.003
β	1.720±0.005	1.714	1.714±0.003
γ	1.735±0.005	1.735	1.735±0.003
$2V_\alpha$ (obs.)	75°±2°	large	
X	*c*, pale yellow	*c*, colorless	*c*, colorless
Y	*b*, golden yellow	lemon yellow	lemon yellow
Z	*a*, golden yellow	lemon yellow	lemon yellow

* Value for α calculated from observed β, γ and V_α.

TABLE 22. OPTICAL DATA FOR SCHOEPITE III

	Present Study	Schoep and Stradiot (1947), for paraschoepite
α	1.700±0.005	1.705
β	1.750±0.005	1.760
γ	1.770±0.005	1.770
$2V_\alpha$ (obs.)		40°±
X	*c*, pale yellow	*c*, colorless
Y	*b*, golden yellow	*b*, yellow
Z	*a*, golden yellow	*a*, yellow

TABLE 23. OPTICAL DATA FOR VANDENDRIESSCHEITE

	Present Study	Frondel (1958)*				Vaes (1947)
		(1)	(2)	(3)	(4)	
α	1.780±0.005	1.790	1.785	1.760	—	—
β	1.850±0.01	1.840	1.810	1.824	1.882	>1.884
γ	1.860±0.01	1.845	1.820	1.828	1.890	>1.884
$2V_\alpha$ (obs.)	60°±2°	medium	medium	50°	medium	large
X	c, colorless	c, nearly colorless				b, nearly colorless
Y	b, golden yellow	b, golden yellow				a, orange yellow
Z	a, golden yellow	a, golden yellow				c, orange yellow

* Values in each column are for crystals with unit cell reported under the corresponding column number in Table 8. Material of (2) from Great Bear Lake; measurements by Palache and Berman (1933). Others from Katanga; measurements by J. W. Frondel.

than normal variation in the values of the β and γ indices of refraction for different crystals. In general, indices of refraction for these minerals must be considered in connection with x-ray evidence for purposes of identification.

CHEMICAL CONSIDERATIONS AND CRYSTAL STRUCTURE

Semiquantitative spectrographic analysis for Pb, Ca, Ba, and Sr was carried out on 2 mg samples of crystals of each mineral except masuyite; schoepite was examined only as schoepite I. So few crystals of masuyite were available that neither spectrographic analysis nor specific gravity determination were feasible. The following results were obtained from the spectrographic analysis:

Sample	*Pb*	*Ca*	*Ba*	*Sr*
Becquerelite from HM No. 106523	.0X	X.	.00X	.0X
Becquerelite from HM No. 106524	.0X	X.	.00X	.0X
Becquerelite from USNM No. R8387	.0X	.X	.00X	.0X
Billietite from HM No. 104445	.0X	.0X	X.	.0X
Schoepite from USNM No. 94712	.0X	.X	.0X	.0X
Fourmarierite from USNM No. R8396	X.	.0X	.00X	.0X
Vandendriesscheite from HM No. 106523	X.	.0X	.00X	.0X

(X is in weight percentage.)
H. J. Rose, Jr., analyst.

These chemical results are best explained in terms of the crystal structure concepts discussed below.

All of these uranyl oxide hydrates yield x-ray patterns on which the strong reflections are distributed according to the demands of a primitive pseudo-hexagonal cell (Figure 1), with cell edges for the several minerals varying from $a' = 4.0$ Å to $a' = 4.2$ Å, and $c' = 7.1$ Å to $c' = 7.6$ Å. The intensities of the strong reflections follow an essentially normal form-factor decline with increasing $(\sin\theta)/\lambda$. These minerals all have perfect (001) cleavage. With these experimental results and a knowledge of the structures of similar compounds, it is immediately possible to derive many of the essential features of the structures of the uranyl oxide hydrates.

A number of compounds containing hexavalent uranium have been studied, including anhydrous uranyl fluoride, UO_2F_2, (Zachariasen, 1948a), calcium uranate, $Ca(UO_2)O_2$, (Zachariasen 1948b), and rutherfordine, UO_2CO_3, (Christ *et al.*, 1955). The structures of these three compounds are alike in that they consist of stacked infinite layers of fluoride, oxygen, or carbonate ions, respectively, with uranyl, $(O\text{-}U\text{-}O)^{++}$, ions normal to the layers, the uranium of the uranyl ion being contained in the layer. A drawing of the structure of the UO_2F_2 layer of uranyl fluoride, taken from Zachariasen (1948a), is shown in Figure 3. Calcium uranat contains similar $[UO_2O_2]_n^{-2n}$ layers, with Ca^{++} ions, in eightfold coordination, located half-way between successive layers. In the uranyl oxide hydrates there are undoubtedly infinite $UO_2(OH)_2$ layers quite similar t those found in UO_2F_2 and $CaUO_2O_2$, and with dimensions close to those c

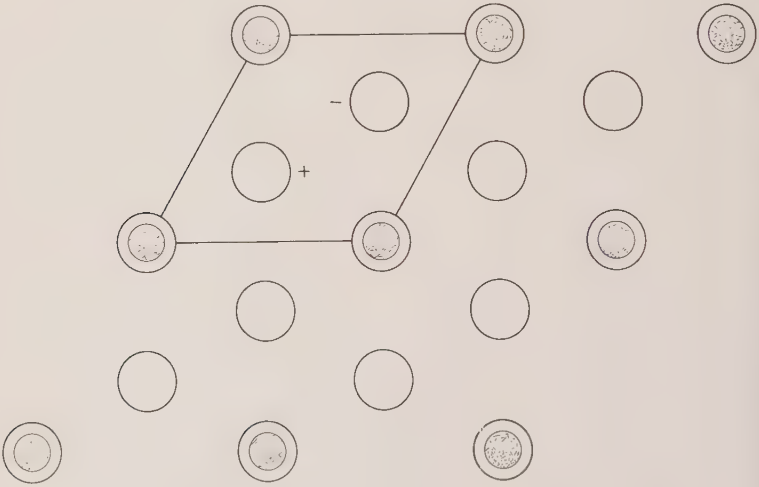

FIG. 3. A drawing of the structure of the UO_2F_2 layer of uranyl fluoride (after Zachariasen, 1948a). Circles with stippled centers represent uranyl groups lying normal to the plan of the drawing with oxygen atoms 1.91 Å above and below the plane, and with the uranium in the plane. The large open circles indicate fluorine atoms at distances of 0.61 Å above (+), and below, (−), the plane. The $UO_2(OH)_2$ layers in the uranyl oxide hydrates ar similar to the UO_2F_2 layer shown here.

UO_2F_2. In crystals of $CaUO_2O_2$ and UO_2F_2 the successive hexagonal layers are displaced, in accordance with the rhombohedral symmetry of the crystals, in order to allow room for the packing of the oxygens of the uranyl groups. The distance between consecutive layers in UO_2F_2 is 5.22 Å, and in $CaUO_2O_2$ is 5.84 Å. The similar hexagonal $UO_2(OH)_2$ layers in the uranyl oxide hydrates are stacked directly over one another with the distance between consecutive layers varying from 7.1 to 7.6 Å. This larger separation presumably serves to provide space to accommodate the water molecules and the cations, such as Pb^{++}, Ba^{++}, and Ca^{++}, contained in the uranyl oxide hydrates.

Although the structure and composition of the layers of the uranyl oxide hydrates seem entirely clear, the structure and even the exact composition of the interlayer content is considerably less apparent, and the clarification of these properties for each of the minerals must await a complete crystal structure analysis. Some preliminary studies with Patterson and electron density maps have been carried out on billietite during the present investigation and the results obtained are in agreement with the conclusions given above. The structure work is continuing and will be reported upon at a later date.

From these crystal structure considerations and the probable chemical content of the minerals, as listed in Table 2, the oxide formulas can be rewritten as follows: schoepite I, $UO_2(OH)_2 \cdot H_2O$; becquerelite, $Ca(OH)_2 \cdot 6UO_2(OH)_2 \cdot 4H_2O$, billietite, $Ba(OH)_2 \cdot 6UO_2(OH)_2 \cdot 4H_2O$, and fourmarierite, $Pb(OH)_2 \cdot 4UO_2(OH)_2 \cdot 2H_2O$. The general formula for these compounds, $x\text{MeO} \cdot yUO_3 \cdot zH_2O$, can be written as $x\text{Me}(OH)_2 \cdot yUO_2(OH)_2 \cdot (z-x-y)H_2O$ (Christ and Clark, 1955). An alternative general structural formulation of the oxide formula, $x\text{MeO} \cdot yUO_3 \cdot zH_2O$, is $\text{Me}_x[(UO_2)_yO_{2x}(OH)_{2(y-x)}] \cdot (z-y+x)H_2O$, where the brackets enclose the layer composition. Under this formulation billietite, e.g., would be written $Ba[(UO_2)_6O_2(OH)_{10}] \cdot 6H_2O$.

The probable chemical formulas listed in Table 2 are those which give the best agreement with all the data available at the present time. The x-ray findings afford two checks on these formulas: densities can be calculated, and a count of the total number of $UO_2(OH)_2$ units per cell can be made. It can be seen from Table 2 that the agreement between calculated and observed specific gravities is excellent. The total number of $UO_2(OH)_2$ units per cell must be an integral multiple of the number of uranium atoms given in a chemical formula, in order for that formula to be acceptable. This rule is obeyed for the chemical formulas listed in Table 2.

The chemical composition of becquerelite has been considered as uncertain (Frondel, 1958); however, the recent work of Protas (1957) clearly establishes becquerelite as a calcium uranyl oxide hydrate, in agreement with the results of the spectrographic analysis of the present study. Protas (1957) gives the formula of becquerelite as $CaO \cdot 6UO_3 \cdot 11H_2O$. The observed specific gravity obtained in the present study, and those found by Protas (1957) for both synthetic and natural becquerelites, are in excellent agreement with the specific gravity calculated on the basis of this chemical formula, as shown in Table 2. In the present study, one becquerelite sample (USNM No. R8387) showed a lower calcium content than the other two examined. Because of the small samples used in the spectrographic analysis, this result may not be real. On the other hand, it may indicate a variable calcium content. It has been suggested that becquerelite may be formulated as a compound in which some of the uranium may be substituted by barium or lead (Frondel and Cuttitta, 1953). This kind of substitution would lead to decreasing density with increasing barium or lead. It is observed, in fact, that the opposite is true, as would be predicted on the basis of the interlayer positioning of cation described above. Because the uranium is undoubtedly present in thes compounds in uranyl groups any substitution of the uranyl by spherica cations seems extremely unlikely.

Billietite is the barium analog of becquerelite, and the formula Ba $\cdot 6UO_3 \cdot 11H_2O$, assigned by Brasseur (1949), is in excellent agreemen with the x-ray and spectrographic results of the present study and with the results of various chemical analyses (Frondel, 1958), including tha for the synthetic billietite prepared and analyzed by Protas (1956).

The formula $PbO \cdot 4UO_3 \cdot 7H_2O$, proposed by Brasseur (1941, 1946) for fourmarierite is consistent with the x-ray results of the present study except for the water content. The cell constants found by us are probably more accurate than those of Brasseur, and when combined with his specific gravity value of 5.74 lead to the formula $PbO \cdot 4UO_3 \cdot 4H_2O$. However, because the contribution of the water to the specific gravity of any of these minerals is small, it is difficult to determine precise water values for them in this way.

No new results on the chemistry of masuyite were obtained in this study.

Frondel (1958) gives the formula of vandendriesscheite as near $PbO \cdot 7UO_3 \cdot 12H_2O$. It will be noted from Table 2 that consideration of the number of pseudo-orthohexagonal cells contained in the large true cell leads to a true cell content of 240 units of $UO_2(OH)_2$. This result would require slight modification of the formula above, since 240 is not an integral multiple of 7. Our observed specific gravity for vandendriesscheite is 5.45, in excellent agreement with the value of 5.46 given for crystal 1 in Frondel (1958), as shown in Table 8. The cell constants of the present study, when combined with the formula $PbO \cdot 7UO_3 \cdot 12H_2O$, yield a calculated specific gravity of 5.86. This disagreement between calculated and observed specific gravities is a second indication that the formula requires modification, and may be variable as stated in Frondel (1958).

Dehydration Phenomena in Schoepite and Vandendriesscheite

As mentioned above, crystals of schoepite commonly occur with an amber-brown core completely or partially surrounded by a derivative golden-yellow rim which retains the morphology of the original crystal, and which itself yields single-crystal patterns. The brown part consists chiefly of schoepite I, and the yellow part mostly of schoepite II or schoepite III. Examination under the binocular microscope reveals that the rim is usually threaded by numerous small tubes, lying approximately parallel to (001), radiating from the brown core to the external surface of the crystal. These tubes are considered to be tunnels that have developed to permit the escape of water from schoepite I, with the resulting formation of schoepite II or schoepite III. *X*-ray study shows that crystals in all stages of alteration occur on the specimen USNM No. 94712. A number of these crystals have been examined from time to time over a period of months, and it has been found that the crystals continually alter, with the alteration process always proceeding with the formation of schoepite II or III and with concomitant decrease in the relative amount of schoepite I. The rate at which the crystals alter varies considerably. Experiments with large *x*-ray dosages have shown that the alteration is independent of the *x*-ray diffraction experiment, and is truly spontaneous. The brown crystals will continue to alter toward the yellow ones, as evidenced by *x*-ray studies, even if the crystals are kept in an atmosphere saturated with water vapor at room temperature; completely yellow crystals (schoepite III) will not alter toward the brown when kept in such an environment. When completely brown crystals are put over concentrated H_2SO_4 in a closed vessel a yellow powder forms in a matter of hours; completely yellow crystals so treated do not alter. The yellow powder yields an *x*-ray pattern designated as that of "dehydrated schoepite" in Tables 13 and 14. Bignand (1955) found that synthetic schoepite heated between 60° and 180° C. lost 5.4% water, and that the remaining product gave an *x*-ray powder pattern different from that of the original schoepite. The pattern obtained by Bignand is in excellent agreement with that obtained by us for dehydrated schoepite, as shown in Table 14. If it is considered that natural schoepite has the formula $UO_3 \cdot 2H_2O$, and therefore contains 11.2% water, the loss of 5.4% water observed by Bignand would lead to the approximate formula $UO_3 \cdot H_2O$, or $UO_2(OH)_2$, for dehydrated schoepite. It has been reported (Katz and

Rabinowitch, 1951, p. 285) that there are four polymorphic crystalline modifications of $UO_3 \cdot H_2O$, all stable at room temperature. For one of these modifications, Zachariasen (1944) gives the following data: orthorhombic, $a = 6.86$, $b = 4.27$, $c = 10.19$ Å, uranium atoms in face-centered array. This form of $UO_3 \cdot H_2O$ will account for nearly all the lines found for dehydrated schoepite (Table 14). Dawson *et al.* (1956) report that UO_3 in contact with water at about 180° C. yields orthorhombic $UO_3 \cdot 0.8H_2O$. The cell dimensions listed by these authors for $UO_3 \cdot 0.8H_2O$ are in excellent agreement with those of Zachariasen for $UO_3 \cdot H_2O$, as given above.

We have also observed that when an amber-brown crystal of schoepite is teased with a dissecting needle the crystal disintegrates into a yellow powder around the point of contact of the needle. X-ray examination shows that this yellow powder is mostly dehydrated schoepite. It is believed that the pressure of the needle results in cleavage on a very fine scale, parallel to (001), thus permitting the rapid escape of water. When an amber-brown crystal with a golden-yellow rim is used in this experiment, or is dehydrated over concentrated H_2SO_4, the rim retains it original form, and remains otherwise unchanged. These experiments ar interpreted to have the following significance. When allowed to alter naturally, the amber-brown crystals will slowly form golden-yellow crystals which are apparently stable toward further change. Schoepite I. corresponding to the amber-brown crystals, and schoepite II or III. corresponding to the golden-yellow crystals, all have slightly different cell constants and x-ray intensity distributions. It seems likely that these differences result from a loss of a small part of the interlayer water (the water in excess of that needed to form $UO_2(OH)_2$ layers) from schoepite I, with consequent slight rearrangement of the atomic structure. The $UO_2(OH)_2$ layers are parallel to (001), and if the interlayer water contributes to the binding together of these layers, then loss of some of the water would result in an increase in c. This increase does occur in going from schoepite I to schoepite III. All of these results indicate that under room conditions, schoepite I is thermodynamically unstable with respect to schoepite II, which in turn is unstable toward schoepite III. Although schoepite I alters to dehydrated schoepite under mechanical pressure, crystals of schoepite II or III do not appear to do so. We have no explanation for this observation. Natural schoepite (schoepite I) (Frondel, 1958), and the corresponding synthetic compound (Hüttig and Schroeder, 1922), (Bignand, 1955) appear to contain slightly more than two moles of H_2O per mole of UO_3. Accordingly, in Table 2 the formula for schoepite I is given as $UO_3 \cdot (2+?)H_2O$. Since schoepite II and III are considered to result from spontaneous loss of water from schoepite I, these are given the formula $UO_3 \cdot (2-?)H_2O$.

That variations in *x*-ray powder patterns of "schoepite" are found is readily understood in view of the foregoing analysis. The patterns will vary both with the way in which material is selected from a given specimen, and with the method of preparation of the powder sample. The results from the powder patterns measured in the present study are given in Table 13. Sample 1 (Table 13) consisted of a mixture of yellow powder and yellow crystal fragments from the specimen USNM No. 94712. It can be seen from Table 13 that this sample contained schoepite II and schoepite III, with a large proportion of $UO_2(OH)_2$ also present. Sample 2 was made up of crystals from the same specimen, selected without regard to their stage of alteration. From Table 13 it can be seen that this sample consisted of a mixture of schoepite I and schoepite II. Apparently, no detectable amount of $UO_2(OH)_2$ was produced in the preparation of this sample.

Vandendriesscheite crystals with varying proportions of phase I and phase II (Table 2) occur on the specimen HM No. 106523. No study was made to determine which of the two phases persisted with time. However, it was found that when a clear orange crystal of vandendriesscheite, consisting principally of phase I, was put in a container over concentrated H_2SO_4, the crystal became cloudy, tiny tubes appeared as with schoepite, and the *x*-ray precession pattern of the altered crystal showed that phase II was now the dominant phase. The *x*-ray powder pattern data, given in Table 15, are indexed on the basis of phase I. It would be difficult to differentiate the two phases with powder pattern data only.

NOMENCLATURE

Throughout this paper, the designations schoepite I, II, and III, and vandendriesscheite I and II have been used for the several phases encountered. These designations are simple and convenient, and are precisely defined in terms of the lattice constants of the phases. In order to relate these terms to the more customary mineralogical nomenclature it is proposed that the name "schoepite" be retained for schoepite I, and that schoepite II be called "metaschoepite." Schoepite III is clearly paraschoepite. Similarly, it seems desirable to use the name "vandendriesscheite" for vandendriesscheite I, and to call vandendriesscheite II, "metavandendriesscheite." These relationships are summarized as follows:

Schoepite I = schoepite
Schoepite II = metaschoepite
Schoepite III = paraschoepite
Vandendriesscheite I = vandendriesscheite
Vandendriesscheite II = metavandendriesscheite

ACKNOWLEDGMENTS

This work was completed as part of a program being conducted by the U. S. Geological Survey on behalf of the Division of Research, U. S. Atomic Energy Commission. We are grateful to Professor Clifford Frondel, Harvard University, and Dr. George Switzer, U. S. National Museum, for the loan of mineral specimens. Professor Frondel and Dr. J. W. Frondel kindly placed at our disposal crystals they had studied, and the results obtained, prior to publication. We are indebted to our colleagues in the U. S. Geological Survey for much help: Mary E. Mrose and Fred A. Hildebrand prepared *x*-ray patterns, Harry J. Rose, Jr. made spectrographic analyses, and D. E. Appleman, Mary E. Mrose, and H. T. Evans, Jr. gave much helpful discussion on various problems.

REFERENCES

BIGNAND, CLAUDE. (1955), Sur les propriétés et les synthèses de quelques minéraux uranifères: *Soc. française Minéralogie et Cristallographie Bull.* **78,** 1–26.

BILLIET, V., AND DE JONG, W. F. (1935), Schoepiet en becquereliet: *Natuurw. Tijdschr Ned-Indië* **17,** 157–162.

BRASSEUR, H. (1941), Contribution à la connaissance de la fourmariérite: *Soc. royale sc Liége Bull.* **10,** 369–372.

BRASSEUR, H. (1946), Contribution à la connaissance de la fourmariérite: *Soc. royale sci Liége Bull.* **15,** 523–526.

BRASSEUR, H. (1948), Properties and chemical formula of fourmarierite: *Am. Mineral.* **33,** 619–621.

BRASSEUR, H. (1949), Etude de la billietite: *Acad. royale Belgique Bull., Cl. Sci., sér. 5,* **35,** 793–804.

BRASSEUR, H. (1950), Etude roentgenographique de la masuyite: *Soc. royale sci. Liége Bull.* **19,** 239–241.

CHERVET, JEAN, AND BRANCHE, GEORGES (1955): Contribution à l'étude des minéraux secondaires d'uranium français: *Sciences de la Terre* **3** (no. 1), 186 p.

CHRIST, C. L., AND CLARK, JOAN R. (1955), Crystal chemical studies of the uranium oxide hydrates [abs.] *Geol. Soc. America Bull.* **66,** 1542.

CHRIST, C. L., CLARK, JOAN R., AND EVANS, H. T., JR. (1955), Crystal structure of rutherfordine, UO_2CO_3: *Science* **121,** 472–473.

DAWSON, J. K., WAIT, E., ALCOCK, K., AND CHILTON, D. R. (1956), Some aspects of the system uranium trioxide-water: *J. Chem. Soc.* (*Lond.*), 3531–3540.

DESTAS, A., VAES, J. F., AND GUILLEMIN, C. (1958), Minéraux d'uranium du Haut Katanga: "Les Amis du Musée royal du Congo belge," Tervuren, Belgium.

FRONDEL, CLIFFORD (1958), Systematic mineralogy of uranium and thorium: *U. S. Geol. Survey Bull.* **1064.**

FRONDEL, CLIFFORD, RISKA, D. D., AND FRONDEL, JUDITH W. (1956), *X* ray powder data for uranium and thorium minerals: *U. S. Geol. Survey Bull.* **1036-G.**

FRONDEL, JUDITH W., AND CUTTITTA, FRANK (1953), Studies of uranium minerals (XII): The status of billietite and becquerelite: *Am. Mineral.* **38,** 1019–1024.

HÜTTIG, G., AND VON SCHROEDER, E. (1922), Über die Hydrate des Urantetroxyds und Urantrioxyds: *Z. anorg. u. allgem. Chem.* **121,** 243–253.

Katz, Joseph J., and Rabinowitch, Eugene (1951), The chemistry of uranium, Pt. 1: New York, McGraw-Hill, Inc.

Larsen, E. S., and Berman, H. (1934), The microscopic determination of the nonopaque minerals: *U. S. Geol. Survey Bull.* **848.**

Mertie, John B., Jr. (1942), Nomograms of optic angle formulae: *Am. Mineral.* **27,** 538–551.

Palache, Charles (1934), Crystallography of the uranium oxides: *Am. Mineral.* **19,** 309–315.

Palache, C., and Berman, H. (1933), Oxidation products of pitchblende from Great Bear Lake: *Am. Mineral.* **18,** 20–24.

Palache, C., Berman, H., and Frondel, C. (1944), Dana's system of mineralogy, 7th ed. Vol. 1: New York, John Wiley and Sons, Inc.

Protas, Jean (1956), Synthèse de la billiétite: *Soc. française Minéralogie et Cristallographie Bull.* **79,** 350–351.

Protas, Jean (1957), Propriétés et synthèse d'un oxyde hydraté d'uranium et de calcium de Shinkolobwe, Katanga: *Acad. sci. [Paris] Comptes rendus* **244,** 91–93.

Schoep, A. (1930), Les minéraux du gîte uranifère du Katanga: *Mus. Congo belge Annales, sér. 1,* **1** (2), 13–22.

Schoep, A. (1932), Le poids spécifique et la formule chimique de la becquerelite et de la schoepite: *Mus. Congo belge Annales, sér. 1,* **1** (3), 5–7.

Schoep, Alfred, and Stradiot, Sadi (1947), Paraschoepite and epiianthinite, two new uranium minerals from Shinkolobwe (Belgian Congo): *Am. Mineral.* **32,** 344–350.

Schoep, Alfred, and Stradiot, Sadi (1948), Additional data on the properties of becquerelite and billietite: *Am. Mineral.* **33,** 503–507.

Thoreau, J. (1948), Caractères cristallographiques de la billietite et de la vandendriesscheite: *Soc. géol. Belgique Annales* **71,** B76–B78.

Ungemach, H. (1929), Précisions cristallographiques sur quelques minéraux du Congo Belge: *Soc. géol. Belgique Annales* **52,** C75.

Vaes, J. F. (1947), Six nouveaux minéraux d'urane provenant de Shinkolobwe (Katanga): *Soc. géol. Belgique Annales* **70,** B212–B229.

Walker, T. L. (1923), Schoepite, a new uranium mineral from Kasolo, Belgian Congo: *Am. Mineral.* **8,** 67–69.

Zachariasen, W. H. (1944), Manhattan Project Report, MP Chicago 6, Reports CP-1249, Jan. 22, and CK-1367, Feb. 25. (From Katz, Joseph J., and Rabinowitch Eugene: The chemistry of uranium, Pt. 1, p. 285: New York, McGraw-Hill, Inc.)

Zachariasen, W. H. (1948a), Crystal chemical studies of the 5*f*-series of elements. III. A study of the disorder in the crystal structure of anhydrous uranyl fluoride: *Acta Cryst.* **1,** 277–281.

Zachariasen, W. H. (1948b), Crystal chemical studies of the 5*f*-series of elements. IV. The crystal structure of $Ca(UO_2)O_2$ and $Sr(UO_2)O_2$: *Acta Cryst.* **1,** 281–285.

Manuscript received June 30, 1959.

THE AMERICAN MINERALOGIST, VOL. 45, SEPTEMBER-OCTOBER, 1960

A SECOND FIND OF EUHEDRAL BORNITE CRYSTALS ON BARITE

G. KULLERUD AND G. DONNAY, *Geophysical Laboratory, Carnegie Institution of Washington, Washington, D. C.*
AND
J. D. H. DONNAY, *The Johns Hopkins University, Baltimore, Md.*

ABSTRACT

Bornite crystals on barite have been found at the Coppercorp Mine in Ontario, Canada, the second locality for this association. The geology resembles that of the Upper Michigan copper area. The bornite cubes, truncated by octahedron faces, prove to be twinned edifices of two kinds, which simulate either cubic ($a=21.94$ Å) or orthorhombic ($a=b=21.90$, $c=10.95$ Å) symmetry.

INTRODUCTION

Bornite, Cu_5FeS_4, although a common mineral in many copper-iron sulfide ore deposits, has rarely been reported in single crystals. Well developed, steel blue, euhedral crystals were found by one of us (G.K.) in August 1956 at the Coppercorp Limited Mine of the Mamainse Point copper area, Ontario, Canada. The hand specimen shows bornite crystals growing on barite (Fig. 2), an association previously reported only from the Cheshire locality in England.

GENERAL GEOLOGY

The Mamainse Point copper area is located on the east shore of Lake Superior in the district of Algoma and lies about 60 miles north of the city of Sault Ste. Marie,* The Keweenawan rocks of this area form the east end of the Lake Superior syncline, are the youngest in the Precambrian era, and are generally unaltered. Amygdaloidal lava flows predominate and are interbanded with a boulder conglomerate. The faults in the area are often well-defined tensional structures. Most of the copper-bearing zones are faulted and the apparent horizontal displacement varies from a few to more than 1000 feet. The faults are considered to be normal and generally dip in the direction opposite to the dip of the strata.

Since the geology of the Mamainse Point area is similar to that of the Michigan copper district, the occurrence of chalcocite and native copper on small fractures led to intensive explorations. These showed that, as to structure and mineralogy, the Mamainse copper deposits, which consist mostly of chalcocite on fissures and fractures, are quite different from the

---

* The areal geology and individual ore deposits of the Mamainse Point copper area have been described by Thomson (1954), who also presented an excellent geological map and thus provided invaluable data for the present report.

Michigan copper deposits, where native copper occurs in flow tops and conglomerates.

The main ore deposits are known as the C zone, the S zone, and the M zone (Fig. 1). The chief ore mineral is chalcocite. Native copper is found on a few localities. Chalcopyrite is much less common than chalcocite. A little massive bornite is found with chalcopyrite and chalcocite in several ocalities and may be secondary. Chemical analyses have shown that a ittle silver occurs with the copper minerals; the silver values are highest where bornite is present (Thomson, 1954).

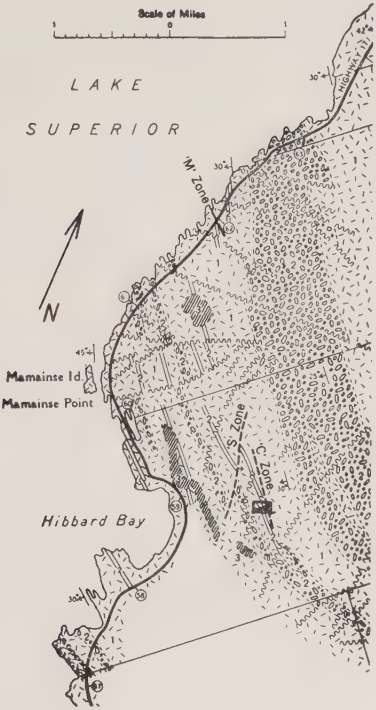

FIG. 1. Sketch map of Mamainse Point area. Numbers in circlets along highway 17 ndicate mileage from Sault Ste. Marie. Black and white rectangle shows shaft of Coppercorp Mine.

GEOLOGY AND MINERALOGY OF THE COPPERCORP LIMITED MINE

The Coppercorp Limited mining operations explored the C zone ore leposit (Fig. 1). The mine shaft is situated about 1 mile east of Hibbard Bay of Lake Superior. The C zone strikes almost parallel to the strata (N 15° W), dips almost normal to them (55–68° E) and may be a strike fault. Geologic information (Thomson, 1954) suggests that it is a normal fault with about 50 feet of vertical displacement. It does not outcrop but has been traced for 5400 feet along the strike by 34 drill holes. It has been estimated to average 8 feet in width. Testing to a depth of 400 feet and on a distance of 2275 feet showed its copper content to average 1.9 per cent. It is a fractured and brecciated zone in interbanded amygdaloidal basalt and conglomerate of the Keweenawan series. The wall rocks, to a depth of about 600 feet along the dip, are mostly lava flows from 20 to 100 feet thick; below this horizon the zone enters a thick conglomerate band. The C zone consists largely of vein breccia which contains massive chunks and sometimes stringers of erratically distributed chalcocite. Sometimes chalcocite also occurs in small fractures and amygdules in the adjacent lava. The breccia carries fragments of wall rocks, quartz, and calcite and is often vuggy (Thomson, 1954).

Bornite crystals growing most commonly on barite (Fig. 2), but also frequently on quartz, were found in vugs of the breccia. Bornite crystals occurring on barite appear with only few exceptions to have grown directly by deposition from a solution, while the bornite found on quartz without exception appears to have been formed by replacement of chalcopyrite (Fig. 3). In some cases some of the bornite which replaces chalcopyrite has in turn been replaced in part by chalcocite. Because of the presence of residual chalcopyrite and replacement chalcocite, it was not possible to obtain pure bornite in amounts sufficient for chemical analysis. The exact bornite composition, therefore, is unfortunately not known.

It was noted on crushing bornite crystals under acetone that fresh surfaces are tombac colored. However, on exposure to the atmosphere such surfaces change their color immediately and will after only a few seconds have acquired a pinkish cast. On continued exposure the pinkish color changes through brownish purple and purple to deep purple and finally an iridescent blue.

CRYSTALLOGRAPHY

Bornite crystals (at first presumed to be single crystals) were detached from the barite crystals found on the hand specimens. Examined under the binocular microscope they show the cube as their dominant form, modified by small faces of the octahedron. Their cube edge ranges in length from 0.2 to about 1.5 mm. The appearance of these edges constitutes the most striking morphological feature of the bornite crystals examined: every cube edge is replaced by a "staircase" of indentations, which consist of alternating octahedral faces, as could be established by a detailed study on the two-circle reflecting goniometer. For instance (Fig. 4) the three edges that meet at the cube corner truncated by (111) are re-

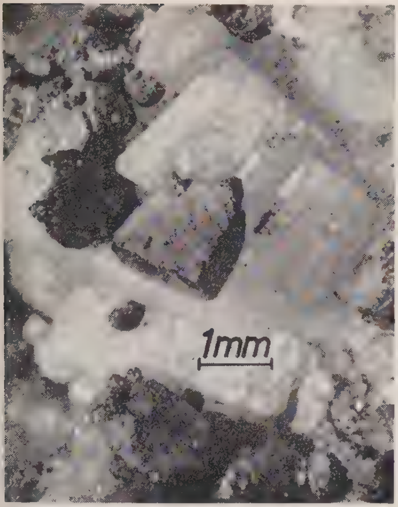

2

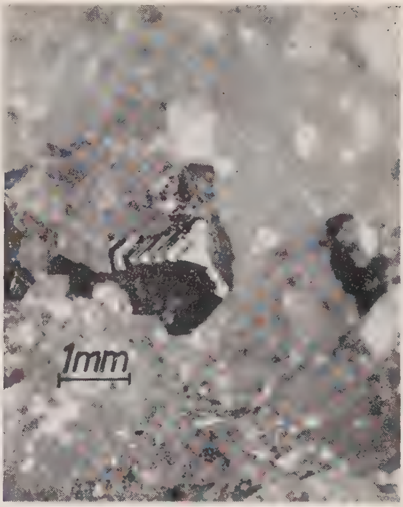

4

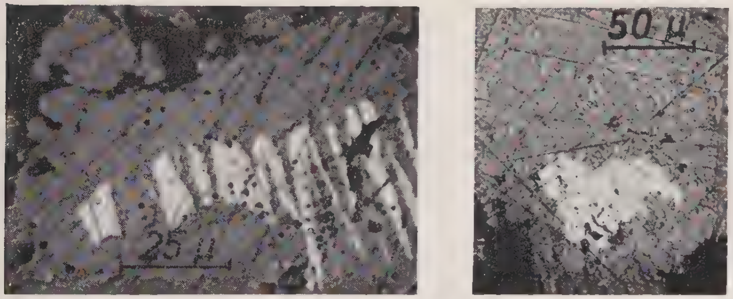

3(a) 3(b)

FIG. 2. Bornite cube on barite crystals. Hand specimen.

FIG. 3. (a) Residual chalcopyrite (white) replaced by bornite (dark gray). Polished section.

(b) Chalcopyrite (white) replaced by bornite (dark gray), in turn replaced by chalcocite (light gray). Polished section.

FIG. 4. Bornite "crystal" with cube truncated by octahedron. Cube edges show staircases due to alternation of octrahedral faces. Hand specimen.

placed by an alternation of (111) faces with $(\bar{1}11)$, $(1\bar{1}1)$, or $(11\bar{1})$, respectively, according as the edge is parallel to the *a*, *b*, or *c* axis. A survey of the available crystals shows that the height of the steps in the "staircase" ranges from 0.01 to 0.05 mm. These steps are visible on the figure, where they appear as small illuminated trapezia, between large and darker cube faces.

Several chips were studied by *x*-ray diffraction, on the rotation, Weissenberg, and precession cameras, using MoKα and CoKα radiations. Two types of crystalline edifices were observed.

One type appears cubic, as shown by rotation patterns taken about the three crystallographic axes. We find cell edge $a = 21.94 \pm 0.06$ Å, and diffraction aspect P***, provided weak reflections are taken into account.

The second type* is metrically tetragonal with $a = b = 21.90 \pm 0.06$, $c = 10.95 \pm 0.03$ Å, but the symmetry of the edifice, as determined from the relative intensities of the diffraction spots, is not higher than orthorhombic, with primitive lattice mode. Our observations agree with those reported by Frueh (1950) on low-temperature bornite from Bristol, Connecticut. Frueh gives the following cell dimensions, $a = b = 21.94$, $c = 10.97$ Å, and considers his material to be primitive orthorhombic and pseudotetragonal. He later informed us, however (priv. comm., July 28, 1958), that he had been dealing with a "multiple crystal." Quoting him: "the reason it was called orthorhombic was that the intensity of reflections did not show 4-fold symmetry. From the smaller fragment it appears to be truly tetragonal with $a = 10.97$ and $c = 21.94$ Å." Since then Morimoto and Kullerud (1959) have established beyond doubt that the true symmetry is indeed tetragonal, with $a = b = 10.95$, $c = 21.90$ Å, space group $P\bar{4}2_1c$, and that the apparent symmetry results from the twinning (by 90° rotation about an *a* axis) of two crystals with *different* volumes. This tetragonal form has been found by Morimoto and Kullerud (1959) on synthetic samples and also on an annealed specimen from the Coppercorp locality. Our cubic type could likewise be explained as a trilling of the tetragonal form, in which the three mutually perpendicular crystals would have *equal* volumes.

A powder pattern of bornite of our "cubic" type was obtained on the Philips diffractometer. With very strong amplification one peak is observed, at $2\theta = 31.9°$ in FeKα radiation, that can be indexed only if the cell edge is 21.90 Å. Its symbol is 643. All other peaks could be indexed on the cell reported first by de Jong (1928) and later by Lundqvist and Westgren (1936): $a = 10.93$ Å, space group $Fd3m$. It is possible that these authors did not observe any weak reflection that would have required doubling the cell edge, or else they were dealing with a structural type that has not been confirmed for low-temperature bornite by later investigators. (A cubic cell with $a = 10.97$ Å and space group $Fm3m$, $F432$, or $F\bar{4}3m$ has been reported by Frueh, 1950, for high-temperature bornite.) For a bornite crystal from Cornwall, Tunell and Adams (1949) reported

---

* In a preliminary report (Carnegie Institution of Washington Year Book 57, 1957–58, p. 248) the limits of error on the value of *a* and *b* are misprinted as ± 0.006.

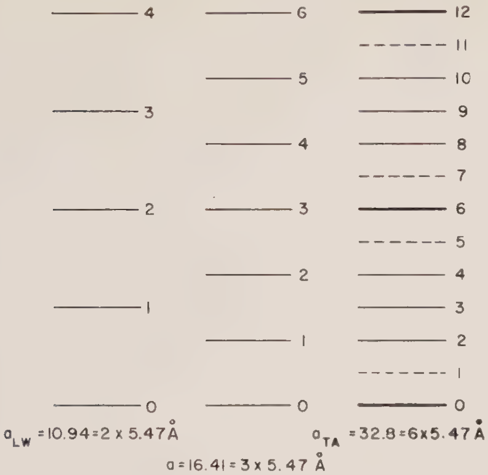

FIG. 5. Schematic explanation of bornite rotation pattern (observed by Tunell and Adams). The proposed intergrowth of two cubic forms, one with $a=2\times 5.47$ Å (found by Lundqvist and Westgren) and a second one with $a=3\times 5.47$ Å (not yet reported in the literature) accounts for the observed absence of first, fifth, seventh, and eleventh layer lines.

a metrically cubic type with cell edge 32.8 Å, but with non-isometric symmetry. They made the intriguing observation that a rotation photograph, which they obtained from a crystal rotating about a "cube" edge and which gave them their value of *a*, does not show the first, fifth, seventh, and eleventh layer lines.

We have attempted to find an explanation for the Tunell-Adams observation. The large cell content of a cube with $a=32.8$ Å—1080 copper atoms, 216 iron atoms, and 864 sulfur atoms—makes us suspect that we are dealing with a complex edifice, either a twin as in digenite (Donnay, Donnay, and Kullerud, 1958) or a syntaxic intergrowth of two distinct phases as with andorite IV and andorite VI (Donnay and Donnay, 1954). Either hypothesis provides an interpretation of the Tunell-Adams rotation pattern. The missing layer lines could be missing as a result of the intergrowth of two phases, one rotating about an edge* of $10.94=2\times 5.47$ Å, the other about an edge of $16.41=3\times 5.47$ Å, as is shown in Fig. 5. The repeat of 10.94 Å is available in the cubic type of Lundqvist and Westgren, as the *c* length of our "orthorhombic" form, or as the *a* length of the tetragonal form. The 16.41 Å repeat has recently been found (Morimoto and Kullerud, in preparation) on synthetic material.

---

* In the preliminary report (C.I.W. Year Book 57, p. 249) two cubic forms had been suggested; their *a* values were misprinted in the legend of Fig. 46 as 2.547 and 3.547 Å, instead of 2×5.47 and 3×5.47 Å.

REFERENCES

DONNAY, G., DONNAY, J. D. H., and KULLERUD, G. (1958), Crystal and twin structure of digenite, Cu_9S_5: *Am. Mineral.*, **43,** 228–242.

DONNAY, J. D. H., AND DONNAY, G. (1954), Syntaxic intergrowths in the andorite series: *Am. Mineral.*, **39,** 161–171.

FRUEH, A. J., JR., (1950), Disorder in the mineral bornite, Cu_5FeS_4: *Am. Mineral.*, **35,** 185–192.

DE JONG, W. (1928), Doctoral dissertation, Delft.

LUNDQVIST, D., AND WESTGREN, A. (1936), On the crystal structure of bornite, Cu_5FeS_4: *Arkiv. f. Kemi, Mineral. och Geologi*, **12B,** (23), 1–6.

MORIMOTO, N., AND KULLERUD, G. (1959), Single-crystal studies of Cu_9S_5-Cu_5FeS_4 solid solutions: *Carnegie Inst. Wash. Year Book*, **58,** 1958–59, 201–203.

THOMSON, J. E. (1954), Geology of the Mamainse Point copper area: *Annual Report of the Ontario Department of Mines*, **62,** pt. 4, 25 pp.

TUNNELL, G., AND ADAMS, C. E. (1949), On the symmetry and crystal structure of bornite: *Am. Mineral.*, **34,** 824–829.

Manuscript received February 6, 1960.

THE AMERICAN MINERALOGIST, VOL. 45, SEPTEMBER–OCTOBER, 1960

AN INTERSTRATIFIED MIXTURE OF MICA CLAY MINERALS

SUSUMU SHIMODA AND TOSHIO SUDO, *Tokyo University of Education, Tokyo, Japan.*

ABSTRACT

Various kinds of mixed-layer minerals are found in close association with the hydrothermal pyrophyllite diaspore deposit of the Yonago mine, Nagano Prefecture, Japan. The reference specimens occur as vein-shaped masses in the pyrophyllite bodies. It almost agrees with allevardite chemically: SiO_2, 43.17%; Al_2O_3, 33.54%; Fe_2O_3, 0.26%; FeO, 0.13%; TiO_2, 0.51%; CaO, 0.52%; MgO, 0.65%; K_2O, 2.84%; Na_2O, 0.38%; P_2O5, tr.; H_2O (+), 10.48%; H_2O (−) 7.75%; Total, 100.23%. *X*-ray data strongly suggest that the 26.1±1 Å spacing can be attributed to a complex combination of the 10 Å mica clay-mineral structure and its more hydrated forms. Ideally three kinds of structures can be considered as "*A*" (10 Å structure . . . a mica clay-mineral structure), "*B*" (12.48 Å structure . . . the silicate layer alternating with a single layer of water molecules), and "*C*" (15.16 Å structure . . . the silicate layer alternating with a double layer of water molecules). It can be appropriately inferred that the 26 Å spacing is nearest to that attributed to a random piling of $A+C$ and $B+C$ structures in equal proportions. It is reasonable to consider that small amounts of potassium ions are still retained even in *B* and *C* structure.

INTRODUCTION

A short time ago, a 26 Å clay mineral was found in the alteration zone around the hydrothermal gypsum deposit of the Tsutsumizawa ore body of the Hanaoka mine, Akita Prefecture, Japan (Sudo and Hayashi, 1955). More recently a 26 Å clay mineral was found in the alteration zone of the Kamikita mine, Aomori Prefecture, Japan (Sudo, Hayashi, and Yokokura, 1958), but the above workers could not provide their detailed mineralogical properties because of difficulty in obtaining pure specimens free from impurities. Subsequently the present writers found the 26° Å clay mineral from the Yonago mine (pyrophyllite diaspore deposit), Nagano Prefecture, and noticed that the mineral also agrees with the Hanaoka and Kamikita materials, and a pure natural specimen was found almost free from impurities. Thus such minerals are not so rare as we have hitherto anticipated, and the present mineral is considered appropriate for the description of its mineralogical and crystallographic properties.

MODE OF OCCURRENCE

Pyrophyllite deposits are found in many localities in Japan, usually accompaning corundum, diaspore, kaolinite, dickite, nacrite etc. Most of them are important mineral resources for the firebrick and paper industries. They are also important because of their mineralogy and geology. But many mineralogical problems remain unsolved because of their very

complex mineral associations. The Yonago mine now being considere
one of the important pyrophyllite-diaspore deposits in Japan.

The area near the ore deposit consists of fine grained sandstone a
shale intruded by porphyrite and andesite dykes. All of these rocks
covered by a lava flow. The ore deposit occurs along the boundary z
between the porphyrite and andesite dykes replacing both of these roc
The ore bodies consist of diaspore, clay minerals, quartz and pyr
Diaspore occurs as compact or powdery masses mostly cemented
pyrophyllite.

About eighty specimens were collected in the area including the
deposit, and the amounts of the minerals in each specimen were e
mated by x-ray analyses using an internal standard of fluorite. Stand
curves were made using pure clay minerals from the other localities. T
confirmed minerals are diaspore, pyrophyllite, quartz, sericite, kaolini
halloysite, montmorillonite, and pyrite. By plotting the result of
qualitative estimations of these minerals except pyrite, zonal distri
tions were confirmed particularly with regard to the distributions
diaspore, pyrophyllite, and kaolin minerals. The center of the zonal
tribution was confirmed in two different places; in both of which
zonal distributions were found to be (diaspore and pyrophyllite
(kaolin minerals) (quartz), going progressively away from the cen
The mineral names written in parentheses are those of the principal m
erals in each zone. The boundaries between these zones are not shar
but gradually grade into one another. Diaspore is rather more domina
in the central area than pyrophyllite, but in most cases both of the
minerals occur mixed with each other in various proportions. Pyri
crystals are dominant in the kaolin mineral zone. Sericite occurs in sm
amounts throughout these zones, but tends to be dominant in the silicio
zone. Montmorillonite occurs locally in the silicious and kaolin mine
zones. Clay minerals showing large spacings in their powder diffractio
data are frequently noted:

Type I (specimens 11 and 63): This mineral shows a 26 Å spacing an
will be discussed in detail in this report. It occurs widely in the ore area
particularly dominantly in the pyrophyllite-diaspore zone, frequently a
vein-shaped masses in the pyrophyllite bodies.

Type II (specimen 1): This mineral also shows a spacing of about 26
and occurs only in the kaolinite zone. Because of difficulty in obtaining
pure sample, we could not ascertain its detailed mineralogical propertie
but it seems to agree with rectorite (Bradley, 1950), or the 26 Å cla
mineral found from the Honami pyrophyllite deposit, Nagano Prefectur
(Kodama, 1958).

Type III (specimen 38): This is found rarely in the silicious zone a thin crusts covering silicious rock fragments. The silicious area usually shows brecciated structures consisting of silicious rock fragments. Because of difficulty in obtaining a pure sample, we could not determine its detailed mineralogical and properties, but it seems to agree with the aluminian mixed-layer mineral recently found from the Kamikita mine, Aomori Prefecture (Sudo and Kodama, 1957).

26 Å CLAY MINERAL (TYPE I)

Macroscopic properties: This mineral occurs as white compact masses with greasy luster resembling the pyrophyllite masses, and is associated with the pyrophyllite-diaspore zone. We could not determine its detailed mode of occurrence, but some of it surely occurs as vein-shaped masses in pyrophyllite bodies.

By *x*-ray testing, we found specimens almost free from impurities, and obtained the following data from the crude specimens. Their *x*-ray reflections consist of the clear and sharp 26 Å reflection and its higher orders except the weak 4.27Å reflection which is probably due to a small amount of impurity. On close examination of the 26 Å reflection under various experimental conditions as studied with a slow scanning speed, or using the internal standard of α-stearic acid, the spacing appears to vary slightly from specimen to specimen. Basal spacings obtained from nine reference specimens and also the mean values of each set of basal reflections are given in Table 1. From each of these mean value the 001 spacings were calculated, and 26.1 ± 1 Å was obtained as the final mean value.

TABLE 1. BASAL SPACINGS OF THE 26 Å CLAY-MINERAL FROM THE YONAGO MINE

001	1		2		3		4		5		6	
	d	I	d	I	d	I	d	I	d	I	d	I
001	28.5 Å	61 s	27.6 Å	66 s	26.8 Å	91 vs	26.8 Å	91 vs	28.5 Å	44 m	26.8 Å	60 s
002	12.8	52 vs			13.0	83 vs	13.0	83 vs	13.0	47 s	12.5	50 s
005	5.12	25 s			5.09	39 s	5.12	40 vs	5.12	27 vs	5.06	34 s
008	3.24	30 s			3.27	48 s	3.24	42 m	3.27	40 vs	3.25	34 m
00.10	2.57	26 s			2.57	32 s	2.57	32 s	2.57	42 vs	2.57	35 s

	7		8		9		Mean	d(001)
	d	I	d	I	d	9	d	
001	27.6 Å	50 m	27.6 Å	20 b	28.5 Å	21 b	27.6 Å	27.6 Å
002							12.9	25.8
005							5.10	25.5
008							3.25	26.0
00.10							2.57	25.7
								Mean 26.1 ± 1 Å

Worthy of notice is that the 26 Å reflection is usually accompanied by a tailed reflection on its small angle side, but we could not find reflections attributable to superstructures of the 26 Å one.

Effects of heat (Table 2): The specimen analysed by x-ray diffraction was heated at each of the temperatures 300° C., 500° C., 700° C., 900° C., and 1000° C. for one hour and sealed into a glass tube immediately after cooling, and kept in the sealed glass tube until it was studied by x-rays. In the specimen heated at 300° C. for one hour, the 26 Å reflection was just visible, and its higher order reflections were somewhat weakened. The 13 Å reflection shifted to a 10.3 Å reflection, and the 5.10 Å reflec-

TABLE 2. X-RAY DIFFRACTION DATA FOR THE AIR-DRYED 26 Å CLAY MINERAL (CuKα, 1.5418 Å)

Room temp.		300° C.		500° C.		700° C.		900° C.		1000° C.	
d	I	*d*	I	*d*	I	*d*	I	*d*	I	*d*	I
26.7 Å	40 vs					24.5 Å	3 vb				
								18.4 Å	2 b		
13.0	33 vs										
				11.5 Å	5 b	11.8 Å	7 b				
		10.3 Å	12 b	10.9	5 b	10.4	8 b	10.3	15 s	10.3 Å	2 b
				9.9	6 b	10.0	10 b				
9.3	3 b										
5.10	16 s	5.01	8 m	5.07	5 b	5.04	9 s	5.07	10 s	5.09	3 m
4.48	19 s	4.51	20 vs	4.53	22 s	4.51	38 vs	4.51	42 vs	4.50	8 m
4.27	10 vs	4.29	21 vs	4.31	3 s	4.27	7 vs				
						3.87	4 vb	3.92	6 b		
								3.80	6 b		
		3.52	3 vb					3.55	5 b		
3.47	3 b										
										3.40	8 vb
3.35	6 s			3.35	10 m	3.34	27 vs	3.35	30 s		
3.27	6 s	3.29	11 b	3.29	8 s	3.24	7 vs	3.27	9 vs	3.25	4 s
								3.10	4 b		
						3.03	2 vb	3.08	4 b		
						2.84	2 vb	2.88	3 b		
										2.70	2 b
2.56	13 s	2.58	15 s	2.59	9 m	2.59	10 b	2.59	11 m		
						2.51	3 vb	2.52	5 b	2.54	3 vb
2.49	3 b	2.46	4 vb	2.49	5 b	2.48	3 vs	2.49	4 b		
2.44	4 b			2.42	3 vb	2.41	3 vb	2.41	4 b		
2.39	4 b					2.35	4 b				
		2.25	3 b	2.26	3 vb			2.26	6 m	2.21	3 b
2.19	3 vb										
2.13	3 vb	2.14	3 b			2.13	4 vs	2.13	2 b	2.13	2 vb
		2.03	2 b			2.01	4 vb	2.01	5 b		
1.99	5 b										
		1.79	4 b	1.72	3 b	1.72	3 vb				
1.69	3 b	1.69	3 b	1.63	3 vb	1.67	3 vb	1.69	5 b	1.68	3 b
		1.65	3 vb								
		1.55	5 s								
1.49	7 m	1.50	9 m	1.51	3 b	1.51	4 b	1.52	4 b		

vs: very sharp. s: sharp. m: medium. b: broad. vb: very broad.

tion was replaced by a 5.01 Å reflection. The 3.27 Å reflection became broader, and its spacing was replaced by a slightly larger spacing of 3.29 Å. In the specimen heated at 500° C., the 26 Å reflection was still just visible. Its higher order reflections became weaker than in the case of the specimen heated at 300° C. The 3.27 Å reflection was replaced by a broad reflection with a slightly larger spacing of 3.35 Å. Worthy of special attention is that the 10 Å reflection acquired a tail toward its low angle side. A very broad reflection at about 11.5 Å could be recognized on its tailed reflection. Such behaviour is closely similar to that of the tailed reflection accompanying the 10 Å reflection in the crude specimen of the Kamikita material. After heating to 700° C., the weak and broad 2.45 Å reflection appeared; the intensities of the 10 Å and 5 Å reflection became somewhat more intense, but the 3.34 Å and 4.51 Å reflections became remarkably intense. The tailed reflection was still confirmed. After heating to 900° C., the intensities of the 10 Å, 5 Å, 4.5 Å and 3.35 Å are similar to those in the specimen heated at 700° C., but the 26 Å reflection as well as the tailed reflection completely disappeared, and the very weak 19 Å reflection appeared. In the specimen heated at 1000° C., the reflections were weakened, except the 4.50 Å and 3.40 Å reflections. The result obtained above suggests that the 26 Å spacing seems to be related to hydrous states of the 10 A structure.

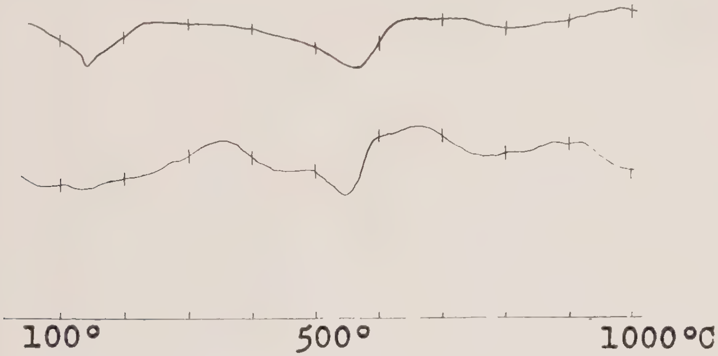

Fig. 1. D.T.A. curves of the 26 Å clay mineral from the Yonago mine. Above: specimen in natural state. Below: specimen treated with piperidine.

Differential thermal analysis curve: The differential thermal analysis curve of the specimen analysed by x-rays shows the broad endothermic peaks at about 600° C., and also between 700° C. and 800° C., except a clear endothermic peak between 100° C. and 200° C. (Fig. 1, above). The specimen was soaked in piperidine for about 10 minutes, and dried on a water-bath. The specimen thus pretreated was analysed thermally (Fig.

1). Its thermal curve shows an additional exothermic peak between 600° C. and 700° C. as in the case of montmorillonite or vermiculite.

Chemical composition: The specimen analysed thermally and by *x*-rays was also analysed chemically. Its chemical composition is as follows: SiO_2 43.17%; Al_2O_3, 33.54%; TiO_2, 0.51%; Fe_2O_3, 0.26%; FeO, 0.13%; CaO, 0.52%; MgO, 0.65%; K_2O, 2.84%; Na_2O, 0.38%; P_2O_5, tr.; H_2O (+) 10.48%; H_2O (−) 7.75%, Total, 100.23%. It is worthy of notice that the mineral almost agrees with allevardite (Caillère, Mathieu-Sicaud, and Hénin 1950; Brindley, 1956), except that the amount of potassium is slightly larger and the amount of sodium is smaller in the present material than in the case of allevardite. The structural formula was constructed on the basis of the number of ions in the octahedral and tetrahedral positions as 12 for the sake of comparison with that of allevardite.

$$(Na_{0.16}K_{0.52}Ca_{0.08})(Al_{3.82}Fe'''_{0.02}Fe''_{0.02}Mg_{0.08})(Si_{6.13}Al_{1.87})O_{17.68}(OH)_{7.44}$$

Treatment with water or ethylene glycol gave no unique results; they seem to vary slightly even from portion to portion in a hand specimen. Treatment with water always caused the 26 Å reflection to be replaced by the 29.2 ± 1 Å reflection, but treatment with ethylene glycol caused no expansion in some specimens, yet clear expansion to about 28 Å in others. Treatment with ammonium nitrate solution (1 N) by boiling for 10 minutes caused no remarkable change except the 26 Å and 13 Å reflections became somewhat broad.

X-ray analysis: In general, the powder reflections are somewhat broad, and we could obtain only five basal reflections for crystallographic considerations even with a slide of well-oriented aggregates. Therefore we could not obtain reliable data for Fourier synthesis of the electron density or the Fourier transform (MacEwan 1956). But we could suggest the probability of occurrences of spacings of about 10 Å, 13 Å, and 16 Å.

DISCUSSION

The present material has mineralogical properties almost agreeing with those of allevardite, but the following slight differences exist between them, which must be considered in drawing a conclusion:

(1) For allevardite, the largest spacing obtained was 24.12 Å in air-dry unheated material, and very many basal reflections were found. In the present case the *x*-ray powder reflections are generally broad, and only five basal reflections are available. The 26 Å spacing varies slightly from specimen to specimen, and even from portion to portion in a hand specimen, and is accompanied by a tailed reflection on its low angle side. But

we could not find reflections due to super-structures by the small-angle scattering technique.

(2) The intensities of the *x*-ray powder reflections of the specimen heated at 900° C. almost agree with the calculated intensities for the regular piling of the 10 Å mica clay-mineral structure and its silicate layer. But the 10 Å reflection is stronger than its calculated value, which implies that the 10 Å structure may be also produced in the firing product.

On this basis, it may be inferred that the 26 Å spacing is not necessarily attributed to a unique regular piling of the 10 Å structure and its more hydrated one, but to a more complex mixed-layer mineral; it is strongly suggested that the 26 Å spacing is due to a random piling of two structures with spacings near to 26 Å.

TABLE 3. OBSERVED VALUES OF SPACINGS AND INTENSITIES OF SOME BASAL REFLECTIONS COMPARED WITH THEIR CALCULATED VALUES OBTAINED FROM A RANDOM MIXED-LAYER STRUCTURE OF A+C AND B+C STRUCTURES

	Observed values		Calculated values	
	d	I	*d*	I
001	26.1 Å	1	26 Å	1
002	12.9	0.52	12	0.40
005	5.10	0.18	5	0.15
008	3.25	0.32	3.1	0.30

As already shown by Brindley (1956), the cell heights of the hydrated forms of the mica clay-mineral structure are as follows:

A: 9.98 Å—mica clay-mineral structure.

B: 12.48 Å—potassium ions are completely replaced by a single layer of water molecules.

C: 15.16 Å -potassium ions are completely replaced by a double layer of water molecules.

Of course these three models are ideal ones. We can consider intermediate states as potassium ions are still associated with water layers. But since the amount of potassium associated with the water layers is small, the fluctuation of these cell heights may be small, and the principal cell heights can be grouped at about 10 Å, 13 Å, and 16 Å, which were already suggested by Fourier-transform diagram.

Various combinations were considered and finally it was shown that the structure of a random piling of 25.1 Å ($A+C$) and 27.6 Å ($B+C$) in equal proportions, gave the calculated intensity values nearest to observed ones (Table 3). Actually, it may be more appropriate to consider that some potassium is still preserved even in the *B* and *C* structures because, as shown above, it seems that the firing product at 900° C. is not solely composed of a regular piling of the 10 Å mica clay-mineral structure, its silicate layer, but also of some amounts of the 10 Å structure.

Worthy of special attention is that a tailed reflection appears associated with the 10 Å reflection on heating. This fact suggests that various spacings slightly different from the 10 Å spacing occur on heating, and also suggests that dehydration did not occur uniformly throughout all the layers on heating. Furthermore in relation to this fact, it is also worthy of notice that effects of treatments with ethylene glycol are not unique. This fact implies that the crystallochemical behavior of the potassium ions is not unique; some of them are exchangeable and others not.

ORIGIN

On the basis of the model, it seems likely that the mineral now in question is a mica clay mineral partially altered by hydration and leaching, the degree of which may vary from place to place, as shown by variation of cell heights and organic complexes. It is believed that with increase of hydration and leaching, potassium ions decrease and the number of layers of water molecules increases. Thus, although potassium ions are still preserved in the water layers, the amount can be expected to be less in the case of a double layer than in the case of a single layer. If the mineral is an alteration product of the 10 Å mica clay mineral it is possible that the mineral is not necessarily represented by the ideal model, but small amounts of potassium ions are still preserved in *B* and *C* structures.

The above statement can be supported by the mode of occurrence of this mineral, namely, in the central area of the deposit closely associated with pyrophyllite-diaspore which may have been formed in a leaching environment. In the case of the Kamikita material, the 26 Å minerals are dominant in the central area of the deposit associating with pyrophyllite and pyrite, and the 10 Å mica clay mineral is rather dominant on going outward.

Recently one of the writers emphasized the concept of the intermediate mineral in clay mineralogy (Sudo, 1957). It means a mineral which behaves as mineral "*a*" in some of its properties but as mineral "*b*" in the other properties. These minerals have frequently been found between certain principal clay minerals such as montmorillonite and chlorite. It is frequently noticed that some of these intermediate minerals have a mixed-layer structure with two kinds of minerals. Thus the present material may be described as an intermediate mineral, formed during the hydration of the 10 Å mica clay mineral.

ACKNOWLEDGMENTS

The writers are indebted to Mr. Miura and S. Ota of the Chugai-mining Company, and Mr. J. Takahashi, of the Yonago Mine, for help of Geological survey. Thanks are due to the officials of the Department of Education for their kindness in granting funds for this study.

The writers wish to express their deep appreciation to Professor G. W. Brindley of the Pennsylvania State University, for critically reading of this manuscript.

REFERENCES

BRADLEY, W. F. (1950) The alternating layer sequence of rectorite, *Am. Mineral.*, **35,** 590–595.

BRINDLEY, G. W. (1956) Allevardite, a swelling double-layer mica mineral. *Am. Mineral.*, **41,** 91–103.

CAILLÈRE S., MATHIEU-SICAUD A., AND HÉNIN S. (1950) Nouvel essai d'identification du mineral de Ia Table pres Allevard, l'allevardite. *Bull. Soc. Franc Miner. Crist.*, **73,** 193–201.

KODAMA H. (1958) Mineralogical study on some pyrophyllite in Japan. *Miner. Journ.*, **2,** 236–244.

MACEWAN, D. M. C. (1956) Fourier transform methods for studying from lamellar systems. 1. A direct method for analyzing interstratified mixtures. *Koll. Zeit.*, **149,** 96–108.

SUDO T. AND HAYASHI H. (1955) New types of clay minerals with long spacings at about 30 Å found from the altered area developed around certain ore bodies of the Hanaoka mine, Akita Prefecture. *Sci. Rep. Tokyo Kyoiku Daigaku* (*Tokyo Univ. of Education*), *Sec. C.*, No. **25,** 281–294.

SUDO, T., HAYASHI H., AND YOKOKURA H. (1958) Mineral association in ore deposits, *Clay Miner. Bull.* **3,** No. 19, 258–263.

SUDO T. AND H. KODAMA (1957) An aluminian mixed-layer mineral of montmorillonite-chlorite. *Zeit. Krist.*, **109,** 4–6.

SUDO T. (1957). The discovery of mixed-layer minerals and its contribution to clay science (in Japanese). *Journ. Miner. Soc. Japan*, **39,** 286–299.

Manuscript received June 19, 1959.

THE AMERICAN MINERALOGIST, VOL. 45, SEPTEMBER–OCTOBER, 1960

RANQUILITE, A CALCIUM URANYL SILICATE

M. Jiménez de Abeledo, María Rodríguez de Benyacar
and Ernesto E. Galloni,

Comision Nacional de Energía Atómica, Buenos Aires, Argentina.

Abstract

A new uranium mineral, named ranquilite, has been found in Mendoza Province, Argentina. The probable formula is $1.5CaO \cdot 2UO_3 5SiO_2 \cdot 12H_2O$. The orthorhombic unit cell has $a_0 = 17.64$ Å, $b_0 = 14.28$ Å and $c_0 = 18.48$ Å. Z. = 8, G. = 3.32. Samples heated to 110–120° and to 130–140° C. show certain changes in the *x*-ray powder pattern suggesting two lower hydrates. After exposure to the air, the original pattern is again obtained.

Introduction

Late in 1957 the Geological Service Laboratory of the Argentine Atomic Energy Commission received samples from the Ranquil-Có area, Portezuelo Hill, Malargüe Department, Mendoza Province, Argentina, consisting of gypsum associated with calcite and some limonite Very small amounts of a fluorescent uranium mineral appeared in fissures in the gypsum. By hand picking it was possible to obtain about 2 mg. of this mineral with small amounts of gypsum. *X*-ray powder photographs and semi-quantitative spectrographic analysis indicated a new calcium uranyl silicate, that was named ranquilite from the occurrence (1, 2, 3).

The fine-grained character of the mineral precluded the measurement of any optical properties other than the mean index of refraction, which for analyzed material is 1.564. The density lies between 2.89 and 3.32. The mineral is easily soluble in acids, and yields a silica gel. It turns ocher-yellow on heating.

With the arrival of new samples it was possible to continue the study of the mineral. From 1.5 kg. of rock, about 2 gms. of relatively pure ranquilite were separated by hand. This was divided into several fractions according to the estimated proportions of gypsum. Several very pure grains were reserved for *x*-ray photographs, electron microscopy and electron diffraction. The chemical analyses and dehydration studies were performed on the fractions containing gypsum (amounts ranging from 1 to 10%).

Chemical Composition

Chemical analyses were performed on three different samples weighing 100 mg. or less each; the proportion of gypsum in those samples ranged from 6.3 to 1%. The results showed good agreement; data from one of the analyses are shown in Table I;* column (e) shows the chem

---

* Chemical Analyses by Enrique Garcia, General Chemistry Laboratory, Argentin Atomic Energy Commission.

TABLE I. CHEMICAL COMPOSITION OF RANQUILITE

	Chemical composition of sample of ranquilite with gypsum impurity				Chemical composition of ranquilite
	On ignited sample		Data recalculated to sample as is		
	(a)	(b)	(c) (b)×.806	(d)	(e) (d)×100/96.72
SiO_2	31.9	31.9	25.71	25.71	26.6
U_3O_8	56.3	56.3	45.38	45.38	46 8
CaO	9.0	8.23	6.63	6.63	6.9
SO_3	1.1	—	—	—	—
H_2O (Loss on ignition on total sample.)	—	—	19.4	19.0	19.6
				96.72	99.9
$CaSO_4$	—	1.87	1.51	—	—
$CaSO_4 \cdot 2H_2O$	—	—	—	1.91	—
Total	98.3	98.3	98.63	98.63	99.9

H_2O^-% 8.1

H_2O^+% Loss on ignition −11.5

Penfield method −11.1

(a) Results of analysis as made.
(b) SO_3 recalculated as $CaSO_4$
(c) and (d) Data recalculated to sample as is, on the basis of total water content, 19.4%.
(e) Results adjusted to 100% after deducting gypsum.

cal composition of ranquilite adjusted to 100% after deduction of gypsum. The probable formula, according to these analyses is:

$$1.5CaO \cdot 2UO_3 \cdot 5SiO_2 \cdot 12H_2O$$

Spectrographic semiquantitative analyses showed the presence of about 1% Al and 1% Mg, but those elements were not determined chemically.

The following elements were looked for, but not found, on the spectrographic plates: Ag, Tl, W, Ti, Sb, Sr, Li, Cr.

According to dehydration experiments, besides water lost at low temperature, (OH) groups are present in the mineral.

X-RAY DIFFRACTION

Owing to the very small size of the crystals no single crystal pattern could be obtained. Table II shows data from a powder pattern taken in a 114.8 mm. diameter camera, with CuK$_\alpha$ radiation. Patterns taken with CoK$_\alpha$ radiation failed to show reflections with spacings larger than 9.3 Å.

From a small block three patterns were taken; the sample, kept stationary, was successively orientated in three directions at 90°. Powder patterns with lines of uniform intensity distribution were always obtained, showing that the sample consisted of microcrystals in random orientation.

Electron Diffraction and Electron Microscopy

Electron diffraction patterns and electron micrographs were obtained in a three stage Philips electron microscope. Many micrographs reveal a stacking of very thin, transparent plates, showing an excellent cleavage parallel to the largest face of the plates (Fig. 1).

The many single crystal electron patterns obtained were all very similar; the spots are arranged on an orthogonal net, and there is a very symmetrical distribution of intensities (Fig. 2). Colloidal graphite patterns, taken with the same settings of the microscope controls, were used for calibration.

Figure 2 shows a selected area diffraction pattern of ranquilite. Assuming it represents the $0a^*b^*$ plane of the reciprocal lattice, two directions at 90° were chosen for a^* and b^*. The values $a = 17.6$ Å and $b = 7.$ Å result. Only $hk0$ reflections with $h+k=2n$ appear.

In many S.A.D. patterns, however, intermediate rows of faint spots

Table II. *X*-Ray Powder Pattern of the Natural Material from Ranquil-C6 (Cu/Ni; λ = 1.4518 Å; Film No. 83).

d (Å)	I	*d* (Å)	I	*d* (Å)	I
9.26	v s	2.508	v f	1.781	f
8.12	s	2.405	f	1.745	w
6.62	f	2.332	f	1.658	w
5.10	w	2.281	f	1.626	v f
4.63	m	2.222	w	1.600	f
4.47	v s	2.186	m	1.566	f
3.68	f	2.067	v f	1.535	v f
3.58	m	1.980	w	1.497	w
3.34	m	1.934	w	1.453	v f
3.21	m	1.892	w	1.351	f
3.03	v s	1.863	w	1.324	f
2.81	w	1.838	w	1.310	v f
2.63	w	1.811	w	1.294	v f

v s = very strong; s = strong; m = medium; w = weak; f = faint; v f = very faint.

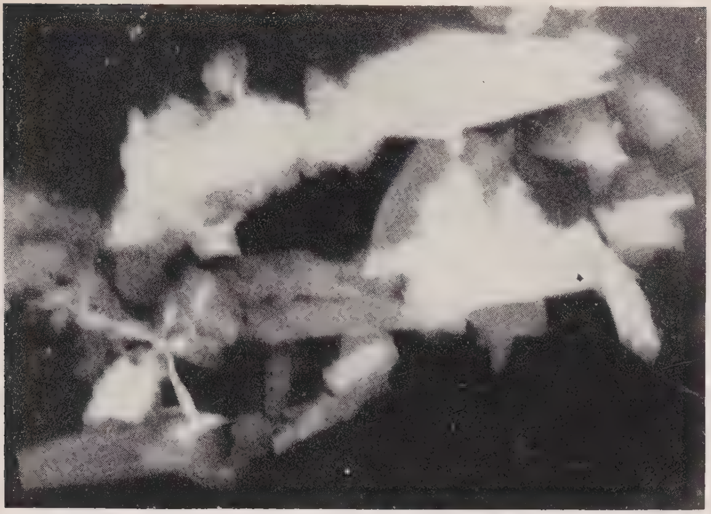

FIG. 1. Electron micrograph of ranquilite.

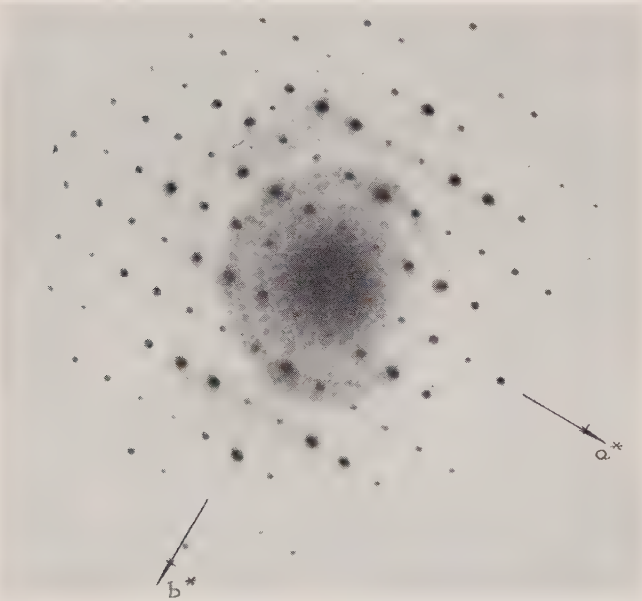

FIG. 2. Selected area electron diffraction pattern of ranquilite. Plane of the grid is approximately normal to the electron beam. 100 KV.

are clearly seen (Fig. 3). Those patterns may be supposed to belong to the thinnest crystals, since they show a larger central dark spot and a stronger blackening. The presence of the intermediate rows has to be accounted for by doubling b, giving 14 Å. With this value for b, and assuming that the faint spots belong to an upper level, only those $hk0$ reflections fulfilling the conditions $h=2n$ and $2h+k=4n$ are present There are no limiting conditions for the hkl reflections.

Considering the easy dehydration of ranquilite (see later), some experiments were performed to determine whether the electron diffraction

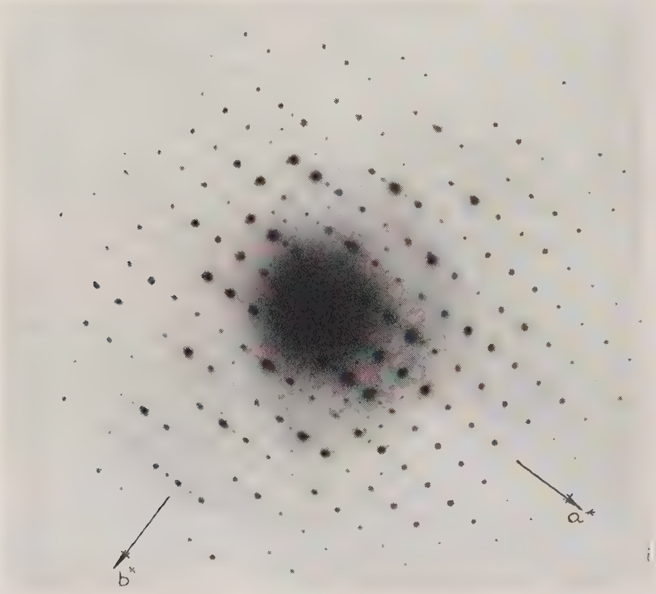

Fig. 3. Selected area electron diffraction pattern of ranquilite showing intermediate spots.

patterns belong to the natural material or to an alteration product r sulting from exposure to high vacuum and electron beam bombar ment. Data from powder patterns obtained in a Siemens Electron Micr scope operated as a camera, and in a Metropolitan Vickers camera both agree with x-ray powder diffraction and S.A.D patterns.

It seems that the spots of the S.A.D. patterns represent reflectio that do not change while the mineral is exposed to high vacuum ar electron beam bombardment.

---

* Both kindly taken Dr. Grünbaum, IDIEM Institute. Santiago de Chile.

DEHYDRATION STUDY

The changes suffered by the mineral on heating were followed by the changes in the *x*-ray powder patterns.

Samples contained in glass capillaries or mounted in the sample holders of the Philips wide range goniometer, were heated to different temperatures for periods ranging from 6 to 24 hours. Photographic patterns or goniometer records were taken immediately afterwards; the capillaries were heat-sealed prior to the taking of the patterns.

Some samples were exposed again to room conditions once the patterns were obtained; others were kept in chambers with known humidities. Later, *x*-ray photographs were taken again.

These experiments show that:

(*a*) There is a change in the diffraction pattern after heating the mineral to 110–120° C. On the photographs several lines shift to positions of smaller spacings; particularly the line $d=9.3$ Å changes to 8.2 Å and the line $d=4.62$ Å to 4.11 Å. The change coincides with the loss of water at 110–120° C. recorded by the chemical analyses.

(*b*) On two experiments the mineral was heated to 130–140° C. for 14 hours. The *x*-ray pattern showed a line with $d=7.3$ Å, while the lines with $d=8.2$ Å and $d=4.1$ Å were not present. A third "hydrate" is suggested.

(*c*) Samples that had been heated, if left for a time at room conditions, gave again the pattern of the "natural" material. Samples kept in chambers with 32, 50 and 75% relative humidities, gave also the original pattern. No intermediate steps could be detected.

(*d*) The goniometer records show that the intensity of some lines, already present in the "natural" pattern, are greatly enhanced after heating, while the intensity of other lines is much reduced (Fig. 4).

(*e*) Goniometer records taken after the dehydrated samples were kept at room conditions for a while, showed again the original spacings, and approximate intensity relationships.

From these results it was concluded that two forms with different amounts of water are present in our samples of ranquilite. On heating, Hydrate I changes to the less hydrated form (Hydrate II). Hydrate II rehydrates easily, by absorption of atmospheric moisture or when wetted, to give hydrate I.

CRYSTAL SYSTEM, UNIT CELL AND UNIT CELL CONTENTS

According to the dehydration experiments, lines belonging to two differently hydrated forms appear on the *x*-ray powder patterns of natural ranquilite. From the study of the lines that shift during dehydration and rehydration, it was concluded that the lines belonging to the form rich in water (hydrate I) are those listed in Table III.

The values $a_0=17.6$ Å and $b_0=14.0$ Å were obtained from electron

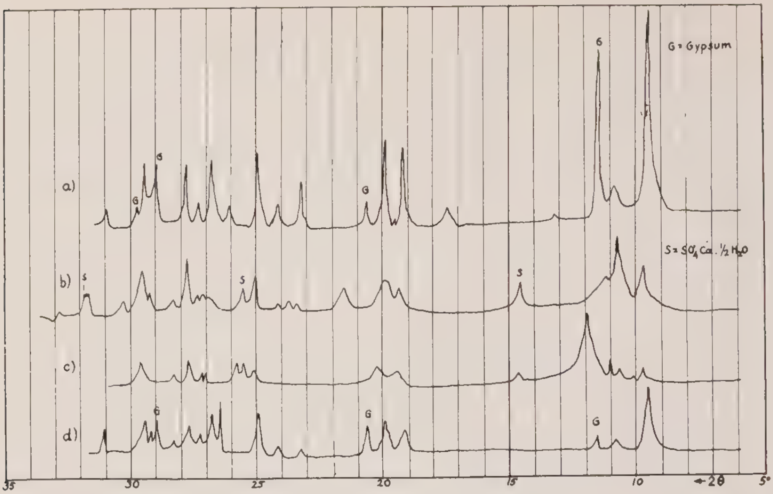

FIG. 4. *X*-ray diffraction goniometer traces of impure ranquilite.

a) Natural material from Ranquil-C6.

b) Sample heated to 110–120° C. for 13 hours.

c) Sample heated to 130–140° C. for 14 hours.

d) Sample wetted with water and kept 12 hours in a chamber with 100% relative humidity, after having been heated to 130–140° C.

The operating constants are: Radiation: Cu/Ni filtered; KVP: 36; MA 20; Divergence slit 1°; Receiving slit: 0.1 mm.; Scatter slit: 1°; Scale factor: 4; Multiplier: 1; Time constant: I seg.; Scanning speed: 0.5°/min.; Chart speed: 800 mm./hr.

diffraction patterns. A value for c_0 was obtained assuming that the lines that shift during dehydration represent $00l$ reflections. Taking the line with $d = 4.62$ Å as 004, we get $c_0 = 18.48$ Å. After having adjusted these values for a better agreement with *x*-ray data, we get:

$$a_0 = 17.64 \text{ Å} \qquad b_0 = 14.28 \text{ A} \qquad c_0 = 18.48 \text{ A}$$

With these values for the unit cell, and assuming orthorhombic symmetry, it was possible to index all of the reflections in the ranquilite (hydrate I) pattern. As shown in Table III, for most of the spacings there were several choices of indices, so it is not possible to determine the space group.

The volume of the proposed unit cell is 4655 Å^3, and if $Z = 8$, the resulting theoretical density is 3.32. The actual density of ranquilite lies between 2.89 and 3.32.

Ranquilite shows a similarity with the mineral zeunerite (4) in its behaviour during dehydration-rehydration; by its *x*-ray diffraction pattern and chemical composition, it is closely related to the mineral named haiweeite by McBurney and Murdoch (5).

Table III. *X*-Ray Powder Pattern of Ranquilite (Hydrate I)

I	d (Å) Measured	d (Å) calculated*	hkl
100.	9.30	9.241	002
0.4	6.63	6.618	120
		6.661	021
13.	5.07	5.050	203
43.	4.62	4.620	004
		4.610	031
		4.595	130
40.	4.47	4.469	104
		4.460	131
		4.509	123
8.	3.67	3.675	421
		3.683	133
		3.655	323
		3.695	005
20.	3.57	3.570	040
		3.578	015
		3.551	224
9.	3.40	3.408	205
		3.424	510
30.	3.34	3.330	042
		3.368	511
		3.315	215
		3.315	034
25.	3.21	3.210	512
		3.205	423
		3.228	125
		3.190	404
28.	3.037	3.035	106
		3.043	143
17.	2.814	2.814	523
		2.819	150
		2.823	051
		2.825	044
13.	2.63	2.633	425
		2.640	007
3.	2.508	2.509	540
		2.512	515
		2.501	630

I	d Å measured
7	2.405
8	2.332
8	2.281
9	2.222
10	2.186
8	2.067
13	1.98
12	1.934
18	1.892
8	1.863
6	1.838
8	1.811
9	1.781
9	1.745
5	1.658

* Calculated for an orthorhombic cell with $a_0 = 17.64$, $b_0 = 14.28$ and $c_0 = 18.48$ Å.

Recently a new occurrence of ranquilite, associated with uranophane, has been reported in the San Sebastian Mine, Sañogasta area, Chilecito, La Rioja province, Argentina. Ranquilite has been identified by its *x*-ray diffraction pattern by Dr. Roberto O. Toubes* who is now studying the samples.

REFERENCES

1. PANDOLFI, C. L. DE, BENYACAR, M. RODRÍGUEZ DE, AND ABELEDO, M. JIMÉNEZ DE. On a new uranium mineral. Paper sent to the Second Conference on Pacific Uses of Atomic Energy. Geneva, September, 1958.
2. PANDOLFI, C. L. DE, BENYACAR, M. RODRÍGUEZ DE, AND ABELEDO, M. JIMÉNEZ DE. On a new uranium mineral from the Ranquil-Có area. Paper read at the 31 meeting of the Asociación Fisica Argentina, Buenos Aires, May 1958.
3. ABELEDO, M. JIMÉNEZ DE, BENYACAR, M. RODRÍGUEZ DE, AND GALLONI, ERNESTO E. Study of ranquilite, a new uranium mineral. Paper read at the fifth meeting of the Sesiones Químicas Rioplatenses Buenos Aires, July 29–31, 1959.
4. FRONDEL, C. Systematic Mineralogy of Uranium and Thorium. *Geological Survey Bulletin* **1064.**
5. MCBURNEY, T. C., AND MURDOCH, J. Haiweeite, a new uranium mineral from California. *Am. Mineral,* **44,** 839–843 (1959).

Manuscript received November 19, 1959.

---

* Geology Department, Atomic Energy Commission, Argentina.

THE AMERICAN MINERALOGIST, VOL. 45, SEPTEMBER-OCTOBER, 1960

NOTES AND NEWS

X-RAY CRYSTALLOGRAPHY OF LARDERELLITE, $NH_4B_5O_6(OH)_4$*

JOAN R. CLARK,
U. S. Geological Survey, Washington 25, D. C.

Because of the minute size of all larderellite crystals available at the time a recent study of ammonium pentaborates was made (Clark and Christ, 1959), neither density nor single-crystal x-ray data could be obtained. Since that time, however, crystals of suitable size for such studies have been found on a specimen of larderellite from Larderello, Italy. The present note describes the results of examinations of these crystals.

The larderellite specimen was given to W. T. Schaller, U. S. Geological Survey, by Professor Stefano Bonatti, Director, Mineralogical Institute, University of Pisa, Italy. I am most grateful to Dr. Schaller for allowing the use of crystals from this specimen and for providing the prepublication results of chemical analyses carried out by himself and Angelina C. Vlisidis, U. S. Geological Survey, and of density determinations by M. K. Carron, U. S. Geological Survey. I am also indebted to my colleague, C. L. Christ, for numerous valuable suggestions.

Single-crystal x-ray data for larderellite, obtained by precession-camera techniques of the kind described in Clark and Christ (1959), are given in Table 1. Similar data found by Marinelli (1959) are also given in Table 1. His results became known to me only after completion of the present x-ray study, and the agreement is gratifying. The optical orientation given by Marinelli (1959), $Y=b$, and the perfect cleavage parallel to (100) as defined by the cell of Table 1, are both confirmed.

The density for larderellite was obtained with a pycnometer for a 1 g. sample, and the value is 1.905 ± 0.004 g. cm.$^{-3}$ (M. K. Carron, oral communication). The chemical formula usually ascribed to larderellite is $(NH_4)_2B_{10}O_{16} \cdot 5H_2O$ (Palache, Berman and Frondel, 1951). For the experimentally determined cell volume of 830.9 Å^3 (Table 1), with two of these formula units per cell, the calculated density is 1.959 g. cm. ^{3}, so that the discrepancy between observed and calculated densities is sufficient to cast doubt on this chemical formula. New chemical analyses by Schaller and Vlisidis (oral communication) are compatible with assumption of either $(NH_4)_2B_{10}O_{16} \cdot 4H_2O$ or $(NH_4)_2B_{10}O_{16} \cdot 4\frac{1}{2}H_2O$. The calculated density based on two formula units per cell of the former is 1.887 g. cm.$^{-3}$, of the latter, 1.923 g. cm.$^{-3}$; both these calculated values are in reasonable agreement with that of the observed density.

---

* Publication authorized by the Director, U. S. Geological Survey.

Table 1. Crystallographic Data for Larderellite
Symmetry: monoclinic

	Marinelli (1959)*	Present Study
a	11.65 ± 0.01 Å	11.63 ± 0.03 Å
b	7.63 ± 0.01	$7.61_5\pm0.02$
c	9.47 ± 0.01	$9.44_7\pm0.03$
β	$97°05'\pm15'$	$96°45'\pm10'$
Volume	835.4 Å^3	830.9 Å^3
Space Group	$P2_1/a$	$P2_1/a$
Cell Contents	$2[(NH_4)_2O\cdot5B_2O_3\cdot5H_2O]$	$2[(NH_4)_2O\cdot5B_2O_3\cdot4H_2O]$
Density (calc.)	1.95 g.cm.$^{-3}$	1.887 g.cm.$^{-3}$
(obs.)	—	1.905 ± 0.004

* Marinelli (1959) interchanged a and c and therefore assigned space group $P2_1/c$; transformation from his cell to the present one: 001/010/100.

Christ (1960) has pointed out that both ammonioborite and larderellite probably contain the pentaborate ion, $[B_5O_6(OH)_4]^{-1}$, known to exist in the two isostructural compounds, $NH_4B_5O_6(OH)_4\cdot2H_2O$ and $KB_5O_6(OH)_4\cdot2H_2O$ (Zachariasen, 1938). The structural formulas for larderellite corresponding to the two chemical formulas are, therefore, $NH_4B_5O_6(OH)_4$ and $NH_4B_5O_6(OH)_4\cdot\frac{1}{4}H_2O$, respectively. Four such formula units per cell are required in each case to obtain the calcu-

Table 2. Comparison of Some Chemical and Physical Properties of Three Ammonium Pentaborates

	Synthetic[1]	Ammonioborite[2]	Larderellite[3]
Chemical composition			
Oxide form	$(NH_4)_2O\cdot5B_2O_3\cdot8H_2O$	$(NH_4)_2O\cdot5B_2O_3\cdot5\frac{1}{3}H_2O$	$(NH_4)_2O\cdot5B_2O_3\cdot4H_2O$
Reduced form	$NH_4B_5O_8\cdot4H_2O$	$NH_4B_5O_8\cdot2\frac{2}{3}H_2O$	$NH_4B_5O_8\cdot2H_2O$
Structural form[4]	$NH_4B_5O_6(OH)_4\cdot2H_2O$	$NH_4B_5O_6(OH)_4\cdot\frac{2}{3}H_2O$	$NH_4B_5O_6(OH)_4$
Symmetry	Orthorhombic	Monoclinic	Monoclinic
a	11.324 ± 0.002 Å	25.27 ± 0.05 Å	11.63 ± 0.03 Å
b	11.029 ± 0.001	$9.65_1\pm0.03$	$7.61_5\pm0.02$
c	9.235 ± 0.004	11.56 ± 0.03	$9.44_7\pm0.03$
β	—	$94°17.5'\pm05'$	$96°45'\pm10'$
Space Group	$Aba2$	$C2/c$ (or Cc)	$P2_1/a$
Cell Contents	$4[NH_4B_5O_6(OH)_4\cdot2H_2O]$	$12[NH_4B_5O_6(OH)_4\cdot\frac{2}{3}H_2O]$	$4[NH_4B_5O_6(OH)_4]$
Volume	$1153\cdot_4$ Å^3	2811 Å^3	830.8 Å^3
Density (calc.)	1.567 g. cm.$^{-3}$	1.758 g. cm.$^{-3}$	1.887 g. cm.$^{-3}$
(obs.)	$1.56_7\pm0.005$	1.765 ± 0.004	1.905 ± 0.004
Volume per oxygen atom	24.0 Å^3	22.0 Å^3	20.8 Å^3

[1] Data from Clark and Christ (1959) except cell constants; these from Cook and Jaffe (1957).
[2] Data from Clark and Christ (1959).
[3] Data of present study.
[4] Proposed by Christ (1960).

TABLE 3. X-RAY POWDER DATA FOR LARDERELLITE, $NH_4B_5O_6(OH)_4$

Monoclinic $P2_1/a$: $a=11.63\pm0.03$, $b=7.61_5\pm0.02$, $c=9.44_7\pm0.03$ Å; $\beta=96°45'\pm10'$

Measured				Calculated[1]	
Marinelli (1959)[2]		Clark and Christ (1959)[3]		Present Study	
I	d_{hkl}	I	d_{hkl}	d_{hkl}	hkl
		50	9.4_5	9.38	001
				6.36	110
39	5.95[4]	18	5.91	5.913	011
17	5.83	25	5.79	5.775	200
48	5.61[4]				
49	5.45	71	5.44	5.429	$\bar{1}11$
				5.198	$\bar{2}01$
34	5.14	50	5.12	5.112	111
77	4.72	100	4.70	4.691	002
				4.679	201
		18	4.60	4.601	210
18	4.31	25	4.30	4.293	$\bar{2}11$
24	4.00	25	3.99	3.994	012
				3.986	211
		4	3.88	3.897	$\bar{1}12$
				3.871	$\bar{2}02$
15	3.82	18	3.81	3.808	020
24	3.68	18	3.66	3.663	112
				3.616	120
32	3.53[4]	4	3.53	3.528	021
15	3.47	12	3.45	3.450	$\bar{2}12$
				3.448	202
				3.436	310
		12	3.42	3.417	$\bar{1}21$
43	3.37[4]	12	3.34	3.341	$\bar{3}11$
				3.333	121
15	3.30[4]				
22	3.185[5]				
				3.179	220
22	3.14	35	3.14	3.141	212
				3.127	003
				3.122	311
				3.072	$\bar{2}21$

---

[1] All calculated spacings listed for $d\geq 2.300$ Å.

[2] X-ray diffractometer data, CuKα radiation.

[3] Correction for film shrinkage negligible. Camera diameter, 114.59 mm; radiation, Cu/Ni, λ CuKα=1.5418 Å. Lower limit of 2θ measurable, approximately 7° (13 Å). Film no. 11101.

[4] Corresponds to a strong or moderately strong line on the x-ray pattern for $KB_5O_6(OH)_4\cdot 2H_2O$ (Clark and Christ, 1959; see Table 4, this paper).

(Continued on next page)

TABLE 3 (*continued*)

Measured				Calculated[1]	
Marinelli (1959)[2]		Clark and Christ (1959)[3]		Present Study	
I	d_{hkl}	I	d_{hkl}	d_{hkl}	hkl
69	2.97	71	2.960	2.956	022
				2.953	221
100	2.92	100	2.921	2.922	$\bar{3}12$
				2.916	$\bar{1}22$
		100	2.887	2.896	$\bar{2}03$
				2.893	013
				2.888	400
				2.881	$\bar{1}13$
				2.856	$\bar{4}01$
24	2.822	25	2.816	2.814	122
13	2.780[4]				
				2.737	113
21	2.723	35	2.713	2.714	$\bar{2}22$
				2.707	320, $\bar{2}1$
				2.700	400
				2.674	$\bar{4}11$
				2.673	401
10	2.675	12	2.663	2.660	$\bar{3}21$
				2.643	312
12	2.637	18	2.623	2.624	203
				2.599	$\bar{4}02$
				2.556	222
10	2.527[4]	6	2.545	2.546	321
				2.522	411
8	2.488	6	2.476	2.481	213
				2.479	130
				2.460	$\bar{4}12$
		6	2.444	2.450	031
				2.444	$\bar{3}13$
				2.433	$\bar{3}22$
12	2.423	9	2.416	2.417	023
				2.412	$\bar{1}31$
				2.410	$\bar{1}23$
10	2.383			2.382	131
21	2.372[4]				
				2.345	004
				2.339	402
		18	2.325	2.324	230
				2.323	123
				2.305	$\bar{2}23$
				2.301	420

TABLE 3 (*continued*)

Measured				Calculated[1]	
Marinelli (1959)[2]		Clark and Christ (1959)[3]		Present Study	
I	d_{hkl}	I	d_{hkl}	d_{hkl}	*hkl*
12	2.270[4,5]				
15	2.253	12	2.257		
		4	2.206		
15	2.186[4]				
29	2.159	25	2.156		
		4	2.138		
11	2.125[5]	4	2.124		
		6	2.094		
24	2.043	35	2.041		
18	2.016	12	2.013		
13	1.995	12	1.989		
6	1.967[6]				
8	1.947	8	1.937		
7	1.920	8	1.923		
16	1.890	25	1.887		
20	1.879	25	1.882		
11	1.854	4	1.855		
		4	1.818		
		2	1.790		
7	1.776	4	1.775		
		2	1.764		
		2	1.730		
6	1.711	4	1.710		
		4	1.683		
		4	1.669		
		4	1.623		
		4	1.615		
		4	1.578		
		4	1.561		
		4	1.536		
		4	1.501		
		4	1.482		
		plus additional weak lines			

---

[5] Corresponds to a strong or moderately strong line on the *X*-ray pattern for sassolite.

[6] Indexes as larderellite $\bar{1}51$; $d_{\bar{1}51} = 1.969$ Å (calc.)

lated densities given above. Symmetry requirements of space group $P2_1/a$ can then be invoked to rule out the second formula, since for $4[NH_4B_5O_6(OH)_4 \cdot \frac{1}{4}H_2O]$ per cell, the total number of oxygen atoms in the cell is 41, whereas the space group contains only general fourfold and special twofold positions, making mandatory an even number of each kind of atom in the cell. On the basis of all available evidence, therefore, the most probable chemical formula for larderellite is $(NH_4)_2B_{10}O_{16} \cdot 4H_2O$, and the most probable structural formula, $NH_4B_5O_6(OH)_4$. A comparison of some of the chemical and physical properties of the three ammonium pentaborates, larderellite, ammonioborite, and synthetic $NH_4B_5O_6(OH)_4 \cdot 2H_2O$, is given in Table 2.

The observed *d*-spacings given by Clark and Christ (1959) for the *x*-ray powder data of larderellite are in excellent agreement with the *d*-spacings calculated from the single-crystal cell constants as shown in Table 3. Intensities of single-crystal reflections conform qualitatively with intensities of corresponding powder lines. All calculated *d*-spacings greater than 2.300 Å are listed in Table 3, together with the observed data found by Clark and Christ (1959), and the diffractometer data reported by Marinelli (1959). Marinelli identifies two sassolite lines

TABLE 4. COMPARISON OF SOME OBSERVED *X*-RAY DIFFRACTOMETER DATA FOR IMPURE LARDERELLITE SAMPLE WITH OBSERVED *X*-RAY POWDER CAMERA DATA FOR $KB_5O_6(OH)_4 \cdot 2H_2O$

Impure Larderellite Sample Marinelli (1959)[1]		$KB_5O_8 \cdot 4H_2O$ Clark and Christ (1959)[2]	
I	d_{hkl} (Å)	d_{hkl} (Å)	I
39	5.95[3]	5.93	15
48	5.61	5.60	71
32	3.53[3]	3.52	84
43	3.37[3]	3.36	100
15	3.30	3.28	18
13	2.780	2.767	50
10	2.527	2.517	12
21	2.372	2.375	9
12	2.270[4]	2.290	9
15	2.186	2.181	21

[1] Selected portion of data (see Table 3 for complete listing); *x*-ray diffractometer, CuKα radiation.

[2] Selected portion of data, all observed lines with I≥9; camera diameter 114.59 mm., radiation Cu/Ni, λ CuKα = 1.5418 Å, measurements not corrected for film shrinkage.

[3] Larderellite observed line occurs here also.

[4] Sassolite observed line occurs here also.

among his observed *d*-spacings. In addition he records appearance of a line at 5.61 Å which he cannot account for, suggesting that it may be a line due to ammonioborite, data for which were not then available to him. Comparison of his data with the calculated *d*-spacings for larderellite (Table 3) shows that the material in his sample gives additionally not only several sassolite lines and the unidentified 5.61 Å line, but also a series of lines clearly due neither to sassolite nor to ammonioborite. These observed lines are listed in Table 4 and compared with the observed *d*-spacings associated with lines of strong intensity of $KB_5O_6(OH)_4 \cdot 2H_2O$ ($KB_5O_8 \cdot 4H_2O$, Clark and Christ, 1959). The matching of these two sets of observed *d*-spacings is preliminary evidence for the appearance of $KB_5O_6(OH)_4 \cdot 2H_2O$ in nature; confirming chemical tests would be of interest.

REFERENCES

CHRIST, C. L. (1960), Crystal chemistry and systematic classification of hydrated borate minerals: *Am. Mineral.* **45,** 334–340.

CLARK, JOAN R. AND CHRIST, C. L. (1959), Studies of borate minerals (VII): *X*-ray studies of ammonioborite, larderellite, and the potassium and ammonium pentaborate tetrahydrates: *Am. Mineral.* **44,** 1150–1158.

COOK, W. R., JR. AND JAFFE, HANS (1957), The crystallographic, elastic and piezoelectric properties of ammonium pentaborate and potassium pentaborate: *Acta Cryst.* **10,** 705–707.

MARINELLI, GIORGIO (1959), Richerche sulla larderellite: *Atti Soc. Tosc. Sc. Nat.* (*Series A*) **66,** 257–272.

PALACHE, C., BERMAN, H., AND FRONDEL, C. (1951). The System of Mineralogy, 7th ed. Vol. II (p. 365–366). New York: John Wiley and Sons, Inc.

ZACHARIASEN, W. H. (1938), The crystal structure of potassium acid dihydronium pentaborate $KH_2(H_2O)_2B_5O_{10}$ (potassium pentaborate tetrahydrate): *Zeitschr. Krist* **98,** 266–274.

THE AMERICAN MINERALOGIST, VOL. 45, SEPTEMBER-OCTOBER, 1960

THE CRYSTAL STRUCTURE OF POTARITE (PdHg) WITH SOME COMMENTS ON ALLOPALLADIUM

K. TERADA AND F. WM. CAGLE, JR.
University of Utah, Salt Lake City 12, Utah.

Potarite is a palladium amalgam which occurs in the Potaro river region of British Guiana (Palache, Berman, and Frondel 1944). It was first described by Harrison and Bourne (1924–5) and more fully characterized by Spencer (1928). Spencer further surveyed the known synthetic palladium amalgams and suggested that potarite might be identical with allopalladium. Cissarz (1930) reexamined simultaneously samples of potarite and allopalladium and found them to be different substances. He described potarite as an isomorphous ground mass with small, irregular, anisotropic inclusions.

M. A. Peacock (1945) examined a sample of potarite by the *x*-ray powder method and reported that it gave a simple cubic pattern with $a_0=5.21$ Å with a unit of cell Pd_4Hg_4. This gave a calculated density of 14.48 g./ml. compared with Spencer's value of 14.88 g./ml. Peacock further reported that attempts to directly synthesize the material had not been successful. He suggested that the structure might be that attributed to FeSi with a space group $P2_13$.

A powder photograph of a synthetic alloy PdHg obtained by Bittner and Nowotny (1952) indicated a face-centered cell $a_0=4.284$ Å, $c_0=3.692$ Å, containing Pd_2Hg_2. In our work we have indexed our patterns for the smaller body centered tetragonal cell $a_0=3.020_5$ Å, $c_0=3.706_7$ Å, cell content PdHg. The crystal structure is that of AuCu type $L1_0$. The space group is P 4/mmm. Trial-structure calculations with Hg at 0, 0, 0 and Pd at $\frac{1}{2}$, $\frac{1}{2}$, $\frac{1}{2}$ are in agreement with the observed line intensities.

EXPERIMENTAL

Samples of PdHg which are identical with the mineral potarite may be prepared either by displacement of palladium from $Pd(NO_3)_2$ solution by mercury or by direct synthesis from powdered palladium and mercury in sealed evacuated tubes. The samples used by Bittner and Nowotny were prepared by direct synthesis from the elements. The compound PdHg can be easily prepared by heating the elements in a sealed Pyrex tube for twelve hours at 400° C. Compositions high in mercury should be annealed for a considerable time at 100° C. to insure uniformity of product. A mixture of palladium powder and mercury in equimolar amounts, which is kept at room temperature, does not show formation of potarite at an appreciable rate. In fact, it has long been known that the rate of penetration of palladium by mercury at low temperatures is slight (Horsford, 1852). A meta-stable system containing an alloy higher in mercury than PdHg and unreacted palladium are found by *x*-ray examination of this system. However, if the system is heated for 4 hours at 200° C., the *x*-ray powder pattern is that of PdHg.

A table showing the observed inter-planar spacings for a natural sample of potarite and for synthetic PdHg prepared from solution and from direct combination of the elements is given. The data given in Table I have been corrected for absorption and beam divergence using the method outlined by Azaroff and Buerger (1958). This method has been programed for use with the Datatron 205 electronic digital computer, and so may be rapidly and easily applied. Patterns were ob-

TABLE I. MEASURED AND CALCULATED SPACINGS OF PdHg.

hkl	*d*(soln)	*d*(direct combination)	*d*(potarite-annealed)	*d*(calculated)
001				3.707
100	3.032	3.029	3.033	3.020
101	2.346	2.343	2.342	2.342
110	2.143	2.141	2.142	2.136
002				1.853
111	1.847	1.850	1.846	1.850
102				1.580
200	1.516	1.509	1.515	1.510
112				1.400
201	1.397	1.399	1.398	1.399
210		1.354		1.351
211	1.273	1.272	1.272	1.269
003				1.236
202	1.170	1.170	1.171	1.171
103	1.139	1.141	1.141	1.144
212				1.092
113				1.069
220	1.071	1.072		1.068
221	1.027			1.026
300				1.007
301	$.973_7$	$.973_5$	$.973_2$	$.971_6$
203				$.956_3$
310	$.957_9$	$.956_5$	$.956_5$	$.955_2$
004				$.926_7$
222	$.926_6$	$.926_0$	$.925_9$	$.925_3$
311				$.925_0$
213	$.910_2$	$.911_5$	$.910_7$	$.911_7$
104				$.885_9$
302				$.884_7$
114				$.850_1$
312	$.850_0$	$.850_2$	$.850_0$	$.849_0$
320				$.837_7$
321	$.819_2$	$.818_7$	$.818_3$	$.817_1$
223				$.807_9$
204	$.789_4$	$.789_0$		$.789_8$
303		$.780_8$	$.780_3$	$.780_5$

The blank spaces in the table represent "d" distances for faint lines which have been observed in pure PdHg patterns exposed under ideal conditions. The last column of interplanar distances were calculated from our $a_0=3.020_5$ Å and $c_0=3.706_7$ Å. By the method of least squares, a_0 and c_0 were recalculated as 3.026Å and 3.072Å respectively.

tained using CuK$_\alpha$ radiation $\lambda(K_{\alpha 1})=1.5405$ Å, $\lambda(K_{\alpha 2})=1.5443$ Å, $\lambda(K_\alpha$ weighted average$)=1.5418$ Å.

It is interesting to note that the potarite sample obtained from the

Table II. Tetragonal and Cubic Indexing of PdHg Powder Photograph

Tetragonal Index	d(observed)	d(calculated with Peacock $a=5.21$)	Cubic Index
100	3.03	3.01	111
101	2.34	2.33	210
110	2.14	2.13	211
111 002	1.85	1.84	220
200	1.51	1.50	222
201	1.40	1.39	321

U. S. National Museum gave broad diffraction lines and thus was quite imperfectly crystalline. This sample was then annealed while still sealed in a Lindemann capillary. Upon heating at 100° C. for 6 hours it recrystallized and sharp diffraction lines were obtained. It is thus apparent that the mineral has not been subjected to elevated temperatures. The sample which Professor Peacock had examined showed normal line breadth and so we may assume that different degrees of crystalline perfection exist in naturally occurring potarite.

It is interesting to compare the indexing assigned by Professor Peacock with that for the tetragonal cell. This is shown in Table II. We have reexamined Professor Peacock's films and find that lines which cannot be explained by his cell may be observed though they are extremely weak. This of course, illustrates the intrinsic danger always present in the interpretation of a powder pattern containing only a few lines.

It would seem that the poorly crystalline mineral appears to be isotropic on microscopic examination and that small islands of crystalline material comprise the "inclusions." The poorly crystalline nature is in accord with an experimental specific gravity of 14.88, rather lower than the theoretical calculated x-ray value 15.09.

Synthetic samples containing less than 15 atomic per cent mercury show a solid solution of mercury in the palladium lattice. This is in accord with the observation of Berzelius (1813) that it is very difficult to remove the last traces of mercury from palladium amalgam. In the mercury rich region, two diffraction patterns have been obtained. These are substances of very low symmetry judged from the complexity of the x-ray patterns.

Allopalladium

Attempts to obtain a sample of allopalladium have been unsuccessful. However, no hexagonal phase of the system PdHg has been found in the range Pd to $PdHg_7$. Thus we must conclude that the hexagonal mineral described by Zincken (1829), Cissarz (1930), and Schneiderhöhn and Ramdohr (1931) is almost certainly not a simple palladium amalgam.

ACKNOWLEDGMENTS

The authors wish to thank Mr. E. P. Henderson of the U. S. National Museum who kindly provided a sample of potarite from the original material found by Sir John Harrison, and Drs. William F. Slawson and E. W. Nuffield of the University of Toronto who sent a sample of the material used by Professor Peacock. We are also indebted to Dr. Bronson Stringham of the University of Utah for many discussions and helpful suggestions as well as Professor Max P. Erickson who made an optical examination of a specimen of potarite. Mr. J. F. Rice and Miss Dee Morgan of the Computer Center at the University of Utah have aided us in our computational work.

REFERENCES

1. Azaroff, L. V., and Buerger, M. J. (1958), The Powder Method in X-Ray Crystallography: New York, 234–235.
2. Berzelius, J. J. (1813), *Kongl. Vetensk. Acad. Handl. Stockholm*, **33**, 175–215.
3. Bittner, H. and Nowotny, H. (1952), *Monatsh Chem.*, **83**, 287–289.
4. Cissarz, A. (1930), *Zeit. Kr.*, **74**, 501–510.
5. Harrison, J. B. (1924), *Official Gazette of British Guiana*, **57**, 212–213.
6. Harrison, J. B. and Bourne, C. L. C. (1925), *Official Gazette of British Guiana*, **59**, 66–68.
7. Horsford, E. N. (1852), *Am. J. Sci.* 2, **13**, 305–318.
8. Palache, C., Berman, H., and Frondel, C. (1944), The System of Mineralogy of James Dwight Dana and Edward Salisbury Dana, Yale University 1837–1892, Vol. I, Seventh Edition, New York, 105.
9. Peacock, M. A. (1945), University of Toronto Studies, *Geol. Ser.*, **49**, 71–73.
10. Schneiderhöhn, H. and Ramdohr, P. (1931), Lehrbuch der Erzmikroskopie, Vol. 2, Berlin, 50.
11. Spencer, L. J. (1928), *Min. Mag.*, **21**, 397–406.
12. Zincken, C. (1829), *Ann. Phys. Chem.* (Poggendorff) **16**, 491–495.

THE AMERICAN MINERALOGIST, VOL. 45, SEPTEMBER-OCTOBER, 1960

A NOTE ON SO-CALLED "PRESSURE INDEPENDENT" MINERALS

Carl W. F. T. Pistorius, *National Physical Research Laboratory, Council for Scientific and Industrial Research, Pretoria, Union of South Africa.*

In a recent note on the stability and synthesis of uvarovite, $3CaO \cdot Cr_2O_3 \cdot 3SiO_2$, Glasser (1959) objected to a statement by Hall (1958) which tended to give the impression that uvarovite, like diamond, is stable only at pressures of the order of 20,000 to 35,000 bars. Glasser then went on to state: "Uvarovite—and several other members of the garnet series mentioned *by Hall* are 'pressure independent' minerals, inasmuch as they also have a thermodynamic stability range at 1 atm. pressure. Hall was apparently unaware of the work of Hummel," (1950) who succeeded in preparing uvarovite at 1 atm. pressure and between 885° and 1400° C.

It should be pointed out, however, that the term "pressure independent mineral" is highly misleading in this context, since it implies that the stability field of such a mineral is actually independent of pressure, something which can only be the case when the phase boundary delineating the stability field of such a mineral in the P-T plane—in the case of uvarovite the phase boundary expressed by

$$3CaSiO_3 + Cr_2O_3 \rightleftharpoons Ca_3Cr_2Si_3O_{12}$$

is a straight line parallel to the pressure axis, *i.e.* with dP/dT infinite. The requirement for this to happen is that ΔV for the reaction be zero, while ΔS be unequal to zero. This is certainly not true for the above reaction, and is, in fact, an extremely rare occurrence for reactions such as the one above or ordinary first-order transitions. Actually, the phase boundary under discussion may be expected to intersect the T-axis at 1370° ± 10° C. (4) and to have a positive slope in the P-T plane, since the garnet is the denser assemblage.

As any geologist knows, geological nomenclature abounds with misnomers, and it would be unfortunate if another is unnecessarily added. One certainly is not justified in ascribing the term "pressure independent" to a mineral merely because it has a thermodynamic stability range at 1 atmosphere.

It is hoped that these remarks will in no way detract from the main point of Glasser's note, with which the present author is completely in agreement.

References

1. Glasser, F. P. (1959), On the stability and synthesis of uvarovite, $Ca_3Cr_2Si_3O_{12}$, *Am. Mineral.*, **44,** 1301–1303.
2. Hall, H. T. (1958), Ultrahigh Pressure Research, *Science*, **128,** (3322), 445–449.
3. Hummel, F. A. (1950), Synthesis of uvarovite, *Am. Mineral.*, **35,** 324–325.
4. Glasser, F. P., and Osborn, E. F. (1958), Phase Equilibrium Studies in the System $CaO—Cr_2O_3—SiO_2$, *Jour. Amer. Ceramic Soc.*, **41** (9), 358–367.

THE AMERICAN MINERALOGIST, VOL. 45, SEPTEMBER–OCTOBER, 1960

PREPARATION AND USE OF A GELATIN MOUNTING MEDIUM FOR REPEATED OIL IMMERSION OF MINERALS

Gordon W. Olcott, *University of Oregon, Eugene, Oregon.**

Presently there is very little information in geologic literature about an inexpensive, easily prepared, isotropic mounting medium that will withstand solvents necessary to wash identifying index oils from microscope slides, thereby allowing the same mineral grains to be repeatedly used until identified. Only two references on the subject were found in the geologic literature. These were papers by Herbert (1942), who used gum tragacanth and Canada balsam to mount detrital mineral grains for demonstration purposes; and by Fairbairn (1943), who refined the original use of gelatin coated lantern slides for refractive index immersion work (Vedeneeva and Melancholin, 1932) by having gelatin coated petrographic slides prepared commercially.

A very satisfactory solution to the problem, both from the standpoint of expense and ease of preparation and use, was found in an article by Marshall and Jeffries (1945). These agronomists modified Fairbairn's mount by decreasing the gelatin concentration. This was necessary to prevent the very small mineral grains of the soil separates, with which they were working, from being engulfed and blanketing the optical effects produced by changing index oils. Their prime contribution to oil immersion technique is publication of the formula of the mount. These "home-made" slides have proven to be every bit as good as the commercial variety, and may easily be made at a fraction of the cost.

Materials Used

The required materials are household gelatin, formalin, acetone and distilled water. Marshall and Jeffries' formula, with the exception of an increase in gelatin concentration, is:

Solution A—	Gelatin	1%
Solution B—	Distilled water	10 cc.
	Acetone	5 cc.
	2% Formalin	2 cc.

Marshall and Jeffries used but 0.1%, but the writer found that a concentration of 1% gelatin was preferable for heavy mineral study.

---

* Present address: Southern Pacific Company, Land Department, San Francisco 5, California.

PREPARATION OF SOLUTIONS

Solution A: Mix the gelatin to a 1% concentration. This is one-fourth gram of gelatin dissolved in 50 cc. of distilled water. The concentration may be altered to accord with the size of the mineral fragments being identified. 1%, however, appears to be satisfactory for most work.

Solution B: Mix 10 cc. distilled water, 5 cc. acetone and 2 cc. of 2% formalin. This is the softening solution that allows the grains to embed themselves in the gelatin. The containing bottle should be well-corked to prevent evaporation.

When these solutions show signs of clouding, they should be replaced by fresh preparations. It was found that small bottles, used by petrology classes several days a week, remained potent about three weeks.

TECHNIQUE OF MOUNTING, USING, AND WASHING SLIDES

1. Spread a generous amount of Solution A on a clean glass slide. An eye dropper works well in applying the liquids. Dry on a hot plate at 75°–80° C. (167°–176° F.). Remove the slide. Besides being better able to control the spreading-on of the grains during the following steps, removal will keep the hot plate clean.

2. Apply two or more drops of Solution B on the dry gelatin and spread lightly. This is easily done with a paper clip. When this evaporates sufficiently so that the gelatin is tacky, sprinkle on the grains. Some semi-soluble minerals may be mounted by allowing the gelatin to become very tacky before applying the grains. Again dry the slide on the hot plate. Remove, cool, apply a suitable refractive index oil and cap with a cover glass. The slide is now ready for petrographic examination. The entire procedure requires about five minutes.

3. Use acetone or carbon tetrachloride to wash oils from the slides. Xylene has too slow an evaporation rate to be used. It is convenient to hold the slide in an inclined position in a small beaker and pour the solvent over it by means of a wash bottle.

PERFORMANCE

That the mount has good holding qualities is demonstrated by the fact that only four grains were detached when an experimental slide, containing approximately 500 grains, was successively subjected to a wide range of index oils in current use and then washed with both acetone and carbon tetrachloride. This mount, however, is generally unsatisfactory for permanent slides. Very careful handling and storage is required, for the grains will rub off if sufficient pressure is exerted.

The main use for this mount is in the rapid identification of mineral fragments. Where great effort and time was formerly consumed in getting a platy mineral particle to stand edge-wise by means of broken pieces of cover glass—only to have the index oil float the particle away—the mineral may now be crushed and sprinkled over the tacky mount. A quick examination of the slide will usually reveal the orientation desired.

The gelatin is neutral to all the immersion oils in current use. However, the mount cannot be used with crystals easily soluble in water or with an immersion media having water as a component. The thin coating allows a ready determination of the Becke line and oblique illumination tests. The mount may be used to good advantage with the universal stage.

References

Fairbairn, H. W., 1943, Gelatin coated slides for refractive index immersion mounts: *Am. Mineral.*, **28**, 396–397.

Herbert, Paul, Jr., 1942, Petrographic microscope slides of detrital mineral grains: *Jour. Sed. Petrology*, **12**, 90–91.

Marshall, C. E., and Jeffries, C. D., 1945, Mineralogical methods in soil research: The correlation of soil types and parent materials, with supplementary information on weathering processes. C. Gelatin slide method for mounting soil separates for microscopic study: *Soil Science Soc. Amer. Proc.*, **10**, 397–405.

Vedeneeva, N., and Melancholin, N., 1932, The theodolite immersion method, etc.: *Trans. Sci. Invest. Inst. Industry, No. 503. Inst. App. Miner., Paper* **54** (Russian and English).

THE AMERICAN MINERALOGIST, VOL. 45, SEPTEMBER-OCTOBER, 1960

DEHYDRATION STUDIES BY INFRARED SPECTROSCOPY

J. M. Serratosa, *Instituto de Edafologia, C.S.I.C., Madrid, Spain.*[1]

While studying the orientation of OH bond axes in layer silicates (Serratosa & Bradley, 1958) by their absorption in the O-H stretching frequency range (≈ 3700 cm.$^{-1}$) some concern was felt because no flexion frequency was certainly correlated with the stretching feature which was utilized. The proper allocation of a band to this expected mode is now arrived at by following the course of dehydration of a montmorillonite from Tidinit, Morocco, and a nontronite from Utah, each previously characterized by *x*-ray diffraction.

Samples of each were dispersed, and $<1\ \mu$ fractions were permitted to evaporate on plastic slides. Dried films were then peeled off for examination.

---

[1] Experimental work conducted while on leave at the Illinois State Geological Survey, Urbana, Illinois.

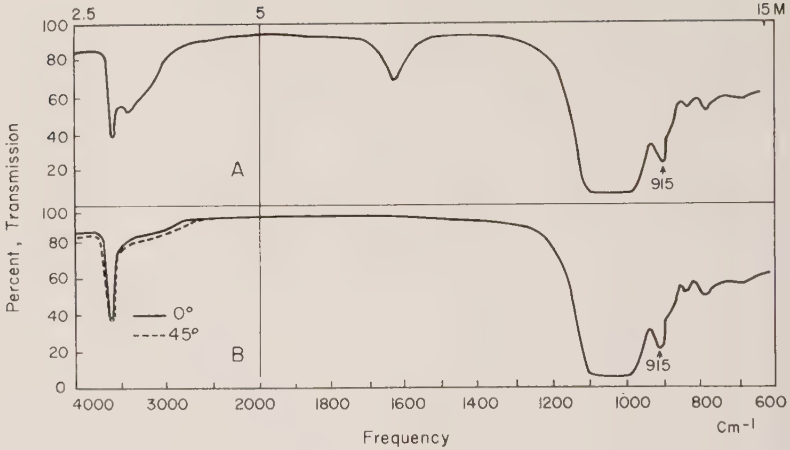

FIG. 1. Infrared spectra of Tidinit montmorillonites: (A) Air dried. (B) Dried at 200° C., and for two incidence angles. The bands from the Nujol have not been included.

Figures 1 and 2 present the absorption spectra of the samples, ai dried, and after drying at 200° C. The heated films were covered wit Nujol to minimize rehydration from the atmosphere. In each case heating dispelled the water absorption bands at 3400, 3240 and 1640 cm.$^{-1}$ but the structural OH stretching frequency between 3600 and 370 cm.$^{-1}$ persisted and was not markedly influenced by change of the angle of incidence of radiation to the clay film (characteristic of dioctahedral composition).

The greatest lower-frequency difference between the two minerals

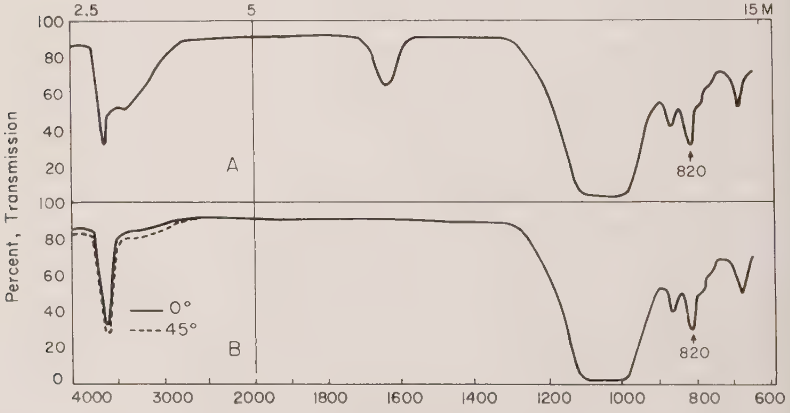

FIG. 2. Infrared spectra of nontronite: (A) Air dried. (B) Dried at 200° C. and for tw incidence angles. The bands from the Nujol have not been included.

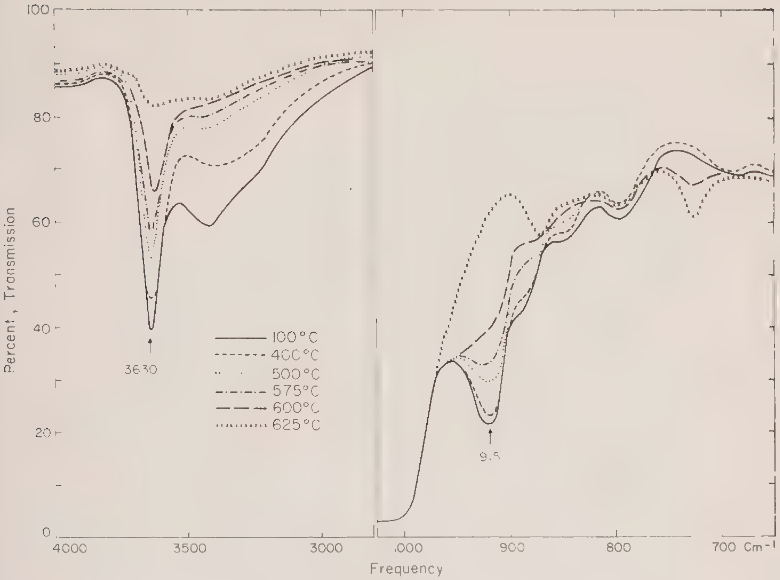

FIG. 3. Infrared spectra of Tidinit montmorillonite heated at increasing temperatures.

was an absorption feature appearing at 915 cm.$^{-1}$ for the Tidinit montmorillonite, but at 820 cm.$^{-1}$ for the nontronite.

In Figs. 3 and 4 are superposed absorption records following heating at successively increasing temperatures. The 915 cm.$^{-1}$ at 820 cm.$^{-1}$ bands decrease in intensity at rates concomitant with those of the stretching frequency in each case, even though practical dehydration of the montmorillonite requires heating to nearly 600° C., but that of the nontronite only to about 425° C.

Although any lowering of the frequency of the stretching vibration by heavier octahedral ion neighbors was within the limits of precision of the frequency measurements in the previous study, the effect of heavier octahedral neighbors on the OH flexion frequency is pronounced.

In these layer structures dioctahedral compositions provide each structural OH with two octahedral ion neighbors, and in the case of the nontronite, it is even possible to speculate that the doubtful feature at about 860 cm.$^{-1}$, which loses intensity less rapidly than the 820 cm.$^{-1}$ feature, represents hydroxyls which have one Fe and one Al or Mg neighbor.

This same allocation of bands at 910 and 938 cm.$^{-1}$ in kaolinite and at 820 cm.$^{-1}$ in nontronite to H-O · · · Al^{+3} and H-O · · · Fe^{+3} respectively has now been authenticated by Stubican and Roy (1960) on the basis

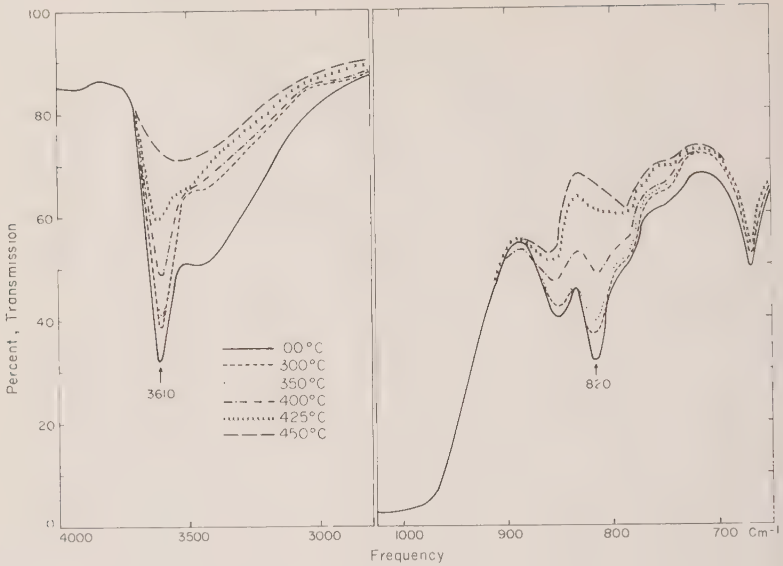

FIG. 4. Infrared spectra of nontronite heated at increasing temperatures.

of comparisons of spectra for these minerals with those of their deuterated synthetic analogues.

REFERENCES

SERRATOSA, J. M. AND BRADLEY, W. F. (1958). Determination of the orientation of OH bond axes in layer silicates by infrared absorption. *J. Phys. Chem.* **62,** 1164–67.

STUBICAN, V. AND ROY, R. (1960). Influence of controlled ionic substitution on the infrared absorption spectra of synthetic clay minerals. Abstracts of Cleveland Meeting of the American Chemical Society, April 1960.

THE AMERICAN MINERALOGIST, VOL. 45, SEPTEMBER-OCTOBER, 1960

X-RAY DIFFRACTION TECHNIQUE FOR SMALL SAMPLES

RONALD K. SOREM, *Department of Geology, Washington State University, Pullman, Washington.*

In work with the *x*-ray powder camera, little difficulty is found in preparing suitable powder mounts from samples weighing several milligrams, but when samples of a much smaller size are used, suitable mounts are not easy to prepare using ordinary techniques. Consider, for example, a few particles perhaps less than 10 microns in size scratched from a mineral grain. A sample of this kind may be required if a pure monomineralic sample is sought. These particles are commonly adequate for producing a good diffraction film, but addition of a mounting medium like gum tragacanth or shellac to so small a sample may result in amorphous scattering which will all but obliterate the mineral pattern. Another problem that may arise is partial loss of the already extremely small sample during mixture with the mounting medium. Capillary tubes are far too large for the samples in question. Although special x-ray cameras may provide means of eliminating these problems, ordinary equipment will yield good results when special mounting techniques are used and certain minor adjustments are made. The methods require no special training and cost no more than ordinary methods.

An ideal way to obtain the powdered sample is to scratch the mineral grain to be sampled, whether in hand specimen or in a polished or thin section, with a sharp diamond point. Either a standard diamond "pencil" or a mounted phonograph stylus can be used. The former is cheaper (about $2.50) and works well, provided that the point is not badly chipped by rough usage, as in writing on glass slides. The stylus, when mounted in a pin vise, is more convenient, however, where sampling is to be done while observing the specimen with a microscope. The point is small and the staff on which it is held can (in some models) be bent so that little clearance is needed above the specimen (Fig. 1). The chief disadvantage other than cost (about $5.00) is that the stylus point is well machined and smooth, and it must be chipped or bevelled in some way before it will bite the sample surface properly. This bevelling can be done by carefully touching the point to a fine grinding wheel, such as the kind used on hand-held power grinding tools.

The sample mount used is a very thin wedge-like gelatin fiber. Three features make gelatin ideal for this purpose. First, a very fine point can be obtained; second, the gelatin is self-adhesive when wet, hence no cement or shellac is needed to bind the sample to it; and third, the gelatin itself produces no amorphous scattering or at worst a very minor amount. Fibers are prepared in advance in the manner shown in Fig. 2, and a supply is kept on hand. The procedure, briefly, is to soften an ordinary gelatin drug capsule by humidification (a closed plastic box containing a wet cotton wad works well), slice off the closed end with a razor blade, and then slit one side of the resulting cylinder. When straightened, the cylinder provides a thin gelatin plate about 1×2 cm. in size. This plate is fastened to a microscope slide with tape and slit in the short dimension by close-spaced razor cuts to yield the fibers. Fibers cut in this orientation show but little tendency to curl when later subjected to changes in relative humidity. The fibers are removed and stored, after air-drying for several hours, in a small closed vial.

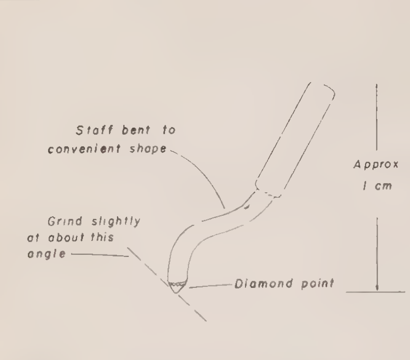
Staff bent to convenient shape
Grind slightly at about this angle
Diamond point
Approx 1 cm

FIGURE 1. Stylus modification for sampling point.

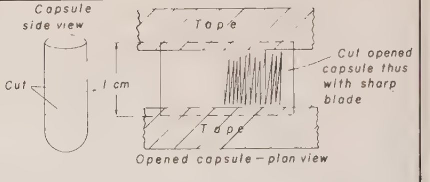
Capsule side view
Cut
1 cm
Tape
Cut opened capsule thus with sharp blade
Tape
Opened capsule — plan view

FIGURE 2. Method of cutting gelatin capsule.

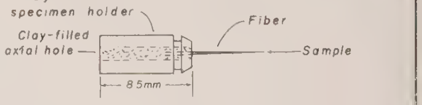

FIGURE 3. Fiber ready for use.

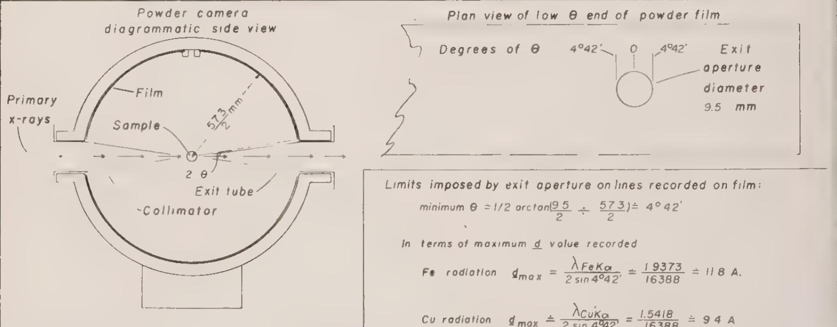
Powder camera diagrammatic side view
Primary x-rays
Film
Sample
57.3 mm / 2
2 θ
Exit tube
Collimator
Plan view of low θ end of powder film
Degrees of θ
4°42′
0
4°42′
Exit aperture diameter 9.5 mm

Limits imposed by exit aperture on lines recorded on film:

$$\text{minimum } \theta = 1/2 \text{ arctan}\left(\frac{9.5}{2} \div \frac{57.3}{2}\right) \doteq 4°42'$$

In terms of maximum $\underline{d}$ value recorded

$$\text{Fe radiation} \quad d_{max} = \frac{\lambda_{FeK\alpha}}{2 \sin 4°42'} \doteq \frac{1.9373}{.16388} \doteq 11.8 \text{ A.}$$

$$\text{Cu radiation} \quad d_{max} \doteq \frac{\lambda_{CuK\alpha}}{2 \sin 4°42'} = \frac{1.5418}{.16388} \doteq 9.4 \text{ A}$$

FIGURE 4. Conventional camera set-up.

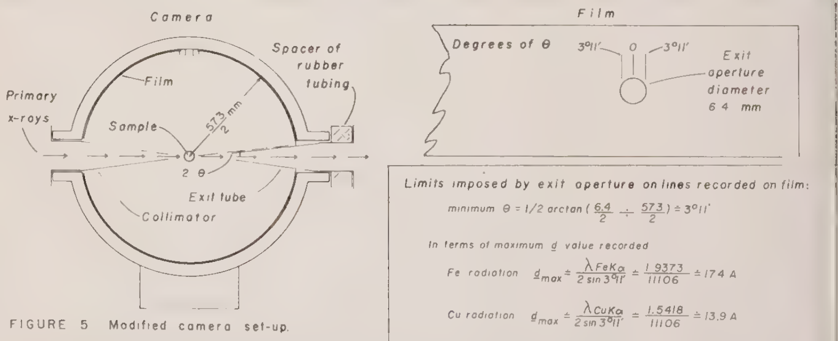

Limits imposed by exit aperture on lines recorded on film:

$$\text{minimum } \theta = 1/2 \text{ arctan}\left(\frac{6.4}{2} \div \frac{57.3}{2}\right) \doteq 3°11'$$

In terms of maximum $\underline{d}$ value recorded

$$\text{Fe radiation} \quad d_{max} \doteq \frac{\lambda_{FeK\alpha}}{2 \sin 3°11'} \doteq \frac{1.9373}{.11106} \doteq 17.4 \text{ A}$$

$$\text{Cu radiation} \quad d_{max} \doteq \frac{\lambda_{CuK\alpha}}{2 \sin 3°11'} \doteq \frac{1.5418}{.11106} \doteq 13.9 \text{ A}$$

FIGURE 5. Modified camera set-up.

When a fiber is selected for sample mounting, it should be examined with the binocular microscope. One that has a marked curvature should be rejected, for it may change shape if the relative humidity changes during the x-ray exposure, thus throwing the sample off center. The fiber to be used should have a sharp, narrow point; this may require additional trimming with a razor blade. This is a tedious job, but with practice the selection and preparation of a fiber takes only a few minutes.

The powdered sample, once obtained, is best left on the surface of the mineral grain temporarily. The next step is to affix the powder—all of it if possible—to the fiber. A vial of water (1 or 2 cc.) containing one or two drops of glycerine to retard evaporation should be at hand. With a clean sharpened toothpick, a drop of water about 1 mm. in diameter is placed on the specimen 1 or 2 mm. from the powder. Next, a gelatin fiber, the thick end mounted in a suitable holder (like the brass specimen holder of the x-ray camera) (Fig. 3) is carefully brought close to the drop (best done while viewing with binocular microscope). In rapid succession, the sharp tip of the fiber is touched to the periphery of the drop and then is touched to the mineral powder and rotated. The sample adheres to the fiber, and in a few seconds the mount is dry and ready for use. Care must be taken that the fiber is not left in contact with the water more than a fraction of a second, for an excess of water will cause the gelatin to expand unduly and the sharp point will be lost. The fiber is now transferred to the x-ray camera and centered and exposed like an ordinary sample. Only the extreme tip of the fiber, with sample intact, should be centered in the field of view of the collimator.

Several comments should be made regarding the x-ray procedure. North American Philips (Norelco) equipment was used in my work, but other brands could no doubt be used as well. A small camera is desirable, because exposure times for very small samples are commonly double those for larger ones, or even longer. In fact, some minute samples may not produce usable patterns in larger cameras regardless of exposure time because of poor contrast between diffraction lines and background fogging. The restriction to small cameras is of no disadvantage, generally, unless it is desired to explore the region below about 10° (2θ). Conventional small Debye-Scherrer cameras (57.3 mm. diameter) made by Norelco allow the recording of lines only as low as about $9°25'$ (2θ), and only above 12°–14° are intensities recorded accurately (Fig. 4). Several means of improving the range exist, however, and it is possible to extend the lower limit to values sufficiently small for most mineral work without great expense or inconvenience.

The general problem of recording reflections in the low θ region has been discussed in some detail by Parrish and Cisney (1948) and more recently by Martin Vivaldi, Girela Vilchez, and MacEwan (1959). Parrish and Cisney describe a special Norelco tube system (collimator and exit tube) which improves quality of the lines to the very edge of the standard 9 mm. film hole. A disadvantage of this system is that reflections at angles greater than 90° (2θ) are not recorded. Martin Vivaldi, *et al.*, describe two means of increasing the low θ range through the use of (a) "an extension tube for the beam catcher," or (b) an "auxiliary beam catcher" which fits inside the camera. These parts, which permit the recording of lines with spacings as great as 29 Å (small camera, Cu radiation), may also be obtained from the Philips Company, according to the authors.

Figure 5 shows a modified camera setup similar in concept to the extension tube method of Martin Vivaldi, *et al.* The modification was used in the Geology Department, University of Wisconsin, in 1957 and 1958, and involves the use of only one accessory, a spacer cut from rubber tubing. The spacer is made to permit the withdrawal of the exit tube to the point at which a film exit hole 6.4 mm. in diameter may be used (Fig. 5). Features of this modification are (a) that the exit tube still fits snugly in the camera and alignment is not disturbed, (b) that the spacer is removable instantly if not wanted, (c) that the hole required is the diameter of an ordinary paper punch, and (d) that the lower limit of the reflections recorded is reduced to about $6\frac{1}{2}^\circ$ (2θ). Corresponding maximum d values are 17.4 Å with Fe radiation and 13.9 Å with Cu radiation.

The combination of gelatin fiber mounts and a camera modification of the kind described permit the x-ray study of particularly small powder samples using essentially standard cameras. Furthermore, the regular use of the modified powder camera provides a constant check on the low θ region for all mineral samples that are commonly run in small cameras and at the same time produces films of particularly good quality. The savings in time and film by extending the use of the small camera are self-evident. It cannot be claimed, of course, that the larger camera is thus supplanted for most powder work, for large films still permit greater accuracy in measurements; but for routine work, modified small cameras should be useful to many investigators.

Acknowledgments

Thanks are due to Prof. S. W. Bailey, in whose laboratory the work was done which led to this paper and who called to my attention the publications cited. Prof. E. N. Cameron headed the project during which the x-ray work was done. Both of these men kindly read the first draft of this paper and made helpful suggestions.

References

Martin Vivaldi, J. L., Girela Vilchez, F., and MacEwan, D. M. C., (1959), Modifications to standard Philips powder cameras for clay mineral work. *Clay Minerals Bulletin* **4,** 110–112.

Parrish, W., and Cisney, E. (1948), An improved x ray diffraction camera. *Philips Technical Review,* **10,** 157–167.

THE AMERICAN MINERALOGIST, VOL. 45, SEPTEMBER-OCTOBER, 1960

A NATURAL OCCURRENCE OF NICKEL HYDROXIDE

K. L. Williams, *Mineragraphic Investigations, Commonwealth Scientific and Industrial Research Organization, University of Melbourne, Parkville, Victoria.*

During the examination of zaratite-bearing specimens from the Lord Brassey mine at Heazlewood, Tasmania (Williams, 1958), a minute amount of a pale greenish blue mineral was observed occurring in a finely banded intergrowth with zaratite on a shear plane in a specimen of serpentinite. This mineral was at first believed to be fine-grained zaratite or hellyerite (which occurs elsewhere in the same specimen), but microscopic and *x*-ray examinations proved it to consist of pure nickel hydroxide, a compound which does not appear to have been found previously in nature.

A complete examination of the mineral could not be made because of the paucity of material; the largest observed area of nickel hydroxide measured $3\times2\times0.7$ mm., and this contained inclusions of zaratite.

The mineral has a dull, earthy lustre and, by contrast with the glassy zaratite, it appears cloudy and rather opaque. It is soft, with an estimated scratch hardness of approximately 2, and it has a white streak.

Microscopically it was found to be transparent but very fine grained, with the aggregates varying from isotropic to weakly anisotropic. The fine grainsize prevented the determination of complete optical data, but the apparent refractive index was found, by immersion methods, to vary between 1.64 and 1.69; the best values were close to 1.68.

An *x*-ray powder diffraction photograph was found to match closely a diffraction photograph of synthetic (chemical reagent) nickel hydroxide, the only significant differences being that some of the lines in the pattern of the synthetic material were relatively diffuse (Table 1). This effect may be due to small crystallite size or poor crystallinity, or both.

Both diffraction patterns match that listed for nickel hydroxide in the American Society for Testing Materials' Index of *x*-ray Diffraction Data. They are both much sharper than the pattern of "anodic nickel hydroxide" figured by Klug and Alexander (1954, p. 385) and they show no evidence of a two-dimensional lattice.

The refractive index of the synthetic material was found to be slightly higher than that of the natural nickel hydroxide; it varied from 1.68 to 1.71, with the best values around 1.69. This difference may also stem from differences in grainsize or degree of crystallinity.

TABLE 1. NICKEL HYDROXIDE $Ni(OH)_2$-*X*-RAY POWDER PATTERN

1		2		3	
d (Å)	$I_{est.}$	d (Å)	$I_{est.}$	d (Å)	I/I_0
4.63	10	4.67b	10	4.60b	0.67
3.67	0.2				
2.71	6	2.72	6	2.70	1.00
2.34	10	2.34b	8	2.33b	0.67
1.757	8	1.75b	2	1.75	0.07
1.562	4	1.56b	4	1.56	0.53
1.480	3	1.48b	3	1.48	0.33
1.352	0.2	1.354	1	1.348	0.07
1.338	3				
1.299	2	1.300	2	1.295	0.07
1.167	1.5	1.17b	1		
1.097	0.5	1.09b	0.5		
1.061	0.2	1.06b	0.2		
1.017	0.5	1.018	0.5		
0.999	1	0.999	1		
0.937	1.5	0.936b	2		
0.929	0.5				
0.903	0.7	0.904b	1		
0.886	0.5	0.887b	1		
0.853	1				
0.796b	0.2				

1. Natural nickel hydroxide, Lord Brassey mine, Heazlewood, Tasmania, $CuK\alpha_1$ radiation, $\lambda=1.5404$ Å
2. Synthetic nickel hydroxide, supplied to the Chemistry Department of the Universit of Melbourne by Hopkin and Williams Ltd.
   $CuK\alpha_1$ radiation, $\lambda=1.5404$ Å
3. Nickel hydroxide pattern from the A.S.T.M. Index of *X*-Ray Diffraction Data
   $MoK\alpha$ radiation, $\lambda=0.708$ Å

The author recognizes that, in the absence of further chemical and physical data, this constitutes a most inadequate description of a new mineral, and accordingly suggests that naming of the mineral be deferred until such time as quantities sufficient for a complete description be obtained, either from Heazlewood or from other localities. On the other hand, the *x*-ray data already obtained leave no doubt as to the identity of the Heazlewood mineral, and its occurrence thus seem worthy of record.

REFERENCES

KLUG, H. P., AND ALEXANDER, L. E. (1954): *X*-ray Diffraction Procedures for Polycrystalline and Amorphous Materials. New York, Wiley and Sons.

WILLIAMS, K. L. (1958): Nickel mineralization in western Tasmania, *Proc. Aus. Ins Min. Met.*, **Stillwell Anniversary Volume, 263–302.**

THE AMERICAN MINERALOGIST, VOL. 45, SEPTEMBER-OCTOBER, 1960

DEHYDRATION AND REHYDRATION OF FERRIMOLYBDITE FROM LOWTHER, NEW SOUTH WALES

H. G. Golding, P. Bayliss and N. Trueman,
The University of New South Wales.

Powder diffraction data has been obtained for ferrimolybdite collected during 1959 from the surface of old prospecting shafts near Lowther, 90 miles west of Sydney, New South Wales. At this locality joint fissures in a porphyritic marginal phase of the Bathurst granite batholith are occupied by hydrothermal quartz veins containing small disseminated aggregates of intimately associated molybdenite, pyrite and chalcopyrite which have partly weathered to ferrimolybdite and goethite.

In addition to films of dull yellow ferrimolybdite coating fracture surfaces in the quartz, the Lowther specimens show radiating groups of sheaf-like units (Fig. 1) of bright yellow colour and silky lustre. Each unit, from 1 to 2 mm. long and about 0.2 mm. wide is itself a bundle of closely packed sub-parallel fibrous crystals. The sheaf-like units are partly embedded in goethite and project into the cells of goethite boxworks or into cavities in the quartz formerly occupied by sulphides.

Single fibres, from 1 to 2 mm. long and about 2 microns wide, are transparent, with refractive indices approximately 1.75 across and 1.8+ along the length and show strong lengthwise light absorption, straight extinction and high birefringence.

The soft and friable character (H=1), colour change from yellow through gray to orange on heating strongly and a chemical analysis on

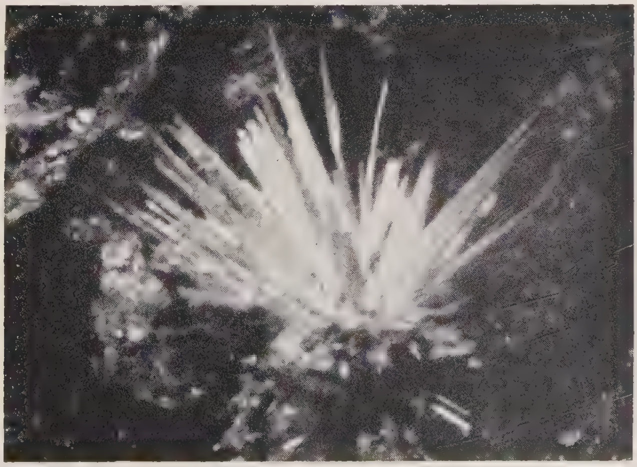

Fig. 1. Ferrimolybdite from Lowther, New South Wales. ×25.

0.5 gm. of goethite-contaminated material served to further verify the mineral as ferrimolybdite (Palache, Berman and Frondel, 1951).

In view of the reported ease with which ferrimolybdite loses water in a warm dry climate (Simpson, 1951) and because the samples although collected during a wet season had been subsequently stored for periods up to several months under variable conditions of summer humidity and temperature, reaching 40° C., *x*-ray determinations have been made on deliberately humidified and dehydrated as well as on untreated powder obtained from the bright yellow well-crystallized material after detaching adherent goethite under the binocular. The samples so obtained were slightly contaminated with quartz, molybdenite and goethite.

X-ray data (Table 1) was obtained by using the powder method, sample 1*a* by means of the geiger diffractometer and the rest photographically. Single crystal data was not obtained because of the small size and fragility of the fibrous crystals.

The sample treatment was as follows:

1*a*: Untreated.
1*b*: Untreated, water-mounted rod.
1*c*: Untreated, glycerol-mounted rod.
1*d*: Humidified over water for 100 hours, water-mounted rod.
1*e*: Desiccated over H_2SO_4 for 50 hours, humidified over water for 100 hours, water-mounted rod.
2*a*: Heated at 50° C. for 1 hour, desiccated over silica gel for 50 hours, glycerol mounted rod.
3*a*: Desiccated over H_2SO_4 for 50 hours, glycerol-mounted rod.
3*b*: Dessicated over H_2SO_4 for 50 hours, heated at 50° C. for 100 hours, glycerol-mounted rod.
4*a*: Heated at 100° C. for 1 hour, glycerol-mounted rod.
4*b*: Heated at 250° C. for 1 hour, glycerol-mounted rod.

Where no significant differences in diffraction patterns are perceptible the data are combined.

The *x*-ray data indicate that the bright yellow, well-crystallized ferrimolybdate was fully hydrated as collected and suffered no perceptible change during storage under normal conditions of summer temperature and humidity. This ferrimolybdite gives characteristic lines of strongest intensity at 9.9 and 8.4 Å.

Progressive dehydration, however, results in significant variations in these low angle reflections indicating the progressive collapse of the crystal structure accompanying loss of water or hydroxyl groups. The data and the line clarity of the photographs suggest that this collapse takes place in definite stages.

The changes observed correspond broadly to the progressive weight

TABLE 1. X-RAY DIFFRACTION DATA FOR FERRIMOLYBDITE

Samples 1a to 1e		Sample 2a		Samples 3a, 3b		Samples 4a, 4b	
d Å	I	*d* Å	I	*d* Å	I	*d* Å	I
9.87	100						
8.40	55	8.40	50				
7.70	2	7.70	50	7.70	100		
6.73	20	6.73	5	6.73	20		
5.91	1	5.91	20	5.91	20	5.91	20
5.83	1	5.83	20	5.83	20	5.83	20
5.16	4						
		5.06	100	5.06	50	5.06	50
4.90	2						
		3.90	40	3.90	20		
3.50	5						
3.20	4	3.20	4	3.20	2		
3.08	20	3.08	60	3.08	60	3.08	100
		2.87	5	2.87	5	2.87	5
2.80	1						
2.70	2	2.70	2	2.70	2	2.70	2
2.59	2	2.59	2	2.59	2	2.59	2
2.55	2	2.55	2	2.55	2	2.55	2
2.50	1						
		2.17	1	2.17	1	2.17	1
		1.95	1	1.95	1	1.95	1
1.78	2	1.78	1	1.78	2	1.78	2
1.73	1	1.73	1	1.73	1	1.73	1
1.70	1						
1.63	4	1.63	1	1.63	2	1.63	2
1.61	2	1.61	1				
1.52	2	1.52	2	1.52	2	1.52	4

loss and to the progressive colour variation accompanying the progressive dehydration of ferrimolybdite from Western Australia as recorded by Simpson (1951).

After partial dehydration as for sample 3*a*, it is found that humidification will restore the sample to the fully hydrated condition as shown by sample 1*e*.

REFERENCES

PALACHE, C., BERMAN, H., AND FRONDEL, C. (1951), The System of Mineralogy, II, 1096. Wiley, New York.

SIMPSON, E. S. (1951), Minerals of Western Australia II, 280–83, Govt. Printer, Perth.

THE AMERICAN MINERALOGIST, VOL. 45, SEPTEMBER–OCTOBER, 1960

THE PREPARATION AND USE OF POLISHED THIN SECTIONS

G. C. Amstutz,
Missouri School of Mines and Metallurgy, Rolla, Missouri.

The literature on the preparation of polished thin sections known to the present author describes only complicated procedures. This may be the main reason why polished thin sections are not widely used, although they can provide the geologist with many detailed criteria for ore genesis, many of which are not available from separate thin and polished sections. These criteria may, in turn, act as guides in exploration. The present paper describes a simpler and faster method for preparing polished thin sections of rocks and ores.

The preparation of the polished thin sections from which the photographs of Figs. 1 to 3 were taken, is simple. It requires only 25 to 35 minutes per section. First a thin section is prepared in the conventional way with Lakeside plastic cement and ground to almost normal thickness with any conventional powder. Quartz may still show yellowish to orange interference colors. The slide is then washed carefully and dried, in order to remove the grinding powder. The next and last step is the polishing on a lead, a lead-bismuth, a silk, or a Trojer (linden-wood) lap with abrasives of 1 or 0.5 micron size. The rotation speed should be rather slow (30–60 rpm.). The slide is placed with only about 50–100 g. pressure on the lap and held there for 5–20 minutes, depending on the nature of the ore and country rock. Frequent checking under the microscope will help to determine the point at which the surface is polished to a satisfactory degree. The powder and the oil is then removed and the section labeled. No further mounting is needed. The polished thin section is of course not covered.

The usefulness of a combined observation with transmitted and reflected light does not have to be pointed out. A combination of thin and polished sections is most needed when alteration is present, or when the exact metallurgical properties of ores are sought.

The frequent association of hydrothermal, deuteric, or supergene alterations with ore minerals is a well known fact. A divergence in geological opinion often takes place, when the discussion centers on the time and the origin of such alterations. Polished thin sections are a refined tool for the determination of the type and nature of these mineral changes. Limonite haloes can be readily recognized (Figs. 1 and 2). True replacements can be distinguished from apparent replacements; congruent and non-congruent features can be differentiated (1), and syngenetic and epigenetic criteria may be observed in more detail (2).

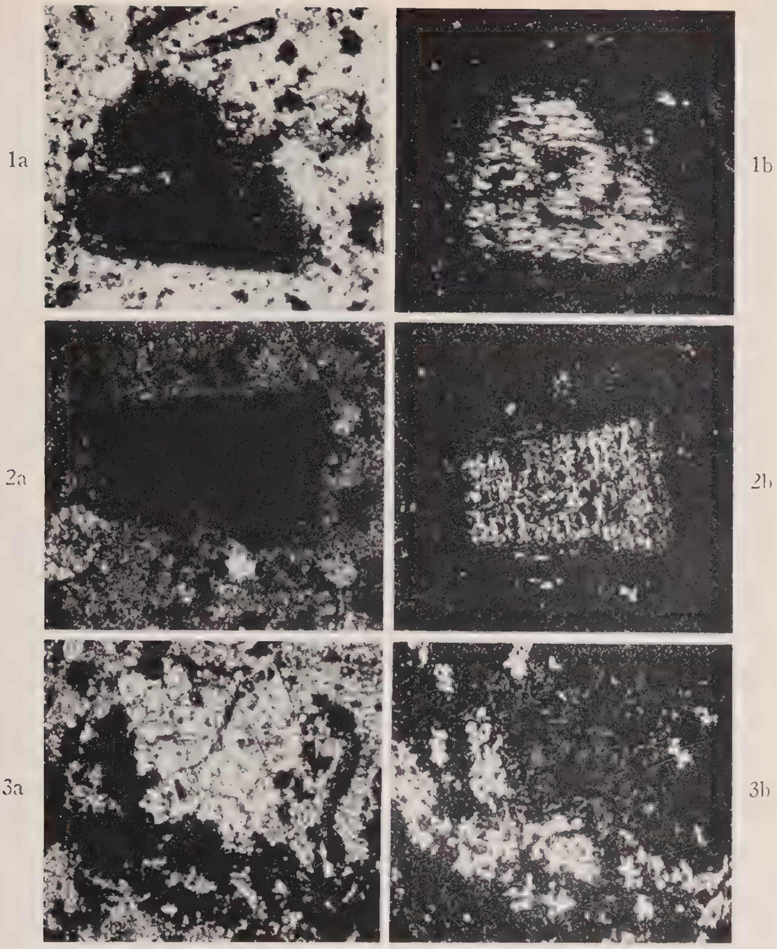

FIGS. 1–3. Pairs of photomicrographs taken of polished thin sections, with transmitted light on left and reflected light on right, all under oil immersion. Enlargement 175×. All three samples from small copper deposits in Carlos Francisco porphyry near Casapalca, Peru. (Geological details, given in (1).)

FIGS. 1, 2. Two examples of pseudomorphically replaced mafic phenocrysts (biotite) are shown. The sulphides also occur as disseminated specks in the matrix of this volcanic rock. During deuteric alteration the early phenocrysts became unstable and were replaced largely by sulphides which now show lamellar orientation in the direction of the original Si_2O_5-lattice sheets. These pseudomorphs are surrounded by a halo of limonite. Note the size difference of the reflected and the opaque areas. The haloes are broad in the elongation of the silicate sheets, but almost absent adjacent to the cleavage plane of biotite. This might indicate the "permeability" of the lattice for the replacement migrations. The sulphides consist of chalcopyrite and bornite, and in Fig. 1 possibly also of some idaite.

FIG. 3. An irregular mass of chalcopyrite in the matrix of the andesite irregularly surrounds a feld-spar phenocryst. Geometrically this is a transition between a true dissemination and an irregular tiny veinlet. Note that all opaque material under transmitted light is not necessarily sulphide mineral. About 25–35% of the visible opaques consist of limonite. This is very fine grained and intermixed with some non-opaques, and therefore, did not take on any polish.

In summary, polished thin sections afford a small but valuable enhancement of the quality and objectivity of observation and help to reduce the quantity of interpretation in ore genesis. These improvements will be welcome when it is recognized that a complete theory needs to be built on a careful combination of geochemical and geometric (fabric, structural) evidence.

Polished thin sections also provide more complete information for ore dressing microscopy, where metallurgical properties of minerals are sought. Coatings, alterations (clay, sericite, etc.), intergrowths or locking types and locking sizes can be seen in more detail and in less time. Typical examples are discussed in detail by the present author (3).

ACKNOWLEDGMENT

The polished sections reproduced in Figs. 1 to 3 were prepared in the Petrology Laboratory of the Cerro de Pasco Corporation in La Oroya, Peru, where the simple method described in this paper was first tried out. Permission for publication of this note is herewith acknowledged with thanks. The author wishes also to thank Dr. P. D. Proctor for the critical reading and valuable suggestions in connection with the content and form of this note.

REFERENCES

1. Amstutz, G. C. (1959a) Syngenetic zoning in ore deposits: *Trans. Geol. Assoc. Canada* **11,** 95–113.
2. ——— (1959b) Syngenese und Epigenese in Petrographie und Lagerstättenkunde: *Schweiz. Min. Petr. Mitt.* **39,** 1–84.
3. ——— (1960) The copper deposits Caprichosa and Antachajra in Central Peru (with notes on ore genesis in general): *N. Jb. Min., Ramdohr Festschrift*, 45 p.

THE AMERICAN MINERALOGIST, VOL. 45, SEPTEMBER–OCTOBER, 1960

VARIATIONS IN INTERFERENCE FIGURES IN SINGLE CRYSTALS OF ZONED SMOKY QUARTZ

L. F. Dellwig and W. E. Hill, Jr.
The University of Kansas, Lawrence, Kansas.

INTRODUCTION

Much attention has been directed to the problem of coloration of smoky quartz and to the related problem of zonation of smoky and colorless quartz in a single crystal. Phillips (1908) recognized a relationship between irradiation and coloration in quartz crystals, noting that coloring and banding developed with exposure of a quartz crystal to radium. He also recognized the significance of impurities in coloration through irradiation, for working with fused boric acid he was unable to effect coloration whereas in impure borax coloration resulted after a few weeks of exposure to radium.

Lind and Bardwell (1923) proposed that the displacement of electrons from their normal position through irradiation was responsible for coloration in quartz and fluorite. Frondel (1945) also favored displaced electrons as a cause for coloration, but at the same time recognized a sensitizing factor (an impurity included during growth) in zoned crystals as evidenced by the differential response of the clear and smoky bands to radioactive emanations. Frondel and Hurlbut (1955) and Cohen and Sumner (1958) attributed coloration to the replacement of a silicon ion by an aluminum ion in the quartz structure. In colorless areas the aluminum content was, in some cases, as great as in smoky areas but in colorless areas it was interstitial rather than replacement. Other structural deviations have been suggested.

Possible explanations for the coloration thus include: (1) inclusion of impurities in either ionic or molecular form, (2) effect of radioactive emanations, (3) structural deviations, and (4) a combination of several of the mentioned factors.

Petrographic examination of zoned quartz crystals from the Wet Mountain Thorium Belt indicates that alternation of colorless and smoky bands is related to a structural change.

Description of Crystals

All of the crystals examined were taken from radioactive veins of the Wet Mountain Thorium Belt in Custer and Fremont Counties, Colorado. This belt includes veins 100 to 5000 feet in length and 10 to 50 feet in width cropping out in a northwest-southeast trending area 10 miles in width and 25 miles in length. Typical minerals of the veins are quartz, barite, and carbonates with minor fluorite, sulfides, iron oxides and thorogummite.

The quartz crystals are euhedral to subhedral with crystal faces generally coated with hematite and sometimes thorogummite. Almost all crystals show some zoning of smoky and colorless quartz (Fig. 1) whether the crystals be only a fraction of an inch or 8 to 10 inches in diameter. Zones may be sharply separated or may show a gradational change from colorless to smoky quartz. Color bands generally continue around the crystal but may be abruptly terminated with a sharp break between colorless and smoky quartz. Color bands parallel the crystal faces and there can be little doubt but that they are also growth bands.

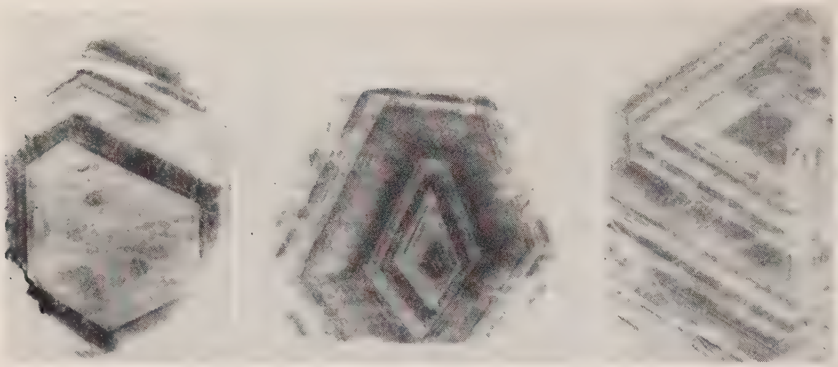

FIG. 1. Thin sections of zoned quartz crystals. Sections cut normal to c axis. ×1.4.

VARIATIONS IN INTERFERENCE FIGURES

A peculiarity common to the majority of the crystals examined is the variation in interference figures in a single crystal between colorless and smoky zones, all sections being cut approximately normal to the c axis. Colorless zones produce either a uniaxial positive figure or a biaxial positive figure with a small (less than several degrees) 2V. Smoky zones in the same crystal, with few exceptions, produce larger 2Vs (up to about $7\frac{1}{2}°$–8°) than do colorless zones. In several crystals no perceptible difference in 2V could be noted with a biaxial figure appearing in each. This might be attributed to strain. In no crystal does a uniaxial figure appear throughout nor does the 2V ever appear larger in the colorless zone. Smoky zones are pleochroic from brown to green in all specimens.

SUPPLEMENTAL DATA

Some crystals have zones sufficiently broad to permit separation of colorless and smoky material for analysis. X-ray powder analyses were made of adjoining zones of colorless and smoky quartz but no structural difference was perceptable.

The abundance of small inclusions throughout the crystals makes highly improbable the detection of an impurity which might be considered to be the cause of the coloration in the smoky material. Semiquantitative spectrographic analyses were run on five pairs of samples (colorless and smoky). Calcium, iron, aluminum, magnesium, copper, and vanadium were found in all samples in trace amounts. Both black and white samples of each pair contained approximately equal amounts of calcium, iron and copper, although small differences in concentration were noted between sample pairs. In general magnesium, vanadium and aluminum were found in slightly larger amounts in the smoky samples.

Aluminum is the impurity suggested by Cohen and Sumner (1958) as responsible for the smoky color.

Loss on ignitions run on three pairs of samples showed the loss of weight between 550 and 600° C. to be greater in colorless quartz than in smoky quartz in two pairs (dark loss 0.08%, colorless loss 0.13%; dark loss 0.03%, light loss 0.05%), thus reducing the possibility of carbon as the coloring agent for the smoky quartz.

CONCLUSIONS

Cyclic inclusion of one or more impurities (probably in ionic form) during growth of the crystal is indirectly responsible for the coloration of smoky quartz. That coloration is directly the result of exposure to radioactive material has been demonstrated on numerous occasions. Recent work indicates that the smoky color develops in quartz in which the impurity is substitutional rather than interstitial. It can thus be concluded that the orderly variation in velocity in smoky quartz in sections normal to the *c* crystallographic axis (biaxial figure resulting) must be due to a structural change resulting from an orderly substitution of one element for another according to a fixed pattern.

REFERENCES

COHEN, A. J. AND SUMNER, G. G., 1958, Relationships among impurity contents, color centers and lattice constants in quartz: *Am. Mineral.*, **43**, 58–68.

FRONDEL, CLIFFORD, 1945, Effect of radiation on the elasticity of quartz: *Am. Mineral.*, **30**, 432–436.

———, AND HURLBUT, JR., C. S., 1955, Investigations into effects of radiation on the physical properties of quartz: **PB111628,** *U. S. Dept. of Commerce Office of Technical Services.*

LIND, S. D. AND BARDWELL, D. C., 1923, The coloring and thermophorescence produced in transparent minerals and gems by radium radiation: *Am. Mineral.*, **8,** 171–180.

PHILLIPS, C. E. S., 1908, Letters to the editor—Coloration of glass and quartz by radium: *Nature*, **77,** no. 2006, 535.

THE AMERICAN MINERALOGIST, VOL. 45, SEPTEMBER–OCTOBER, 1960

CALCIOSTRONTIANITE FROM PULASKI AND ROCKINGHAM COUNTIES, VIRGINIA

R. V. DIETRICH, *Virginia Polytechnic Institute, Blacksburg, Virginia.*

Strontianite with approximately eight per cent CaO, hereinafter referred to as calciostrontianite, has recently been found to occur in calcite-lined vugs at two Virginia localities other than the one mentioned by Pharr and Mitchell (1959). These are: 1) at the Salem Rock Corp. Quarry on the west side of Virginia Route 100, ca. 315 miles (by road) south of Dublin, Pulaski County and 2) beneath the Maude Liskey Property about 0.4 mile southeast of U. S. Route 11, ca. 2.7 miles northeast of the center of Harrisonburg, Rockingham County.

The Rockingham County calciostrontianite was found in a drill core. It occurs as white to cream-colored, radial groups of spear-shaped crystals in calcite-lined vugs in limestone of the Athens formation of Middle Ordovician age. Its identity as calciostrontianite is based chiefly on its *x*-ray diffraction pattern.

The Pulaski County calciostrontianite occurs as nearly colorless, white and buff, radial and sheaf-like groups of spear-shaped crystals (Fig. 1) in vugs and on joint surfaces in dolomite of the Elbrook formation of Middle and/or Late Cambrian age. Most of the formation is highly laminated at the locality. Nearly all of the vugs are lined with colorless to white calcite crystals, typically scalenohedra terminated by rhombo-

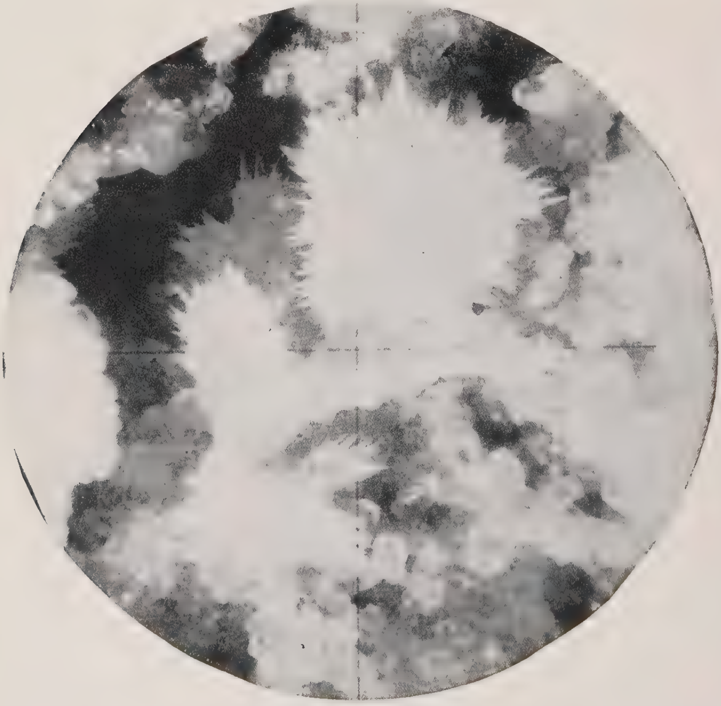

FIG. 1. Calciostrontianite in a calcite-lined vug from Pulaski County, Virginia. The largest radial group is approximately 3.0 mm. in greatest dimension. Most individual radial groups thus far found at the locality are less than 3.5 mm. in greatest dimensions, a few range up to 6 mm.; some radial groups comprise composite masses up to 12 mm. in greatest dimension.

hedra. A few of the calcite crystals are citrine to amber in color. In some vugs groups of calcite crystals are arranged so as to form ridges arranged radially away from a central mass of silica. Such central silica typically consists of granular, loose to partly aggregated, colorless to white quartz around a light gray to milky white, solid, chalcedonic silica core. Typically the size of the core varies directly with the size of the containing vug. Contrariwise, there appears to be no such size relationship between core size and thickness of surrounding granular quartz. Rather, the thickness of the granular quartz appears to be nearly constant (about 10 mm.) in all vugs. In fact, some central masses of granular quartz with greatest dimensions of less than about 20 mm. have no massive chalcedonic cores. Apparently exceptional is one specimen with a large (greatest dimension of ca. 90 mm.) core which has a direct junction with the surrounding dolomite. The granular quartz consists of angular, irregular-shaped grains and crystals (!!?!), nearly all of which pass .062 mm. mesh screen and many of which pass .044 mm. mesh screen. A mass of light blue celestite was found spatially associated with the calciostrontianite in one vug. Also, it is perhaps of at least passing interest that numerous, nearly colorless tabular celestite crystals that range up to eight millimeters in longest dimension were found to occur in three, calciostrontianite-free, calcite-lined vugs (—within dolomite which is more massive than typical, *i.e.*, it is essentially nonlaminated). No granular quartz or chalcedony occurred in these three vugs.

Relationships observed suggest that the vugs occupy space which was occupied by some material other than dolomite, perhaps silica, at the time of the original sedimentation. The paragenetic sequence of the minerals in the vugs, if listed from oldest to youngest on the basis of position with respect to the vug walls, would be calcite, light blue celestite, calciostrontianite, and silica. (As mentioned, the nearly colorless celestite appears to be postcalcite but no interrelationships have been observed between it and the other vug minerals.) However, it appears that this apparent sequence possibly needs to be modified at least so far as the silica is concerned. It seems likely that the silica was not introduced into the vugs after the other minerals but, instead, that it may be residual and derived from silica that previously filled the present vug space. If such silica was a gel and/or calcareous-rich or something similar the lack of enough silica to fill the vugs completely at present might reflect such things as loss of water, loss and/or redistribution of calcareous and/or other material(s) or removal of part of such material(s) during passage of the solutions which, if ever existent, may have been responsible for deposition of the carbonates and/or sulfates. In any case, the granular quartz and massive chalcedony may represent diverse modifications of a common parent. Observable interrelationships between vug boundaries and adjacent surrounding dolomite laminae appear to support removal or partial removal of the pre-existing filling material(s) after consolidation of the sediment, *i.e.*, deposition of the original filling material(s) was at the sediment-water interface. Otherwise, this aspect remains unsolved.

The following data, except where noted otherwise, were derived from investigation of the Pulaski County calciostrontianite.

1. *X-Ray:* Powder data are presented for calciostrontianite with 8.1 per cent CaO (Table 1). These data are presented despite the fact that they are, to a large extent, repetition of those of Pharr and Mitchell (*op. cit.*) because of the difference in methods used in their and V.P.I.'s laboratories.* The spacings for the calciostrontianite, *e.g.*, 4.34, 3.51, 3.41, 2.54, 2.43, and 2.04, when compared to equivalent reflections of essentially calcium-free strontianite (see Swanson, Fuyat, and Urginic)—4.37, 3.54, 3.45, 2.55, 2.45, and 2.05, respectively—appear to reflect the substitution of smaller radius calcium for some of the larger radius strontium. The Rockingham County material gave *d* values and relative intensities nearly identical to those given on Table 1 except that the 4.17*d* reflection was not apparent.

TABLE I. *X*-RAY POWDER DATA FOR CALCIOSTRONTIANITE FROM PULASKI COUNTY, VIRGINIA

d (Å)	I	*d*(Å)	I
4.34	w	1.885	m
4.17	vvw	1.81	m
3.51	vvs	1.80	mw
3.41	vs	1.75	vvw
2.98	w	1.705	vvw
2.815	w	1.66	vw
2.58	vw	1.60	mw
2.54	s	1.55	mw
2.46	m	1.53	vw
2.43	vs	1.49	vvw
2.25	vw	1.47	vvw
2.165	m	1.44	vw
2.075	vw	1.41	vvw
2.04	s	1.30	vw
1.96	m	1.27	mw
1.935	mw	(75 degrees 2θ, end of scan)	

---

* The *x*-ray setup used by the writer is a General Electric XRD-5 diffractometer with a No. 2SPG geiger counter type spectrogoniometer. CuKα radiation with a Ni filter was used. A scanning speed of 2 degrees 2θ/min. was used for the complete scan; the lowest 2θ reflection ($d=4.34$) and the three strong reflections with *d* values of 3.51, 3.41, and 2.04 were checked at a scanning speed of 1 degree 2θ/5 mins.

2. *Optical:*

Indices of refraction—α—1.522
β—1.663 (calc.)
γ—1.664
Biaxial (−)
2V = 8°
Slight dispersion with r < v.

3. *Chemical:*

$CaO = 8.1$ per cent* (equivalent to ca. 14.5 per cent $CaCO_3$).

4. *Thermal:* An exemplary differential thermal analysis curve for pure calciostrontianite is presented (Fig. 2). The heating curve is marked by two sharp endothermic reactions and the cooling curve has two exothermic reactions. The lower temperature endothermic reaction has been found to occur at ca. 860° C. in all runs; the higher temperature endothermic reaction has been found to peak at 925° C. in all runs except one in which the temperature was 915° C. In all cooling runs, both exothermic reversals occurred at lower temperatures than the complementary endothermic reactions of the heating runs. The higher temperature exothermic reversal occurred at ca. 875° C. in all runs except one in which the temperature was 840° C.; the lower temperature exothermic reversal occurred

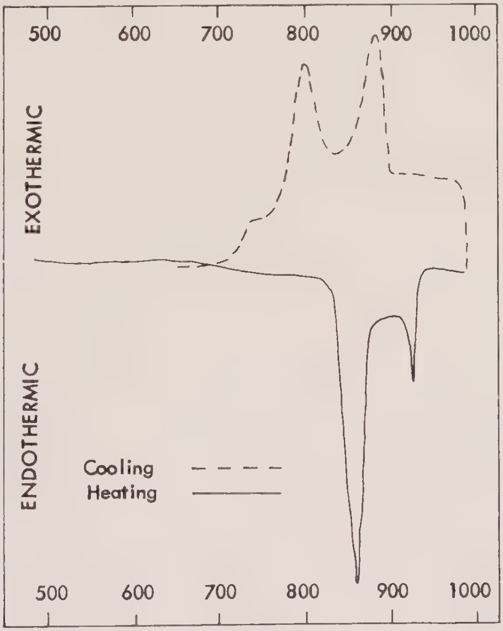

Fig. 2. Tracing of thermal (D.T.A.) curve of calciostrontianite from Pulaski County, Virginia. Curve between room temperature and 500° C. was essentially straight.

---

* Analyst—Dr. J. W. Murray, Department of Chemistry, Virginia Polytechnic Institute; analyses by Beckman flame photometer with Aminco photomultiplier photometer.

at 790° C. to 795° C. in all runs. The relative peak areas (defined as suggested by Webb and Heystek, p. 352) were remarkably similar in all runs with that of the lower endothermic reaction about 7.5 times that of the higher, that of the higher exothermic reversal about 2 times that of the lower temperature one, etc. In all runs, the conductivity of the material existent between the two endothermic peaks appears to be notably different from the conductivities of the phases existent originally and after the second reaction.

On the basis of the purity of the samples used and the reversibility of both endothermic reactions, as shown by the cooling curve, the writer believes that both reactions reflect inversions—probably from orthorhombic to hexagonal and thence to isometric forms of calciostrontianite. This suggestion is made with complete awareness of the fact that both Cuthbert and Rowland (1947) and Gruver (1950) suggested similar curves for strontianite to reflect only the orthorhombic to hexagonal inversion (one peak) and some reaction involving impurities (other peak). Apparently neither of these reported investigations included the running of cooling curves. The cooling curves plus determination that the material existent at the end of each run is identical to the original material appear to support best the suggested two-inversions interpretation. Permissively corroborative is the fact that differential thermal analyses of structurally similar witherite manifest two such inversions (see, for example, Cuthbert and Rowland; Gruver; and Webb and Heystek—all *op. cit.*).

5. *Miscellaneous:*

Density—3.67 ± 0.02
Fluorescence —white to yellowish (long wave)
white (short wave).

The writer gratefully acknowledges that W. D. Lowry of the Department of Geological Sciences of Virginia Polytechnic Institute supplied the core from the Rockingham County locality, and that R. S. Mitchell of the Department of Geology of the University of Virginia made available unpublished x-ray data for calciostrontianite from Wise County, Virginia.

References

Cuthbert, F. L. and Rowland, R. A. (1947) Differential thermal analysis of some carbonate minerals: *Am. Mineral.*, **32,** 111–116.

Gruver, R. M. (1950) Differential thermal-analysis studies of ceramic materials: I, Characteristic heat effects of some carbonates: *Jour. Am. Ceram. Soc.*, **33,** 96–101.

Pharr, R. F. and Mitchell, R. S. (1959) Celestite and strantianite from Wise County, Virginia (abst.): *Va. Acad. Sci. Proc.* 1959.

Swanson, H. E., Fuyat, R. K. and Urginic, G. M. (1954) Standard x-ray diffraction powder pattern: Nat. Bur. Stan. (U.S.), circ. **539,** 73.

Webb, T. L. and Heystek, H. (1957) The carbonate minerals: in McKenzie, R. C., "The differential thermal investigation of clays": *Min. Soc.* (*Clay Min. Grp.*), *London,* 329–364.

THE AMERICAN MINERALOGIST, VOL. 45, SEPTEMBER–OCTOBER, 1960

THE OCCURRENCE OF ORTHOPYROXENE WITH LOW OPTIC AXIAL ANGLE

J. F. LEWIS
Victoria University of Wellington, Wellington, New Zealand.

Orthopyroxene with $2V_X$ as low as 35° has been found in the dacitic rocks of the Tauhara volcano, which is situated in the active volcanic belt of the North Island, New Zealand. The volcano consists of several cumulo-domes, one of which has been breached exposing the core. The core rocks are highly oxidized while those on the margin of the dome are not oxidized, but have a similar composition. There is no other alteration of the rocks. It is in the oxidized rocks that the orthopyroxene with very low $2V_X$ occurs.

Investigation into the literature showed that no orthopyroxene with $2V_X$ less than 45° has been recorded. Kuno (1954) considers that the $2V_X$ of orthopyroxenes in volcanic rocks is not less than 50°. However, orthopyroxenes in hypabyssal and plutonic rocks possess a lower $2V_X$ at the same Fe:Mg ratio (Poldervaart, 1950; Hess, 1952; Kuno, 1954). These authors consider this to be due to the lower Al_2O_3 and CaO content of hypabyssal and plutonic orthopyroxenes.

$2V_X$ of orthopyroxene crystals in the marginal unoxidized rocks of the dome ranges from 72°–54°, av. 67° ($\gamma = 1.697 - 1.720$). In oxidized rocks from the core of the dome $2V_X$ ranges from 70°–35° ($\gamma = 1.700$–1.736). The average 2V varies with the degree of oxidation of the rocks, but is generally about 60°, considerably lower than in the corresponding unoxidized rocks. Crystals with optic axial angle below 45° always have a rim of opacite, are discrete, or occur as inclusions in plagioclase. Only one or two crystals in a thin section possess the very low 2V. The variation in optical properties of the orthopyroxene in the unoxidized rocks indicates a wide range in composition for this mineral. However, variation in composition alone is probably not the primary cause of the low 2V of the orthopyroxene in the oxidized rocks.

Confirmation that the mineral is an orthorhombic pyroxene was made by taking Weissenberg and rotation photographs of the zero and first layer lines about the *c* axis of a crystal of the pyroxene in question. These were compared with those taken about the *c* axis of a crystal of common orthopyroxene from an unoxidized rock.* The unit cell dimensions and optical properties of these two crystals are given together with a comparative set of values from Kuno (1954) for orthopyroxene with composition Fe_{50}.

---

* Single crystal determinations made by Mr. P. P. Williams, Dominion Laboratory, Wellington.

Optic orientation: $a=Y$, $b=X$, $c=Z$.

Common orthopyroxene (Unoxidized rock)	Abnormal orthopyroxene (Oxidized rock)	Orthopyroxene, Fe_{50} (Kuno, 1954)
$a=18.320$ Å	$a=18.340$ Å	$a=18.360$ Å
$b=$ 8.850 Å	$b=$ 8.945 Å	$b=$ 8.925 Å
$c=$ 5.14 Å	$c=$ 5.16 Å	$c=$ 5.230 Å
$N_X \doteq 1.685$**	$N_X \doteq 1.720$	$N_X = 1.710$
$N_Y = 1.693$	$N_Y = 1.733$	$N_Y =$ —
$N_Z = 1.697$	$N_Z = 1.734$	$N_Z = 1.728$
$2V_X =$ 71°	$2V_X =$ 36°	$2V_X =$ 52°

Pleochroism distinct:

X = pale reddish brown	X = pale pinkish brown
Y = pale straw yellow	Y = pale pinkish yellow
Z = pale green	Z = smoky green
Absorption: $X>Y=Z$	Absorption: $Z=X>Y$

The photographs obtained were identical except for the larger unit cell dimensions of the abnormal orthopyroxene. The unit cell dimensions given are not absolute, but the relative values between the two crystals are accurate. It is not assumed that the two crystals measured have the same Fe:Mg composition ratio.

Because of practical difficulties in obtaining a pure sample, the abnormal pyroxene has not been chemically analyzed, but it is probable that the unusual optical properties of the mineral are due to oxidation and heating rather than to extreme primary composition.

REFERENCES

Hess, H. H. (1952), Orthopyroxenes of the Bushveld type, ion substitutions and changes in unit cell dimensions. *Am. J. Sci.*, Bowen vol., 173–187.

Kuno, H. (1954), Study of orthopyroxenes from volcanic rocks. *Am. Mineral.*, **39**, 30–46.

Poldervaart, A. (1950), Correlation of physical properties and chemical composition in the plagioclase, olivine, and orthopyroxene series. *Am. Mineral.*, **35**, 1067–1079.

THE AMERICAN MINERALOGIST, VOL. 45, SEPTEMBER-OCTOBER, 1960

BIREFRINGENCE OF SYNTHETIC GARNETS

A. B. Chase and R. A. Lefever, *Hughes Research Laboratories, Malibu, California.*

Single crystals of the synthetic garnets $R_3Ga_5O_{12}$ and $R_3Al_5O_{12}$ (where R is Y, Yb, or Tm) were grown from lead oxide-lead fluoride melts,

---

** R.I. = ±0.003.

using compositions and procedures approximating those suggested by Nielsen for gallium garnets (1). The melts were heated to 1250° C. in covered 50-cc. platinum crucibles, soaked for 12 to 24 hours, and cooled at a uniform rate of 4.2° C./hr. to 1000° C. The majority of the $R_3Ga_5O_{12}$ crystals were subhedral to euhedral and approximately 0.2–1 cm. in size, with faces parallel to dodecahedral $\{110\}$ and trapezohedral $\{211\}$ crystal planes. The trapezohedron was the dominant form, with dodecahedral modification occurring only in the very early and late growth stages. The crystals usually contained an array of inclusions and voids oriented parallel to the growth surfaces. The inclusions contained normal components of the melt and varied from sub-micron to about 1 mm. in size. The voids were approximately the same in size and all degrees of filling by the flux components were observed. The refractive index of the gallium garnets was approximately 1.95 (measured with white light and standard index oils.)

The $R_3Al_5O_{12}$ crystals were euhedral to subhedral and approximately 1–3 mm. in size. The dominant form was dodecahedral, with trapezohedral modification occurring near the end of the crystal growth. Inclusions and voids similar to those encountered in the gallium garnets were also present in these crystals. The refractive index of the aluminum garnets was approximately 1.85.

Under the microscope, sections of the garnets exhibited marked birefringence. Two types of structures were observed under crossed nicols: a birefringent halo around large inclusions and a well defined banding or zoning resembling twinning in the plagioclase feldspars. The birefringence varied from near zero to approximately 0.002. All of the crystals examined exhibited banding birefringence but the birefringent halo associated with the larger inclusions was rarely encountered. The birefringence was best observed in polished sections of 1–2 mm. thickness.

The birefringent halos associated with large inclusions extended outward for a distance of about one tenth of the diameter of the inclusion. The extinction was undulatory and pivoted about any sharp angles formed by the surfaces bounding the inclusion. The birefringence had a maximum value of about one quarter of that associated with banding and decreased in the vicinity of voids. This birefringence decreased sharply on annealing the sections for 24 hours at 1200° C., suggesting that it was caused by strain developed in the crystal during cooling, probably as a result of differences in the coefficients of expansion of the garnet and the included materials (2).

The banding normally exhibited the greatest birefringence in the peripheral zones of the crystals. The bands were parallel to the crystal faces and not to a single set of equivalent crystallographic planes. The bands varied in thickness from 0.01 to 1 mm. and did not possess observable boundaries. However, a becke line could be seen between bands in the regions of greatest difference in birefringence. The bands exhibited an undulatory extinction that varied plus or minus six degrees to the direction of the bands. The birefringence of individual bands decreased in the vicinity of voids. Sections prepared parallel to a growth face and at the periphery of the crystal appeared isotropic, except around inclusions. These sections showed off-centered biaxial optic axis figures with 2V varying from 5 to 20 degrees. The banding birefringence also decreased on annealing the samples at 1200° C.

The sections were more strongly birefringent in areas where edges and corners were formed by crystal faces during growth than in regions along the faces. When this condition was well developed, the crystal appeared to have rays of birefringence extending from the center to the corners and edges. When both the general banding and the rays were well developed, changes in crystal morphology that occurred during growth could be observed.

X-ray back reflection photographs provided information concerning the source of the birefringence in the banded areas. Birefringence in natural garnets is generally attributed to twinning (3). However, no evidence of twinning was observed in the synthetic garnets. In all crystals examined, the Laue spots exhibited a weak asterism oriented perpendicular to the line formed by the intersection of the nearest crystal face with the surface of the section. The asterism was greatest when the crystal face nearest to the area examined was perpendicular to the surface of the section. The asterism is interpreted as resulting from strain. The fact that the birefringent banding is oriented with respect to the asterism indicates that the birefringence is also due to strain, rather than twinning. Preliminary work with natural garnets indicates that birefringence in these crystals may also be primarily the result of strain. The strain probably results from variations in such properties as composition, purity and perfection of the crystals which, in turn, reflect variations in growth conditions.

We wish to express our appreciation to Dr. John Reed for assistance with the *x*-ray work and Mrs. Juanita W. Torpy for assistance with the crystal growth and sample processing.

References

1. Nielsen, J. W., *J. Appl. Phys., Supplement*, **31, 51S** (1960).
2. A more detailed treatment of birefringence and strain associated with inclusions is contained in the paper, "Pressure and Temperature of Crystallization from Elastic Effects around Solid Inclusions in Minerals," by J. L. Rosenfeld and A. B. Chase (to be published by *Am. Jour. Sci.*)

3. See for example, E. Ingerson and J. D. Barksdale, *Am. Mineral.* **28,** 303 (1943); A. N. Winchell and H. Winchell, "Elements of Optical Mineralogy. Part II." John Wiley and Sons, Inc., New York, 1956, 4th ed., p. 490.

International Mineralogical Association

The papers in the two symposia given at the Zürich meeting of the I.M.A. (*Am. Mineral.* **44,** 460, 1319) have now been published in magnificent quarto form of 106 pages with numerous illustrations by the Instituto Lucas Mallada (Paseo de la Castellana 84, Madrid) as Fasc. VII, May 1960. Copies are available for residents of North America by sending $1.50. to D. J. Fisher, Rosenwald Hall, University of Chicago, Chicago 37, Illinois before January 1961. Others may order from Madrid, from where later orders will also be handled. The table of contents of this Fasciculo is as follows:

Pimera Reunion de la Asociación Internacional de Mineralogia 1
Symposium on Twinning 3
  M. J. Buerger, Introductory remarks 3
  M. J. Buerger, Twinning, with special regard to coherence 5
  H. Curien, Sur les axes de macle d'ordre supérieur à deux 9
  J. D. H. Donnay y H. Curien, The concept of (lattice) complex in the theory of twinning 13
  P. Hartman, Epitaxial aspects of the atacamite twin 15
  W. T. Holser, Relation of pseudosymmetry to structure in twinning 19
  I. Kostov, Relationship between stability of crystal habit and twinning 31
  A. von Neuhaus, Zur Symmetrie und Zwillingsbildung des Diamanten 33
  I. Sunagawa, Surface structure of the twin boundary of hematite crystals 47
Symposium on Alpine Fissure Minerals 59
  G. Fagnani, Alpine fissure minerals and their relationship to the minerals of Baveno 59
  D. P. Grigoriev, The origin of quartz as a fissure mineral of the Alpine type with special reference to occurrences in the U.S.S.R. 63
  M. A. Kaschkai, On the Alpine-type veins of the Caucasus 77
  J. Leitz y M. R. Hänisch, The colouring of smoky quartz 83
  Robert L. Parker, The fissure deposits of the Swiss Alps. Their distribution and character 91
  T. von Schadlun, Einige metamorphische Bildungen vom Typus der alpinen Gänge in den Sulfidlagerstätten 97
International Mineralogical Association 101

ERRATUM

In the May-June, 1960 issue of the American Mineralogist, page 615, the equation $2ZnO+3S=2ZnO+SO_2$ should read $2ZnO+3S=2ZnS+SO$.

NEW MINERAL NAMES

Chudobaite

H. Strunz. Chudobait, ein neues Mineral von Tsumeb. *Neues Jahrb. Mineral., Monatsh.* **1960,** No. 1, 1–7.

This was listed as Mineral R in a preliminary note (*Am. Mineral.*, **44,** 1323 (1959)) Analysis by W. Schneider gave K_2O 2.0, Na_2O 5.0, CaO 1.0, MgO 12.0, ZnO 11.5, CuO 0.2, MnO 2.0, Co none, As_2O_5 49.7, H_2O^+ 17.0, sum 100.4%. This corresponds to $(Na, K, Ca)(Mg, Zn, Mn)_2\,H\,(AsO_4)_2 \cdot 4H_2O$. Water is lost at 140°.

The mineral occurs at the 1,000 m. level of the Tsumeb Mine, SW Africa, in the "second oxidation zone," and is associated with conichalcite, cuproadamite, and zincian olivenite. Crystals up to 0.5 cm. in size show the forms $a\{100\}$, $b\{010\}$, $c\{001\}$ dominant, also $m\{110\}$, $n\{120\}$, $L\{\bar{1}80\}$, $d\{101\}$, and $y\{\bar{1}84\}$, and perhaps $x\{186\}$. An angle table is given. Triclinic, $a{:}b{:}c = 0.6830{:}1{:}0.5827$, α 115° 10′, β 95° 54′, γ 94° 06′. Cleavage (010) very good, (100) good. Hardness $2\frac{1}{2}$ 3, G 2.94 measured, 3.0 calcd. Color pink, like kunzite. Optically biaxial, negative, *n*s (Na) α 1.583, $\beta \sim 1.608$, γ 1.633, 2V 79°. Extinction angle $\gamma'{:}C$ on (010) −24°, on (100) 110°. Not fluorescent in U V light.

Rotation photographs gave: triclinic, $P\bar{1}$, a 7.69, b 11.37, c 6.59 Å, $a{:}b{:}c$ (x-ray) $= 0.676{:}1{:}0.580$. Unindexed x-ray powder data are given (99 lines); the strongest lines are 10.163 (10), 2.979 (9), 3.440 (8), 3.273 (8), 2.730 (7), 3.859 (5), 3.746 (5), 2.831 (5), 2.637 (5), 2.417 (5), 1.817 (5).

The name is for Karl F. Chudoba, German mineralogist. Pronounced koo-dō-baite.

Michael Fleischer

Oregonite

Paul Ramdohr and Margaret Schmitt. Oregonit, ein neues Nickel-Eisenarsenid mit metallartigen Eigenschaften. *Neues Jahrb. Mineral., Monatsh* **1959,** No. 11–12, 239–247.

The mineral occurs as water-rolled pebbles in Josephine Creek, Oregon; the pebbles have a smooth brown crust. Under the microscope, the mineral is metallic white with high reflectivity, about 65%, in both air and oil. Anisotropism is weak, but visible in air along grain boundaries. Hardness about 5. Associated minerals are an unidentified mineral ("mineral y"), and small amounts of native copper, bornite, chalcopyrite, molybdenite, chromite, and perhaps niccolite. The gangue (about 40% by volume) consists of penninite and serpentine.

X-ray fluorescence analysis (data not given) corresponds to $Ni_{10}Fe_6As_9$ or Ni_2FeAs_2; the data indicate that the compound has intermetallic properties. A little Co is present, and traces of Cu. Attempts to synthesize the mineral melts in evacuated silica tubes failed.

From x-ray powder data and a Guinier photograph, oregonite is hexagonal, a_0 6.083 ± 0.003, c_0 7.130 ± 0.005 Å., c/a 1.1732, $Z = 3$ (Ni_2FeAs_2), G. calcd. 6.92. An indexed x-ray pattern is given; the strongest lines are 2.314 (vs), 2.1195 (vs), 1.991 (s), 1.7885(s), 1.757 (s), 1.739 (s). There is some similarity to the pattern of heazlewoodite, but the latter is rhombohedral.

The name is for the state of Oregon.

E. H. Rooseboom

Matraite (ZnS-3R)

S. Koch. The associated occurrence of three ZnS modifications in Gyöngyösoroszi. *Acta mineralog. petrog. Univ. Szegediensis,* **11,** 11–22 (1958).

Kalman Sasvari. ZnS mineral with ZnS-3R crystal structure. *Ibid.*, pp. 23–27.

The deposit contains wurtzite $2H$, galena, chalcopyrite, and pyrite, and brownish-yellow pyramidal crystal aggregates which are oriented intergrowths of sphalerite (ZnS-$3C$) with ZnS-$3R$ (called β' ZnS). Analysis by Mrs. Eve Klivenyi of the aggregates gave Zn 61.70, Fe 5.10, S 33.22, sum 100.02%. Spectroscopic analysis showed Pb significant traces, Cd traces, Sn weak traces. The ZnS-$3R$ is transparent; some crystals show pronounced anisotropy. The sphalerite present shows polysynthetic spinel-type twins, the aggregates are commonly scepter-shaped. The ZnS-$3R$ has $a_h = 3.8$, $c_h = 9.4$ Å.

The name is for the locality, the Matra Mountains.

Discussion.—This is the first natural occurrence of a modification first prepared by Buck and Strock, *Am. Mineral.*, **40,** 192–(1955), who showed it to be a new polymorph of ZnS, not merely a member of the multi-layered stacking series of wurtzites. They named it γ=ZnS, which is to be preferred to the β'-ZnS of the present authors.

Brian Skinner

Hydrosodalite

V. I. Gerasimovskii, A. I. Polyakov, and L. P. Voronina. Hydrosodalite, a rock-forming mineral of nepheline syenites of the Lovozero Massif. *Doklady Akad. Nauk S.S.S.R.,* **131,** no. 2, 402–405 (1960) (in Russian).

K. A. Vlasov, M. V. Kuz'menko, and E. M. Es'kova. The Lovozero alkaline massif. *Akad. Nauk S.S.S.R., Inst. mineralog., geokhim., i kirstallokhim. redkikh elementov,* **1959,** 272–274. (in Russian)

The first intrusive phase of the Lovozero Massif, Kola Peninsula, consists of poikilitic syenites occurring as xenoliths in the later intrusives. An abundant constituent is an isometric mineral, formerly thought to be sodalite or analcime, commonly replaced by zeolites. Analyses by L. P. Voronina and V. A. Moleva gave, respectively, SiO_2 32.71, 41.05; Al_2O_3 26.12, 28.36; Fe_2O_3 0.64, –; MnO –, 0.05; MgO –, 0.18; CaO 1.48, 0.60; Na_2O 26.67, 19.02; K_2O 0.14, 1.46; Cl 2.10, 0.16; S 1.12, 1.38; H_2O^+ 4.93 (total H_2O), 5.40; H_2O^- –, 1.25; insol. 6.48, –; sum 101.75, 99.55; ($O=Cl_2$, S) (not given in originals) = 1.03, 0.73 = 100.72, 98.82%. These correspond, respectively to the formulas $Na_{10}Al_6(O,OH)_{25}(O_{1.33}Cl_{0.67}$, and $2NaAlSiO_4 \cdot H_2O$. Soluble in HCl. Dark inclusions of a sulfide (pyrrhotite?) were observed and may account for the S (but the hackmanite variety of sodalite is common in the area—M.F.). The first formula is near that of sodalite, with Cl replaced by OH.

The mineral is gray to dark gray, hardness 5–6, G. about 2.3. Isotropic, n 1.487–1.490. X-ray powder data are given; they agree closely with those of sodalite. The strongest lines are 3.69(10), 3.25 (8), 3.44 (7), 2.63 (6).

The mineral may be of primary origin in these rocks or may be formed by autometasomatic processes. It is also formed as a secondary mineral after nepheline in other rocks.

Discussion.—The name hydrosodalite was used previously by Wyart and Michel-Levy, *Compt. rend.*, **229,** 131–133 (1949) for a synthetic mineral containing OH and CO_3 in place of Cl. Probably to be regarded as a variety of sodalite.

M. F.

Manganosteenstrupine

K. A. Vlasov, M. V. Kuz'menko, and E. M. Es'kova, The Lovozero alkaline massif, *Akad. nauk S.S.S.R.* **1959,** 421–422.

Analysis by M. E. Kazakova gave SiO_2 21.36, P_2O_5 0.65, Al_2O_3 0.91, TiO_2 1.49, ZrO_2 1.08, Fe_2O_3 1.99, MgO 0.70, MnO 17.98, ThO_2 11.28, UO_2 0.20, PbO 0.10, Ce_2O_3 9.79, La_2O_3 10.27, Y_2O_3 0.13, CaO 4.66, Na_2O 0.48, K_2O 0.24, H_2O^+ 12.86, H_2O^- 3.58, sum 99.75%, corresponding to (Ce, La, Th, Ca) (Mn) (SiO_3) $(OH)_2/2H_2O$. Spectrographic analysis also shows Sr, Ba, and Be. X-ray spectrographic analysis of the rare earths gave La 41.1, Ce 32.8, Pr 8.6, Nd 16.3, Sm 0.77, Gd 0.14, Dy 0.24%. A D.T.A. curve showed endothermal breaks at 90–200° and an exothermal effect at 850°.

The mineral occurs in aggregates up to 10 cm. in diameter. Color black, opaque, brownish-red in fine fragments. Luster resinous. Streak dark brown. Brittle, fracture conchoidal. Optically isotropic, $n > 1.80$. G. 3.288. H. 5½–6. Amorphous.

The mineral occurs in pegmatites on the north-east slope of Mt. Karnasurt in hackmanite syenites, associated with microcline, natrolite, hackmanite, aegirine, schizolite, and nenadkevichite. It is altered to various hydrous rare earth silicates, including hydrocerite.

M. F.

Hydrocerite

K. A. Vlasov, M. V. Kuz'menko, and E. M. Es'kova. The Lovozero alkaline massif. *Akad. Nauk. S.S.S.R.*, **1959,** 427–429 (in Russian).

Analysis by M. E. Kazakova gave SiO_2 22.30, P_2O_5 5.76, BeO 0.30, Al_2O_3 3.66, TiO_2 3.33, ZrO_2 0.49, Nb_2O_5 2.00, Fe_2O_3 6.15, MgO 0.14, CaO 2.83, Ce_2O_3 4.83, La_2O_3 12.33, ThO_2 15.14, H_2O^+ 5.65, H_2O^- 14.14, total 99.95%, corresponding to (La, Ce, Th, Ca) (Al, Fe, Ti, Nb) $(Si, P)_2O_7 \cdot 5H_2O$. Spectrographic analysis also showed Zn, As, Mn, Pb, and Cu.

Color yellow to honey-yellow, luster vitreous. Isotropic with n 1.580. Brittle. Amorphous to x-rays; after being heated gives a powder pattern close to that of cerite. Strongest lines 3.03 (10), 2.91 (10), 1.87 (8) , 2.20 (5), 2.16 (5), 1.97 (5), 1.75 (5), 1.335 (5), 1.275 (5), 1.235 (5).

The mineral occurs as pseudomorphs after manganosteenstrupine in natrolite-albite pegmatitic veins of Mt. Karnasurt, associated with neptunite in hackmanite-bearing pokilitic syenites.

Discussion. The composition is very close to that of karnasurtite.

M. F.

Chukhrovite

L. P. Ermilova, V. A. Moleva, and R. F. Klevtsova. Chukhrovite, a new mineral from Central Kazakhstan. *Zapiski Vses. Mineralog. Obshchestva,* **89,** no. 1, 15–25 (1960) (in Russian)

Analyses by V.A.M. of samples from depths of 50 m. and 2 m., respectively, gave Al_2O_3 10.56, 10.70; $(Y, Ce)_2O_2$ 18.00, 18.12; MgO 0.40, 0.44; $(Na, K)_2O$ trace, –; ThO_2 trace, –; SO_3 10.38, 10.30; F 28.32, 27.88; H_2O^- 12.00, 12.20; H_2O^+ 10.80, 11.00; insol. trace, trace, sum 111.98, 111.64, $-(O=F_2)$ 11.89, 11.71 = 100.09, 99.93%. Sp. gr. 2.353, 2.40. These correspond to the formulas $Ca_{3.03}Al_{1.62}(Y, Ce)_{0.95}(SO_4)_{1.00}(F_{11.46}OH_{0.40}) \cdot 9.55H_2O$ and $Ca_{2.97}Al_{1.64}(Y, Ce)_{1.02}(SO_4)_{1.00}(F_{11.37}OH_{0.55}) \cdot 9.72H_2O$, which may be $Ca_6Al_3(Y, Ce)_2(SO_4)_2F_{23} \cdot 20H_2O$, or more probably $Ca_3Al_2(Y, Ce)(SO_4)F_{13} \cdot 10H_2O$. Spectrographic analysis also showed Pb, Fe, Si (very weak), Mo, Mn, Cu, Ag, Ti, Sr (traces).

The proportions of the rare earths were determined by the *x*-ray spectrographic method by R. L. Barinskii who obtained (total rare earth oxides 18.00%) La_2O_3 5, Ce_2O_3 15, Pr_2O_3 4, Nd_2O_3 12, Sm_2O_3 7.2, Eu_2O_3 0.2, Gd_2O_3 6.5, Tb_2C_3 0.9, Dy_2O_3 4.1, Ho_2O_3 0.8, Er_2O_3 1.7, Tu_2O_3 0.3, Yb_2O_3 1.2, Lu_2O_3 0.2, Y_2O_3 0.2, Y_2O_3 (by diff.) 40.9%.

The D.T.A. curve shows a sharp endothermal break at 280°, ascribed to loss of water of crystallization, a smaller one at 780°, and an exothermal break at 480°. The loss of weight curve shows 26.7% loss at 280°, the loss above the water content is ascribed to loss of HF. Above 280° there is a continuous gradúal loss in weight (SiF_4?) up to 55.6% at 1000°. Material heated to 550° is isotropic, *n* 1.540, and gives sharp *x*-ray pattern, not corresponding to any known compound. Before the blowpipe, swells and fuses easily to a creamy-white enamel. Readily dissolved by dilute HCl and H_2SO_4.

The mineral occurs in crystals ranging from less than 0.5 mm. to 1 cm. in size, showing *a* (100) and *o* (111). Colorless and transparent, or white porcelain-like, sometimes with a lilac tint. The white material contains many liquid inclusions. Luster vitreous when transparent, weakly pearly when white, greasy on fracture surfaces. Cleavage octahedral, indistinct; fracture irregular. Brittle. Hardness about 3. G 2.274–2.398, av. 2.353. *n* (Na) 1.440–1.42; the mineral is anomalously birefringent.

X-ray study (by R.F.K.) shows the mineral to be cubic, *a* 16.80±0.005 Å. Indexed powder data are given (37 lines); the strongest lines are 2.193 (10), 1.834 (10), 3.261 (9), 2.572 (9), 2.843 (8), 1.684 (8), 1.512 (8), 1.460 (8), 1.417 (8), 1.279 (8), 4.256 (7), 2.664 (7), 1.616 (7).

The mineral occurs in the secondary oxidation zone of the Kara-Oba molybdenum-tungsten deposit, Central Kazakhstan, associated with gearksutite, creedite, halloysite, supergene fluorite, anglesite, and hydrous Fe oxides. Oxidation of sulfides such as pyrite have dissolved primary fluorite of the deposit which contains up to 3% rare earths.

The mineral is named for the Russian mineralogist, F. Kh. Chukhrov, who has published many papers on minerals of the zone of oxidation. It is probably the same as the unnamed mineral from Greenland described by Bøggild, *Z. Krist,* **51,** 608 (1913), *Medd. on Grønland,* **149,** no. 3, 97 (1953) without any analysis.

Presumably to be classed with creedite.

M. F.

Karnasurtite (Kozhanovite)

M. V. Kuz'menko and S. I. Kozhanov. The new mineral karnasurtite. *Trudy inst. mineral., geokhim. i kristallokhim. redkikh elementov,* **2,** 95–98 (1959) (in Russian).

K. A. Vlasov, M. V. Kuz'menko and E. M. Es'kova. The Lovozero alkaline massif. *Akad. Nauk S.S.S.R.,* **1959,** 423–425 (in Russian).

The mineral occurs as individual grains up to 1 cm. in diameter or as accumulations of platy crystals up to 10×6×2 cm. One good cleavage. Color honey-yellow when fresh to pale yellow when altered. Streak yellowish. Luster greasy. Hardness 2, brittle. G. 2.89–2.95. In section pale yellow, no pleochroism. Optically uniaxial, negative, *ns,* O 1.617, E 1.595. Sometimes anomalously slightly biaxial. Extinction parallel.

The four analyses given lead to the formula (La, Ce, Th) (Ti, Nb) (Al, Fe) $(Si, P)_2O_7$ $(OH)_4 \cdot 3H_2O$. Spectrographic analysis showed also Zn (strong lines), As, Cu, and Ga (very weak lines). A dehydration curve showed that half the water is lost up to 150°, the rest gradually to 650°.

Hexagonal (?). The mineral is amorphous to *x*-rays; after being heated at 900°, it gives a pattern close to that of huttonite. The strongest lines are 3.10 (7), 2.88 (7), 3.29 (6), 3.49 (5), 1.723 (5).

The mineral occurs in a zoned pegmatitic stock in the intermediate replacement zone consisting mainly of microcline. It is associated with schizolite, natrolite, and epididymite, and is replaced by polylithionite.

Analyses of Karnasurtite

	1	2	3	4
SiO_2	22.33	20.47	30.27	24.91
P_2O_5	5.55	3.29	2.42	6.81
BeO	0.35	—	—	—
Al_2O_3	6.40	7.46	8.43	5.52
Fe_2O_3	3.50	1.10	0.75	1.07
MgO	0.45	0.91	3.41	0.60
TiO_2	10.73	12.14	6.65	12.33
ZrO_2	none	—	—	1.20
Nb_2O_5	6.25	8.20	5.00	2.20
ThO_2	5.40	6.22	2.82	6.04
Ce_2O_3	6.55	17.58	5.15	8.11
La_2O_3	9.82	—	10.63	8.55
CaO	2.23	1.66	1.73	3.20
BaO	—	0.68	—	—
Na_2O	0.50	0.91	0.97	—
K_2O	1.57	0.76	1.05	—
H_2O^+		7.22	8.68	7.29
H_2O^-	17.90	10.84	10.67	12.29
F	—	0.91	—	—
	99.53[a]	100.35	98.63	100.12
$-(O=F_2)$	—	−0.38		
		99.97[b]		
G.	2.89	—		

[a] Given as 99.43; [b] given as 99.47; both in the second reference. Analyses 1, 3, and 4 by M. E. Kazakova, 2 by K. P. Sokova, 1–3 from Karnasurt Mt., 4 from Punkaruaiv Mt.

The name is for the locality. It had previously been called kozhanovite without a description (see *Am. Mineral.*, **42**, 119–120 (1957).

Discussion.—Presumably related to huttonite, cheralite, and monazite.

M. F.

Sakharovite

Ivan Kostov. Bismuth jamesonite or sakharovite — a new mineral species. *Trudy Mineralog. Muzeya Akad. Nauk. S.S.S.R.*, **10**, 148–149 (1959) (in Russian).

A mineral called bismuth jamesonite was described by M. S. Sakharova in 1955 (*Am. Mineral.*, **41**, p. 814 (1956)), with formula $Pb(Sb, Bi)_2S_4$, Sb : Bi = 1 : 1. No new data are given; Kostov considers the mineral to be a new species and suggests the name sakharovite.

M. F.

NEW DATA

Erikite

K. A. Vlasov, M. V. Kuz'menko and E. M. Es'kova. The Lovozero alkaline massif. *Akad. Nauk. S.S.S.R.* **1959,** 425–427.

Material called erikite had been described from Mt. Punkaruaiv by Gerasimovskii in 1937 (*Mineral. Abs.*, **8,** 222 (1942)). A new analysis by M. E. Kazakova for erikite from Mr. Karnasurt gave SiO_2 10.82, P_2O_5 20.06, BeO 0.50, TiO_2 0.25, ZrO_2 0.43, Fe_2O_3 1.80, Al_2O_3 0.66, MnO 0.50, MgO 0.20, ThO_2 1.15, Ce_2O_3 21.06, La_2O_3 29.24, CaO 1.90, BaO 0.76, SrO 0.60, Na_2O 1.36, K_2O 0.38, H_2O^+ 4.70, H_2O^- 2.72, sum 99.09%, corresponding to (La, Ce, Ca, etc) $[(P, Si)O_4]\cdot H_2O$.

Discussion.—The type erikite from Greenland has been discredited (*Am. Mineral.* **44,** 1329 (1959)); should the name be transferred to the Kola material? In any case, further optical and *x*-ray study is needed. Perhaps related to rhebdophane?

Oryzite or Orizite

G. Cocco and C. Garavelli. *Atti soc. Toscana Sci. nat., Mem.* **65,** 262–283 (1958) (Pub. 1959).

Oryzite (Grattarola, 1899; *Dana's System, 6th Ed.*, 576) has been supposed to be heulandite; the old analyses are similar to those of heulandite. *X*-ray powder data (28 lines) are given; they are considered to be different from those of heulandite. The strongest lines (2 samples) are 8.92 (100, 100); 3.21 (36, 42); 3.45 (30); 3.44 (27); 1.778 (20); 1.777 (12); 3.88 (17); 3.87 (16); 2.92 (16, 12); 4.92 (16, 12); 6.92 (10); 6.93 (14).

Further study will be made.

M. F.

DISCREDITED MINERALS

Gearksite (=Gearksutite)

I. F. Grigor'ev and E. I. Dolomanova. Gearksite. *Trudy Mineralog. Muzeya Akad. Nauk S.S.S.R.*, **10,** 185–186 (1959) (in Russian).

Three new analyses of gearksite, described by G. and D. in 1951 (*Am. Mineral.*, **41,** 371 (1956), show that the original analysis was in error and that gearksite is gearksutite. It is in fine fibrous aggregates with birefringence not above 0.009; mean *n* 1.458.

M. F.

Plinthite (=mixture)

Jessie M. Sweet. What is plinthite? *Mineralog. Mag.*, **32,** 455–458 (1960).

Plinthite (Thomson, 1836) Dana's System, 6th Ed., p. 695) is shown to be a mixture of kaolinite and montmorillomite colored by hematite. Other similar red material contains various zeolites.

M. F.

G. Cocco and C. Garavelli. *Atti soc. Toscana sci. nat., Mem.*, **65,** 262–283 (1958) (Pub. 1959).

This paper gives the results of re-examination of type specimens of several zeolites from San Piero, Elba.

Pseudonatrolite (=Mordenite)

Pseudonatrolite (Grattarola, 1879; Dana's System, 6th Ed., 573) is shown by *x*-ray study to be mordenite.

Foresite (=mixture Stilbite+Cookeite)

Foresite (Rath, 1874; Dana's System, 6th Ed., p. 585) is shown by *x*-ray and optical study to be a mixture of stilbite and cookeite.

Hydrocastorite (=mixture)

Hydrocastorite (Grattarola, 1876; Dana's System, 6th Ed., p. 312) was re-examined optically and by *x*-ray study. Samples were found to be heterogeneous mixtures of stilbite, petalite, mica, and quartz; one was montmorillonite.

M. F.

Glottalite (=Chabazite)

M. H. Hey. Glottalite is chabazite. *Mineralog. Mag.*, **32,** 421–422 (1960).

Glottalite (Thomson, 1836; Dana's System, 6th)Ed., p. 599) was found by *x*-ray study to be chabazite. The analysis, except for H_2O, is evidently erroneous.

M. F.

SHALE'S

LISTING OF FINE MINERAL SPECIMENS

RUBIES IN CHROME DIOPSIDE MATRIX (Belgian Congo, Africa) Two 1″ flat hexagonal crystals imbedded in matrix. Very showy—$50.00

BARITE CRYSTAL GROUP (Palos Verdes, Calif.) One of the largest ever found. 9x16 brown crystal group—$75.00

KYANITE GROUP (Minas Geraes, Brazil) 7x12 fine massive crystal group—$17.50

BERYL var AQUAMARINE CRYSTAL (Brazil) Fine 6x5 green-blue opaque crystal—$45.00

ZIRCON CRYSTALS IN MATRIX (Ontario, Canada) Two long crystals in 6x9 matrix. Very fine specimen—$40.00

AQUAMARINE CRYSTAL (Brazil) Green mostly gemmy 1½x2¼ crystal 172 grams—$165.00

FIRE OPAL (Virgin Valley, Nevada) 1½x2½ fire opal limb section—$75.00

CUPRITE AND SOME COPPER CRYSTALS. (Santa Rita, New Mexico) Bright 2x4 crystal specimen—$15.00

MINERALS FOR COLLECTIONS & STUDY

APATITES IN LIMESTONE MATRIX (Iron Mountain, Durango, Mexico) Fine yellow crystal specimens—$1.00, $1.50 and $2.00. Single crystals—25¢, 50¢ & 75¢

KYANITE CRYSTALS (Brazil) Blue crystal blades up to 3″—50¢, 75¢, $1.00 ea.

SAPPHIRE CRYSTALS (Mozambique, Africa) Blue opaque crystals. Up to 2x3″ specimens—$1.50, $2.50 and $3.00 each

RUBY CRYSTALS (Ampanihy, Madagascar) Up to 1″ flat hexagonal crystals—75¢, $1.00 and $2.00 each

QUARTZ CRYSTALS WITH INCLUSIONS OF PHANTOMS, ETC. (Brazil) 1″ to 2½ crystals showing 1 or more phantoms and sometimes other inclusions—75¢, $1.00 & $2.00

"CHINESE JADE" JADEITE (Mogaung Upper Burma) Cores and cuttings from Hong Kong from Jade cutting factories—$5.00 per lb.; 3 lbs. $12.00

SPODUMENE var TRIPHANE (Brazil) up to 1″ crystals partly clear—3 for $1.00

SEND FOR LISTINGS—WE ARE BUYERS OF COLLECTIONS

SHALE'S

9226 W. Pico Blvd.
Los Angeles 35, Calif.

Phone CR-5-8222

WARD'S BIG GEOLOGY CATALOG

Our largest and finest geology catalog offers you the widest choice of the best:

1. Mineral, rock and fossil teaching, study and reference collections.
2. Mineral, rock and soil specimens; individually and in bulk.
3. Special series of reference clay minerals.
4. Individual fossil specimens.
5. Paleontology and animal kingdom charts.
6. Light weight plastic relief maps.
7. Aids for crystallography (models, goniometers, protractors).
8. Geomorphological models.
9. Color slides for geology, mineralogy, paleontology; black and white transparencies on glaciers, astronomy.
10. Field and laboratory equipment—the largest listing ever.
11. Superb selection of the finest storage and display equipment.
12. Petrographic supplies; refractive index media.
13. Thin section and lapidary equipment.
14. A full line of weather instrument.
15. Fluorescence and radiation equipment.

Ward's big geology catalog, #603, is the answer to every geologist's needs. We are just as anxious to send you this new catalog as we think you will be to receive it. If you are affiliated with a teaching, industrial or research institution, your copy is absolutely free. Just write on your school or business letterhead. Ask for Ward's Geology Catalog #603.

WARD'S *NATURAL SCIENCE ESTABLISHMENT, INC.*
P.O. BOX 1712
ROCHESTER 3, N.Y.

GEORGE BANTA COMPANY, INC., MENASHA, WISCONSIN, U.S.A.